CONDITIONING 3D BIOMIMETIC SCAFFOLDS FOR THE CULTIVATION OF TRANSPLANTABLE BETA CELLS

JAMES DAVID BOCKHART

A thesis submitted in partial fulfilment of the requirements of the University of Brighton for the degree of doctor of philosophy

September 2013

The University of Brighton in collaboration with the Porvair Filtration group

Abstract

Islet transplantation holds vast potential as a treatment for type 1 diabetes mellitus and provides recipients with short term insulin independence. A major limitation of this treatment is the lack of donor beta (β) cells available for transplantation. Significant progress has been made with stem cell differentiation protocols; current methods have generated cell populations which possess a functioning β cell phenotype. However, these cells are not suitable for clinical transplantation. Two dimensional cell culture systems do not accurately mimic the complexity of the *in vivo* pancreatic environment, reducing the effectiveness of current β-cell differentiation protocols. The paradigm shift into three dimensional tissue culture provides an attractive area of investigation, and the use of three dimensional culture methods has improved growth in a variety of cell types *ex vivo*. The mass culture of β cell analogues on a 3D biomimetic environment is now necessary, and may offer a new platform on which an alternative source of transplantable cell populations can be differentiated and cultured successfully.

This thesis aims to develop and condition BioVyon™, a high density polyethylene (HDPE) based biomaterial, for use as a mass β cell cultivation system. In order to achieve this, a number of objectives will need to be met: (i) Complete characterisation and assessment of all properties of Biovyon™ that have a direct influence on cell culture, (ii) modification of the BioVyon™ surface chemistry to promote cell adhesion and growth, (iii) absorbance of proteins to mimic the pancreatic environment and aid proliferation of the Min-6 cell line, (iv) assessment of the Min-6 cell line phenotype after extended period of culture on the modified BioVyon ™ environment.

Scanning electron microscopy and Atomic Force Microscopy were used to characterise the surface of the HDPE material post plasma etching. Advancing and receding (ARCA) and Fourier Transform Infrared Spectroscopy were used to analyse the elemental changes to the polymer surface. The HDPE biomaterial was conditioned using plasma etching, subsequent adhesion and growth of Min-6 cells was quantified using a lactate dehydrogenase assay. Min-6 populations were seeded at a density of $1x10^6$ on BioVyon™ and tissue culture plastic of comparable surface area, and analysed after extended periods of growth. An insulin ELISA was used to quantify insulin released by populations of β cells at different time points witin the BioVyon™ in response to fluctuating glucose concentrations.

The results obtained in this thesis indicate that BioVyon™ offers an appropriate structural environment for cell culture. Pore size and frit dimensions allow for cell infiltration and the effective diffusion of oxygen and nutrients. Plasma etching incorporated oxygen groups and a novel surface topography that improved cell adhesion and growth. β-cell phenotype was protected and sustained in cell populations cultured within the BioVyon™ environment.

In conclusion, BioVyon™ can be conditioned to function as an effective 3D cell culture system. Modification of the surface chemistry has enabled BioVyon™ to harbour and sustain large populations of the Min-6 cell line. The protected β cell phenotype in the Min-6 populations suggests BioVyon™ could hold potential as a stem cell culture and differentiation platform.

Contents

List of Figures

List of Tables

Acknowledgements

Thank you Dr Wendy Macfarlane, Dr Claire Marriott and Dr Dave Cowieson for your support, advice and wisdom, I couldn't have asked for better supervisors during this process. My appreciation extends to the staff at Porvair Filtration and and my colleagues the University of Brighton, in particular Dr Barry, Miss Holling, Mr Kumar, Miss Alhasawi and Mr Lacey who joined me in an estimated 4380 cups of coffee required to complete this work.

Finally, thank you to my parents as well as the friends and family who had to endure my commitment to this project, your love, support and encouragement made it possible.

Declaration

I declare that the research contained in this thesis, unless otherwise formally indicated within the text, is the original work of the author. The thesis has not been previously submitted to this or any other university for a degree, and does not incorporate any material already submitted for a degree.

James David Bockhart

1 Introduction

1.1 Type 1 Diabetes

Type 1 diabetes mellitus (T1DM) is a metabolic disease limiting a person's capability to maintain optimal blood glucose concentrations. This can be attributed to a near complete destruction of the cells responsible for synthesising and secreting insulin. Beta cells (β-cells) are found in the pancreas and contribute to approximately 60% of the cells in clusters known as the islets of Langerhans; these islets function as a part of the endocrine system [1-3].Secreted insulin stimulates the uptake and metabolism of glucose as well as stimulating glycolysis in the liver. If endogenous supply of insulin is removed, homeostasis of blood glucose becomes impossible.

1.1.1 Complications

Fluctuating concentrations of blood glucose can result in major complications, such as retinopathy, coronary heart disease and neuropathy of the peripheral nervous system. Neuropathy is caused by oxidative stress placed on the neurons exposed to a hyperglycaemic environment; this can affect the sudomotor, gastrointestinal, genitourinary and cardiovascular function of an individual. Dysfunction of these systems can lead to several debilitating symptoms including pain, decreased mobility and ulceration of the feet [4].

The most serious risks however, are associated with large and sudden fluctuations in blood glucose concentrations. Hypoglycaemia is one of the most common issues in T1DM, occurring mainly due to the overuse of insulin, low calorie intake or exercise without accounting for the loss of blood glucose. Rapid decreases in blood glucose levels lead to convulsions, unconsciousness and death and may be the reason for “dead in bed syndrome”. It is suggested nocturnal hypoglycaemia combined with neuropathy of the autonomic nervous system can cause the failure of cardiac repolarisation and therefore fatal ventricular arrhythmias [5, 6] .

Severe hyperglycaemia is equally lethal and is caused by insulin deprivation; without this hormone the transport of glucose out of the blood into skeletal, muscle and adipose tissue slows significantly. Escalation of hyperglycaemia from food causes these cells to metabolise proteins at a high rate leading to muscle break down. Urea and fatty acids build up in the liver and result in increased aceto-acetate levels in the blood. This can lead to ketoacidosis which has a toxic effect on neurones in the brain and can cause lethargy and comas, regrettably this was usually the fate of all individuals suffering from T1DM prior to the discovery of insulin [6, 7].

1.1.2 Pathophysiology and Etiology of T1DM

The World Health Organisation (WHO) has classified T1DM into two subtypes. Type 1A (T1ADM) is a chronic autoimmune disease, compared to Type 1B (T1BDM) of unknown, referred to as idiopathic T1DM [8].

In the early stages of T1ADM, autoantibodies directed against the islet cell population are present within the peripheral blood, alongside pancreatic infiltration of T cells (CD4 and CD8), B-cells and macrophages. This in turn contributes to insulitis and the destruction of the β-cell population [9]. This pre-clinical period can last for years before symptoms arise, however this is not normally the case [10]. Hyperglycaemia usually occurs when at least 80-90% of the β-cell population has been eradicated [11].

There are genetic susceptibilities to T1ADM, associated with the Human Leukocyte Antigen (HLA) gene cluster located on chromosome 6. 90% of individuals with T1DM possess polymorphisms within this HLA gene cluster [6, 12]. These alleles are associated with a selection of auto antigens identified from autoantibodies against glutamic acid decarboxylase [13], insulin and a zinc transporter known as Slc30A8 [13].

Interestingly, T1DM is developing in children with intermediate-risk HLA alleles, postulating genetic influence is not the single contributory factor [9]. Several environmental factors have been indicated as a potential cause for the onset of T1DM. Many proposed environmental factors include diet (Gluten intake, wheat-derived proteins), malnutrition (vitamin D deficiencies), and infection (Coxsackie virus) [9, 12]. Although patterns between these environmental factors and development of T1DM exist the exact mechanisms are not fully understood. Environmental agents may cause direct damage to the β-cell population, trigger an autoimmune response in genetically susceptible individuals (mimicking T1ADM), increase insulin resistance, or generate susceptibility in the β –cell population that leads to damage [11].

1.1.3 Epidemiology

The onset of T1DM occurs primarily in children under 15 years of age, 48% of which are between 10 and 14 [9]. Studies indicate that the incidence of T1DM is increasing; between 1985 and 1995 in children under 5 and children between 10 and 14 years of age there was a 4% and 11% increase in incidence in the UK respectively [12]. Despite on-going investigation, the incidence of T1DM is predicted to increase by 70% in children under 5 over the next 8 years [14].Currently, 36 million people globally are suffering from T1DM; this has increased from 15 million in 2000 and is predicted to rise further to 55 million in 2030 [6, 15]. In the UK, 2.6 million people suffer from diabetes, of which 260,000 suffer from T1DM. Overall diabetes costs the NHS approximately £9 billion per year [15, 16].Therefore, research into potential cures and treatments is easily justified

1.1.4 Islet transplantation

To date, the primary treatment for T1DM consists of subcutaneous administration of purified insulin [17]. Since the discovery and isolation of insulin in 1921, diabetes has been treatable but not cured [18]. Even the most rigorous and consistent administration of insulin cannot replace the precise insulin secretion of an endogenous β- cell population. This can result in the complications and hypo/hyperglycaemic episodes previously discussed [5, 6].

Islet transplantation is an alternative treatment for T1DM involving the replacement of the lost β-cell population with cadaveric donor cells. 6000 islet equivalents per kg of the recipient's body weight are usually implanted into the liver via the hepatic portal vein

with the aid of fluoroscopic guidance [19, 20]. Initial islet transplantation techniques conducted on 267 recipients between 1990 and 2002 showed that 73% of patients could successfully produce insulin after 1 month but, only 11% remained insulin independent after 1 year [20].

Success rates improved drastically after the introduction of the "Edmonton protocol" [19], in which transplantation of more than 10,000 islet equivalents per kg of recipient body weight was followed by a course of glucocorticoid-free immunosuppressants. Unlike previous drugs, these glucocorticoid-free immunosuppressants are not associated with islet toxicity [17, 19].

The introduction of the Edmonton protocol resulted in a 100% transplant success rate with all patients showing insulin independence. Furthermore, 80% of patients remained insulin-independent after 1 year, and 10% after 5 years [21]. However, at present islet transplantation does not provide a long term treatment for T1DM and has two major disadvantages. Firstly, the recipient receiving the allograft islet tissue must be on lifelong immunosuppressants. This is to prevent an immune response caused by immunologically offensive, foreign islet cells. Furthermore the immunosuppressants are associated with serious complications including anaemia, ulcerations, weight loss and decreased renal function [22]. However, one of the most impeding limitations of islet transplantation is a lack of suitable islet cells. Currently, the cadaveric donor β-cells supply approximately 0.5% of the type 1 diabetic population [23]. Before islet transplantation can be applied effectively to treat the type 1 diabetic population an alternative supply must be established.

1.1.5 Alternative supply of beta cells

Embryonic stem cells (ESCs) form the mammalian blastocyst or embryo approximately 5 days after fertilisation. These cells are totipotent and genetically uncommitted to any lineage. They are able to proliferate indefinitely, provided they are cultured in a suitable environment [24]. The first ESC line was derived in 1998 from the inner cell mass of human blastocysts produced via *in vitro* fertilisation (IVF)[24]. Due to their ability to differentiate into all adult cell lineages there is a promising capacity for ESCs in regenerative medicine and the treatment of tissue and organ loss due to injury, disease or congenital abnormality [25]. Various disciplines have explored the use of ESCs in neurological diseases, heart disease and skin grafts, forcing these cells through complex protocols via *in vitro* cell culture [26-31].

Over the last 10 years significant progress has been made in differentiating ESCs into functional β-cells. In 2000, Soria *et al* developed the first successful differentiation protocol that engineered murine ESCs into expressing and producing insulin. ESCs were transfected with an insulin producing gene combined with a hygromycin/neomycin resistant gene within a DNA vector, enabling selection of the differentiated cell population [32]. The next protocol advancement was achieved by Lumelsky *et al* (2001) who utilised a 5-stage culture protocol to isolate mouse ESCs expressing the neural filament protein nestin [33]. Research has identified an association between neural and pancreatic cell lineages during embryogenesis, suggesting nestin-expressing ESCs are pancreatic cell progenitors and have the ability to differentiate into specialised islet cells [34]. *In vivo,* these cells were able to vascularise, respond to insulin and form 3D structures similar to islet clusters after 12 days in STZ diabetic mice [33]. However, these

cells did not consistently prevent hyperglycaemia despite mice surviving longer with the implants [33].

These protocols were originally designed for mouse ESCs, and the knowledge surrounding differentiation of these cells exceeded that of human ESCs by 17 years [35]. However, they provided the important steps to developing a human ESC differentiation protocol.

In order to mirror the natural development of a β-cell during human embryogenesis the stages of growth were mimicked by D'Amour *et al* (2006) [36]. This protocol induced differentiation of human ESCs from endoderm, primitive gut tube, posterior foregut, pancreatic endoderm and finally, the pancreatic β-cell. Although this *in-vitro* development is not identical to the environmental signalling in a developing foetus, it mimics it well enough to have produced a β-cell population expressing endocrine markers NeuroD1, ISL1 and PAX 6 as well as insulin, amyloid polypeptide and C-peptide [36]. When compared to primary human β-cell populations, the differentiated ESC produced similar quantities of insulin and cell morphology showed granules of insulin. However, as little as 7% of the cell population undergoing this protocol expressed insulin. It has been suggested that this low differentiation efficiency is caused by different ratios of partially differentiated cells within the ESC cell population. This in turn contributed to the differentiation process while in culture [36]. This cell population demonstrated a limited C-peptide response to high glucose concentrations in comparison to mature β-cells, indicating the cell line resembled a foetal β-cell population. These cells were an ideal basis to begin further differentiation and development protocols [36].

The environment of the developing embryo is complex, to date β-cell differentiation protocols have been unsuccessful in accurately mimicking the lengthy and intricate signalling process required to generate a mature β-cell population. Further environmental factors must be identified and applied before the desired cell line can be harvested and used clinically to treat diabetic patients [37].

1.1.6 Benefits of 3D cell culture

Current two dimensional (2D) *in vitro* cell culture systems offer limited success in stem cell differentiation. They do not accurately mimic the complex 3D niche in which cells differentiate *in vivo* during embryogenesis. Molecular gradients cannot be maintained in the absence of three dimensions and do not interact with cells as they would in the developing embryo. This limits several important biological mechanisms dependant on gradients such as differentiation and signal transduction mechanisms [38]. Cells often adapt to the 2D environment; alterations in oxygen levels and nutrients *in vitro* can result in a cell with altered metabolism [38]. The position of cell surface molecules may also be affected by 2D environment as cells orientate their transmembrane, transport molecules to the media and oxygen above in the flask. This may have an effect on cell to cell adhesion; reducing the number of cadherin interactions between cells. Therefore reducing communication which can affect growth and gene expression [39].

3D matrices appear to overcome these limitations and mimic the *in vivo* environment more accurately, aiding cellular adhesion to surrounding attachment molecules and growth factors [40, 41]. This facilitates gene expression promoting proliferation,

differentiation and migration. Differentiation studies have shown a tenfold increase in proliferation rate of insulin-producing pancreatic cell lines attached to extracellular matrices [42, 43]. A more recent study incorporated differentiation factors activin A and BMP4 in matrigel acting as a 3D scaffold; following differentiation, human ESCs showed partial islet cell phenotype and consisted of between 5-20% of the total cell population [44]. Furthermore, studies surrounding regenerative medicine have found 3D culture matrices useful in differentiation of osteoblasts [45], chondrocytes [46, 47] and neurones [48] as well as mimicking cellular behaviour in organs and large structures in the body [49].

An optimised version of the protocol developed by D'Amour *et al* (2006) involved taking cells differentiated from the protocol at stage four and seeding them into a 3D gelatin foam, prior to transplantation into mice [37]. This study shows that *in vivo* development of immature β-cell lines into fully differentiated β-cells is a promising method. Not only did the cell population function to the same levels of human adult islets, but also protected mice from hyperglycaemia for up to 100 days [37]. Work implanting ESC derived β-cell lines into STZ induced diabetic mice identified 92% of recipient mice were resistant to hyperglycaemia; however this was after a 3 month time period in which the cells matured and produced maximal insulin response to elevated glucose levels [37]. These studies indicated that β-cells cultured and transplanted differentiated in a 3D environment prior to analysis improved function. Cells require cell to cell cadherin adhesion in order to maintain expression of mature β-cell phenotype, as cadherin loss results in dedifferentiation in pancreatic cells [50]. These studies highlight the importance of extracellular adhesion molecules in the differentiation and continuous

expression of pancreatic phenotype. In order to incorporate these signalling molecules effectively, the use of 3D differentiation culture systems is required to more accurately mimic the natural environment of the developing foetus.

The success of 3D biomaterials is not simply due to structure alone. A degree of mimicry is a common theme in successful 3D culture systems [45-47]. In order to generate a 3D biomaterial that mimics the pancreatic islet, it is advantageous to hold a detailed understanding of the *in-vivo* tissue structure at the cellular and molecular level.

1.2 The functional structure of the pancreatic islet

In order to successfully mimic a tissue in-*vitro* a thorough understanding of its structure is necessary; the environment that sustains the cell population must be understood and simulated at the micro and nanoscale. The function of the β cell is supported by the unique structure of the pancreatic islet, which will be explored in detail in this section.

The human pancreas is a lobulated gland lying transversely in the posterior of the abdomen. It consists of three regions; the head, connecting the pancreatic duct to the duodenum, the body, and the tail, relating to the spleen and the left kidney [51]. The incomplete lobules of the pancreas are composed of two functional tissue types; exocrine and endocrine cells contained in tubular and ellipsoidal clusters, respectively. These are surrounded by enteroendocrine, loose connective tissue, consisting of mast cells, muscle cells and neurones [51-53].

The pancreas exhibits two primary functions. Exocrine tissue is formed of acini, groups of often columnar or pyramidal shaped cells, as a tubular cluster these cells secrete pancreatic juice containing a variety of zymogens into ductules. These connect to larger intralobular ducts. Upon arrival into the duodenum, zymogens are activated and work synergistically with brush border enzymes. In combination, these enzymes function to break down food by cleaving peptides, fatty acids and sugars from their corresponding substrates for effective digestion and absorption of food [51].

Endocrine tissue is also found in clusters, named the islets of Langerhans. Approximately one million islets contribute to 1-2% of the tissue mass of the pancreas [54], and are scattered throughout the pancreas, but concentrated primarily in the tail region. Five cell types exist within the pancreatic islet. Alpha (α) and β cells function to regulate blood glucose levels by secreting glucagon and insulin, respectively. Delta (δ), PP cells and Epsilon (ε) cells hold a regulatory role within the islet, secreting hormones affecting cell proliferation, neurotransmission and hormone secretion [55]. The functional significance of the pancreatic islet is mirrored by the extensive vascularisation and neurological branching observed throughout its macrostructure. This structure optimises the speed at which hormones can enter the blood and generate a physiological effect, as well as providing the sympathetic nervous system with appropriate control over the homeostatic control of blood glucose.

1.2.1 Microstructure

The islet microstructure has been investigated extensively. The dimensions and cell populations per islet varies considerably; pancreatic islets contain between 100 and

5000 cells, 60% of which consist of β cells (Figure 1-1) [3]. Islet diameters of approximately 50 and 500µm have also been observed [56, 57]. Supplied by 1-3 arterioles, a significant commitment of capillaries have been observed to supply pancreatic islet tissue relative to the size of the cell populations (Figure 1-1) [57]. It is estimated to be up to five times as dense and ten times as divaricating as capillary networks in exocrine tissues, further emphasising the functional structure of the islets of Langerhans [58, 59]. Although some variance exists in capillary structure between islets, divarication appears to occur centrally, allowing the blood flow to supply the centrical β cell population before it reaches the other cell types in the islet periphery [56].

Similar to other tissues, the islet capillaries are approximately 5µm wide, approximately 600nm separates the arterial blood flow from secretory insulin granules, due to distance through the basement membrane (BM) and endothelial cell body [60]. This, in combination with a unique basement membrane and complex endothelial cell - β cell association, makes hormone secretion extremely efficient. β-cells initiate insulin exocytosis and secretion in response to circulatory, intra-islet and neuronal triggers, all of which increase intracellular calcium ions (Ca^{2+}) [11]. The regions of β-cell membrane in close proximity to capillaries are known to hold a density of membrane receptors. Among them glucose transporters promote the uptake of glucose which acts on the β-cell metabolism. This results into potassium ion (K^{+}) channels closing, in turn, intracellular K^{+} concentration increases triggering voltage gated Ca^{2+} channels to open [11, 61].

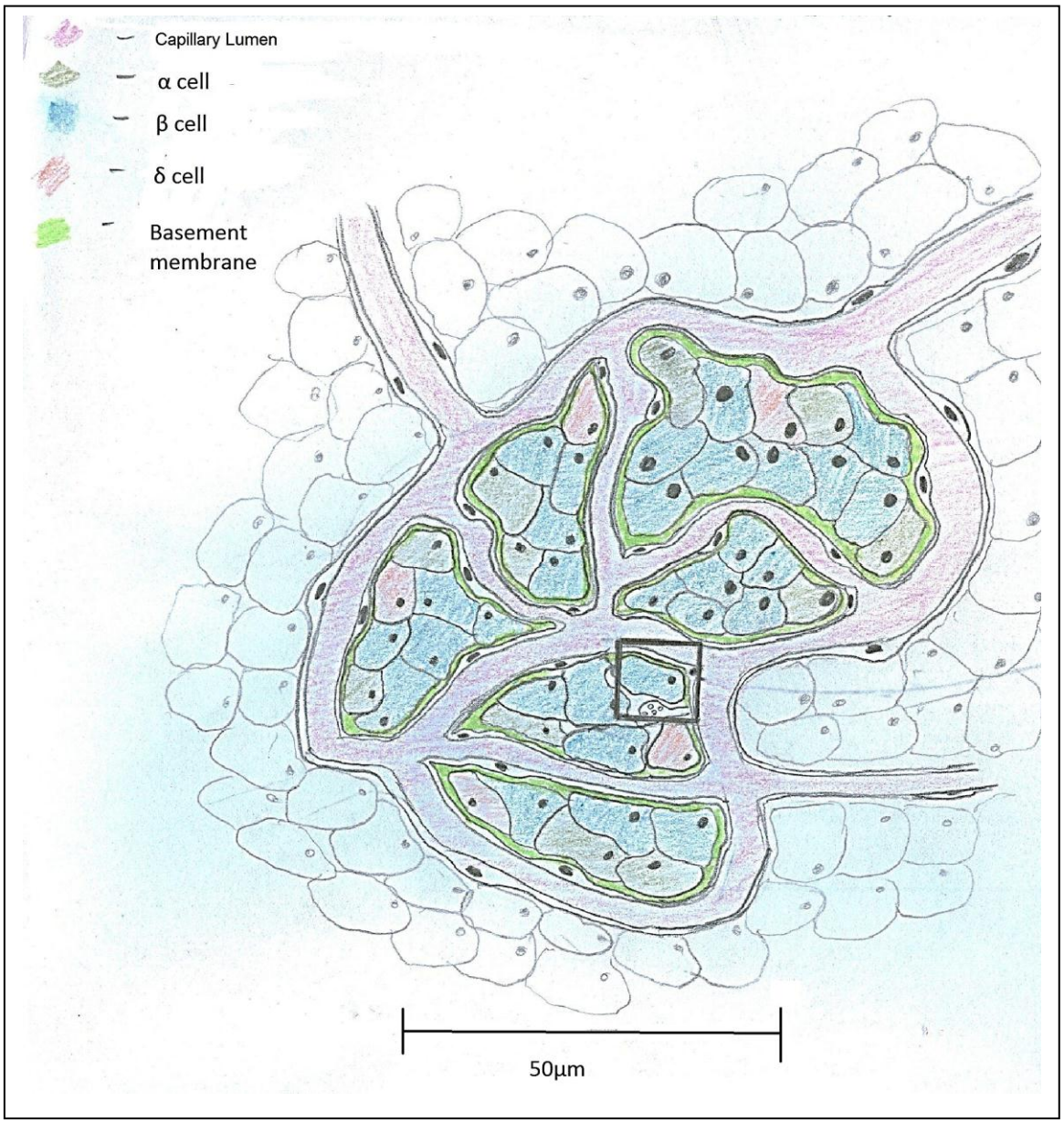

Figure 1-1: Diagram of pancreatic islet microstructure.

Diagram indicates scale and structure of islets relative to capillary divarication. Cell types are at a similar ratio and position of natural pancreatic islets. Basement membrane is present between islet cell populations and capillary endothelial cells. Central square is magnified in Figure 1-2. Adapted from Gray, HL. Grays' Anatomy. 38th ed: Chruchill Livingstone; 1995, P1794.

Pancreatic islet cell populations are also innervated with parasympathetic and sympathetic neurones, which form neuro-insular complexes with β-cells (Figure 1-2). Neurohormones noradrenaline and adrenaline interact with α-adrenergic and β-adrenergic receptors. These receptors potentiate intracellular mechanisms which stimulate and inhibit insulin secretion respectively [11]. This provides the central nervous system with a degree of control over insulin secretion. These triggers in combination with the influx of Ca^{2+} between β-cells via gap junctions (Figure 1-2), function to increase intracellular calcium ion concentration [11]. The presence of intracellular Ca^{2+} is known to be vital for exocytosis of insulin granules [62]. The microstructure of pancreatic islets ensures that β-cells are provided with access to capillaries, neuro-insular complexes and stable adhesion with other β-cells, thus promoting an environment for insulin secretion (Figure 1-2).

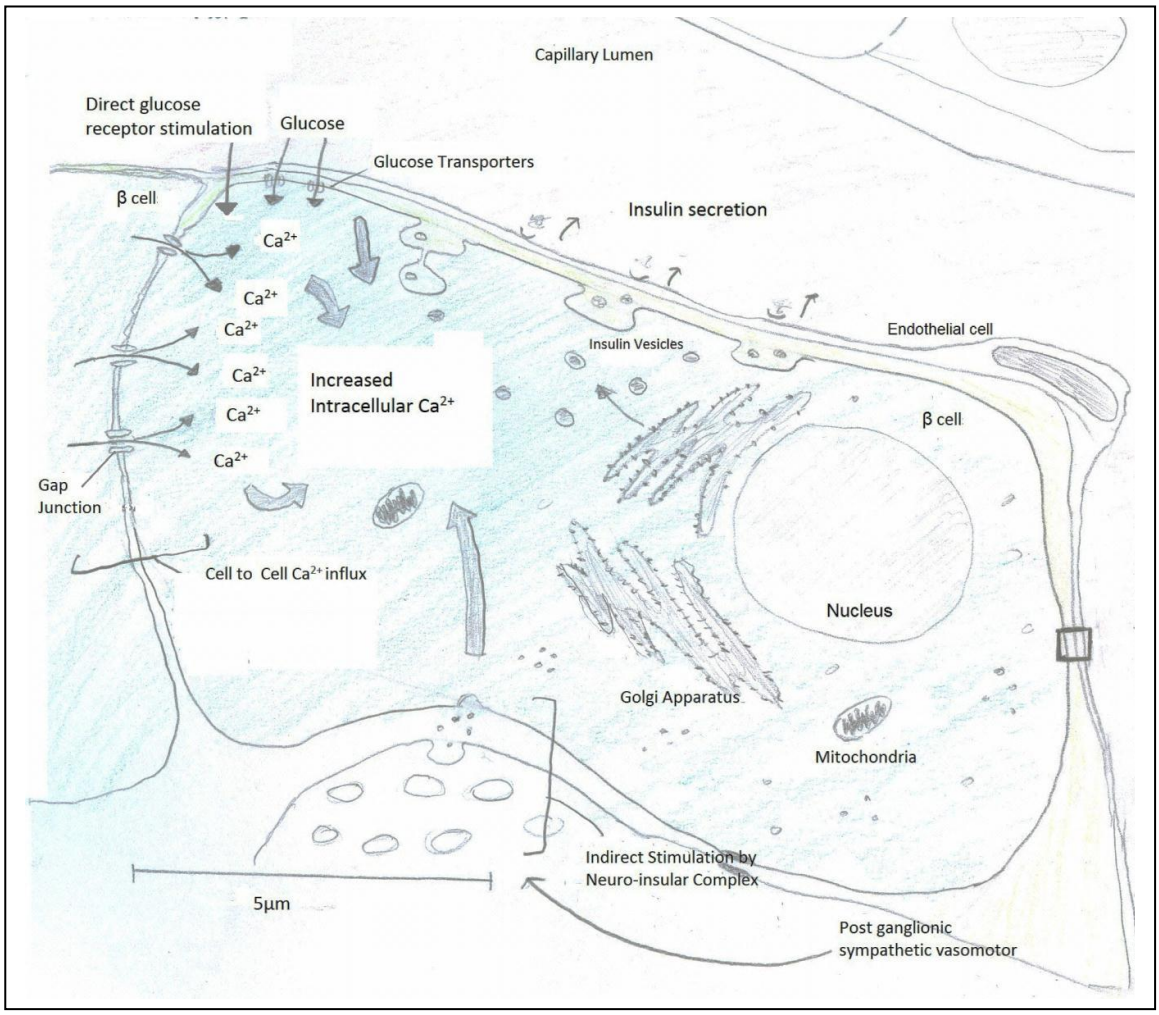

Figure 1-2: Diagram of β-cell

Diagram shows three primary mechanisms promoting insulin granule exocytosis and insulin secretion. Glucose uptake from the capillaries, indirect stimulation via neuro-insular complexes and influx from adhered β-cells function to increase intracellular calcium ions. Square is magnified in Figure 1-3. Magnified from square in Figure 1-1. Adapted from Gray, HL. Grays' Anatomy. 38th ed: Chruchill Livingstone; 1995, P1794.

1.2.2 Nanostructure

In order to influence a cell population *in-vitro,* a clear understanding of the tissue nanostructure is arguably most important to the success of any biomaterial. The extra cellular matrix (ECM) describes a variety of proteins organised into functional structures, providing tissues with structural support and molecular cues at a cellular level. The basement membrane (BM) describes the basal laminae and its constituent layers; it is one of the most significant types of ECM. It is located in all tissue adjoining epithelia and contributes not only to tissue organisation and architecture, but also regulates cellular function, adhesion and in some cases differentiation [63, 64].

Capillary endothelial cells are enveloped by a 20-200nm-thick BM throughout the body, consisting of layered collagen IV (Col IV) and laminins (Lm) connected by smaller heparin sulphate proteoglycans (HSPGs) such as perlecan and entactin. This forms a sheath called the lamina densa [65]. This is sandwiched between two less dense layers named the lamina lucida externa and lamina lucida interna, which associate with the cell membrane and the connective tissue of the stroma, respectively (Figure 1-3) [63, 66, 67]. Cells may bind to the lamina lucida externa or directly to the lamina densa via integrin adhesion to Lm. Several other cell surface receptors can interact with the BM relative to the tissue type [68, 69]. LMs are secured to type IV collagens that are not fibrillated on account of regions of non helicated domains, forming a 2D layer. These layers of the basal laminae are cross-linked and anchored to the stroma via fibrillated types I, III and VII collagens [63].

Human endocrine tissue has a second BM referred to as the peri insular BM that directly encapsulates the islet cell populations via intra islet vascularisation [70-72]. This BM possesses a similar structure to endothelial BM, containing collagens bound to LMs via HSPGs. The majority of literature has observed that the isoforms Lm 511 and Col IV are the primary constituents of the adult peri-insular BM matrix (Figure 1-3) [70, 71, 73]. However, other proteins and isoforms have also been identified such as fibronectin and the collagens I, III, V and VI [72, 74, 75].

The prevalence of different proteins may change during the development of the islet. They can also be influenced by the location within the pancreas and the type of endocrine cells contained within the islet [72]. Vitronectin (VN) is one such protein that has been observed in the foetal pancreatic BM but appears to become redundant during development. Supporting evidence has found VN to positively influence the motility and expression of integrins in progenitor β-cell cells when compared to adult β-cells [72, 76]. Variance exists between studies investigating the composition of BM proteins, particularly between the ratios of collagen isoforms [77, 78]. The complexity of the literature surrounding islet ECM is mirrored by the complexity of the islet itself. The endocrine system is multifunctional and so demands a multiplex of cells and supporting tissue architecture.

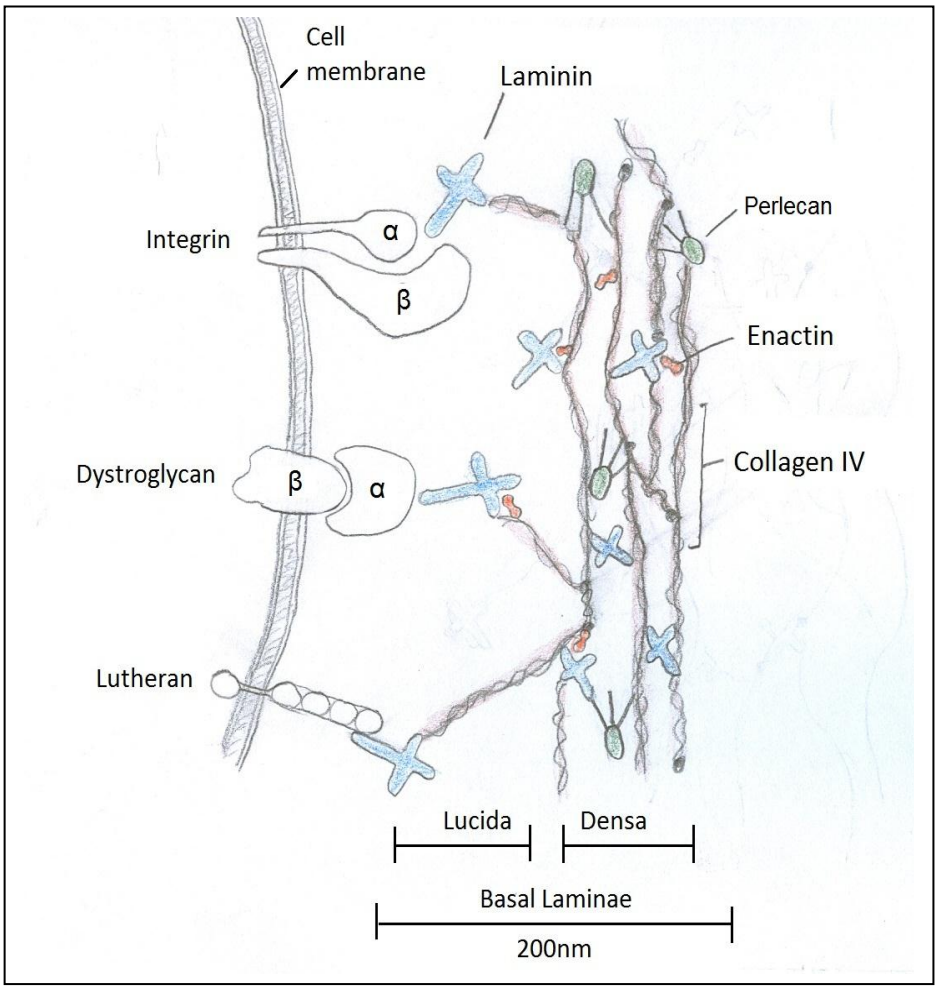

Figure 1-3: Diagram of peri-insular basement membrane

Diagram shows protein constituents of the lucida and densa layers which form the basal laminae. Collagen IV chains are linked by enactin, perlecan and laminin proteins. Laminins interact with cell membrane molecules; Integrins, dystroglycans and lutherans. Diagram magnified from Figure 1-2. Adapted from Kragl M, Lammert E. Basement membrane in pancreatic islet function. Adv Exp Med Biol. 2010;654:219, 222.

1.2.2.1 Collagen IV

Collagen IV (Col IV) is particularly plenteous in the endocrine BM [69]. Three combinations of Col IV are known to exist; these protomers are made up of three different α chains; α1 α1 α2, α3 α4 α5, and α5 α5 α6 of which all contain integrin binding motifs [69, 79]. The primary role of Col IV in the BM is to provide structural integrity to the adjacent cell population; however, it is known to possess a high affinity for integrins α1β1 and α1β2 [80]. It can be speculated that collagen binding motifs share a similar structure, as α1 β1 and α2 β1 integrin adhesion was completely inhibited by the peptides containing the GFOGER sequence [81]. Despite the similarity in motif sequence the evidence suggests that a subtle molecular difference can create a preferential affinity towards specific integrins [80].

Studies culturing islet-like clusters and adult β cells demonstrate Col IV -based integrin adhesion promotes high levels of insulin secretion [80, 82]. Over 18 hours of culture a significant depletion of intracellular insulin was also observed in β cells, this was not associated with a decrease in cellular viability [82]. The authors attribute this secretion to increased Ca^{2+} levels in response to the intracellular integrin adhesion process [82].

Improved motility was also observed on a collagen IV surface; a significantly higher number of adult and foetal β cells were observed to migrate into a matrix coated in collagen IV when compared to collagen I, fibronectin, vitronectin and laminin [80]. Foetal β cells were more mobile than adult β cells. This was not entirely due to a decreased expression of α1 β1, as up to 80% of the migrated adult β cell population still

expressed the integrin. Another intracellular mechanism repressing adhesion signals or cytoskeletal architecture may have been responsible for the diminished motility [80].

The literature investigating Col IV has found that it holds multiple functions in the endocrine BM; it has been implicated in insulin homeostasis, motility and adhesion. The massive insulin secretion observed from α1 β1 /collagen IV adhesion suggest that while it is involved in insulin homeostasis, it is also highly regulated in the islet BM environment to prevent inappropriate insulin secretion. This may be especially true in the developing islet as foetal β cells have a restricted expression of α1 β1 integrin [82]. However, the improved motility of foetal β cells when in contact with Col IV show it is important during islet neogenesis. Once the structure has developed the adult β cells migratory response is reduced to preserve the integrity of the mature islet architecture [80]. The effects of Col IV integrin adhesion seem almost detrimental to β cell function if taken out of the context of the BM. A combination of integrins adhered to a range of BM proteins must be highly regulated for appropriate β cell function.

1.2.2.2 Laminin

Laminin (Lm) is a trimeric glycoprotein reported to directly influence cell function. Disulphide bonds connect three chains to form a characteristic cross shape [63]. The α chain is linear and spans the length of the molecule, containing globular domains at the amine and carboxy termini (Figure 1-4) [83]. The β and γ chains are half the weight of the α chain and convolute together around it, branching out opposite each other approximately two thirds along the length of the α chain from the carboxy terminus (Figure 1-4) [83].

Up to 15 isoforms of Lm exist, formed from combinations of 5 α, 3 β and 3 γ chain variants [84, 85]. These chain variants possess different lengths of epidermal growth factor repeat, affecting the overall structure of laminin isoforms. Only specific chains can associate, which is why merely 15 Lm isoforms have been identified *in vivo* despite a wide selection of chain variants. Four structural morphologies have been identified; classical (Figure 1-4). Long, possessing an extended α chain at the amine termini. Topless, which has a reduced α chain at the amine termini and truncated, which has shortened α, β and γ chains at the amine termini [85].

The most significant feature of Lm is the abundance of adhesion sites. It binds to a variety of BM proteins such as Col IV, perlecan and enactin, known to be associated with the amino termini of all three chains. These sites also promote m polymerisation and maintain the overall integrity of the BM [67, 86, 87]. Lm also possesses binding motifs for cell adhesive molecules in the β cell. Specifically these include integrins, dystroglycans and Lutheran [88-90].

Binding motifs that adhere cell adhesion proteins have been investigated extensively, they have been located primarily at the carboxyl termini of the α chain and associate with regions of the globular domains as well as regions in the β/ γ intersection [65, 91]. Immunohistochemical staining from two different studies has found that Lm 511 is the primary isoform of Lm present in the adult human islet endocrine BM [70, 71]. Lm 111 and 411 have also been detected in smaller quantities in the foetal endocrine BM [70].

These isoforms function to improve β cell viability and to up-regulate insulin gene expression in insulinoma cell lines [92]. Min-6 cell populations cultured in a polyethylene glycol gel containing a selection of ECM constituents were stimulated with glucose; it was

observed that significantly higher levels of insulin were secreted after 10 days of culture in the laminin enriched gel than any other ECM protein [78].

More recently, adult β cell proliferation was analysed when cultured in the presence of specific isoforms of Lm, detected in the endocrine BM of adult and developing islets. It was observed that Lm isoform 511 promoted the highest proliferation in the adult β cell populations [93]. This Lm isoform has also been found to have an affinity for the β1 integrin subunit, which has been confirmed by an observed reduction in insulin secretion in the presence of anti β1 mouse antibody (mAb). This was supported by the function of siRNA which reduced β1-integrin mRNA and in turn surface expression by 60 to 80%. Application of these methods resulted in significantly reduced insulin gene expression [92].

Min-6 populations also demonstrate a significantly decreased insulin secretory response when cultured with anti α 6 mAb [92]. This study supports earlier findings that integrin α6 β1 is the primary cell adhesive molecule expressed in adult rat β cell populations. Cell populations cultured in α6 β1 antibodies showed reduced spreading, furthermore, there was a clear correlation between α6 β1 expression and insulin secretion [94].

Observations of the molecular architecture suggest that specific isoforms of Lm provide appropriate structural and molecular cues for endocrine cell populations. However, some complexity surrounds the adhesion molecules that promote the β-cell phenotype. Laminins are known to hold an affinity for lutheran [95], dystroglycan [88] and a selection of integrins; α1β1, α2β1, α3β1, α5β1, α6β1, α6β4, α7β1, α9β1, α6β4 are all known surface receptors of laminin [69, 78, 88, 94, 96-100].

Once adhered, intracellular mechanisms promote insulin secretion by up-regulating genes associated with the β cell phenotype. This is achieved directly through physical stimuli, the mechanisms of which are yet to be fully defined. However, observations have suggested that integrin initiated complexes promote cytoskeletal activity, which in turn could influence insulin granule locomotion and secretion [78, 101] .

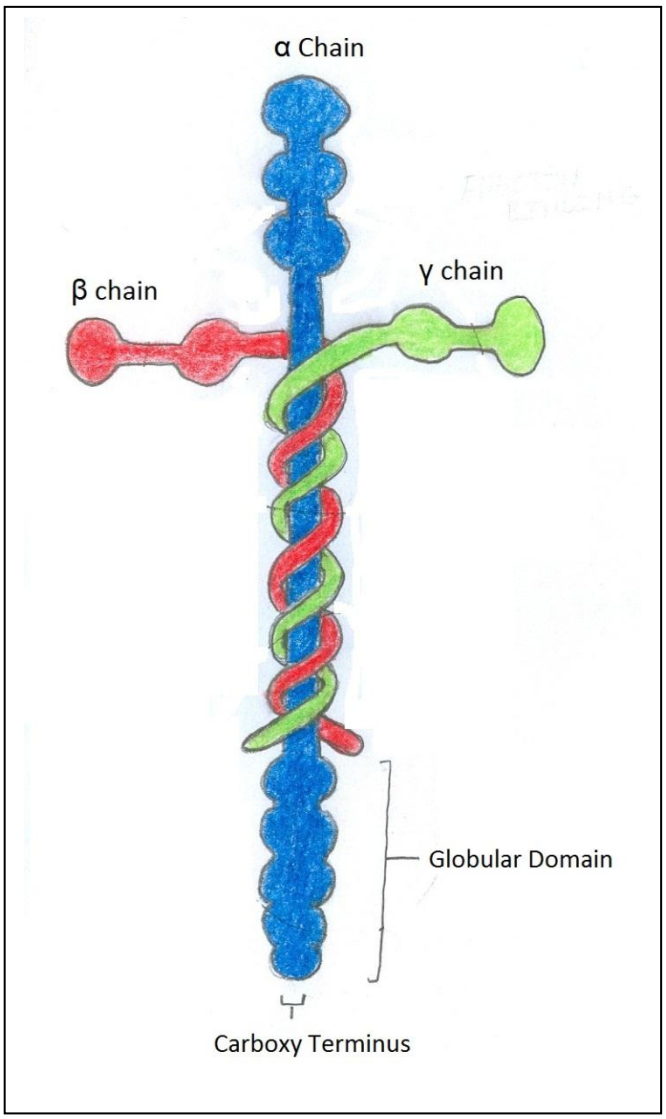

Figure 1-4: Diagram of Laminin

Diagram showing the α, β and γ chains that form the classical laminin structure. The bottom of the α chain ends with the carboxy terminus and consists of five globular domains, which hold several binding sites. Adapted from Colognato H, Yurchenco PD. Form and function: The laminin family of heterotrimers. Developmental Dynamics. 2000;218:213-34.

1.3 Factors influencing cell culture *in-vitro*

Multicellular organisms often rely on a transport system to provide cells with the molecules necessary to function. In mammals, the circulatory system ramifies nearly all tissue; this, combined with regulatory homeostatic systems, ensures a consistent supply of oxygen and nutrients. Glucose, amino acids, fatty acids and vitamins are all vital in order to sustain cell populations and functional tissue. Due to the nature of cell metabolism, the *in-vivo* environment also enforces an optimal physicochemical environment, regulating temperature, PH and CO_2 levels in the blood. At optimal conditions, mammalian blood is isotonic. Osmolality of the blood has a significant influence on the diffusion of inorganic ions through the cell membrane required for intracellular function.

In order to culture cells *in-vitro,* these factors must be considered and a similar environment must be supplied to the cell populations. Established 2D culture techniques have accounted for the primary requirements of the cell. The development of cell culture media can be traced back as far as 1880 with the work of Sydney Ringer who discovered that amphibious heart contractions were sustained with a solution containing inorganic ions [102]. The discovery was in part due to Ringers' lab assistant who used tap water in place of distilled water, perhaps to keep up with a demanding schedule [103]. At that time tap water supplied to the University College London contained various inorganic ions, including calcium, potassium and sodium. An improved saline solution was derived and tested, the basic constituents of which are still used today.

Ringer's contribution founded medicinal saline as well as the development of Eagle's media, the first standardised mammalian cell culture media [104]. Early attempts at long term cell culture used undefined isotonic salt solutions combined with various serums, plasma clots, tissue extracts and ultra filtrates [104, 105]. Harry Eagle was first to determine the minimum constituents required to sustain a human uterine carcinoma (HeLa) and a mouse fibroblast cell line. These included a collection of amino acids, vitamins, glucose, and serums [104].

These advances in cell culture technology have made nearly a century of cell culture possible. However, as discussed in section 1.1.6, 2D cell culture has several disadvantages which limits progress with current stem cell differentiation protocols. In order to mimic stem cell niches, novel 3D biomaterials are currently being investigated. The 3D element to these new culture systems presents new obstacles.

1.3.1 Nutrient and oxygen access

Mammalian cells require a specific physicochemical environment that is sterile, and at approximately 37°C. A cell population must also be submerged in culture media at a pH of 7.2 to 7.5. CO_2 concentration must be within physiological parameters at 2-5%, and the osmolality of the solution between 280 – 320 mOsmol/kg [106]. The use of incubators and cell culture media account for these factors, and overcome the initial risk of cell death by necrosis in response to inappropriate, external parameters.

Culturing cell populations becomes more complex when considering the nutritional requirements; these can vary massively between cell lines. A wide selection of culture

media exist supplemented with various energy sources, amino acids, vitamins, growth factors and proteins tailored to sustain different cell types [106].

The cell culture environment is also affected by time; cells can alter the physicochemical environment, as they proliferate vital constituents of the media are consumed, and metabolites from intracellular processes build up in the media to create a suboptimal environment. Media must also be appropriately replenished. However, if changed too often the cell population may not be able to modify and optimise the media to suit their specific physicochemical requirements [106].

In a 2D cell culture system with optimal physicochemical and nutritional requirements, oxygen and carbon dioxide can readily diffuse into the cells. The supply is constant due to the exchange with the atmosphere. However, the volume of media must be of a suitable volume for a cell culture flask or 2D container to allow gases to reach the cell monolayer. The solubility of oxygen in culture media is limited and oxygen gradients can occur with a linear relationship to the depth of media [40]. This gradient is increased with the presence of a cell monolayer. It has been estimated that at a depth of 2mm a cell monolayer containing 10^7 MCF7 breast cancer cells consume 4.5µmol of oxygen per hour, reducing the oxygen concentration to 10-50% of that at the surface [107].

The diffusion limit of oxygen is the primary consideration when designing a 3D biomaterial for cell culture. Oxygen gradients are depleted quickly by large cell populations. Studies investigating pathological angiogenesis of tumours, as well as histological observations of capillary ramification, have concluded that the diffusion limit of oxygen through tissue is approximately 200µm [108-110]. This can generate a

hypoxic environment which, in turn can have an effect on cell metabolism and gene expression.

The number and type of biomaterial commercially available and under investigation is extremely varied, so too is the level of control over the internal structure of these biomaterials. A common advantage between all 3D biomaterials is the ability to generate 3D cell clusters, or microtissues. To completely avoid the risk of hypoxia and hyponutrition, cell cluster size must not exceed 250µm in diameter [111, 112]. This can be prevented by modifying the macro structure of the biomaterial to suitable parameters.

Solid scaffolds normally have a partially defined, tortuous porous structure. Often, the internal structure is unable to directly regulate the size of microtissue structures; as a result the size of the whole scaffold must be restricted [113]. Alvetex® is a polystyrene based biomaterial possessing an internal structure of spherical voids of between 10-20 µm [111]. This material is designed for complete cell infiltration and growth via interconnecting pores. The overall design compensates for the limit of oxygen diffusion as discs are commercially available at a thickness of 200µm. If the scaffold is at total capacity, cell populations will never be more than 100µm from a supply of oxygen enriched media [111, 112].

Solid free-form fabrication (SFF) is a type of additive manufacture, describing construction of a 3D object by adding layers using a 3D printer that works off a digital design [114]. This manufacturing technique has enabled strict control over internal architecture of 3D biomaterials. The precision of SFF holds the potential to generate structures that guide and control the size of microtissues, overcoming existing hypoxic

limitations [109]. Attempts to actively generate a vasculature from a 3D scaffold *in–vivo* involved the use of degradable fibres on which endothelial cells proliferate to form a tube, or capillary like structure. After initial seeding, these scaffolds were implanted into mice; flow of blood was observed through the engineered capillary like structures after 2 weeks [115]. This indicates that while efforts to overcome hypoxia and hyponutrition in 3D culture are currently underway, a solution that mimics *in-vivo* vasculature is required before large tissue structures can be cultured *in-vitro.*

So far the immediate requirements of a cell population grown in 2D and potential obstacles in 3D have been discussed. However, in order to generate functional tissue structures in a 3D culture system, cell signalling molecules must also be influenced.

1.3.2 Cell adhesion

Integrins are one of the most significant adhesion molecules expressed by mammalian cells. These transmembrane glycoproteins are responsible for anchoring cells to the ECM. This interaction stimulates intramolecular signalling cascades that regulate gene expression and ultimately control cell movement, proliferation and differentiation [105]. The significance of integrin based adhesion cannot be overlooked when conditioning a biomaterial for cell culture. Polymer surfaces can be conditioned to mimic the ECM and exploit the cells' adhesive properties [116].

In vitro adhesion begins with the attachment of a cell in suspension to a binding motif on a biomaterial surface. This is mediated by integrins; extra cellular heterodimers consisting of two subunits [117]. The α and β subunits are both involved in ligand

binding and have large extracellular presence relative to the cytoplasmic tail. Divalent cations located on binding sites of the α subunit enable interaction and attachment to integrin ligands [118, 119]. Currently, 18 α and 8 β subunits have been identified, the presence of which in the membrane varies between cell type. The integrin binding sites themselves also vary in specificity [120].

Interestingly, there is a 30% and 45% similarity between α and β subunits, respectively, with the primary divergence in the cytoplasmic tail [119, 121]. This indicates that the integrin family are able to initiate a vast number of molecular cascades. Integrin binding is the primary mechanism that initially anchors cells to the surface of a biomaterial, providing mild resistance against shear forces [121]. Cell adhesion by integrin subunits triggers a series of molecular responses, initiating the formation of actin filaments that act as stress fibres. These converge together to form focal adhesions. As the cellular membrane flattens along the substrate more, focal adhesions are generated and can also be degraded enabling migration [121-123]. The intracellular mechanisms that anchor the cell cytoskeleton to the integrin subunits involve a vast number of proteins. Figure 1-5 shows both cytoskeletal and regulatory proteins that function to generate focal adhesions as well as pathways that affect cell survival. After initial integrin binding, primary cytoskeletal proteins form links between actin filaments and integrins. This is initiated by talin, which binds to the β chain and functions to crosslink actin filaments while also interacting with vinculin, paxcillin and focal-adhesion kinase (FAK) (Figure 1-5) [124, 125]. Talin and α-actinin promote the migration and adhesion of multiple integrin molecules.

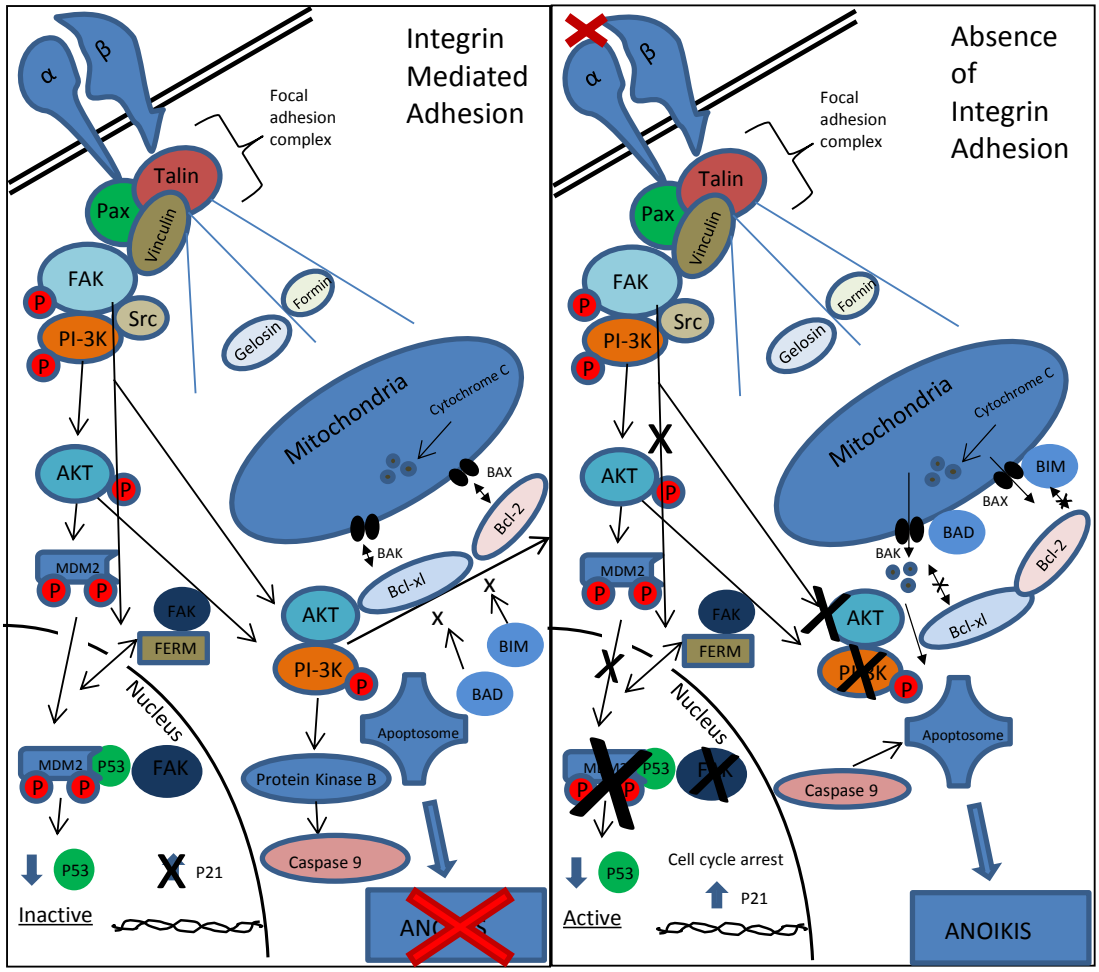

Figure 1-5: Intracellular mechanisms of adhesion

Diagram showing cytoskeletal and regulatory proteins involved in the generation of focal adhesion complexes and their effect on cell survival; Diagram (left) depicts normal integrin mediated adhesion and the pathways promoting cell proliferation and inhibition of apoptosis, diagram (Right) depicts absence of intergrin adhesion and lack of factors promoting cell proliferation and inhibiting apoptosis. Integrin adhesion initiates the formation of the focal adhesion complex mediated by formin and gelosin, this results in Akt and PI-3K sequestering Bad and Bim which function to initiate apoptosis via Bak and Bax apoptosome formation. Akt activation also mediates the suppression of P53 via Mdm2 and FAK. Without integrin adhesion apoptosis is mediated via Bad and Bim, and the P53 pathway is not suppressed.

These engage formin and gelosin which function to construct actin filaments and cap and sever individual actin molecules, respectively [105, 123, 126]. During this process vinculin modulates the site at which talin and actin are connected. Absence in this connection results in reduced adhesion and increased migration in ESCs [123, 127].

A lack of integrin-mediated cell adhesion results in apoptosis among several cell lines [128]. Paxillin (Pax) is a regulatory protein associated directly to the α4 integrin chain, talin and vinculin, Pax recruits cytoplasmic signalling factors such as FAK (Figure 1-5) [7, 124]. After FAK interacts with pax, tyrosine phosphorylation occurs, opening the binding site Tyr397 for PI-3K and src this in turn activates several cascades [123, 129-131]. Briefly, PI-3K signals a cascade via Akt which activates Mdm2 an ubiquitin E3-ligase; this in turn enters the nucleus and inactivates p53 via ubiquitination [128, 132]. FAK is also directly involved in promoting cell survival and is translocated into the nucleus via FERM and acts to enhance p53 ubiquitination, leading to p53 degradation [133]. The absence of active p53 prevents activation of p21 which arrests the cell cycle, therefore promoting cell survival and proliferation [133].

The integrin adhesion platform generates other cascades which directly prevent apoptosis. FAK indirectly prevents apoptosis by increasing the production of Akt and protein kinase B; a molecule downstream of PI-3K [134]. These factors directly function to inhibit caspase-9, phosphorylate the apoptosis-inducing protein Bad as well as up regulating NF-κB, respectively [135-137]. A combination of different integrin adhesion complexes are required to sustain cell survival via a large number of cascades; these may vary between cell lines and are affected by the surrounding biomaterial surface [124, 138].

In the absence of any integrin-based adhesion all the mechanisms (Figure 1-5) are suppressed. The pro-apoptotic proteins Bad and caspase 9 function to suppress the action of Bcl-2, unleashing other pro-apoptotic proteins onto the outer mitochondrial membrane (OMM). This forms the apoptosome molecule which initiates the apoptotic process [139-141]. Without any external stimuli, focal adhesion complexes are not generated, decreasing the number of pro- survival molecules such as FAK, PI-3K and Akt. FAK is unable to suppress the activation of p53, initiate the signal cascade to Akt or the mdm2 ubiquitin E3-ligase [136]. PI-3K sequesters BIM and BAD by phosphorylation, in its absence these factors translocate to the OMM and invalidate the effect of anti-apoptotic protein Bcl-xl, which induces OMM permeabilization via bax and bak oligomers [128, 142]. If apoptosis is triggered, this leads to the release of cytochrome c from the inner membrane of the mitochondria and the activation of apoptosomes, along with caspase-9 activation the machinery responsible for apoptosis becomes operational [105].

Overall the absence of cellular adhesion severely sensitises the cell to apoptosis [128]. This can pose a significant problem if cells are under stress while being seeded onto a biomaterial. Before progress can be made in developing a biomaterial, integrin mediated adhesion is the foremost priority for cellular survival. Progression from simple plastics to complex cell culture systems is intertwined in the history of cell culture.

1.3.3 Influencing cell adhesion on biomaterials

For nearly a century, research has pursued methods to stimulate *in-vitro* cell adhesion in order to overcome programmed cell death, in response to deficient integrin binding.

After the discovery of a compatible cell culture media, anoikis became the most limiting factor of 2D cell culture. Cell adhesion is a complex phenomenon which must be well understood in order to appropriately condition biomaterials.

1.3.3.1 The history of biomaterial surface chemistry

In 1923, Alexis Carrel created the first tissue flask; canted neck D flasks were made from heat resistant glass known as PYREX®[143]. During this early period of tissue culture, Carrel endeavoured to improve the efficiency of his aseptic technique. D flasks could withstand the high temperatures of a Bunsen flame during sterilisation, making it easier to add culture media without the risk of bacterial infection. It also provided a non-cytotoxic environment [143].

However, these early flasks were not optimal for cellular adhesion; between 1960 and 1975 polystyrene flasks became extremely popular. Untreated polystyrene is unsuitable for cellular adhesion and growth and so various chemical and physical industrial processes were used to improve adhesion [144-146]. One of the main processes employed was glow discharge treatment, which was successful enough to warrant a patent and led to the modern tissue culture flasks used today [146].

Radio frequency glow discharge (rfGD) describes a method in which gas at a low pressure can be ionized by radio frequency typically between two electrodes to generate plasma. The term plasma refers to the state of a highly excited gas consisting of atoms, molecules, ions and free radicals [147]. In this state, gas contributes to the modification of the most inert surface chemistries and can be tailored to generate a

range of charges and species. RfGD was used to generate oxygen moieties on the polymer surfaces of cell culture flasks [146].

Studies during this time speculated that the treatment was responsible for increasing the negative charge on the surface of the polystyrene which improved its wettability. This in turn was thought to improve cellular adhesion [145, 146]. It is important to note that cells possess a net negative charge. This is common to the micro filamentous filopodia of cells which function to flatten and increase the strength of the cells adherence [144]. During contact with a substratum, any positively charged groups present on the surface of a biomaterial was thought to induce an electrostatic force between the cell itself and the surface. While this is not true adhesion, observations of this phenomenon in early cell studies gave rise to the theory of "passive adhesion". This was no doubt the cause of the divided opinion between the roles of protein in cell adhesion [148, 149].

The nature of cell adhesion to polystyrene was rigorously investigated in studies undertaken during the 1980's. The concept of wettability and whether cells required protein to adhere to plasma treated substratum was largely undecided [150].

Curtis *et al* (1983) used X-ray photoelectron spectroscopy to show that hydroxyl and carboxyl groups were of high density on the surface of tissue culture plates. In order to prove which group is responsible for cellular adhesion, the crystal violet method was used to block specific anionic groups. These studies indicated that hydroxyl groups yielded the highest number of adhered cells [150]. Furthermore, BHK cells were cultured on a variety of treated surfaces with serum free media and treated with cycloheximide to prevent protein synthesis. Despite this, adhesion was observed on bacteriological and

tissue culture grade polystyrene, with 7,880 and 22,159 cells adhering per cm^2 respectively [150].

These data supports the theory that hydroxylation of polymer surfaces by plasma treatment causes direct cellular attachment. This was at variance with one of the most widely referenced cell adhesion studies, which supports the significant role of absorbed proteins to cell interaction, adhesion and spreading on the substratum surface [144]. Several explanations for the binding and spreading of the BHK cells in a serum-free environment were suggested, the most likely explanation was that the cells secreted proteinaceous micro exudate such as fibronectin that was endogenously stored during cycloheximide treatment [151].

With the discovery of the Arg – Gly – Asp – Ser (RGDS) tetra-peptide sequence, and its corresponding integrin binding site on fibroblasts, it was observed that cells were unable to bind to a substrate after being cultured with the RGDS peptide sequence [152-154]. This was due to the peptide-blocking integrin-binding sites vital for cellular adhesion. This provided significant evidence that contributed to the paradigm shift into the theory of peptide-based cell adhesion. Despite these findings, the optimal surface chemistry required for protein absorbance was unknown, with several studies observing poor cell adhesion on highly charged biomaterials [155, 156].

1.3.3.2 Protein absorbance

Proteins often possess a negative charge. This charge affects the structure proteins in a solution or adhered to a material. In a polar solution, proteins are folded in such a way

as to protect the non-polar or hydrophobic amino acid chains. *In-vivo* this structure provides a function which can be utilised by cells [157].

The interaction of proteins in solution with a polymer surface is complex. Literature spanning back one hundred years has been caught between two paradigms, one supporting the 2D water polymer interface, with a simplistic view of irreversible protein absorption[158]. The other, incorporates a third dimension allowing for the reversal of absorbed molecules as well as several layers of solutes from the polymer surface [159]. These are known as the Langmuirian and Gibbsian paradigms, respectively (For a detailed review see [158]).

A hydrophilic, polar surface is highly wettable and interacts with polar substances. A hydrophobic surface is often non-polar of low wettability, repelling polar substances like water [158, 160]. The physics of water self-association, interfacial tension and miscibility, in response to surfaces, cannot be so easily grouped into these out-dated terms, but are suitable to describe simplistic models of protein absorption [158].

A useful tool for measuring wettability, and therefore surface chemistry, is water contact angle (CA). Briefly, this method involves placing a drop of water onto a polymer surface and measuring the angle of the drop surface interface (Figure 1-6). It is a widely used method in biomaterial research, despite variation in opinion regarding the ranges associated with either hydrophobicity/hydrophilicity. Current opinion identifies a surface CA of > 65° to be hydrophobic and < 65° to be hydrophilic [158] and that 0 - 90° is wettable and 90 - 180° is non wettable [160].

Figure 1-6: Scaffold wettability

Diagram to show contact angle (CA) of water droplet on different surfaces, left image shows hydrophobic surface with a high contact angle, right image shows hydrophilic surface with a low contact angle.

Lee *et al* (1993) worked with a range of organic polymers and plasma treatments exploring their effect on cell adherence. Initial work focused on three polymer films made of polypropylene (PP), polystyrene (PS) and polyethylene (PE). A rfGD plasma chamber was used to plasma treat the samples. A motorised mask was incorporated into the chamber; as the mask was moved it gradually exposed the sample. This generated a plasma treatment time gradient, removing the necessity of multiple samples and potential variation while increasing sample exposure time to the plasma environment. With increasing exposure time there was a decreasing CA, indicating more oxygen moieties formed and gave the material a more hydrophilic surface [161].

Each sample produced a different contact angle with PS, PE and PP giving a CA of approximately 25°, 65° and 70°, respectively, after 8 seconds. Interestingly, these CAs are at variance with the percentage of atomic oxygen calculated by electron spectroscopy for chemical analysis (ESCA). Percentage atomic oxygen was 18, 16 and 10% in PE, PS, and PP samples after 8 seconds, respectively [161]. It was observed that although PS had the highest CA, it did not have the highest percentage atomic oxygen, suggesting that certain species of oxygen moiety may contribute to contact angle more

than others. A later study using low density PE films and corona discharge treatment included cell adhesion trials [162]. PE samples were plasma treated using knife shaped electrode connected to an RF source, as the samples were moved the RF was increased generating a wettability gradient resulting in a CA range between 100 and 40° (Figure 1-7) [162].

Lee *et al* (1993) was the first to identify that a CA of approximately 55° is optimal for cell adhesion, as shown in Figure 1-7 [162]. Higher CA results in a rapidly decreasing percentage cell adhesion. However, cell adhesion decreases slowly and consistently as the CA decreases [162]. Protein absorption was also studied on the PE samples. Human albumin is well characterised and has a known nitrogen content of 14-15% [162]. ESCA was used to find the albumin absorption by detection of the nitrogen content on the PE surface; Figure 1-8 shows that nitrogen % increases with decreasing CA. This is most likely due to the external hydrophobic regions of albumin adhering with the increasingly hydrophobic surface [162].

If the surface chemistry of the polymer is hydrophobic, then the interaction of water can be described as weak. This means that at the water/surface interface, proteins are able to unfold unimpeded by a strongly bound layer of water and bind to the hydrophobic surface via a range of different bonds [157, 163]. Ionic bonds between the hydrophobic side chains within proteins on hydrophobic surfaces can result in the deconformation or unfolding of proteins that are irreversibly bound unable to support cellular adhesion [164]. This chemical phenomenon explains why cell adhesion is so low on non wettable, hydrophobic surfaces.

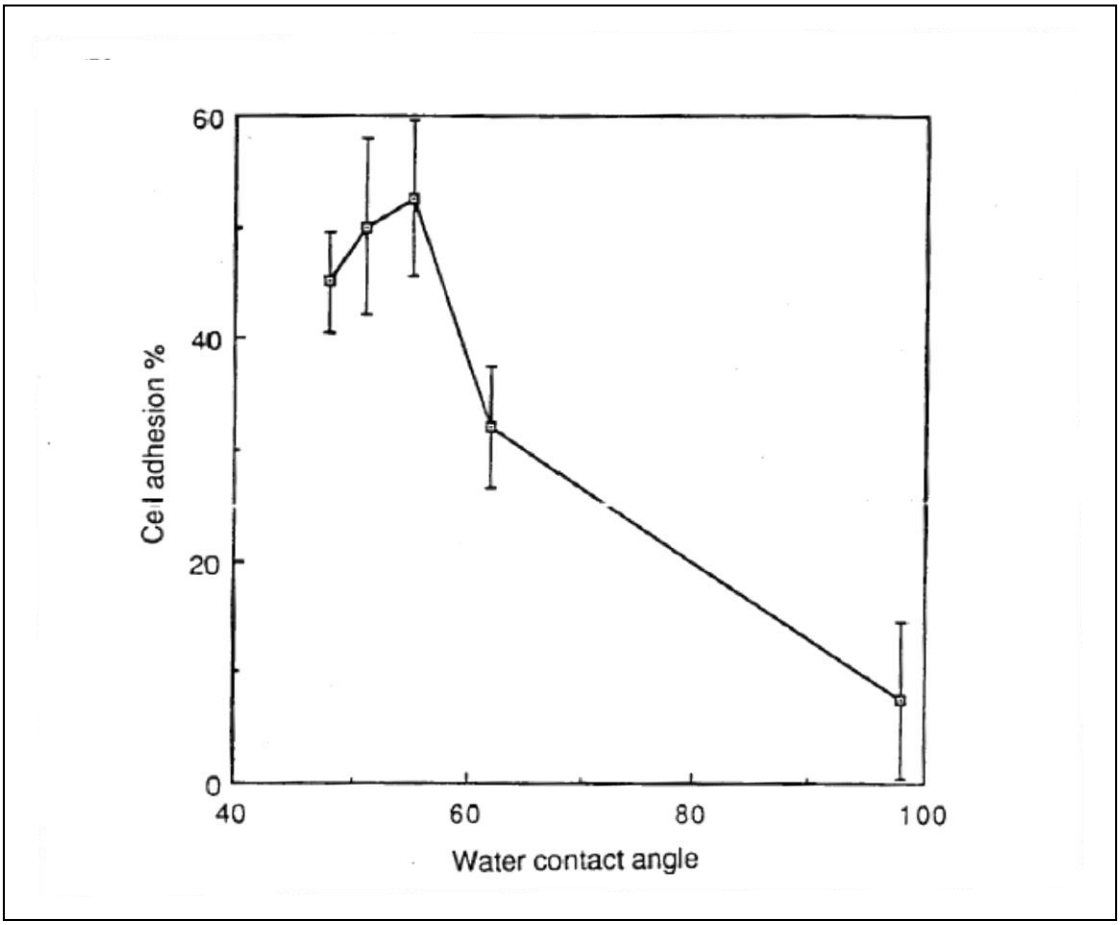

Figure 1-7: Cell adhesion and water contact angle

CHO cell adhesion seeded at 4 × 10^4/cm^2 on corona-treated PE surfaces of increasing contact angle for 2 hours. Number of cells adhered peaks at 55° before decreasing rapidly with increasing contact angle. n=3. Reproduced from Lee JH, Lee HB. A wettability gradient as a tool to study protein adsorption and cell adhesion on polymer surfaces. J Biomater Sci Polym Ed 1993;4(5):467-481.

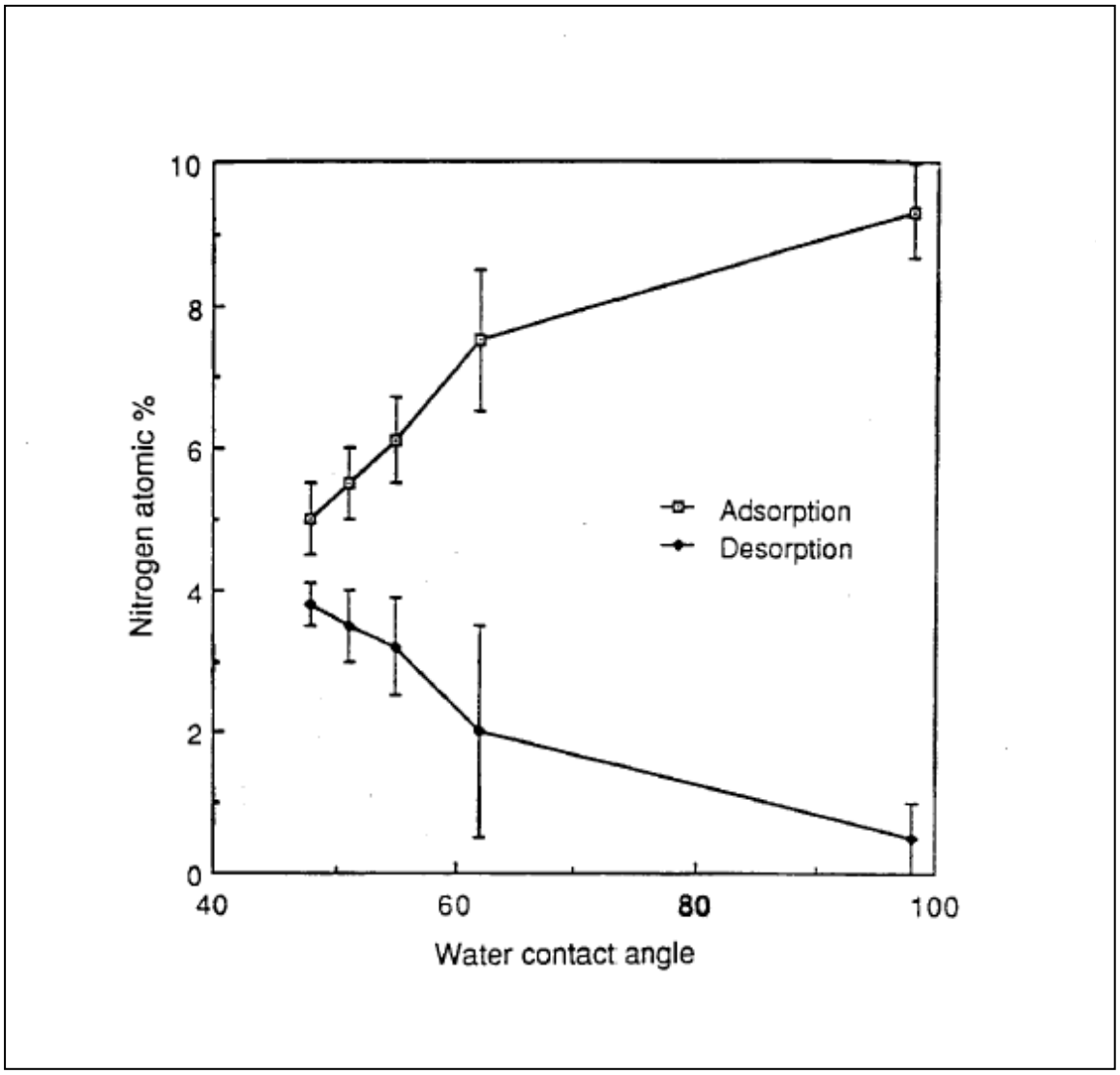

Figure 1-8: Percentage atomic nitrogen and water contact angle

Nitrogen atomic (%) after adsorption and desorption of 1mg/ml albumin solution for 1 hour and 30 minutes respectively on corona-treated PE surface. Desorption achieved with 1mg/ml Tetronic 1504 solution. The (%) of nitrogen adsorbed increases with increasing water contact angle.Reproduced from Lee JH, Lee HB. A wettability gradient as a tool to study protein adsorption and cell adhesion on polymer surfaces. J Biomater Sci Polym Ed 1993;4(5):467-481.

A strongly hydrophilic polymer, however, may create a strong enough force on the surrounding water that the interface is impenetrable to the proteins. This phenomenon is known as solvation and accounts for the decrease in cell adhesion observed at CA's lower than 55° [165]. Several studies have observed these phenomenons in the past without understanding the nature of the chemistry involved. Jin Ho Lee's studies provide an excellent proof of principle, as well as identifying intermediate surface chemistries between these extreme states that are optimal for protein adsorption [161, 162, 166-169].

1.3.4 Topography and cell growth

Topography describes the features present on an area of substrate and is an important factor when considering cell adhesion and growth. A range of topography scales, from micro to nano scale, can impact a wide range of cell responses on biomaterial surfaces. Cell adhesion, proliferation, morphology, orientation and differentiation have all been investigated. Surface topographies can be generated synthetically to guide cells into a specific pattern or structure. Alternatively surface topography can be caused from the processes generating materials, surface abrasion during manipulation or coalescence. Even the smoothest surfaces are at the macroscopic scale are often mountainous at the microscopic level [170].

Detailed work utilising well characterised, controllable, unalloyed titanium investigated MGS63 osteoblast adhesion and proliferation relative to micro and nano scale topographies [171]. 15mm diameter discs were engineered with hemispherical cavities of which the diameters were 10, 30 and 100 μm [171]. These cavities were then treated

to possess a range of topographies. The control surface was electrochemically polished generating an extremely smooth surface relative to the other treatments. Chemical etching and porous anodization are common techniques used to increase rugosity of surfaces and were used to generate extremely rough and porous nano scale topography, respectively [171]. Sand blasted large grit acid etching is another common technique adopted to generate micro scale topography, involving blasting surfaces with coarse grit between 250-500µm [172]. Each surface treatment was applied to the different microscale cavitied surfaces and cell responses observed by immunofluorescence labelling and Scanning electron microscopy (SEM) imaging [171].

The primary findings were that osteoblasts appeared not to interact with the hemispherical cavities of below 10µm (Figure 1-9). Larger scale hemispheres were infiltrated and in the 30µm cavities even encouraged 3D growth. This infiltrative behaviour has also been observed in macrophages and silica pits 10µm diameter and 6µm deep [170]. The larger hemispheres were infiltrated by several osteoblasts, which spread around the perimeter (Figure 1-9). These findings are at variance with previous studies which have found that groove widths as low as 1 - 5µm affected the orientation of rat dermal fibroblasts [173]. These cells were also observed to partially infiltrate or protrude into the 5 and 10 µm wide grooves only. However studies have observed that rat osteoblasts orientate in a similar way in 42µm wide grooves, regardless of depth. These findings suggest cell interaction is due to the width of topographical structures compounded by cell size [170, 174].

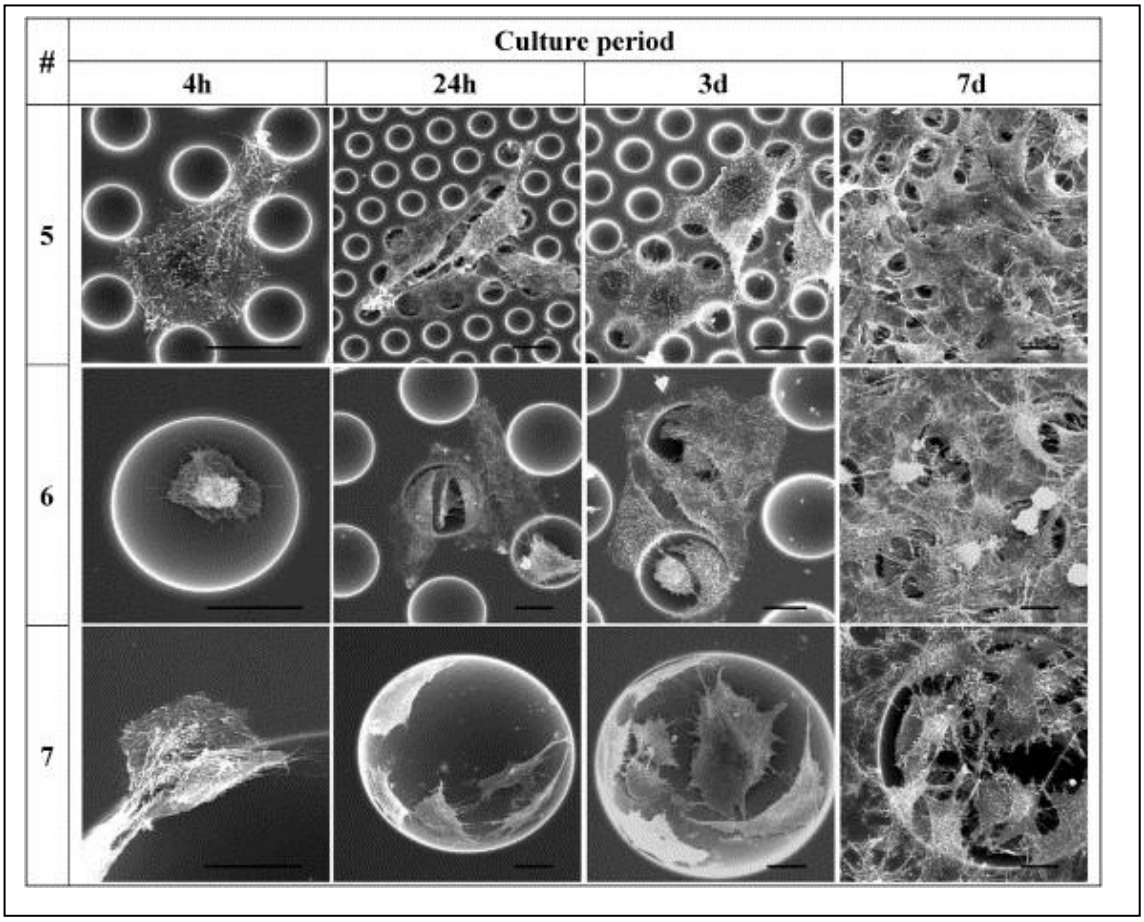

Figure 1-9: MG63 cells and micro-topography

SEM pictures of MG63 cells cultured on 10/1 smooth (5), on 30/1 smooth (6), and on 100/1 smooth (7) surfaces, after 4h (4h), 24 (24h), 3 days (3d) and (7d). Scale bar = 15µm [171]. Reproduced from Zinger O, Anselme K, Denzer A, Habersetzer P, Wieland M, Jeanfils J, et al. Time-dependent morphology and adhesion of osteoblastic cells on titanium model surfaces featuring scale-resolved topography. Biomaterials. 2004;25:2695-711.

However, earlier literature has repeatedly shown that cells respond primarily to depth rather than width. Groove cliffs between 1 - 25µm were shown to promote orientation [170]. The effect seen with osteoblasts bridging 10µm hemispheres has also been observed before in studies where cells covering channels of approximately 50nm. However, it is argued this effect was due to the immediate presence of the channel cliff edge opposed to the channel depth [175]. While these studies have highlighted very in-depth factors affecting cell response to micro scale topographies, differences in cell types may offer an explanation to the vast number of disparities observed. Nano scale topography is another area that has been heavily investigated and one which can significantly alter cell response to biomaterials.

1.3.4.1 Surface roughness

Groups conducting the earliest studies patterning surfaces with proteins to guide cell growth were forced to question whether the chemistry of the protein itself generates a response. Or, if the physical presence of the protein generates topography responsible for cell growth [170]. Favour for the first viewpoint was found in a study that raised the topographical profile of a protein pattern by molecular distances, the elicited cell growth was widely agreed to be due to chemistry alone [176]. This work should not suggest that even very small scale topography cannot alter cell growth. Macrophages have been observed to respond to topographies as low as 44nm [177]. Micro to nano scale topography, which is smaller than cells and follows no pattern on a surface, can be referred to as roughness. This type of topography is a natural feature on almost all material surfaces.

Investigation of roughness on cell behaviour has been performed on a vast number of materials and between several cell lines. The majority of literature surrounds the responses of osteoblasts. There are several studies supporting that, in general, with increasing surface roughness, osteoblast proliferation increases and differentiation decreases [178-181]

A study investigating different sized hemispheres on MG63 response did not support this generalisation. There was no significant difference between cell densities on smooth electro polished 2D titanium surfaces compared to anodised porous surfaces. However, the combined micro and nano topography of the hemispheres and anodising treatment was shown to increase osteoblast proliferation [171]. Furthermore the levels of Alkaline phosphatase (AlP) (Often used as a differentiation marker) was analysed and indicated no significant change in response to the surfaces tested. Despite this, osteoblasts showed a clear increase in focal contacts and appeared thicker under SEM analysis on the rougher surface treatments [171]. This study investigated the proliferation, adhesion and morphology of cells encountering a range of surfaces possessing micro scale topography and nanoscale roughness. It highlights the complexity of the cell response even in well characterised cell lines.

In order to gain a wider view of cell response to surface roughness, a range of cell lines must be considered. Work comparing the effect of roughness to osteoblasts and fibroblasts explored three main cellular responses, morphology, adhesion, proliferation and production of fibronectin [182]. The cells were cultured on two types of nickel titanium (NiTi) alloy, the rough surface containing grooves, the smooth surface generated as a result of mechanical polishing. These surfaces were shown to be

considerably different under SEM analysis [182]. It was observed that after two hours of incubation the initial rate of adhesion between the two cell lines was different, with osteoblasts adhering more readily than the fibroblasts to the rough NiTi surface [182]. Osteoblasts proliferated faster on the rough surface than fibroblasts, which were observed to generate less fibronectin on rougher surfaces and showed reduced proliferation over 7 days. This study suggests roughness is more beneficial for osteoblasts than other cell lines perhaps due to the nature of the *in-vivo* environment expected by their lineage [182].

This study contradicts with another groups finding. HUVEC endothelial cells were seeded on polyurethane surfaces modified with two different lengths of polyethylene glycan (PEG) and the short chain peptide GRGD. The nano scale roughness increased with the addition of PEG, PEG combinations, and PEG combinations conjugated with GRGD, respectively [183]. The difference in PEG heights generated a 16nm increase in surface roughness. This study found that cell growth rate was significantly improved after 36 hours on the PEG combinations conjugated with GRGD. This indicates that subtle differences in the nano topography may improve the growth of endothelial cell lines. Unfortunately, the lack of roughness quantification in the studies discussed earlier prevents direct comparison [183]. The relationship between cells and surface roughness is complex, and cannot be considered independently from the cell line and surface chemistry of the material [184].

A wide range of responses have been observed between cell types, thus suggesting that the genetic lineage of a cell has an influence on its response to the surrounding environment. Roughness is one of the three major factors contributing to the

biocompatibility of a biomaterial and must be considered during modification and conditioning of a biomaterial [184].

1.4 Tailoring the *in-vitro* environment for beta cell populations

The differentiation and expansion of β-cell populations *in-vitro* depends upon more than the basic supplementation provided by cell culture media and 2D culture systems. In order to progress and build upon existing work, a critical analysis of the literature surrounding β-cell interaction with their in-*vivo* environment was required.

The nanoscale structure of the pancreatic islet has already been explored (Section 1.1.1). In order to apply this knowledge to an *in-vitro* environment, this section will explore the range of adhesion molecules that are expressed in β-cell populations, the intracellular signalling pathways they stimulate and the regions on BM proteins to which they adhere. In combination this evidence can be applied toward accurately mimicking the BM of the islet.

1.4.1 Importance of the islet-matrix interaction

The peri-insular basement membrane is known to maintain β-cell populations via interactions with specific proteins. Literature has found both isolated natural ECM and synthetically mimicked BM can influence the proliferation [185], insulin secretion [78, 186-189], and in all cases survival of β-cell populations.

The peri-insular BM may also play an important role during pancreatic embryogenesis. Various developmental studies have incorporated BM proteins such as fibronectin, collagen IV [190, 191], and Laminin [191, 192]. The presence of these molecules in culture can influence the expression of insulin within foetal endocrine cells. 3D biomaterials augmented with BM proteins have also been successful in harbouring, expanding and promoting differentiation in endocrine progenitor cells [193].

The peri-insular BM cannot be overlooked when culturing β-cell populations *in-vitro.* Although it is partially mimicked through serum in culture media, it lacks the complexity and specificity of the natural BM. The cell population responsible for the production of the BM during pancreatic genesis is of relevance to the conditioning of a suitable islet cell expansion system. If β-cell populations are capable of synthesising and secreting their own ECM proteins, this could be exploited to improve a 3D culture environment.

1.4.1.1 Peri-insular basement membrane genesis

Detailed studies investigating the endocrine environment have found that the BM is generated by vascular endothelial cells. Immunocytochemistry was used to stain laminin and collagen IV in mouse pancreatic tissue, the fluorescence observed was concentrated in the peri-insular BM. This was limited to the periphery of capillaries in endocrine tissue, but not the intercellular voids of the islet mass [92]. Earlier work supports these findings, using immunocytochemistry and electron microscopy it was observed that there is a complete absence of ECM proteins between islet cells. Vitronectin, fibronectin, nidogen and collagen isoforms were not found to support the intra islet in

mouse, pig, dog, rat and man [73, 75, 194] These studies suggest that the functional and architectural integrity of the intra islet are directly maintained through cell to cell adhesion and soluble growth factors alone [73]. They also indicate that the pancreatic islet is structurally optimised for the passage of hormones through the intercellular environment to the blood.

Further work incorporating Cre recombinase under a Pdx-1 promoter in mice was successful in preventing the up-regulation of VEGF within endocrine cell populations [195]; as a result no endothelial cell growth was observed in islets of the mutant mice compared to heterozygous controls [196]. To confirm these findings immunocytochemistry targeting laminin and collagen IV was incorporated. A distinct absence of intra islet BM was imaged in the mutant mice. The cell adhesion molecule PECAM1 indicated a lack of endothelial cell populations in the smaller mutant islets [196].

The absence of BM with the loss of endothelial cells combined with the observation that islet cells do not synthesise BM proteins during different stages of embryogenesis [197], provides strong evidence that islet populations and more specifically β-cells cannot generate their own BM [92]. This poses a unique challenge to tissue engineers trying to grow β-cell populations *in-vitro.* Often, cells synthesise and secret their own ECM constituents, effectively supporting themselves once seeded into porous biomaterials [198]. A biomaterial harbouring a functional β-cell population must compensate for the endocrine environment completely, in order to protect and induce the expression of the valuable β cell phenotype.

1.4.2 The Min-6 cell line

Due to the expense, rarity and poor proliferative rate of primary islet cells, genetically modified cell lines are often used as analogues in their place for *in-vitro* studies [199]. These cell lines offer a cheap and expendable option to research groups investigating the cellular response to experimental environments where there is a high risk of cell death.

Early studies used cell lines isolated from a rat insulinoma and transformed using the simian virus 40 (SV40), respectively [200, 201] .These cell lines were limited as they did not produce insulin or respond to glucose as efficiently as β cells. In 1990 the mouse insulinoma (Min-6) cell line was established. Transgenic mice were created by microinjecting a human insulin promoter gene connected to the SV40 T antigen gene into the pronuclei of mouse eggs. Once grown, the founding mice developed pancreatic tumours at 13 weeks from which the novel cell line was harvested [199]. The Min-6 cell line is immortalised and retains the β-cell phenotype, responding more appropriately to increases in extracellular glucose compared to previous model β cells providing a more precise β cell analogue.

Several studies have utilised the Min-6 cell line to investigate cell adhesion, gene expression and proliferation in a wide range of culture environments. Disadvantages are inherent in all transformed cell lines, including the Min-6. However, the difference in their proliferative capabilities compared to primary β-cell populations makes them ideal for the investigation of experimental culture environments.

1.4.3 β cell adhesion molecules

β-cells interact with their surrounding environment through several different adhesion molecules, as mentioned the BM plays a key role in influencing the β-cell morphogenetic processes via three main glycoproteins; integrins, lutherans and dystroglycans [69, 70].

1.4.3.1 Integrins

Integrins are membrane bound adhesion molecules formed of two subunits named α and β chains (Section 1.1.1). These chains combine non-covalently to form up to 24 integrin receptors, possessing binding sites specific to regions within BM proteins [202]. Integrin expression in β-cells is a subject of much disputation, compounded by islet age and variation between species. However, the majority of recent literature agrees on a significant expression of 6 primary chains α3, α5 and αv in combination with β1, β3 or β5 by human adult islets [71, 72, 76, 80, 99, 203]. In β-cells these subunits have been collectively observed in combination as α1β1, α3β1, α5β1, α6β1, αvβ1, αvβ3 and αvβ5 [78, 80, 94, 98-100].

In a study comparing mature and progenitor β-cells, integrin αvβ5 mediated adhesion in both cell types, αvβ1 promoted spreading and movement in foetal β-cells, but was not present in significant quantities to promote the same effect in mature β-cells [100]. Separate studies have also found that integrin α3β1 promotes adhesion in adult β-cell populations [93, 100].

There appears to be variance between the integrin expression of mature and progenitor β-cells during islet development. αvβ3 and αvβ5 integrins are highly expressed in the foetal islet cells, aiding differentiation of the ductal epithelium into the early pancreas [76]. This combined with evidence that α1β1 improves foetal β-cell motility suggests that integrin adhesion is labile, and changes during development in order to generate an appropriate islet architecture [72, 76, 80].

There are differences in the integrins expressed by β-cells of different species. Murine β-cells show clear differences in integrin expression to human β-cells, rat and mouse cells were found to express α6 and β4 subunits, respectively, which are not regularly expressed in human β-cells [73, 94]. Integrin expression even varies between species of the same subfamily, variation between rat and mouse β-cells has caused a deal of discrepancy between integrin investigations [73, 94]. The differences suggested by these studies are supported by the observation that unlike humans the mouse pancreas does not possess a BM duplex. The BM in contact with the endocrine cells is similar to that of the endothelial BM containing laminin 411 and 421 [70]. This in turn has an influence on the type of integrins expressed, as the extracellular environment will affect the affinity of the integrin up-regulated.

β-cells are known to be in influenced by outside-in signalling, the type, combination and clustering of integrins adhered can influence the intracellular function of a cell and its genetic phenotype [204]. Evidence supporting this has been observed in the min-6 cell line. Populations cultured in media containing soluble laminin 111 required a specific concentration of laminin (30μg/ml) before insulin gene expression was observed [92],

indicating a specific number of integrin interactions were required to initiate a focal adhesions which promote the appropriate signalling cascades.

Literature directly linking β-cell integrins to BM proteins is limited. However, it can be speculated that the number and type of integrin promoting survival, proliferation and insulin expression in cell culture trials (Covered in sections 1.2.2.1 and 1.2.2.2) are similar to those expressed in functioning human β-cells. The BM proteins found most abundantly in the peri insular matrix such as Lm 511 are responsible for promoting specific integrin up-regulation via outside –in signalling [70].

1.4.3.2 Dystroglycan

Dystroglycan (DG) consists of two subunits, the transmembrane β-subunit and a glycosylated α chain which shows specificity towards several BM proteins including laminin 111 and 211 [205]. As a complex these subunits are involved in linking intracellular actin filaments to glycoproteins within the BM [206]. In mice DG has been observed in the epithelial cells of several tissues types including; the glands, testis, skin, kidney, trachea, digestive tract and skeletal muscle [205]. These observations in combination with death in DG null mice after 3.6 days suggest that DG plays a crucial role in linking epithelial cells to the BM and providing structural integrity [207].

DG is also thought to play more complex functions in cells; studies have found DG co-localised with cell to cell adhesion molecules and co-purified with intracellular signalling molecules such as FAK, ERK, Src (Section 1.1.1) [208, 209]. Furthermore, work blocking the interaction between DG and laminin in foetal mouse β-cells resulted in cell death

[210], these findings allow speculation towards DGs function in β-cell survival and proliferation.

1.4.3.3 Lutheran

Investigation of laminin (Lm) receptors in human islets found a significant expression of the Lutheran. This glycoprotein is part of the immunoglobulin superfamily. It is most commonly found on erythrocytes, but is also expressed in human β-cells. [70, 71, 95].

Antibodies against α3 and β1 integrin subunits in combination with soluble Lutheran completely prevented β-cell adhesion to Lm 511. Immunochemical staining showed that Lutheran was co-aligned with Lm 511 on the peri-insular matrix indicating that Lutheran may play a role in β-cell adhesion [71].

Investigations into the binding domains of Lutheran support its role in adhesion; it is known to bind to the Lm α 5 chain giving it specificity to Lm 511 and 521. The adhesive characteristics of Lutheran are strongly linked to the pathology of sickle cell anaemia; lm is a primary constituent of the vascular BM, any damage to the vascular endothelium exposing sickle cells to lm can cause increased adhesion between sickle cells and the damaged region. This in turn can lead to complications such as vaso-occlusive crises [95, 211]. The isoform of Lutheran expressed in human β-cells possesses a significant cytoplasmic domain, although characterisation of Lutheran has shown this tail contains phosphorylation sites at present, its interaction with intracellular pathways can only be speculated [70].

1.4.3.4 Cell to cell adhesion molecules

Cell to cell adhesion involves a number of different membrane bound molecules. These molecules mediate selective adherence between cells of the same tissue type. The specificity of these interactions is necessary to segregate tissues during embryonic development and is a characteristic which is sustained throughout the adult pancreatic tissue architecture [105, 212].

Transient cell to cell adhesion describes a passive interaction mediated between the binding sites of the adhesion molecules [213]. This type of adhesion is the first to occur between dispersed cells free in solution and is achieved through selectins, cell adhesion molecules (CAM) and integrins [105, 213]. *In-vitro* cell work observations provide an example of transient adhesion. Despite brief contact and considerable shear force once trypsinised Min-6 cells floating in solution adhere. This promotes aggregation and potential for more complex adhesion.

Stable adhesion is a more durable interaction and involves the formation of adherens and gap junctions between cells, in which the transmembrane molecules interact with intracellular molecules and generate a connection to internal actin based architecture [105]. Actin based stable adhesions are mediated through the calcium dependant, cadherin family proteins E-cadherin (E-CAD) and N-cadherin (N-CAD) are known to be expressed by β-cells [62].

It is well established that β-cells require appropriate cell to cell contact to maintain a functional β-cell phenotype in combination with external ligand adhesion. Studies culturing min-6 cells as pseudoislets observed a significant increase of insulin secretion

in response to glucose compared to monolayer populations. The quantity of insulin secreted was also comparative to primary islets [214]. The increased insulin secretory response observed in these pseudoislets was linked to the presence of E-CAD, as pseudoislets failed to form when Min-6 populations were cultured in the presence of anti-E-CAD antibodies which blocked cell-to-cell interaction.

E-CAD is a transmembrane protein that functions in combination with other cadherins to create an adherens junction. Two isoforms of E-CAD exist weighing 50 and 120 kDa [214]. The latter is heavier due to the presence of an intracellular region which interacts with the three proteins p120, β-catenin and α-catenin [105, 215, 216]. These form a complex that anchors E-CAD to the intracellular actin architecture creating a stable adherence to adjacent cells [215]. Min-6 pseudoislets were found to possess significantly higher levels of the 120kDa E-CAD isoform than monolayers, suggesting that the increased cell-to-cell adhesion and adherens junctions may have an influence on intracellular pathways [214]. Later studies found that increased E-CAD in islet like structures resulted in a decreased proliferation, ensuring a confluence between cells in a 3D structure [217].

E-CAD may have a more complex role in intra-islet communication as they directly influence the formation of gap junctions. Gap junctions are channels formed between adhered cells, enabling the flow of signalling molecules. In primary β-cells and Min-6, six connexion 36 molecules form a cylindrical structure between two cell membranes, opening a pore that is large enough for the transport of small molecules and ions [105, 218]. The addition to the fluorescent molecule luciferase to one side of a Min6 pseudoislet resulted in its diffusion throughout the cell population. This provides an

example of the effectiveness of molecular transport between cells possessing gap junctions. This effect was impeded by the presence of anti E-CAD antibodies suggesting that E-CAD has some involvement in the formation and stability of gap junctions [219]. Gap junctions are vital to the pulsatile secretion of insulin from the islets of Langerhans. The rapid intracellular influx of Ca^{2+} is synchronised between β-cells of within pseudoislets due to the presence of gap junctions (Figure 1-2) [218, 220, 221]. The loss of connexion 36 in mice was shown to have a negative effect on the secretion of insulin in response to glucose [222].

β-cells express a variation of adhesion molecules, all of which are conserved in the environment of the pancreatic islet. Any 3D biomaterial attempting to harbour functional β-cell populations would have to completely compensate for the molecule interactions provided by the peri-insular membrane. However, observations have found that populations of min-6 are capable of restoring adherence junctions *in-vitro* and communicating in a similar way to cells of a functional islet [214]. This suggests the 3D element of a culture system should suffice in generating communication between Min-6 cells and potentially primary β-cells.

1.5 Polyethylene

Polyethylene (PE) refers to a commonly used plastic, its molecular form is that of repeating units of methylene, which form hydrocarbon chains (Figure 1-10) [223]. PE is produced by the polymerisation of ethylene gas, which generates a homopolymer under specific pressures and temperatures [223]. Low density polyethylene (LDPE) was first

generated in 1936 by Eric Faraday and the process later patented in 1937 by Imperial chemical industries [224, 225].

LDPE is formed at high pressures, between 1000-3000 atm, and temperatures of 80 and 300°C, the presence of oxygen is minimal at less than 10ppm [226]. Later in 1956 the Philips and Ziegler processes generated High density polyethylene (HDPE) [227]. The use of metal oxide catalysts functioned to lower the temperature and pressures of the polymerisation reaction to approximately 10-80 atm and 70-300°C, respectively.

LDPE and HDPE were found to possess very different physical properties. HDPE has a higher melting point, yield point, permeability to gases and overall hardness than LDPE. These differences are due to the effect temperature has on the polymerisation of the hydrocarbon chains [223]. The angles of the bond between methylene chains possess three states of rotation; the stable *trans* position (Figure 1-11) and two potential *gauche* positions, in which the methyl group is orientated with the opposing hydrogen atoms on the same side (Figure 1-11). In LDPE the high pressures and temperatures used during polymerisation promote *gauche* rotations.

These contribute to the random structure of PE chains, which, due to rotations of the C-C bonds, can adopt complex non-linear forms. This, in combination with the generation of free radicals during polymerisation, results in branching of hydrocarbon chains.

Overall the molecular chains produced in LDPE are complex and highly branched, with approximately 30-40 methyl groups at the end of branches, per 1000 carbon atoms which make up the primary chain [226]. This results in a plastic primarily composed of non-crystalline, amorphous regions of low density. In contrast the lower temperatures

used during the polymerisation of HDPE promote short, linear chains with less gauche rotations and an inconsequential amount of branching on the hydrocarbon chain, with approximately 7 methyl groups per 1000 carbon atoms [226]. These chains pack together more efficiently during polymerisation and generate a crystalline structured plastic of high density.

HDPE and LDPE describe the earliest grades of PE. At present there are hundreds of different PE grades available which possess variations in the number and lengths of branches along the primary chain as well as the addition of comonomer residues and impurities [226]. Each grade can be described in terms of branching and density such as linear Low density polyethylene (LLDPE), very low density polyethylene (VLDPE) and ultra-high molecular weight polyethylene (UHMWPE). As an industrial material, PE offers electrical insulation, chemical resistance, inertness, toughness, flexibility and transparency all at a low cost and easy production. Electrical insulation of sea cable and radar equipment during WWII were some early uses of PE and due to its flexibility and transparency in thin films currently a vast percentage of consumption is in packaging of food and other products [226]. Due to its chemical inertness, early work in the 1950's even pioneered HDPE for use in surgical techniques. The success of these trials is mirrored by its use in medicine today [228, 229].

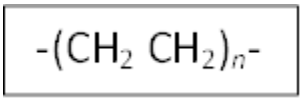

Figure 1-10: Monomer forming polyethylene

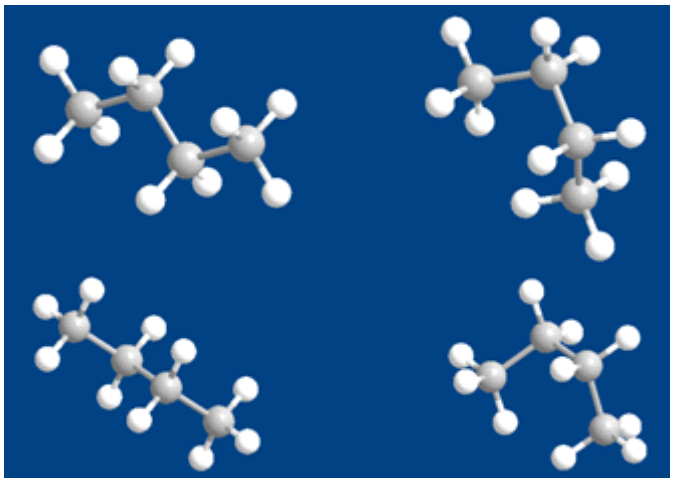

Figure 1-11: 3D polyethylene rotations

Diagrams showing; linear *trans* (Left) and *gauche* (Right) rotation of two methyl groups bound in a polyethylene chain,-(Image generated on Chemdraw). Gray and white spheres represent carbon and hydrogen respectively.

1.5.1 Conditioning PE surfaces:

Polyethylene (PE) has played a key role in the advancement of plastics from the early 1900's. Arguably, one of the most significant areas of plastic research after the initial production is surface modification. PE is a naturally inert and resistant material due to the net negative charge of the hydrocarbon chains which possess a low surface energy. The primary aim related to biomaterial research is to improve the wettability of polymers in order to promote interaction with cells and mimic an *in vivo* physiological environment. This has been achieved with polystyrene; the polymer which currently monopolises the 2D cell culture market. Various techniques exist to modify the surface chemistry of polymers. In general, these techniques do not alter the bulk polymer properties but instead modify a surface thickness of up to 100μm [230]. One of the earliest modification techniques employed on PE was chemical etching, sulphochromic and chromic acids were used extensively to etch a variety of polymers [231]. It was observed that these acids function to remove the amorphous regions of the polymer structures, SEM images show deep pits and hollows due to the removed amorphous regions of PE (Figure 1-12) [232]. The susceptibility of the amorphous regions to acid etching can be attributed to the difference in the rate of reaction between chromic acid and methyl groups found at the end of PE chains and the methylene groups mid chain. The rates of reaction are 184:3 , respectively. This explains why branched amorphous regions of PE degrade more readily during etching as they possess more methyl groups [233]. The difference in etching rate has been observed as (92μg/cm^2-hr) and (75μg/cm^2-hr) for branched amorphous and unbranched crystalline PE regions, respectively [231]. The reaction with chromic acid results in oxidation of the PE chains, generating a variety of oxygen moieties such as aldehydes, carboxylic acids and ketones.

Continued oxidation leads to chain scission and eventual dissolution of the amorphous PE regions causing the hollows observed in the SEM images (Figure 1-12) [230]. Other methods of PE surface modifications include flame and thermal treatment, the process of generating polar groups is effectively the same for these methods. Free radicals such as O, NO, OH and NH are generated at high temperatures and remove hydrogen on contact with the polymer chains [234]. Polymer oxidation follows from the reaction between oxygen and surface polymer free radicals generated from the reaction in **Figure 1-13** [230]. Flame treatment differs from thermal treatment in that an oxygen rich flame contacts the polymer surface for 0.01 to 0.1 seconds as opposed to a blast of air at approximately 500°C [235, 236]. Plasma treatment is the most common technique used to modify the surfaces of a varied number of biomaterial surfaces. Described as the fourth state of matter, plasma is, in essence, ionized gas. In this state, plasma appears luminous, containing a mixture of electrons, ions, atoms, excited molecules, UV radiation and free radicals. There are three main types of plasmas: thermal, cold and hybrid, each one generated by electrical discharges using different techniques. Thermal plasma can be produced via flames and sparks and are often of extremely high temperatures [237]. These are at contrast with cold plasmas which are generated at low pressures of between 0.1 and 10 torr. This can be achieved using either direct contact between gas and electrodes and low frequency voltages, or in isolated chambers via high or low frequency oscillations of between 10-50 kHz and 1.5-5 MHz, respectively [238]. Hybrid plasmas are produced at atmospheric pressures and involve generating several sparks in unison at high voltages of between 5-50kVs. All of these plasma treatment methods can be used to modify polymer surfaces [230]. The primary plasma-PE reactions are due to free radicals and less commonly UV radiation, (Figure 1-14)

these reactions can ultimately lead to chain scission and ablation as well as crosslinking. In oxygen based plasma modification oxygen radicals also generate a variety of groups on the surface PE chains, altering the surface chemistry as well as the topography (Figure 1-12). Chain scission and crosslinking occur simultaneously, and similarly to acid etching chain scission results in a decrease in polymer weight due to the scission product evaporation and ablation. Crosslinking describes the formation of bonds between parallel PE chains. It can be speculated that as hydrogen radicals are generated, they may react with nearby vinyl groups resulting in C-C bonds in place of the original C-H groups (Figure 1-14). Crosslinking increases the density of PE and therefore its strength and melting point, this effect is more prominent in HDPE due to the linear chained, crystalline regions that are less susceptible to cross linkage relative to the amorphous regions that comprise LDPE [230, 239]. Oxygen based plasma results in a higher abundance of oxidation groups on a number of polymers relative to noble gas based plasma [230]. Two methods exist which can directly assess the presence of oxygen based groups on polymer surfaces: Fourier Transform Infrared Spectroscopy (FTIR) and Electron Spectroscopy for Chemical Analysis (ESCA) also known as X-Ray Photoelectron Spectroscopy (XPS). Theoretical correlations exist between the absorption bands possessed by certain structural groups and the infrared spectrum. These structural groups must have a changeable electric dipole moment as part of a bond in order to absorb photons from infrared radiation; this is observed in heteronuclear groups. FTIR utilises infrared radiation by firing it at samples and measuring the frequency of the reflection emission, the remaining wavelengths reflected can be analysed to calculate absorption from heteronuclear species on the sample [240].

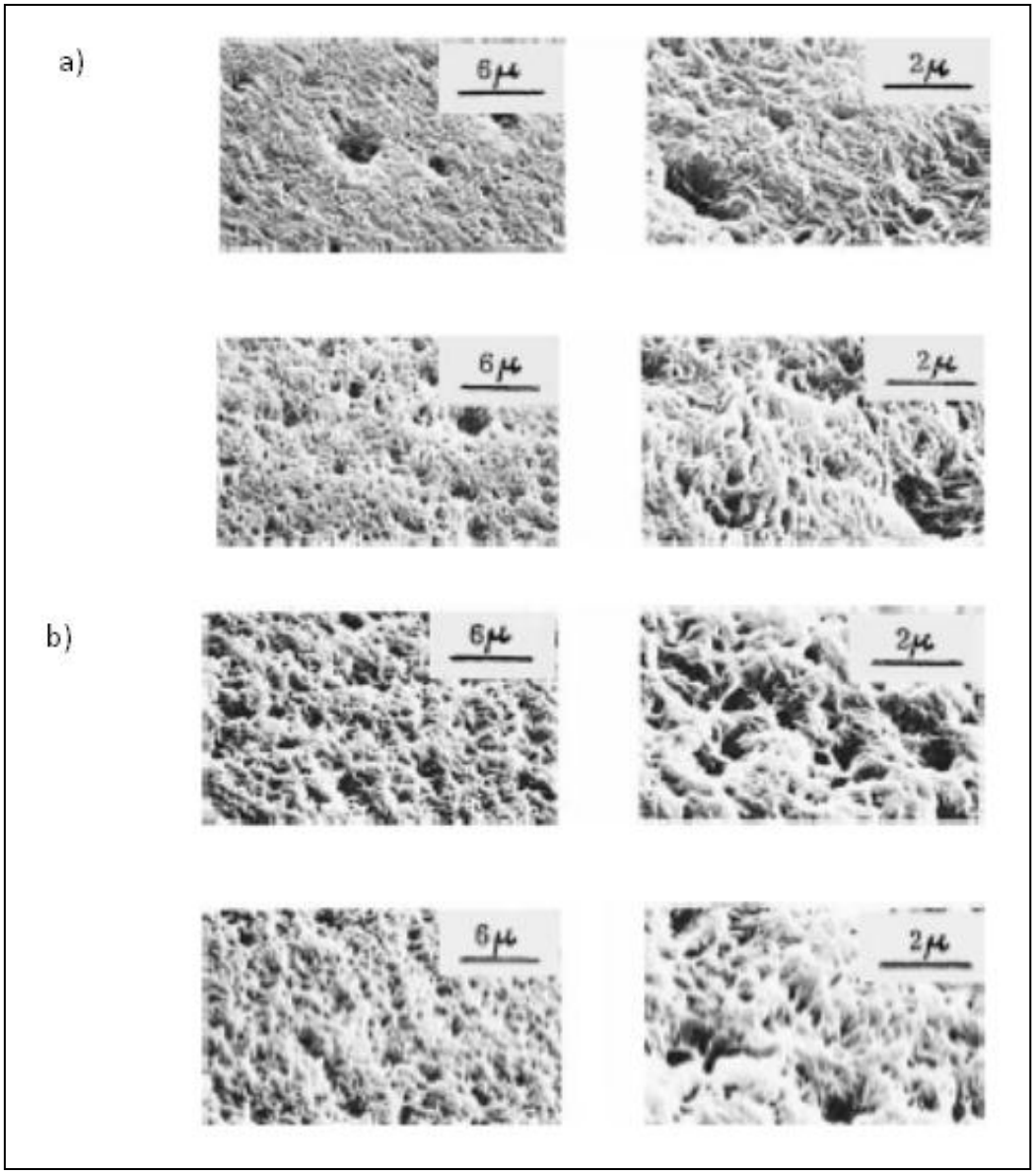

Figure 1-12: Polyethylene etching

Scanning electron micrograph of the surfaces of HDPE a) LDPE b) treated with chromic acid mixture. Reproduced from Kato K. Investigation of high-density polyethylene film surface treated with chromic acid mixture by use of 2,4-dinitrophenylhydrazine. II. Film surfaces treated at 70°C. Journal of Applied Polymer Science. 1977;21:2735-43.

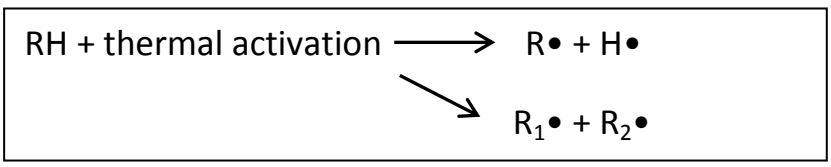

Figure 1-13: Thermal activation of a polymer.

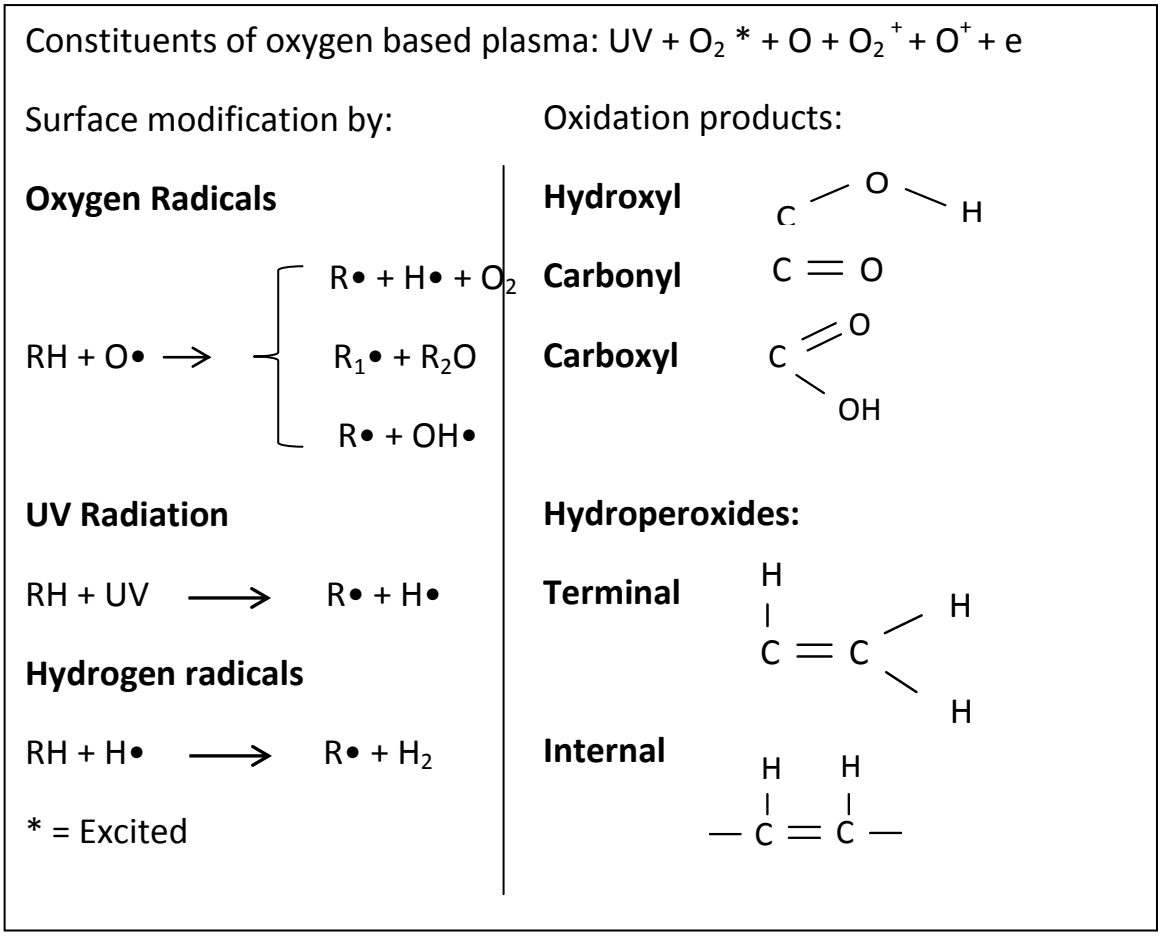

Figure 1-14: Polyethylene and oxygen plasma

Diagram showing the reaction process and products of oxygen plasma treatment on the surface of polyethylene.

In the case of polymers, the specificity and consistency of these absorption reflections can be plotted to generate a reproducible “footprint”. Footprints are unique wavelength patterns which provide information about the quantity and type of C-H bonds in the polymer based sample. Figure 1-15 shows infrared spectra of LDPE and HDPE, respectively. Three peaks of low transmittance can be seen between approximately 720-730, 1360-1500 and 3000-3200 cm^{-1}. The lowest two band wavelengths correspond to the absorbance of IR by CH_2 groups. This group has three degrees of rotational freedom: wagging, bending and rocking [240]. These bond vibrations results in IR absorption, the first peak between 720-730 cm^{-1} corresponds to CH_2 rocking, a smaller peak at 1369 cm^{-1} is due to CH_2 wagging as the charge or dipole moment fluctuates between the carbon and hydrogen atoms. And finally, the larger peak at 1475 cm^{-1} is absorption from CH_2 bending. C-H stretching is one other type of bond vibration observed and results in the absorbance peak at approximately 3000 cm^{-1}.The differences between LDPE and HDPE can be seen by three main observations of Figure 1-15. A larger peak at 1378 cm^{-1} represents CH_3 group absorbance and so would be higher in the branched amorphous regions of PE in LDPE. The *trans* and *gauche* rotational state of methyl groups provide different absorbance peaks which can be used quantitatively, providing an idea of crystalline to amorphous region ratio in PE samples. Finally, due to the linear packing of PE chains in crystalline regions a phenomenon known as crystal field splitting can be observed. This is due to an interaction between two methyl groups in adjacent chains leading to two small peaks at the apex of a larger one, this effect is more prominent in HDPE samples [240]. This technique can also detect the presence of oxygen based moieties within the polymer sample; this has been shown in two separate papers investigating oxygen based plasma modification of polyethylene [241, 242].

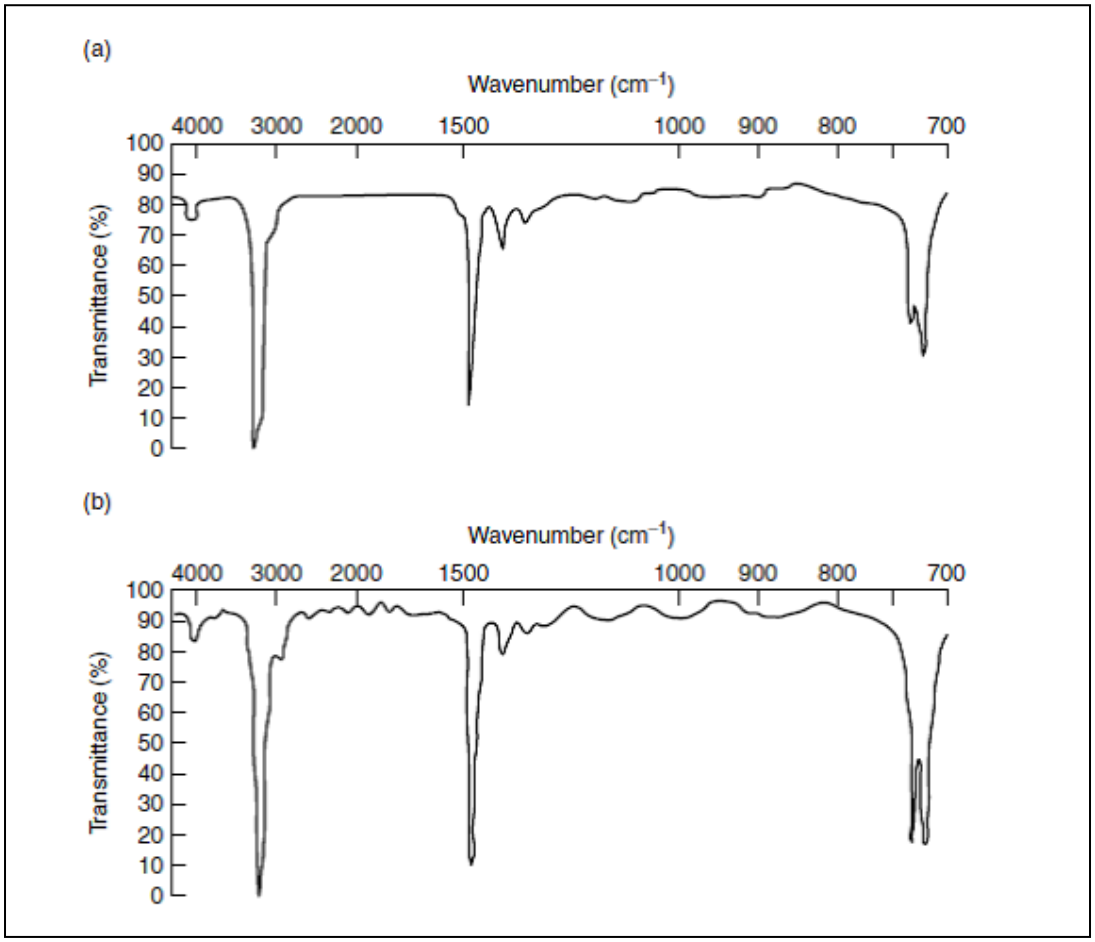

Figure 1-15: FTIR spectra of polyethylene grades

FTIR spectra of untreated a) LDPE and b) HDPE. The first peaks between 720-730 cm^{-1} corresponds to CH_2 rocking, smaller peak at 1369 cm^{-1} is due to CH_2 wagging, the larger peak at 1475 cm^{-1} is absorption from CH_2 bending [240]. Reproduced from Barbara HS. Infrared Spectroscopy: John Wiley and Sons; 2004.

Evidence of oxidation products can be seen from peaks in Figure 1-16; peaks at 1737 cm^{-1} and 1368 cm^{-1}-1646 cm^{-1} are due to the presence of carbonyl and carboxylic groups respectively [241] . A reversed spectra of peaks subtracted from an untreated PE sample in Figure 1-7 indicates similar absorbance of carbonyl groups at approximately 1700 cm-1 and carboxyl groups at 1400 cm^{-1}, as well as strong peaks at 1255 cm^{-1} which correspond to ethers [242].

These studies provide an example of the different oxygen species generated from oxygen plasma treatments, and are not exhaustive. A major disadvantage of FTIR is the selective absorbance of radiation. This often provides data regarding the primary molecular constituents of the material, reducing the significance of rarer oxygen groups relative to the hydrocarbon chains being analysed. Although it can be used for qualitative analysis of oxygen moieties in polymer samples, the full extent of oxidation may be missed by FTIR, which penetrates beyond the nm thick layer which has been in highest contact with oxidising plasma. It is known that the depth of penetration in plasma etched polymers is in the region of 5- 50µm, oxidation product concentration decreases with depth due to the decrease in oxygen diffusion; oxygen groups of interest can be missed as a result [230]. Furthermore, the all infrared inactive bonds are effectively invisible, as the lack of dipole moments does not absorb infrared radiation. As a result active bonds must be used to deduce the overall molecular constituents of samples being analysed.

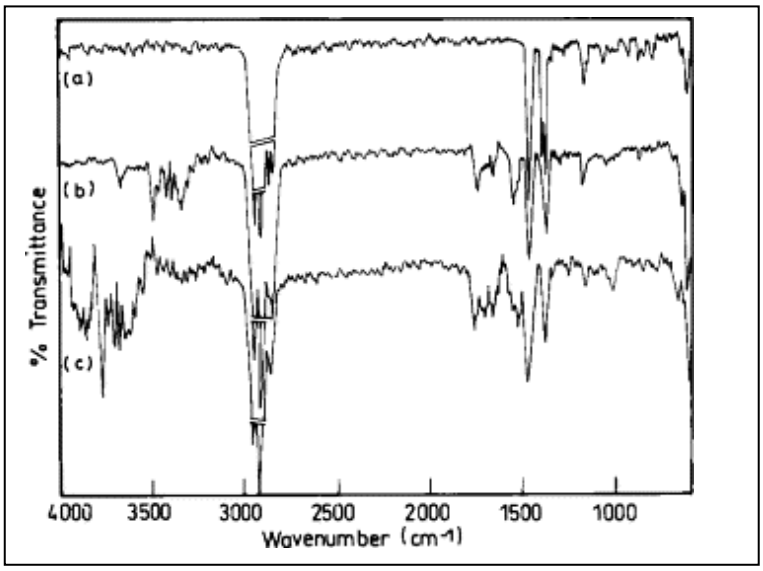

Figure 1-16: FTIR spectra of polyethylene and plasma

FTIR spectra of polyethylene treated with argon and oxygen plasma: (a) untreated; (b) 200 W, 120 s (argon plasma); (c) 200 W, 120 s (oxygen plasma). Reproduced from Guruvenket S, Rao GM, Komath M, Raichur AM. Plasma surface modification of polystyrene and polyethylene. Applied Surface Science. 2004;236:278-84.

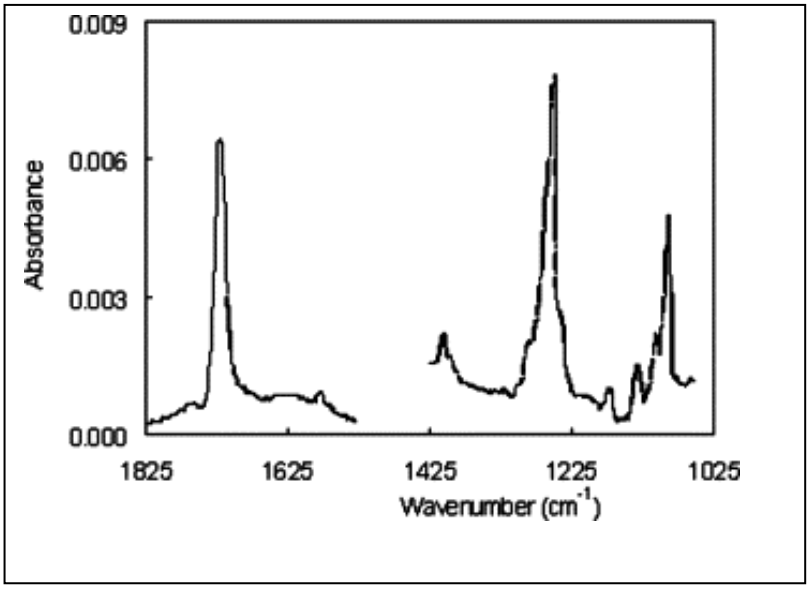

Figure 1-17: Reverse spectra FTIR of polyethylene and oxygen

FTIR reverse spectra of Polyethylene treated with oxygen radio frequency plasma. Reproduced from Lehocký M, Drnovská H, Lapčíková B, Barros-Timmons AM, Trindade T, Zembala M, et al. Plasma surface modification of polyethylene. Colloids and Surfaces A: Physicochemical and Engineering Aspects. 2003;222:125-31.

FTIR is often used in combination with electron spectroscopy for chemical analysis (ESCA). This method utilises x-ray spectroscopy to provide information about the chemical and atomic profile of a sample. The high frequency of x-rays enables the detection of elements with an atomic number above three and can analyse a surface layer of 1-10nm [243]. Studies incorporating this method in analysis of oxygen plasma treated PE have identified a strong spectra corresponding to hydroxyl, ether and hydroperoxides, in support of FTIR spectra and previous studies [242].

Wet chemistry can also be applied to quantify oxygen species generated by plasma. Detailed analysis of fluorescence labelling reactions for quantification of hydroxyl, carbonyl and carboxyl groups found these techniques had a significantly higher detection limit when compared to ESCA [244]. Thionine acetate (THA) is an example of a fluorescent labelling reagent that binds exclusively to carboxyl groups at a ratio of 1:1 (Figure 1-18). Providing sensitive spectrometry equipment is available, this dye can be incubated with the surface of a plasma treated polymer sample prior to the solutions fluorescence intensity measured at 618nm. Changes in the solution absorbance can be compared with a standard curve to calculate the change in molarity and therefore quantify the number of carboxyl groups generated [244]. An alternative method of quantifying carboxyl groups would be to wash away unbound THA molecules after incubation and cleave the remaining bound molecules with a HCL solution. This method would provide a direct measurement of carboxyl groups. However, there is potential error in the wash steps and the solution must be diluted before measurement [244]. One further complication with this method is the penetration of THA molecules into PE, a linear increase in carboxyl group concentration was observed with increasing sample

thickness, carboxyl group concentration increased by four over 150nm thickness [244]. THA chemistry has been applied successfully in previous literature to accurately characterise plasma treatment alone or as a complementary technique [244-248].

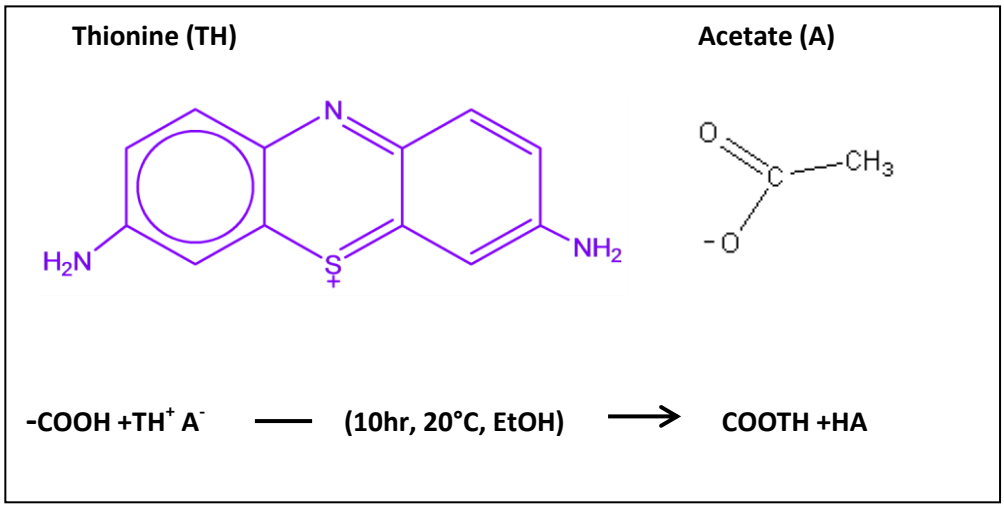

Figure 1-18: Molecular structure of thionine acetate and fluorescent labelling reaction

1.5.2 Surface roughness

The nature of plasma etching can modify not only the surface chemistry of PE but also the surface topography; the action of PE chain scission and ablation is known to cause hollows as observed in Figure 1-12. The amount of roughness generated is dependent on the type of etching process and the density of the PE being treated (Figure 1-12).

Reliable, quantitative assessment of surface roughness has become possible with the discovery and production of commercial scanning probe microscopes in the 1980's and 1990's respectively [249]. An atomic force microscope (AFM) physically probes the surface of samples by "tapping" along the surface with a nano scale tip. Lasers detect the tiny movements in the position of the tip in response to changes in surface topography and convert it into a digital signal. AFM can produce extremely detailed 3D images of surface structure, and if the tip end is small enough imaging can be achieved down to a molecular level! [250]. Many AFM microscopes have software that is capable of calculating surface roughness by the root mean square average (R_q) or the arithmetic average roughness (R_a) [172]. R_q is the most appropriate roughness measurements for nano scale surface analysis, as it takes into account peaks and valleys by generating an average of the absolute roughness profile ordnance. As opposed to the R_a, this is more commonly applied but generates a value for the average roughness making no distinction between peaks or valleys.

There are several papers that have investigated the effect of various types of plasma treatment on PE surfaces incorporating AFM. One study characterised not only the changes to surface topography but also the oxidation groups generated from CO_2,

microwave produced cold plasma. LDPE samples surfaces were homogeneous and unremarkable compared to LDPE surfaces post plasma treatment, which were found to possess distinct peaks. The peaks appear to increase in height with increased plasma treatment time; and are between 0.1 to 3μm in size (Figure 1-19) [247].

The authors speculate these peaks are due to the readily degraded amorphous regions of PE. These regions are removed by scission reactions discussed earlier and ablated via gas flow causing rapid degradation of the polymer surface. This is supported by the observation that weight loss occurs during plasma treatment with approximately 20μg/cm^2 of PE being removed over 300 seconds. The peaks seen are presumed to be resistant crystalline regions of PE [247]. Similar topography has been generated by Ar based RF plasma treatment of UHMWPE, AFM software analysis presented in Figure 1-20, clearly demonstrating an increase in surface roughness and the generation of hollows in the PE surface [251]. Differences in the topography of Figure 1-20 and Figure 1-19 are relative to the ratio of amorphous branched regions of PE in their structure. UHMWPE is contains more crystalline regions, this in turn affects the type of topography seen.

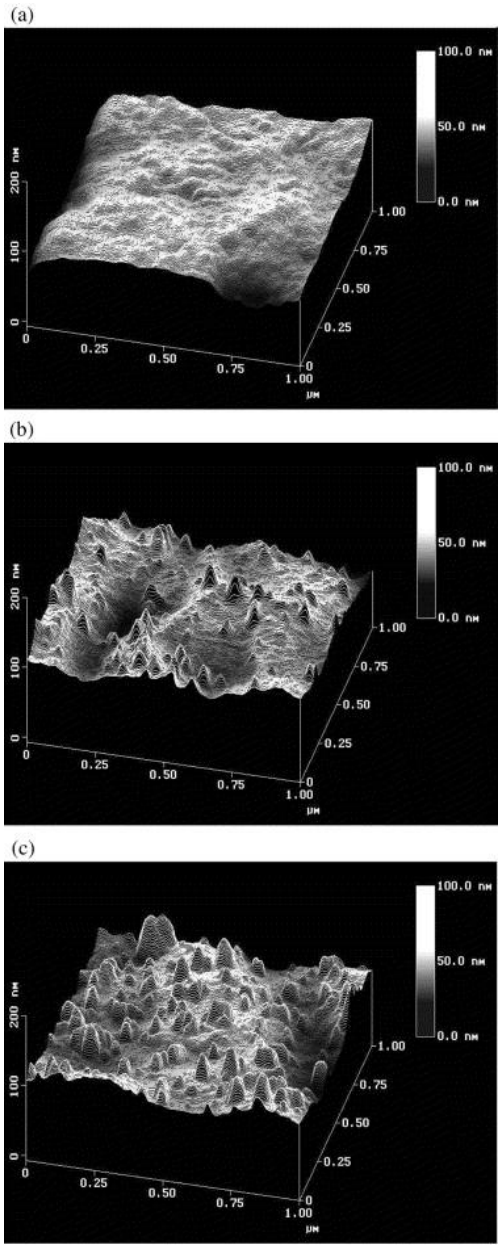

Figure 1-19: AFM of plasma etched high density polyethylene

AFM images (1×1 µm) of: (a) Untreated HDPE; (b treated) HDPE (P=40 W, d=5 cm, $Q(CO_2)$=10 sccm, p=0.3 mbar, t=2 min); (c) treated HDPE (P=40 W, d=5 cm, $Q(CO_2)$=10 sccm, p=0.3 mbar, t=4 min). Reproduced from Médard N, Soutif JC, Poncin-Epaillard F. Characterization of CO_2 plasma-treated polyethylene surface bearing carboxylic groups. Surface and Coatings Technology. 2002;160:197-205.

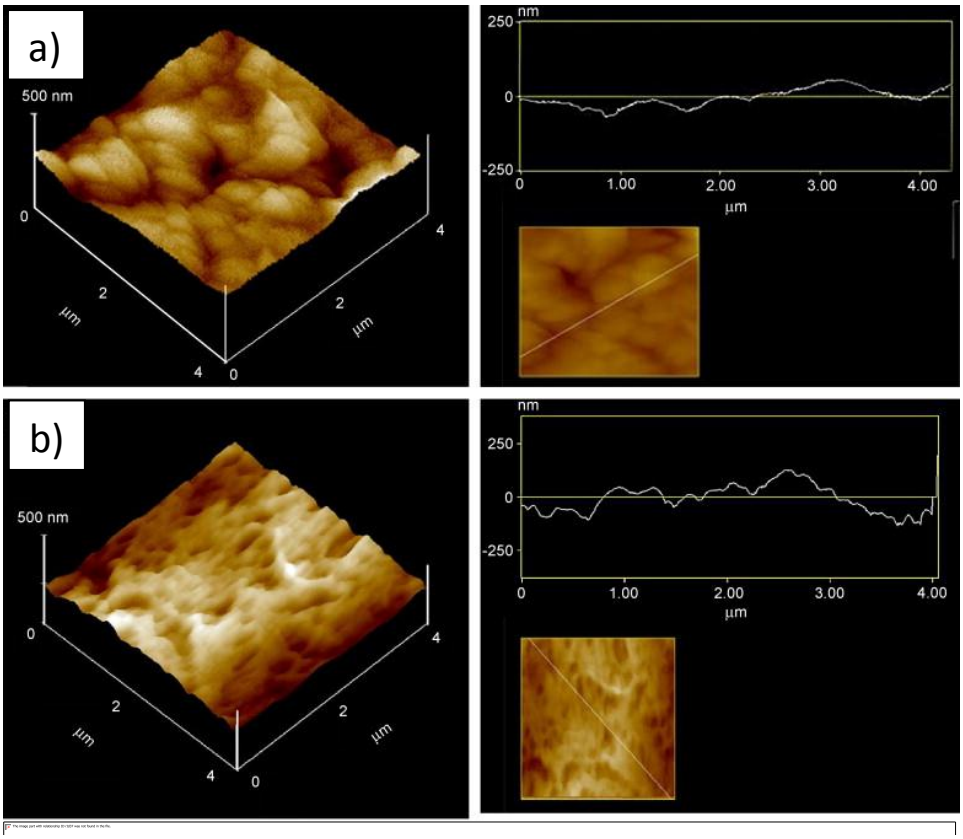

Figure 1-20: AFM of plasma etched ultra-high molecular weight polyethylene

AFM micrographs of (a) untreated and (b) Ar-treated UHMWPE, left hand images show 3D topography of an area of 4µm^2. Right hand images show side 2D view of topography. Reproduced from Rhodes NP, Wilson DJ, Williams RL. The effect of gas plasma modification on platelet and contact phase activation processes. Biomaterials. 2007;28:4561-70.

1.5.3 Polyethylene biomaterials

Since the 1960s, one of the most significant uses of PE has been orthopaedic hip and knee prosthesis. In both cases ultra high molecular weight polyethylene (UHMWPE) provides a surface on which a metal femural head or condyles couple and function to restore movement in the patient [252].

Due to the stress exerted in place of the original hip joint, high density molecular weight polyethylene (HDMWPE) offers the highest level of toughness and abrasion resistance of all PE grades and due to its inertness holds a low risk of immunological rejection after surgery. Despite these properties, decay and loss of prosthesis function due to wear of the HDMWPE component is a continuing problem. This includes poor artificial lubrication between the metal and PE components of the hip prosthesis compounded with patient movement [252]. Friction generated between components during articulation of the hip prosthesis generates particles of PE estimated at around 1 – 5 μm in diameter [252]. Similar problems have arisen with knee prosthesis. It was reported that of 51 retrieved knee prostheses, 22 cases had traumatically dislocated due to failure of the PE meniscal bearing component. Further histological inspection of surrounding synovial tissue found PE particulates between 10 and 100 μm [253].

Osteolysis has been observed in surrounding tissue of failed hip prosthesis. This has been attributed to nano scale PE particulates of between 0.2 and 0.8 μm which induce macrophage activation, periprosthetic inflammation and in turn aseptic loosening of the prosthesis [254, 255]. An additional requirement of PE used in prosthetic roles is complete sterility, due to the damage caused by autoclaving ionizing gamma and beta

radiation are used to sterilise PE prosthetics prior to implantation. Under the right conditions, beta radiation can be used to crosslink PE chains, thus generating a stronger form of PE. However, in the presence of oxygen, chain scission and oxidation can occur [252, 256]. These potentially damaging reactions can be overcome by storing any PE based products in a vacuum to prevent oxygen diffusion into the PE structure. Alternatively, the oxidation can be reduced and crosslinking improved using stabilisation techniques [252].

Crosslinking has been shown to significantly improve the abrasion resistance of UHMWPE hip prosthetics. Studies incorporating hip simulation equipment demonstrated that standard UHMWPE degraded at a rate of 141 mg/million cycles as opposed to 37 mg/million cycles of cross-linked UHMWPE [257]. In addition, abrasion resistance and strength are dependent on the segmental mobility between the PE chains, increased crosslinking reduces this [258]. By varying the temperature at which UHMWPE samples are irradiated and the dose rate, a crosslinking gradient has been achieved through a UHMWPE prosthetic by one group [258]. These samples provide a high level of resistance on the active surface of the acetabular cup which in direct contact with metallic femoural head, the opposite side is less cross linked preventing wear against the supporting shell [258]. The overall gradient is also constant which reduces any internal mechanical stress between cross linked regions in the plastic during use [258].

PE has also been used for catheters, as early as 1951 LDPE was identified as a material that could be used for long periods of time without causing discomfort due to its hydrophobicity, inertness and flexibility [228]. An early use in Jejunostomy feeding has

now been superseded by its potential as a urinary catheter. Current research has incorporated the antimicrobial agent triclosan at different concentrations in the generation of LDPE catheter tubing, generating a biocidal polymer [259]. It was observed that with increasing concentrations of triclosan there was a decrease in biofilm formation as well as a decrease in bacteria present in the artificial urine after flow through the material over 30 days [259].

Current uses of PE in medicine provide an excellent example of how this polymer can be altered and conditioned to suit a wide range of requirements. As research into polymers advances and more control is achieved over the generation of polymeric materials further use may be found in more specific roles in the body.

1.5.3.1 Medpor®

Further uses of PE in surgery include craniofacial surgery reconstructing ears, spherical orbits, nasal passages and facial abnormalities (Figure 1-21) [260]. A vast quantity of literature has observed success using a PE based porous surgical prosthesis material Medpor®. One study found that out of 187 patients receiving nasal reconstruction, only 2.6% suffered complications [260, 261]. A more recent study assessed 285 patients and found a failure rate of 6.2% which is comparable to other large studies [260, 262]. Failure was often due to infection, particularly in regions such as ear and nasal cavities where the skin covering the implant was thin [262]. Overall, Medpor® is considered by several surgical groups as a material second only to autologous bone and cartilage. PE offers physical integrity, proving a platform which can be easily crafted into the desired

shape and pore size. However, It has been shown to be completely biocompatible with no signs of degradation during long-term use [262].

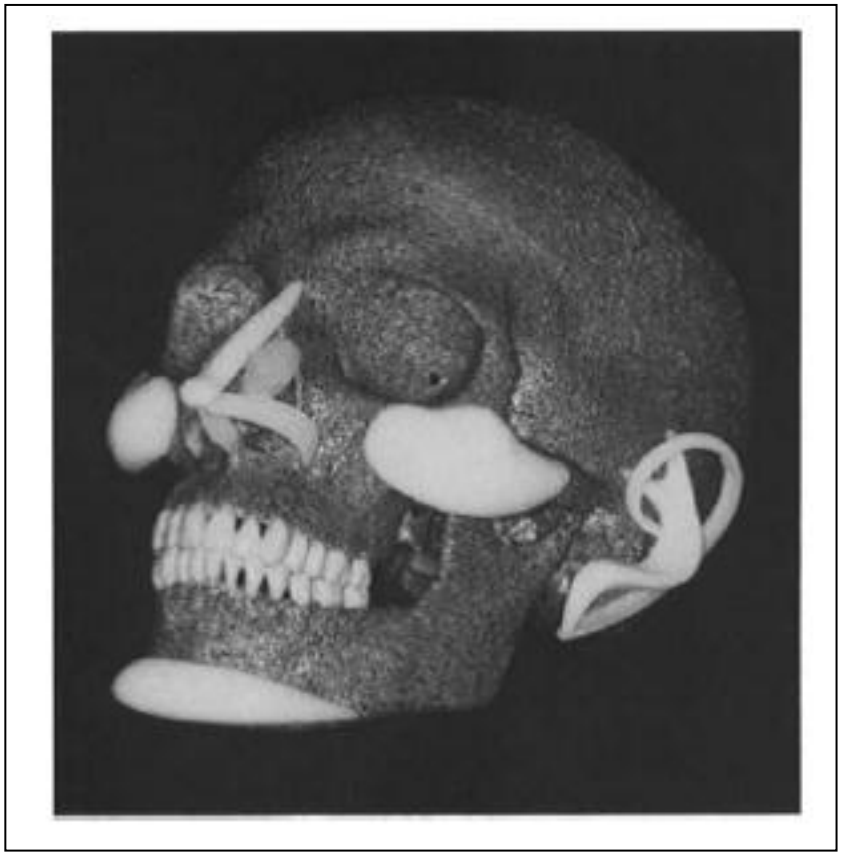

Figure 1-21: Medpor® facial implants

The applications for the Medpor® implant are demonstrated in the chin, malar, nasal areas and as a frame work for ear reconstruction [260]. Reproduced from Wellisz T. Clinical experience with the medpor porous polyethylene implant. Aesthetic Plastic Surgery. 1993;17:339-44.

1.5.3.2 The potential of polyethylene cell culture systems

There is currently a vast amount of literature investigating a range of polymer based biomaterials for use in culturing cells. The priority in many is the manipulation of surface chemistry. As a result, the benefits of structural integrity and inertness possessed by PE have not warranted significant investigation. It can be speculated that the success of similar polymers like polystyrene in early trials has resulted in the lack of interest in PE as a cell culture biomaterial. This may have been due to the lower abundance of oxygen groups generated from plasma in PE relative to polystyrene, especially in HDPE which possesses a low amount of CH_2 groups which are more readily oxidised [146, 150, 230].

It is well established however, that plasma modification can incorporate useful chemical species onto PE surfaces improving the wettability, and in turn the compatibility of PE with proteins and cells. These oxygen species can also be used to conjugate more complex growth factors and adhesion peptides. The direct involvement of PE in cell culture systems is limited. Two studies have incorporated HDPE as an internal material coated to promote the growth of chondrocytes [263, 264]. An early study was investigating the use of different materials in combination with the hydrogel F-127; this gel acts as a biocompatible, non-toxic environment in which chondrocytes can grow and generate their own extracellular matrix. One major disadvantage however, was the lack of structural control over the gel; 5 different materials including HDPE were tested as internally supporting biomaterials for the gel. 1mm layers of gel infiltrated with chondrocytes were syringed over the materials until they solidified. It was observed that the HDPE control sample implanted independently caused mild

inflammation in mice, but performed well as an internal support structure. Gel coated HDPE promoted the growth of mature elastic cartilage as supported by the histological analysis of reclaimed scaffolds [263]. This study highlights the success of untreated HDPE in the *in-vivo* environment, despite its chemical inertness the surface was successfully covered in a gel layer, with 95% of the surface being covered in cartilage and 5% in a fibrous tissue after 8 weeks of growth [263]. Further work incorporating HDPE as a scaffold coated in polyglycolic acid (PGA) showed similar success in cell compatibility. HDPE rods were wrapped in PGA fibres, seeded with chondrocytes and incubated for 3 weeks prior to subcutaneous implantation and a further 8 weeks *in-vivo* growth [264]. A consistent cartilage structure was observed in the PGA fibres histologically after reclamation of the samples. Furthermore, the cartilage grew to the HDPE rod central to the samples. This indicates that biocompatibility between untreated HDPE and chondrocytes [264].

Although PE has not had much direct use in cell culture, it has a long history as an implant material. Biocompatibility and cell in growth has been observed in current PE based surgical materials, BioporeTM and Medpor® are materials used in craniofacial surgery that promote the infiltration and ingrowth of surrounding tissues [262]. Fibrovascular ingrowth was observed in Medpor® which has been successfully implemented in thousands of operations for long term prosthesis [260-262]. Made from sintered HDPE particulates, Medpor® is known for its complete inertness and biocompatibility *in-vivo*. Histological analysis of sections of Medpor® reclaimed after 3 months have shown the generation of functional blood vessels and collagen secretion from surrounding tissues [260]. The structure of Medpor® may also aid the infiltration of

surrounding tissues. Standard pore size is approximately 100µm. This combined with 50% porosity have proven effective at establishing an internal cell population [260, 265]. Overall these studies suggest that HDPE has a certain amount of biocompatibility before conditioning with plasma, and in combination with other biomaterials has proven to be a powerful structural asset in the field of tissue engineering.

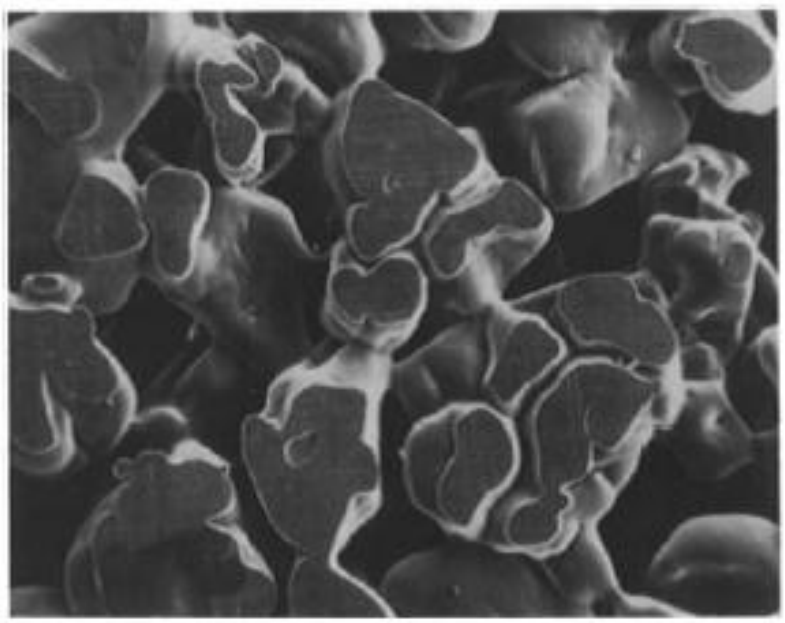

Figure 1-22: Medpor® particulates

Scanning electron micrograph (x20) of the Medpor implant demonstrating the contiguous, large pore structure [260]. Reproduced from Wellisz T. Clinical experience with the medpor porous polyethylene implant. Aesthetic Plastic Surgery. 1993;17:339-44.

1.6 BioVyon™

BioVyon™ is a porous plastic material made from industrial grade HDPE produced by the Porvair Filtration Group. The term “frit” describes a porous 3D disc generated from HDPE. The size, porosity and surface chemistry of the BioVyon™ frits can be altered and tailored to specification by sintering (Figure 1-23).

Sintering is a process by which PE particulates are partially coalesced at high temperature for a known period of time. This process results in the PE particles partially melting or coalescing together, pores then form from the voids between the particulates as coalescence takes place (Figure 1-24). If the particulates are sintered too long or at too high a temperature, over sintering can occur, complete coalescence takes place, and the particles condense filling the voids resulting in a translucent solid frit. Conversely, if the particulates are under sintered initial coalescence is not uniform throughout the frit and a powdery, brittle structure results.

The surface of the HDPE particulates is altered during the coalescence process. Amorphous regions of PE have a lower melting point and so coalesce more readily than the crystalline regions generating a novel topography. BioVyon™ is currently sold in a range of filtration and separation products; in the form of cartridges and micro plates. BioVyon™ is resistant to a wide range of acids, bases and organic solvents and retains structural integrity at temperatures of up to 80°C. This material is extremely versatile with vast applications in the bioscience industry. Untreated hydrophobic BioVyon™ has been applied in venting, aerosol retention, pipette tips and catheters. Further applications are possible after plasma treatment including chemical wicking and process

chromatography as well as offering valuable functional groups for advanced modification. Functionalised BioVyon^{TM} holds the most potential. Oxidation groups can be conjugated to biologically active molecules making applications in affinity chromatograph and antibody purification possible.

Figure 1-23: Sintered Vyon frits produced by Porvair Filtration.

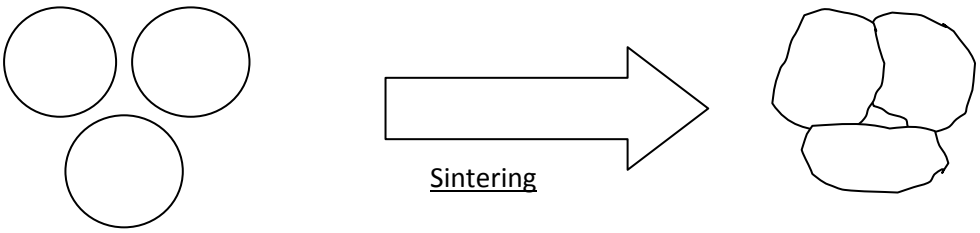

Figure 1-24: Coalescence of polyethylene particles as a result of sintering.

1.7 Aims

Type 1 diabetes affects a significant proportion of the population worldwide, causing potentially lethal fluctuations in blood glucose. Although treatments such as subcutaneous insulin administration are effective at providing short term relief, they are often associated with long term complications [4, 6, 15]. Islet transplantation is an alternative treatment and potential solution to long term complications and has been successful in proving patients with insulin independence over 5 years. The major disadvantage however, is the lack of donor cells available for transplant [21, 23]. Embryonic stem cells hold the potential to be differentiated into β-cells *in-vitro,* offering an alternative supply for transplantation [25]. Current differentiation protocols however, are inefficient, and require optimisation before the complex phenotype of a mature β-cell can be accurately mimicked, mass cultured and used for transplantation [36, 37].

Novel 3D culturing methods have shown an improvement in cell growth and viability. These materials hold potential to completely mimic all significant factors that result in natural tissue structures formation. In order to accurately mimic the pancreatic basement membrane, the type and number of integrin adhesions *in-vivo* must be identified and reproduced using proteins that form the architectural basement membrane of the islet ECM. In combination with current and future β cell differentiation protocols 3D biomaterial culture systems could provide a solution to the donor β-cell shortage, by mass culturing β- cell populations with a sustainable phenotype.

Polyethylene has been used as a biomaterial for the last 30 years. It is well characterised and can be augmented for cell culture by modifying its surface chemistry and creating 3D structures that resemble the vasculature of tissues. BioVyon ™ holds excellent potential as a 3D culture system to mimic the pancreatic islet at the macro and nano scale to ultimately mass culture transplantable β cells.

Research question: Could BioVyon™ be conditioned to mimic the environment of the endocrine pancreas, in order to mass culture and preserve the phenotype of transplantable beta cells?

The project aims were to::

- Fully characterise and assess the potential of BioVyon™ for use as 3D cell culture system.
- Modify the surface chemistry of BioVyon™ to promote cell adhesion, spreading and growth.
- Adsorb proteins at ratios reflecting the BM of the endocrine system.
- Condition the environment of BioVyon™ to harbour viable Min-6 cell populations for an extended period of time.
- Maintain insulin secretory phenotype in Min-6 cell line after 15 days growth on the BioVyon™ scaffolds.

2 Materials and methods

2.1 Materials

Cell culture materials: DMEM 5mmol/L glucose with L-glutamine media was purchased from PAA. Foetal bovine serum and trypsin was purchased from Invitrogen (Glasgow, UK).

Bichonininic acid (BCA) assay was purchased from Thermo Scientific (Hemel Hempstead, UK).

Lactate dehydrogenase (LDH) assay was purchased from Promega (Southampton, UK).

Insulin ELISA was purchased from Mercodia (Uppsala, Sweden).

BioVyon™ frits were supplied by Porvair Filtration plc (Wrexham, Wales).

Unless otherwise specified all chemicals were purchased from sigma (Gillingham, UK).

2.2 Methods

2.2.1 Statisticsal analysis

Minitab 16 statistical software, was used for all statistical analysis, all data was tested for normal distribution prior to analysis.

2.2.2 Multiple comparisons

A two way analysis of the variance (ANOVA), was used to directly compare significance of the means of multiple data sets between treatments over different time points. Individual data sets were analysed using a one way ANOVA. Tukey's wholly significant difference test (Tukeys test) was further employed for the multiple comparison of these data sets and identification of the means which were significantly different. Student's two sample T-test was used to compare two sets of data.

2.2.3 Vyon powder parameters

Industrial grade polyethylene powders were used during sintering trials (Table 2-1); three different grades of known sizes were used yielding various porosities of BioVyon™ disc after sintering.

Name	% of Particle size (µm)						Bulk density (g/cm^3)
Vyon M	<63	63 - 125	125 – 250	>250			0.57
	14.3	75.6	10.1	0			
Vyon F	<63	63 – 106	106-150	150 – 212	212 – 300	>300	0.529
	0	5.69	18.89	49.55	24.00	1.87	
Vyon HP	< 300	300 - 425	425 - 600	>600			0.57
	0	2.4	96.0	1.6			

Table 2-1*: Parameters PE powder grade*

Table to show percentage particle size and bulk density (g/cm^3) of three different high density polyethylene (HDPE) Vyon powder grades; Vyon M,F and HP possess the highest percentage of particulate sizes between 63-125, 150-212 and 425-600 µm respectively. Vyon F has the highest range of particulate sizes, with percentages contributing to the powder particulate sizes between 63 and 300µm. All powders possess a similar bulk density, indicating all powders are HDPE.

2.2.4 Sintering Process

The high density polyethylene (HDPE) powders were poured into a sintering tool which also acted as a mould (Figure 2-1) and heated in a vacuum oven for 30 minutes at 180°C. After sintering the frits were checked, BioVyon™ structural integrity was considered optimal if there were no loose particulates, and the porous structure was intact, indicating partial coalescence between the particulates. The Vyon F grade powder was sintered using this method prior to porosity measurement; all BioVyon™ F frits (D 14.4mm, W 1mm) used in the remainder of the project were produced using similar, optimised industrial processes, tailored to the powder grades and density.

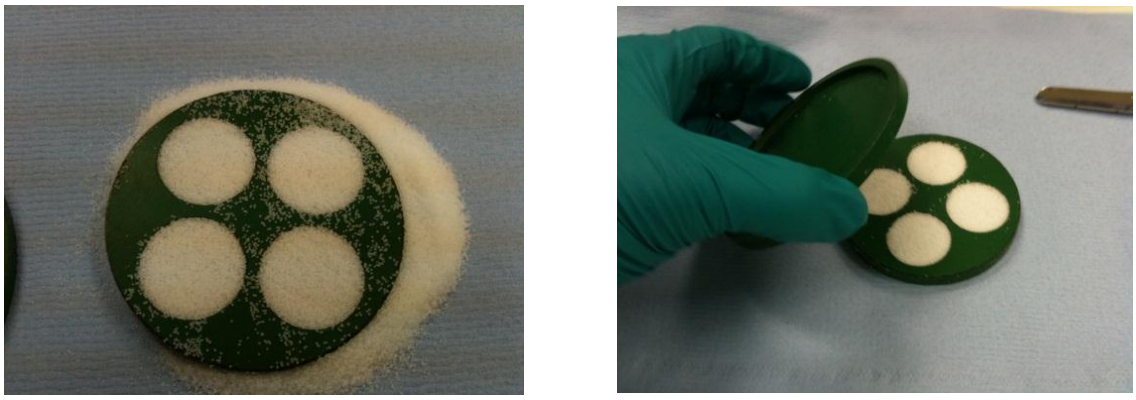

Figure 2-1: GHR 8020 sintering

Images of polyethylene powder in sintering tool (left) and sintered BioVyon frits™ (right).

2.2.5 Porosimetry

Sintered frits were submerged in wetting fluid of known viscosity once placed in the porosimeter (Coulter porosimeter II, Quantachrome). The equipment software calculated the pore sizes of each frit from the extrusion pressure and a standard curve of pressure against flow of porofil. The frit total volume, apparent density, theoretical density and percentage porosity were calculated using the frit dimensions and formulas below respectively:

Frit total volume (cc) = ((Frit diameter (mm) ^{2} × ¼ × π) × (height (mm)))/1000

Apparent density (g/cc) = Frit weight (g) / Frit volume (cc)

Theoretical density (g/cc) = Frit volume (cc) × Density of PE (g)

Porosity (%) = (Density of PE (g) – Apparent density (g/cc) / (Density of PE (g) × 100))

2.2.6 Mercury porosimetry

The porous structure of BioVyon™ was also investigated using a PoreMaster mercury porosimeter (Quantachrome Instruments, Farnborough, UK). Half sections of BioVyon™ (0.0528 g) were dried in a vacuum oven at 60 °C for 3 h prior to analysis. Porosimetry analysis was carried out using Quantachrome Autosorb data reduction software (Quantachrome Instruments, Farnborough, UK).

2.2.7 Plasma treatment

Radio frequency generated cold plasma was produced in an inductively coupled barrel etcher (Polaron pt7150 plasma barrel etcher, chamber size approximately 10 x 14 cm) (Figure 2-2). A polystyrene 24 well plate lid was utilised as a makeshift stage on which the BioVyon frits were etched. Pressure control was automated and supplied by a tank of pure oxygen. Prior to plasma treatment (PT), chamber pressure was 2 mbar (1.5 torr) which increased gradually over a consistent time period to a final pressure of to 0.8 mbar (0.6 torr). BioVyon™ frits were plasma etched at varying pressures, radio frequencies and lengths of time.

A larger industrial plasma etcher was also used to treat BioVyon™ frits; this equipment followed an automated run program (Figure 2-3).Two batches of 700 Biovyon F frits were placed on one of 10 shelves and plasma etched with pure oxygen for 116 seconds at 807 watts. 2D HDPE analogues were added to the batches to calculate advancing and receding contact angle (ARCA) which was approximately 40° throughout the platform. Post plasma etching all 1400 BioVyon frits were immediately stored in PBS to preserve the oxygen moieties generated by the plasma [266].Prior to plasma treatment both chambers were purged of atmosphere, chamber pressure was reduced to 2mbar and 0.33 mbar in the plasma etcher and industrial etcher respectively. These purges functioned to remove any compounds or gas present from previous experiments. Prior to plasma etching all BioVyon™ frits were washed three times in 100% ethanol for 30 minutes each in an ultrasonic bath to remove debris and polymer chains from the sintering process.

Figure 2-2: Plasma etcher

Image of Polaron pt7150 plasma barrel etcher (University of Brighton). Chamber size approximately 10 x 14 cm.

Figure 2-3: Industrial plasma etcher

Image of industrial plasma etcher at Porvair Filtration plc, (Wrexham, Wales).

2.2.8 Advancing and receding contact angle measurement

The advancing and receding (ARCA) contact anlge of polymer samples was measured, it provided data of droplet hysteresis, or the interaction of the water across regions of the surface [267]. Maximal and minimal contact angles were derived from the advancing and receding stages of the method respectively, this provided more substantial data on the interaction between the water and the polymer surface. ARCA measurements were conducted on an OCA 15plus contact angle goniometer (Data physics, Hailsham, UK). A 100µl syringe (Hamilton™) was filled with RO water prior to every experiment measurement and used to generate 5µl drops. The drops were produced automatically by the goniometer software, which then recorded the changes in drop volume on the sample surface at a rate of 1 frame per second. The instrumental dosing rate was set at 0.25 µl/sec; increasing the initial 5µl drop volume by 5µl over 20 seconds for the advancing stage followed by a 5µl decrease over a following 20 seconds for the receding stage. Individual frames from the recordings were used to measure individual contact angles, generating approximately 40 measurements per sample. Once measured the contact angle data was plotted and advancing and receding contact angles calculated using the instruments software.

Sessile drop technique (Described as contact angle (CA)) was also used to measure low density polyethylene (LDPE) samples during the characterisation of the plasma treatment and etching systems. This method involved producing between 5 and 10 static 5µl drops on the surface of a material, the contact angle was then measured on both sides per drop.

Before analysis of the plasma treatment could be achieved reliably the goniometer protocol required optimisation, the variation between drop sizes was tested on untreated low density PE samples (LDPE) films which was used as an analogue of the BioVyon™ surface.

Figure 2-4 indicates that a drop volume of between 2 and 5 µl was associated with the least variation in CA. It was also observed that as drop volume decreased lower than approximately 3µl there was a rapid decrease in CA. This effect was due to the relationship between drop surface tension and drop radius. After a threshold radius of curvature has been passed the drop surface tension has a negative effect on drop contact angle [267].

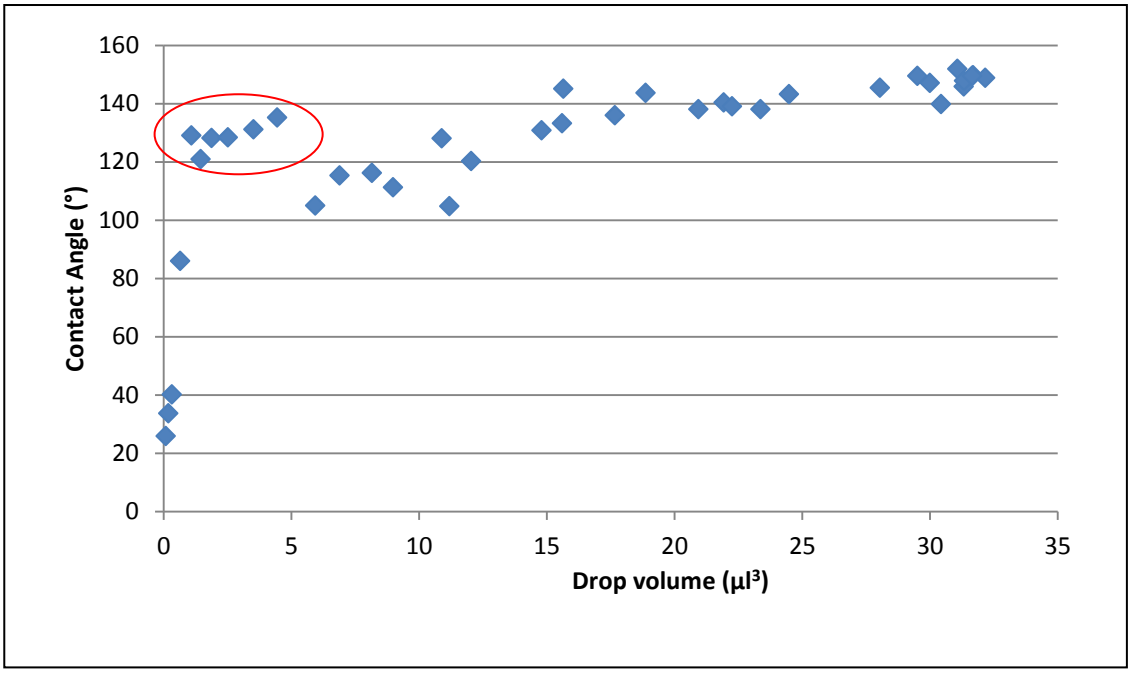

Figure 2-4: Effect of drop volume on contact angle

Drops of water were applied to untreated low density polyethylene film using a syringe and contact angle was measured. Circled region represents drop volume range with least variation; it can be seen that below 2µl there is a rapid increase in contact angle, above 5µl and there is a large amount of variation in CA from 100° to 160°.

2.2.9 Thionine Acetate

Biovyon™ F frits were plasma etched and incubated in atmosphere for 15 minutes prior to staining with thionine acetate (THA). The treated frits were then submerged in 500µl of 2.5mmol/L THA solution for 24 hours. After incubation stained frits were then washed three times with 100% ethanol and blotted with blotting paper to remove excess liquid in the porous frit structure. To cleave the bound THA molecules stained frits were submerged in 500µl 0.01mol/L HCL and diluted in 1:1 ethanol: water for 1.5 hours on a shaker. 300µl of the cleaved THA in solution was then transferred to a 96 well plate and measured using a spectrometer (Thermo, multiscan ascent) at 540nm; the THA concentration was calculated using the calibration curve in Figure 2-5.

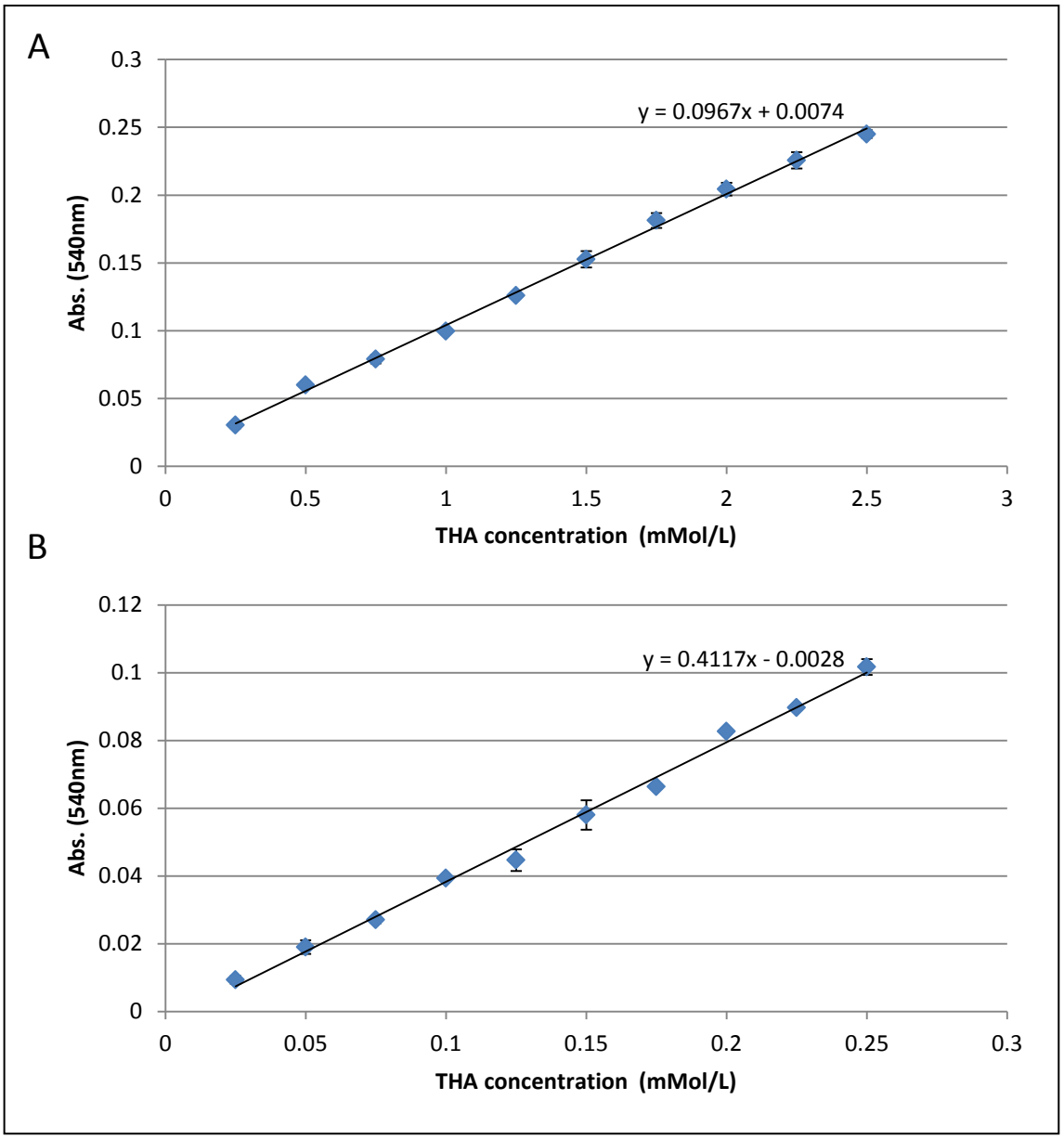

Figure 2-5: THA calibration curves

Increasing concentrations of THA in 300µl 0.01mol/L HCL and diluted in 1:1 ethanol: water, from 0.25 - 2.5 (mmol/L) (Graph A) and 0.025 – 0.25 (mmol/L) (Graph B) top and bottom graphs respectively. Absorbance was measured at 540nm. Line of best fit was used to calculate samples of unknown concentration via absorbance reading.

2.2.10 Toluidine blue

Biovyon™ F frits were plasma etched and incubated in atmosphere for 15 minutes prior to staining with toluidine blue (TBO). The treated frits were then submerged in 500µl of 0.25 mmol/L TBO solution for 6 hours. After incubation stained frits were then washed with 10ml RO water (Figure 2-6) and blotted with blotting paper to remove excess liquid in the porous frit structure. To cleave the bound TBO molecules stained frits were submerged in 500µl acetic acid (50% w/v) and placed on a shaker for 5 minutes. 300µl of the cleaved TBO in solution was then transferred to a 96 well plate and measured using a spectrometer (Thermo, multiscan ascent) at 595nm; the TBO concentration was calculated using the calibration curve in Figure 2-7.

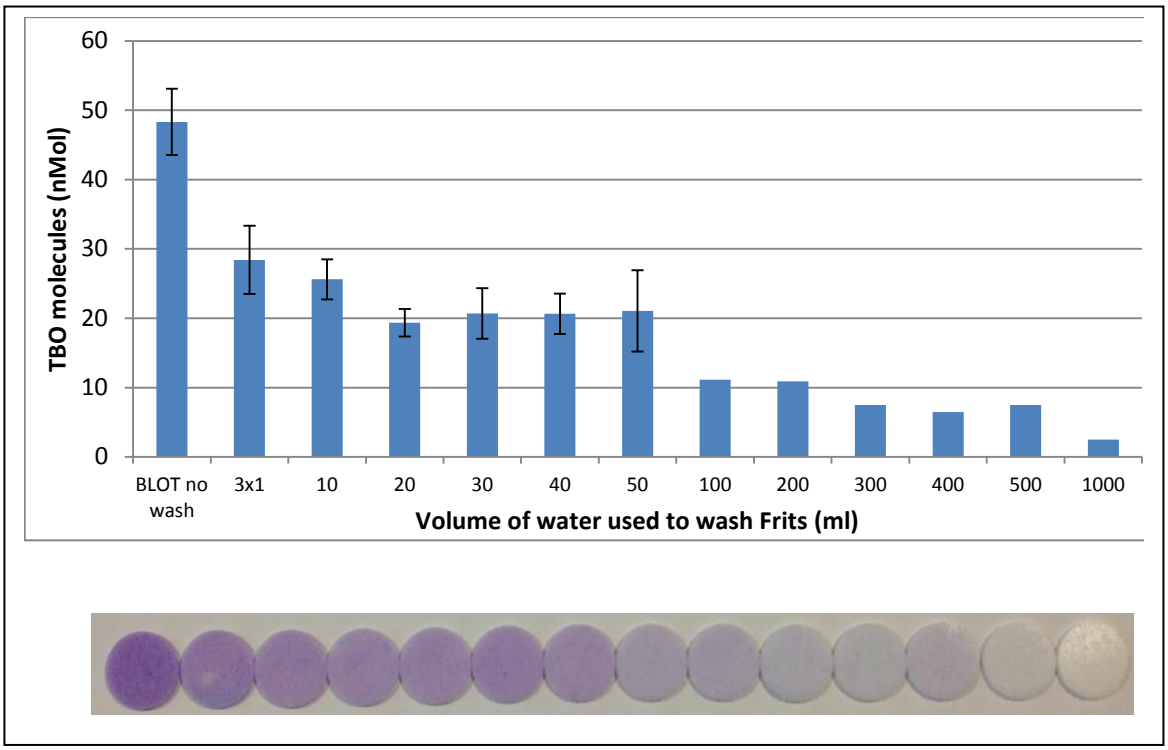

Figure 2-6: Optimal washing volume for toluidine blue assay

Graph and figure to show changes in toluidine blue (TBO) molecules bound to frits after washing with increasing volumes of RO water. Graph (top) indicates that larger volumes of water result in less TBO molecules remaining bound to the frit surface. This is reinforced by the image (Bottom) of frits after washing. A plateau in TBO molecules can be seen between 10ml and 50 ml, suggesting these are the smallest volumes capable of washing away unbound TBO molecules without removing significant quantities of bound TBO molecules.

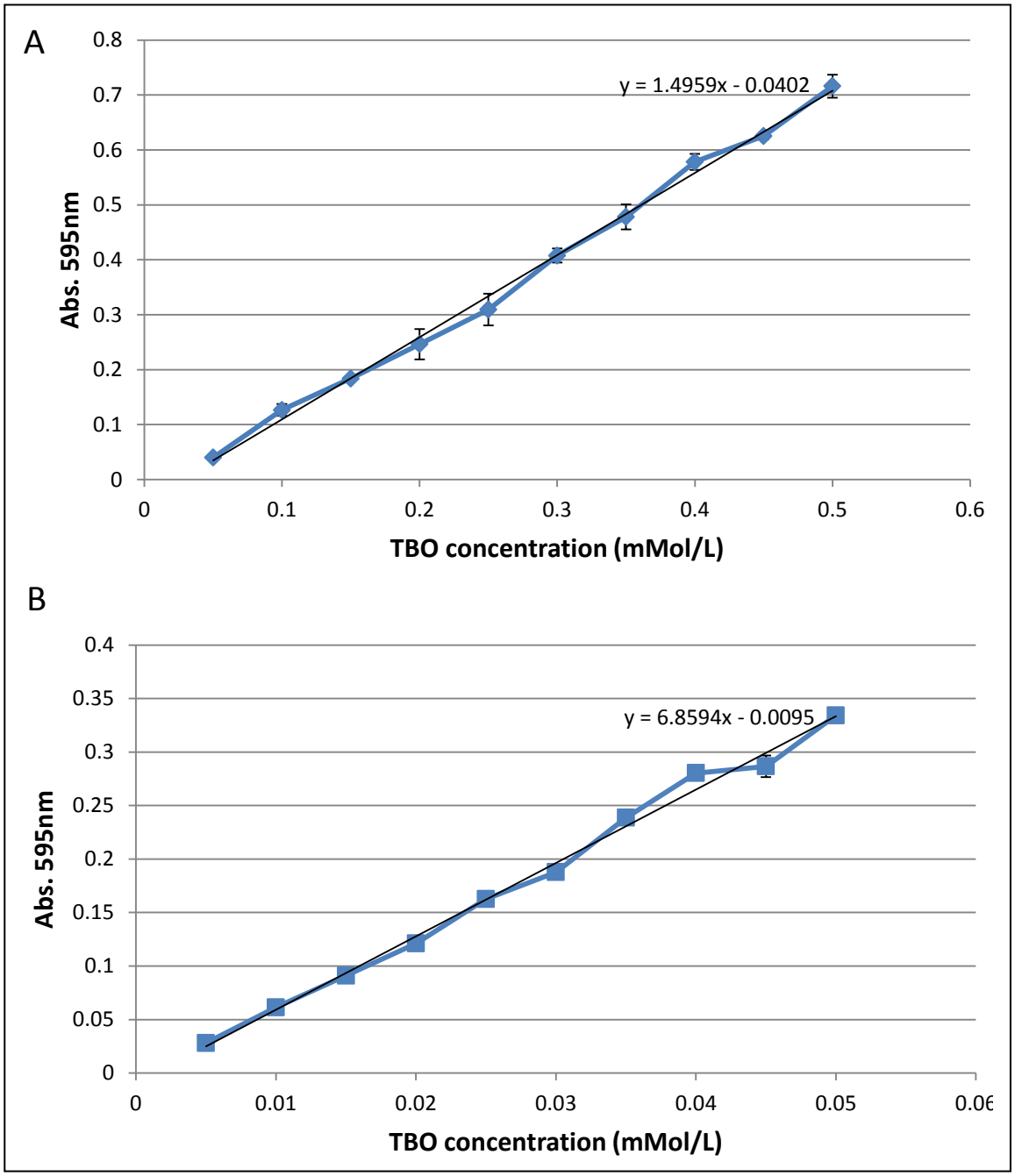

Figure 2-7: TBO calibration curves

Increasing concentrations of TBO in 300µl acetic acid (50% w/v), from 0.05 - 0.5 (mmol/L) (Graph A) and 0.005 – 0.05 (mmol/L) (Graph B) top and bottom graphs respectively. Absorbance was measured at 595nm. Line of best fit was used to calculate samples of unknown concentration via absorbance reading.

2.2.11 Fourier transform infrared spectroscopy

BioVyon™ frits were analysed using attenuated total reflectance (ATR) Fourier transform infrared spectroscopy (FTIR), performed on a spectrum 65 FTIR spectrometer (Perkin Elmer, Cambridge, UK). Frits were clamped down onto a Germanium crystal surface. 4 scans were performed at a 4cm^{-1} resolution between 4000-650cm^{-1}.

2.2.12 Atomic force microscopy

Imaging and surface roughness measurements were carried out using a Nanoscope III atomic force microscope (AFM) (Digital Instruments), a silicon nitride micro cantilever "tip" was used to image the samples. BioVyon™ frits possess one side which has been smoothed by the action of heating and contact with a flat edge during production, this was exploited for roughness measurement. 8 scans were completed for 5 different samples, 4 scans were completed on individual untreated frits, another 4 in the same location after plasma etching for 60 seconds at 0.8 mbar at 60 Watts. Scans were produced at room temperature at a rate of 0.5Hz, scan sizes ranged from 50, 10, 5 and 1µm respectively per frit. Scan data scales are presented at 1, 0.3, 0.3 and 0.1µm for each size respectively. Roughness measurements were calculated by the instrument software and are presented as root mean-squared (RMS). Difference in roughness was calculated by subtracting roughness measurements of untreated frits from plasma etched frits for each scan size.

2.2.13 Scanning electron microscopy

Prior to analysis frits were sectioned and positioned appropriately on metal stubs for analysis with scanning electron microscope (SEM). Samples were sputter coated in 4nm of palladium and 2nm of platinum for analysis on EVO LS15 SEM (Oxford instruments, Abingdon, UK), or Σigma SEM (Oxford instruments, Abingdon, UK), respectively. Samples were magnified and images generated at 100, 1000, 20,000, 50,000 and 100,000 times magnification.

2.2.14 Silane linker modification

Plasma etched BioVyon™ frits were submerged in 10ml of a 50, 10, 1 and 0.1% 3-Aminopropyltriethoxysilane (APTES) solution diluted in toluene, and incubated for 24 hours at 90°C. Once dried, frits were washed three times with 1ml PBS to remove excess, unlinked APTES.

2.2.15 Methyl orange (MO)

Frits were transferred to a 24 well plate and submerged in 500µl of 0.016% (w/v) MO dissolved in 0.1 molar solution of sodium dihydrogen phosphate (PH 4.7). Frits were shaken at 200rpm for 1 hour before being washed three times with RO water. MO molecules were removed from NH_2 groups by the addition of 500µl 100% ethanol. 50µl samples were then transferred to a 96 well plate and the absorbance measured using a spectrometer (Thermo, multiscan ascent) at 492nm. The MO concentration was then calculated using the calibration curve (Figure 2-8).

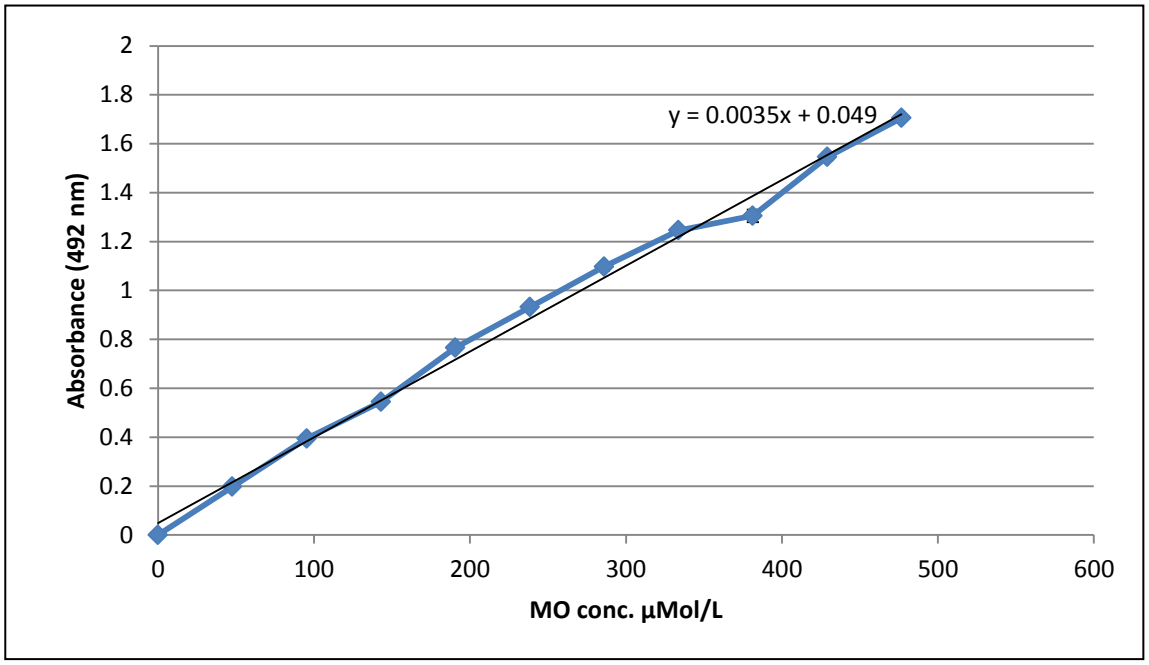

Figure 2-8: MO calibration curve

Increasing concentrations of MO in 50µl 100% ethanol from 0 - 500 (µmol/L). Absorbance was measured at 595nm. Line of best fit was used to calculate samples of unknown concentration via absorbance reading.

2.2.16 Min-6 cell culture

In 1990 the mouse insulinoma (Min-6) cell line was established. Transgenic mice were created by microinjecting a human insulin promoter gene connected to the SV40 T antigen gene into the pronuclei of mouse eggs. Once grown, the founding mice developed pancreatic tumours at 13 weeks from which the novel cell line was harvested [199].

Min-6 cells were incubated in humidified 5% CO_2/95% air at 37°C. DMEM 5mmol/L glucose with L-glutamine, 25mmol/L HEPES culture media was supplemented with 10% Foetal bovine serum (FBS) and 1% penicillin/streptomycin. Cells were passaged by trypsinisation (concentrated Trypsin/EDTA) at approximately 80% confluency and were not used above a passage number of 35.

In order to ascertain the rate of proliferation or doubling time within the Min-6 cell line a known number of Min-6 were seeded and the number counted after 6 days of culture. The data obtained was used to calculate the theoretical population doubling time (Figure 2-9) using the equation below:

Population doubling time = 3.32 (Log number harvested – Log number seeded) / time of culture

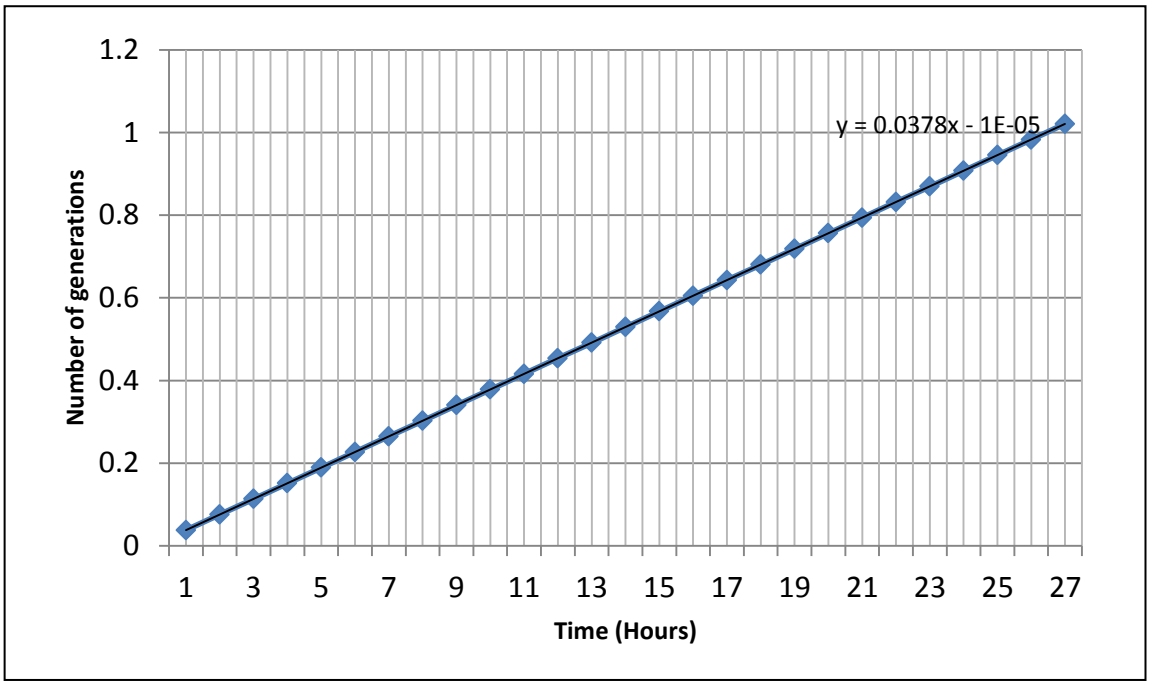

Figure 2-9: Min-6 population doubling time

Three T75 flasks were seeded with cell suspension containing 435,000 Min-6 using a method similar to that described in Section 2.2.16.2. And cultured for 6 days, 12ml of media (Described in section 2.2.16) was replaced every two days. After culture, cell populations were trypsinised and counted using a haemocytometer. A theoretical population doubling time was calculated from the data obtained. Graph shows linear increase in generations over time.

2.2.16.1 Preparation of BioVyon™ frits for cell culture.

Plasma etched frits were washed in 10 ml RO water and blotted on blotting paper, before being transferred to a 24well plate and submerged in 70% ethanol for 30 minutes. After sterilisation, first were washed three times with Phosphate buffered saline (PBS) consisting of 1M potassium phosphate (Monobasic and dibasic) and 5M sodium chloride (pH ~ 7.4) , and transferred to a 24 well suspension plate using forceps sterilised with a flame prior to manipulation. Frits were treated in triplicate with 40µl of a protein solution; DMEM (10% FBS) and basement membrane proteins (BM) derived from the Engelbreth-Holm-swarm murine sarcoma cell line (Sigma Aldrich, Gillingham, UK). Collagen (250µg/ml), laminin (250µg/ml) and a combination of both at 125µg/ml), were pipetted onto the centre of sterile frits and incubated for 2 hours. After incubation frits were diluted with 200µl of PBS and 50 µl samples were collected for analysis using the Bichonininic acid (BCA) assay (Section 2.2.17). Frits were then washed once with PBS and blotted on sterile blotting paper; dried, coated frits were stored at 4°C prior to cell seeding.

2.2.16.2 Cell seeding on frits

Min-6 of a passage number below P35 were cultured for a minimum of 5 days on T-75 flasks prior to being washed with approximately 12ml of PBS and trypsinised using 2ml of ×1 trypsin solution. Cells were incubated at 37°C for 5 minutes and observed until cell populations were seen to have lifted from the flask surface. 8ml of 10% DMEM was added to each flask being trypsinised and transferred to a 10ml tube for centrifuging at

500G for 5 minutes (Hereaus multifuge 2, Kendro laboratory products). Media was then aspirated from the cell pellets, which were re-suspended in 500µl - 1ml of culture media (Re-suspension media either supplemented with 10% FBS or serum free depending on the experiment), 10µl samples of the cell suspension were removed and counted using a haemocytometer.

After counting and calculation of cell number $1x10^6$ Min-6 were seeded via capillary action, at a volume ≤ 60µl, to the centre of sterile treated BioVyon™ F frits in 24 well suspension plates. Seeded frits were normally incubated at 37°C for 2 hours (Adhesion incubation time varied between experiments). After adhesion, frits were washed three times with PBS to remove unadhered cells and transferred to new 24 well suspension plates using sterile forceps, frits were re-suspended in 1ml low glucose DMEM (10% FBS). Entire volume of media was replaced after the first 24 hours; after which 500µl of media volume was changed every 24 hours. 12 well plates functioned as TCP controls and possessed an approximate, comparative surface area to a 1x14mm Biovyon™ frit. Seeding protocol was identical, except during the addition of cell populations in which 1ml of media was added to seeded cell volume to ensure entire surface of the wells was submerged.

Min-6 were seeded onto the frits using basic capillary action, after a set incubation time capillary action was used to wash away unadhered cells, adhered cells are exposed to a shear force that remains consistent between experiements, as described in previous literature [156].

2.2.16.3 Glucose challenge and insulin secretion

After 3, 9 and 15 days of incubation BioVyon™ frits harbouring Min-6 populations were washed three times with PBS and transferred to a new 24 well suspension plate, and submerged in 1ml of 0mmol/L glucose DMEM (10% FBS) for 1 hour at 37°C. After incubation frits were washed three times with PBS and transferred to a new 24 well suspension plate, and submerged in 1ml of 25mmol/L glucose DMEM (10% FBS) for 1 hour at 37°C. After incubation, 1ml of the surrounding media was collected and stored in eppendorf tubes at -20°C. Samples collected for data on Min-6 insulin secretion to a range of glucose concentrations (Figure 5-22)**,** were submerged in 1ml of 5mmol/L, 0mmol/L and 25mmol/L glucose with three PBS washes in between. Each 1ml sample was collected and stored in Eppendorf tubes at -20°C.

A two site solid phase enzyme Insulin immunoassay (Mercodia, Uppsala, Sweden) was used to quantify insulin secretion from Min-6 populations in response to increased glucose levels in the surrounding media. Samples were thawed at 37°C and diluted 1:50 (20µl in 980µl PBS) for 3 days and 1:100 (10µl in 990µl) PBS for 9 and 15 day time points. Once diluted, Insulin concentration in each sample was obtained following the assay protocol. 10 µl of each sample was pipetted into the ELISA 96 well plate, 100µl of a prepared enzyme conjugate solution was added to the samples and the plate was incubated for 2 hours on a plate shaker, at room temperature. Plate was then inverted to move conjugate solution and washed six times with 200µl wash buffer; between each wash the plate was tapped firmly against absorbent paper to remove excess liquid. 200 µl of substrate solution was added to wells post washing procedure and incubated for

15 minutes at room temperature. Finally 50µl of stop solution was added to each well and the plate was read using a spectrometer (Thermo, multiscan ascent) at 450nm. Sample absorbance values were compared against calibration curve to quantify insulin content (Figure 2-10).

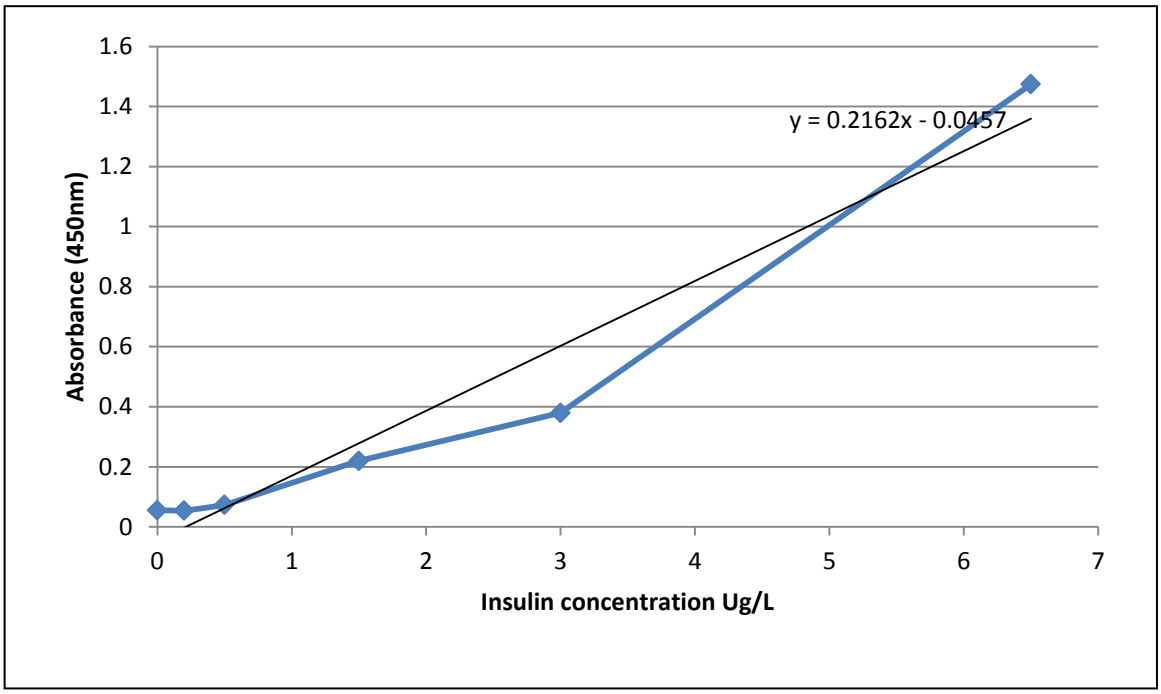

Figure 2-10: Insulin ELISA calibration curve

Calibration curve was generated by pipetting 10 µl of 6.5, 3, 1.5, 0.5, 0.2 µg/L control samples into an ELISA 96 well plate, 100µl of a prepared enzyme conjugate solution was added to the samples and the plate was incubated for 2 hours on a plate shaker, at room temperature. Plate was then inverted to move conjugate solution and washed six times with 200µl wash buffer; between each wash the plate was tapped firmly against absorbent paper to remove excess liquid. 200 µl of substrate solution was added to wells post washing procedure and incubated for 15 minutes at room temperature. Finally 50µl of stop solution was added to each well and the plate was then measured using a spectrometer (Thermo, multiscan ascent.) at 450nm; Line of best fit was used to calculate samples of unknown concentration via absorbance reading.

2.2.16.4 Cell quantification with Lactate dehydrogenase assay (LDH)

A cyto tox 96® non-radioactive cytotoxicity assay (Promega, Southampton, UK) was modified to quantify total cell population. Before seeding onto Biovyon™ or tissue culture plastic (TCP) controls a calibration curve was generated by counting and quantifying lactate dehydrogenase (LDH) in cell populations from 1 $x10^6$ down to 1 $x10^5$, with samples every 100,000 cells. These populations were pipetted into 3ml tubes and quantified using the same method as the frits and TCP. A calibration curve was generated for each experiment to ensure a cell population with the same passage number was used to calibrate cell number. Frits were transferred to a new 24 well plates and, along with TCP controls, washed three times with PBS to remove unadhered cells after culture for specific periods of time. Cell populations adhered to Frits, TCP controls and in calibration samples were submerged in 200µl lysis solution (9% triton X diluted in RO water) and incubated for 45 minutes at 37°C.

Once lysed the cell supernatant for each frit was diluted with 200 µl PBS to aid diffusion of the LDH in solution throughout the frit structure. All other samples were diluted with 260 µl to account for excess liquid contained within the Frit structure prior to lysis. Three 50µl samples of supernatant were transferred to a 96 well plate for quantification with LDH assay (samples were also collected for analysis using the BCA assay total protein). The absorbance values of LDH in the samples were obtained following the assay protocol, assay substrate was reconstituted in 12ml thawed assay buffer, 50µl of

substrate mix was added to the supernatant samples and incubated protected from light for 30 minutes. Samples were then measured using a spectrometer (Thermo, multiscan ascent) at 492nm; cell population number was calibrated against a standard curve unique to its initial passage number (Figure 2-11).

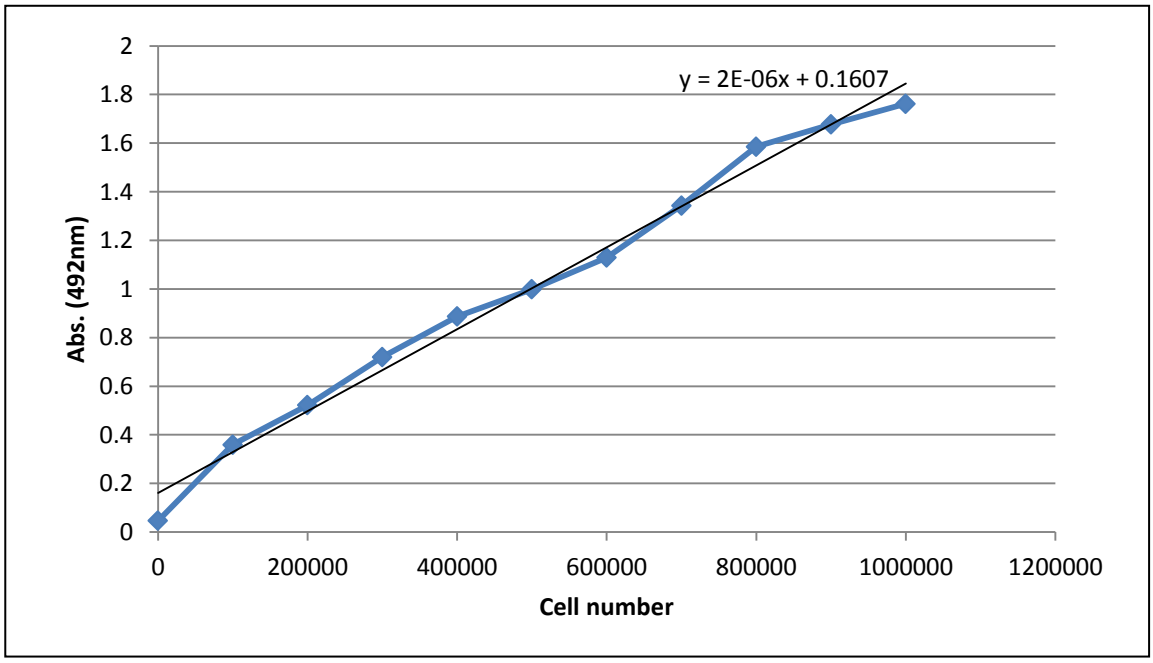

Figure 2-11: LDH Calibration Curve

Calibration curve was generated by counting cell populations from $1x10^6$ down to $1 x10^5$, with samples every 100,000 cells. Three 50µl aliquots of supernatant were transferred to a 96 well plate for measurement with LDH assay. The absorbance values of LDH in the samples were obtained following the assay protocol, assay substrate was reconstituted in 12ml thawed assay buffer. 50µl of substrate mix was added to the supernatant samples and incubated protected from light for 30 minutes. Samples were then measured using a spectrometer (Thermo, multiscan ascent.) at 492nm; Line of best fit was used to calculate samples of unknown concentration via absorbance reading.

2.2.16.5 Cell imaging

Fluorescent stains were used to visualise cell populations on top and within the BioVyon™ frit structure, once stained frits were observed under fluorescent microscopy (Axiovert 25, HBO 50) and under a confocal laser scanning microscope (Leica TCS, SP5). Before staining all frits containing cell populations were washed three times with PBS and transferred to a new 24 well plate.

2.2.16.6 Hoescht and Propidium Iodide (HPI)

0.1 mg of Bisbenzimide (H33258) powder (Sigma, Gillingham, UK) was dissolved in Dimethyl sulphoxide (DMSO), to generate a stock solution of 0.1mg/ml; this was diluted further 1:10 to 10µg/ml for the working solution. 50µl aliquots of bisbenzimide working solution were mixed with 50 µl of 0.1mg/ml propidium iodide and diluted in 900µl cell culture media prior to cell staining. 200µl of the HPI stain was pipetted onto the frits, which were protected from sunlight for 5 minutes before observation under fluorescence microscopy.

2.2.16.7 Calcein AM

1 mg of Acetomethoxy derivative Calcein (Calcein AM) (Sigma, Gillingham, UK) was dissolved in 1ml DMSO to generate a stock solution of 1mg/ml; 10µl aliquots were diluted in 5ml of media to make a 2µg/ml working solution. 250µl of the working

solution was pipetted onto the frits and protected from sunlight during observation under fluorescence microscopy.

2.2.16.8 Phalloidin

0.1 mg of Phalloidin (Sigma, Gillingham, UK) was dissolved in 1ml of DMSO to generate a stock solution of 0.1mg/ml; 10µl aliquots were diluted in 1ml of media to make a 10µg/ml working solution. 250µl of the working solution was pipetted onto the frits and protected from sunlight during observation under fluorescence microscopy.

2.2.17 Protein assay

A Bichonininc acid (BCA) assay (Thermo scientific) was used to measure protein free in solution, protein bound to the surface of frits , removed from the frits and total protein in lysed cell supernantents. In each case the assay working reagent was made up from a solution of reagent A (Sodium carbonate, sodium bicarbonate, bicinchoninic acid and sodium tartrate in 0.1M sodium hydroxide) and reagent B (4% cupric sulphate) combined at a ratio of 50:1.

Bound protein samples were prepared using the same protocol in 2.2.16.1, however, once the protein was absorbed to the surface, BioVyon™ frits were washed once in PBS, blotted dry and 500µl working reagent (WR) added to the frits directly, after 1 hour 300µl samples per frit were collected and measured at 1 and 48 hours.

Bound protein was also calculated using the reverse method, once protein was adsorbed to the surface, BioVyon™ frits were diluted in 200 µl PBS and 50µl samples

incubated with 625 µl of working reagent for 1 and 48 hours. The quantity of protein bound was calculated by subtracting the amount free in solution from the amount added to the frits.

To remove protein once bound samples were prepared using the same protocol in 2.2.16.1, frits were then submerged in 250µl of a 1% sodium dodecyl sulphate (SDS) solution, and incubated for 1 hour. SDS and unbound protein were then diluted with 750µl PBS, 25µl samples were transferred to a 96 well plate and incubated with 200µl BCA working reagent for 30 minutes before measurement at 1 hour.

The preparation of protein samples free in solution is described in section 2.2.16.1, Increasing concentrations of each protein used to treat the BioVyon™ frits were used to construct calibration curves, protein concentration of unknown protein sample were then quantified using the calibration curve. 5 - 50µl volume samples of FBS, Collagen, Laminin and Laminin/Collagen increasing in 5µl accumulations were diluted to a total volume of 50µl. These samples were measured at 1 and 48 hours.

All 50µl samples were then incubated with 625µl of BCA working reagent for 1 or 48 hours depending on the experiment. Two 300µl samples of the protein/WR solution were collected and transferred to a 96 well plate before being measured. All samples measurements were acheived using a spectrometer (Thermo, multiscan ascent) at 540nm; the protein concentration was calculated using the calibration curves in Figure 2-12 and Figure 2-13.

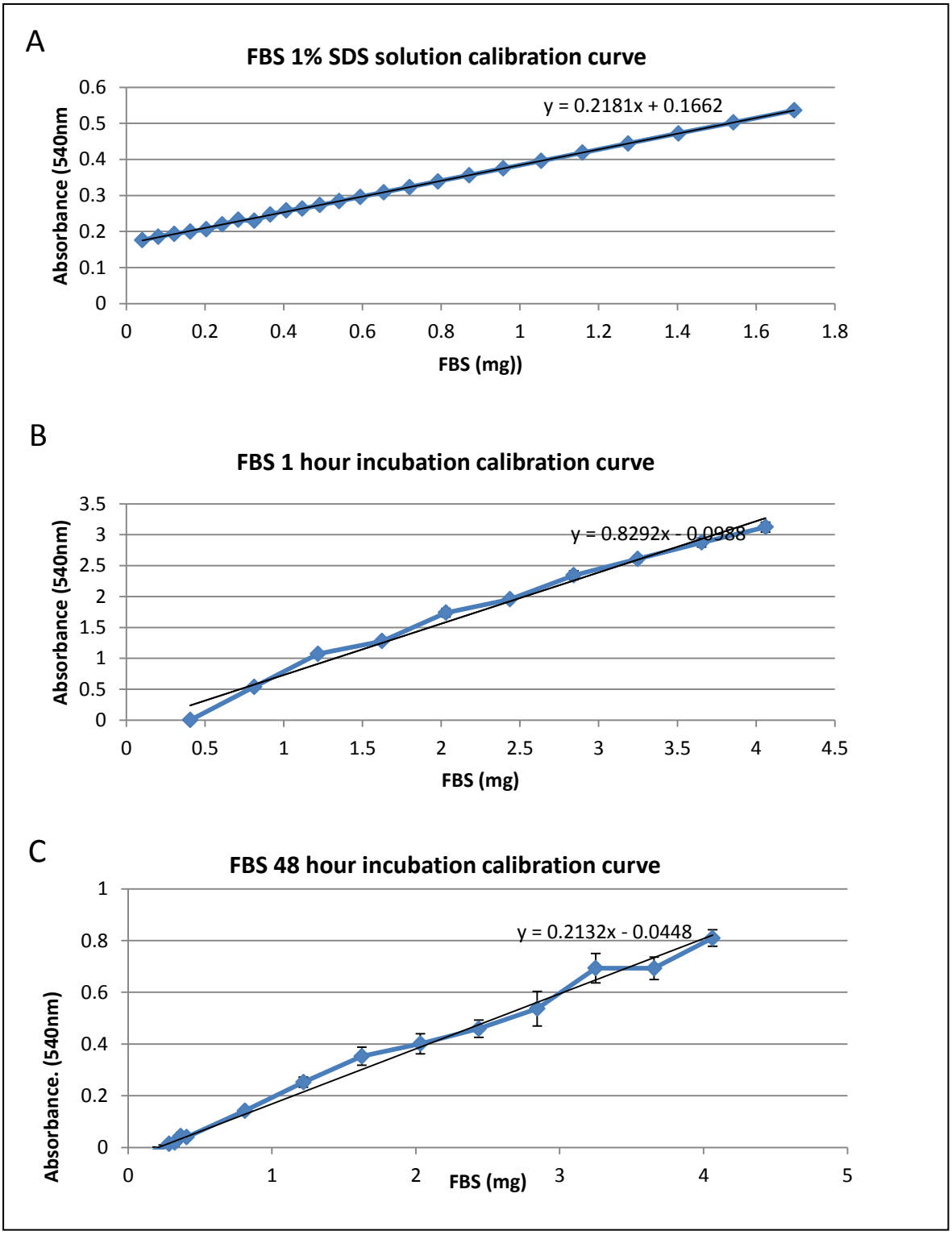

Figure 2-12: BCA calibration curves

Increasing concentrations of: 25µl samples of foetal bovine serum (FBS) 1% SDS solution incubated for 30 minutes in 200µl Bichonininc acid (BCA) working reagent (WR) (Graph A), 50µl samples of FBS incubated for 1 hour in 625µl BCA WR (Graph B), 50µl samples of FBS incubated for 48 hours in 625µl BCA WR (Graph C) Concentrations increase from 0.0406 – 1.7mg for FBS in SDS(Graph A), 0.406 – 4.06mg for FBS (Graphs B and C) Line of best fit was used to calculate samples of unknown concentration via absorbance reading.

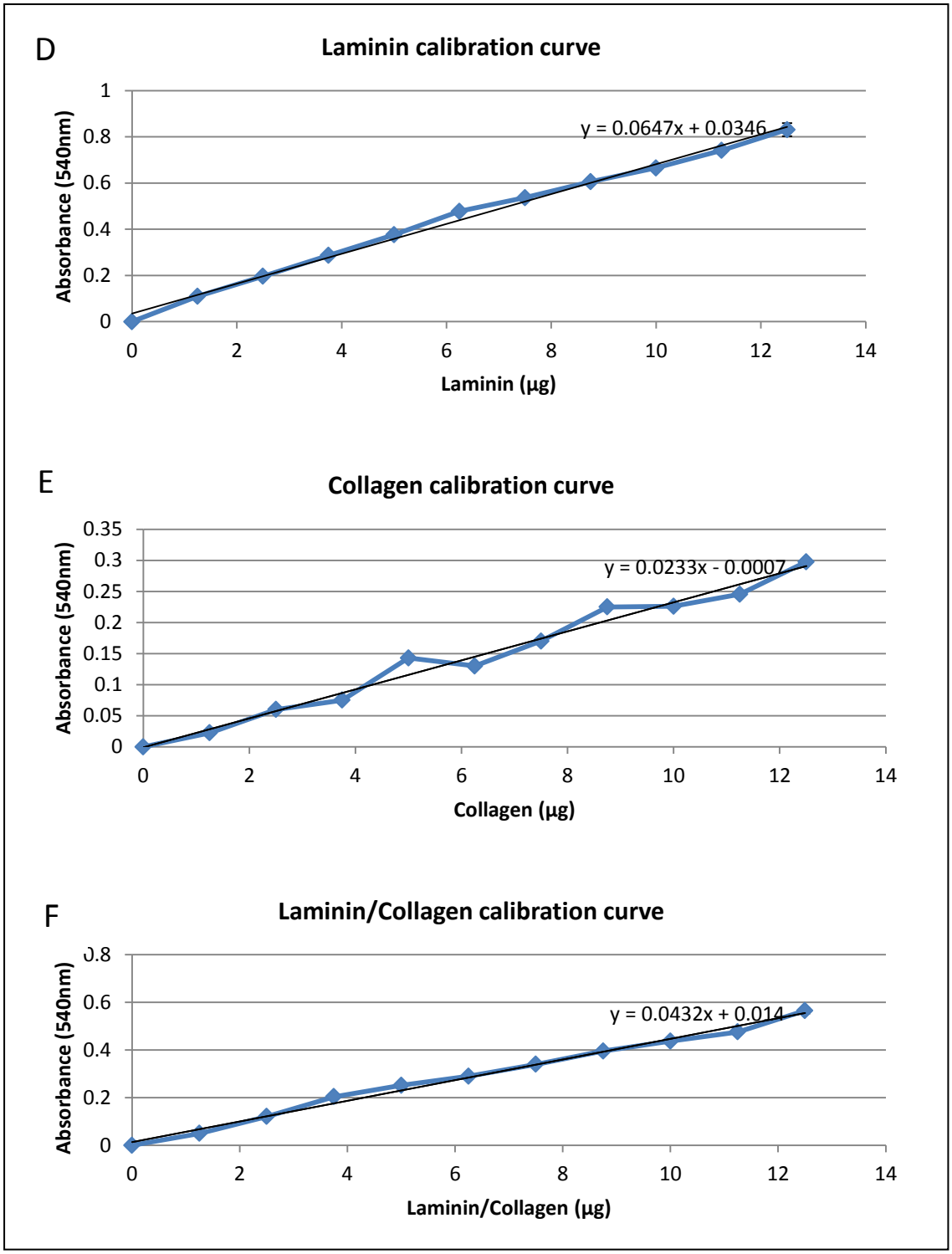

Figure 2-13: BCA calibration curves

Increasing concentrations of: 50µl Laminin samples incubated for 1 hour in 625µl of BCA WR (Graph D), 50µl of Collagen samples incubated for 1 hour in 625µl of BCA WR (Graph E) and 50µl of Lamini/Collagen samples incubated for 1 hour in 625µl of BCA WR (Graph F). Concentrations increase from 1.25 – 12.5µg of Laminin, collagen and laminin/collagen (Graphs D-F). Absorbance was measured at 540nm. Line of best fit was used to calculate samples of unknown concentration via absorbance reading.

3 BioVyon™ characterisation

3.1 Introduction

All biomaterials must undergo an in-depth characterisation before coming into contact with cells. Initial assessment of the constituent materials and the manufacturing process used to generate the biomaterial is vital to ascertain overall suitability as a cell culture environment. Various factors could potentially make a biomaterial unsuitable, such as residual chemicals from the manufacturing process causing cytotoxicity, genotoxicity and carcinogenicity [268].

Biomaterial structure is another important factor to consider, a cell-harbouring biomaterial must possess a high level of porosity and interconnectivity aiding nutrient and oxygen flow via diffusion [269]. Furthermore the biomaterial surface chemistry must allow cellular adhesion, spreading and differentiation via conjugation of peptides and growth factors [119, 270]. In order to develop BioVyon™ into a functional biomaterial capable of harbouring large cell populations, a detailed characterisation of its structure, surface chemistry and surface area was required. Understanding of this would aid the augmentation and conditioning of the BioVyon™ for cellular adhesion and growth.

3.2 BioVyon™ internal structure

In order to characterise BioVyon™ frits, porometry and porosimetry were used to analyse the internal 3D structure. Different grades of high density polyethylene (HDPE) powder were sintered to form M, F and HP BioVyon™ frits. These frits were analysed to calculate the pore size, void volume and surface area. This data was then used to choose an appropriate grade to use in the remainder of the investigation.

3.2.1 Porometry

A liquid of known surface tension was used to wet the BioVyon™ M, F and HP grade frits. Increasing pressure was then exerted on the frit until all liquid in the pores was displaced with gas. The average pore diameter of the frits was extrapolated by calculating the pressure required for liquid displacement. The frit weights and the density of the PE powders were recorded to find the frit volumes.

	Pore size (µm)		
Name	Min	Max	Mean
Vyon M	7.24 ± 2.26	56.63 ± 23.9	15.4 ± 7.12
Vyon F (Median)	15.25 ± 7.75	83.9 ± 61.26	55.9 ± 33.23
Vyon HP (Coarse)	14.77 ± 3.55	83.9 ± 0	43.5 ± 12.25

Table 3-1: Frit pore size

Porometry data showing frit minimum, maximum and average pore size. Three different high density polyethylene powder grades were used to sinter 25 x 3 mm frits, these where then used with the porometer to calculate pore size.

Name	Volume (cc)	Apparent density (g/cc)	Theoretical density (g/cc)	Void volume
Vyon M	1.47262	0.546645	1.41312	43%
Vyon F (Median)	1.47262	0.504543	1.41312	47%
Vyon HP (coarse)	1.47262	0.608439	1.41312	37%

Table 3-2: Frit dimensions and density

Porometry data showing frit volume, apparent density, theoretical density and percentage void volume. Three different high density polyethylene powder grades were used to sinter 25 x 3 mm frits, these where then used with the porometer to calculate void volume.

Table 3-1 shows that BioVyon™ grades M and F possess the lowest and highest mean pore sizes, respectively. Vyon M holds the lowest pore sizes due to the small particulate size of the constituent HDPE powder. The relatively high void volume (Table 3-2) combined with the low average pore size is likely due to a high porosity.

The larger grade particles rendering BioVyon™ F and HP share similar pore sizes, but different void volumes (Table 3-1 and Table 3-2). The higher void volume of BioVyon™ F is due to a high mean pore size in combination with a lower particulate size. Overall the data shows that Vyon F offers the highest void volume and largest mean pore size; this in turn indicates that it will provide the highest porosity and surface area.

3.2.2 Porosimetry

BioVyon™ F frits were analysed further using mercury porosimetry, untreated and frits plasma etched for 120 seconds were cut in half to fit into the mercury chamber prior to weighing. Liquid mercury was intruded and extruded throughout the Biovyon™ structure, the pressures required were recorded and the Quantachrome Autosorb data reduction software calculated the Vyon F surface area at approximately 45.4 cm^2/g prior to plasma etching. The porosimetry data supports the porometry data in Table 3-1; the largest peak indicates that there is an average pore size of 70µm (Figure 3-1). The smaller peak between 600-900 µm represents the voids between the sample and the walls of the chamber.

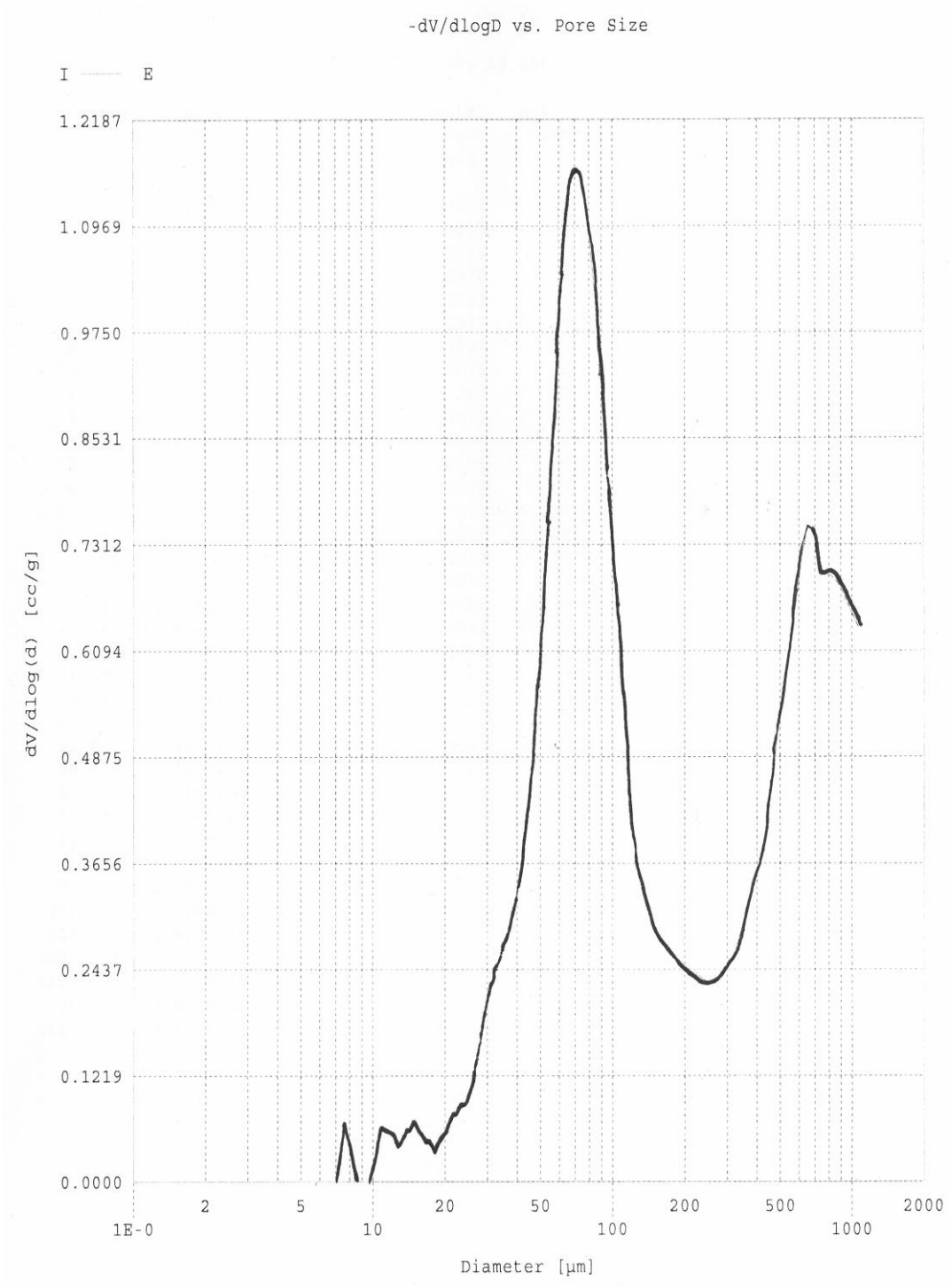

Figure 3-1: Average pore size of Vyon F frit

Graph to show the mean pore size of a BioVyon™ F frit, calculated by Quantachrome Autosorb data reduction software. Peak at 70µm represents the average sized pore throughout the frit structure.

3.3 BioVyon™ surface chemistry

To create an internal environment suitable for cell culture the hydrophobic, untreated BioVyon™ was exposed to oxygen based plasma. Plasma functioned to modify the surface chemistry throughout the BioVyon™ frits internal structure. It was necessary to investigate the effects of plasma for several reasons; quantifying the effect of oxygen plasma made it possible to optimise the methodology. Factors affecting plasma intensity were identified and maintained to prevent inconsistencies between plasma treatment runs. By using well established quantification techniques this work was directly comparable to previous literature [166, 266].

3.3.1 Characterising the plasma systems

Plasma treatment (PT) functions to add oxygen groups to the surface of polymer. It is commonly used in tissue engineering to aid cellular adhesion and integration of proteins onto polymer surfaces [162]. Oxygen moieties generated can function as anchors for the conjugation of other more complex molecules promoting cellular growth and differentiation [271].

There are various types of plasma generating apparatus all of which function influencing the surface chemistry of inert materials [147]. This study incorporated cold plasma via a polaron barrel etcher and a larger industrial model (Section 2.2.7). Plasma itself, is a state of matter consisting of highly energetic moieties excited by radio frequency [147]. Chamber size, mass of the sample being treated, wattage, pressure and time of contact

are all factors that may affect the intensity of plasma and in turn the density of oxygen groups generated on polymer based materials.

In order to quantify the effects of plasma on the BioVyon™ surface, contact angle (CA) goniometry was used to measure surface wettability. This method observes the effect of a materials surface energy on a drop of sessile water. Known volumes of water are placed on the surface of a material, the angle at which the periphery of the drop meets the surface is measured. This angle acts as a measurable boundary condition, providing a consistent quantification of surface polarity. Contact angle goniometry is a well-defined and commonly used method to characterise surface wettability [267, 272, 273]. Wattage and pressure are known to be key factors influencing plasma, in order to quantify their impact on BioVyon™ analogues were treated at varying watts and pressures prior to analysis of CA. Figure 3-2 indicates a consistent surface chemistry is generated between 60 and 10 watts, with a significant increase in CA at 5 watts ($P<0.001$).

Low density polyethylene (LDPE) films were plasma etched at a range of different chamber pressures at 60 watts for 120 seconds and the CA generated was measured. A trend can be seen in Figure 3-3, as chamber pressure decreases so does the CA, more hydrophilicity is generated at lower pressure with a significant difference between 4 and 1 mbar ($P<0.05$).

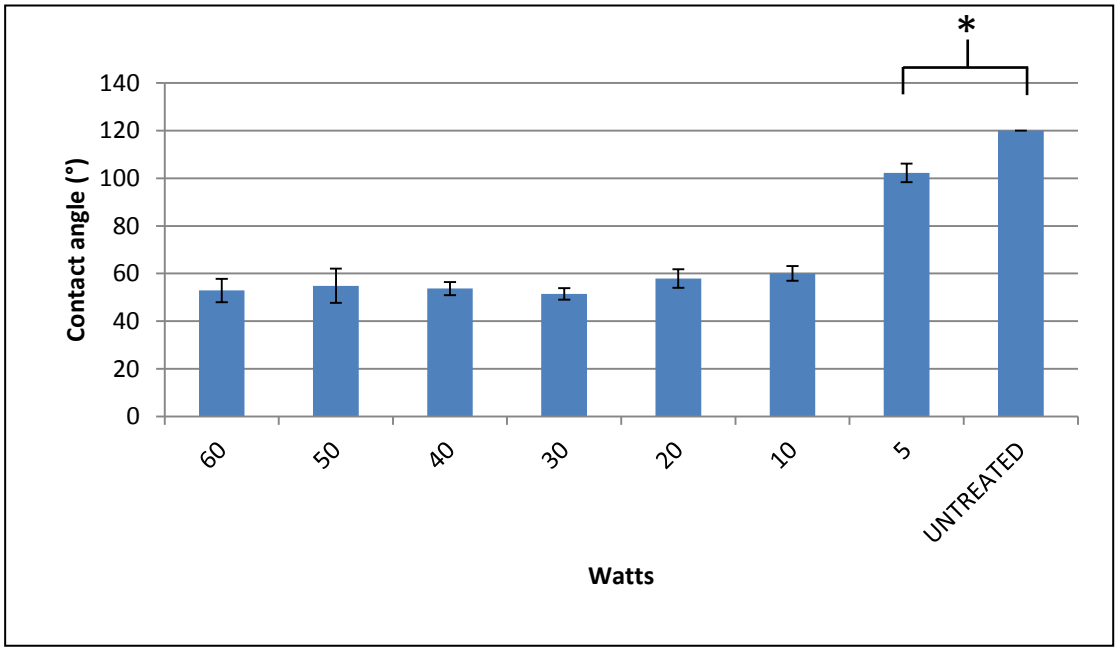

Figure 3-2: CA and increasing Watts

Low density polyethylene films were plasma etched for 120 seconds, at a range of Watts between 60 and 5. Contact angle (°) of water was measured 5 times along each plasma etched film and compared; error bars represent standard deviation between average ARCA of ≥ 4 different samples. Graph shows a increase in CA from 60 to 10 watts, with a statistically significant increase at 5 watts and the untreated sample ($P<0.001$). * indicates contact angles significantly different to other treatments.

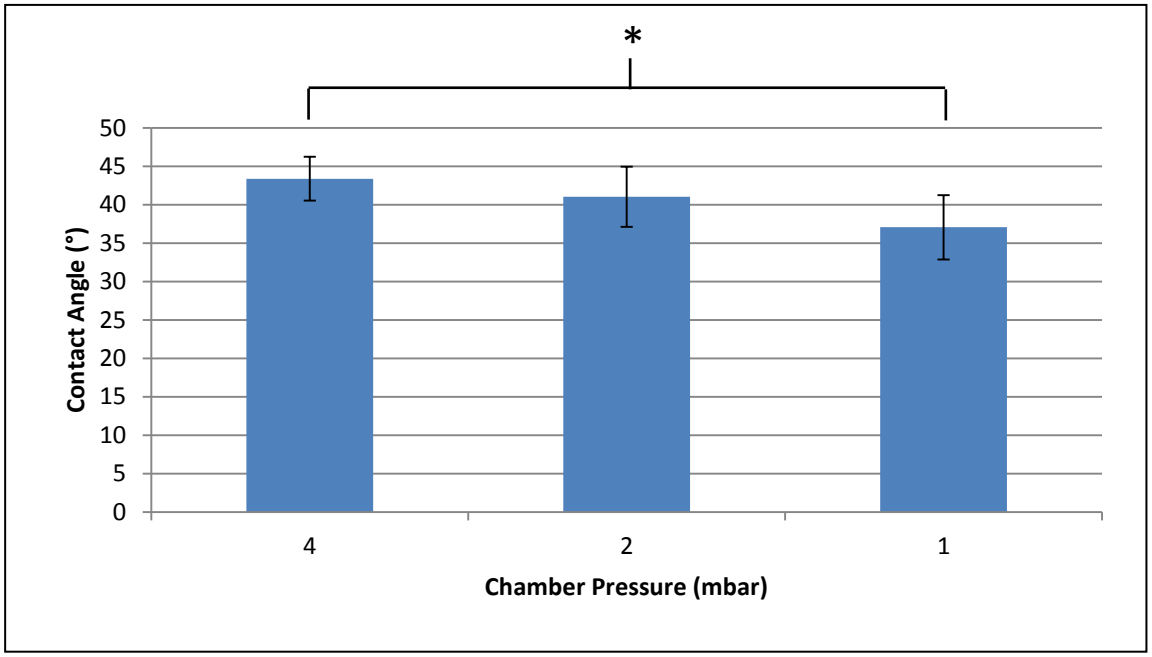

Figure 3-3: CA and increasing chamber pressure

Low density polyethylene films were plasma etched for 2 minutes at 60 watts at a chamber pressure of 4, 2 and 1 mbar. Contact angle (°) of water was measured 5 times along each plasma etched film and compared; error bars represent standard deviation between average ARCA of≥ 4 different samples. Graph shows a decrease in contact angle with decreasing chamber pressure, and a significant difference in the contact angle between 4 and 1mbar ($P<0.05$), as indicated by *

One of the most significant factors effecting surface wettability is plasma contact time. In order to quantify the effects of increasing plasma contact time HDPE films were plasma etched for 15, 30 and 60 seconds and wettability measured using ARCA. It is important to note that samples exposed to plasma longer than 60 seconds were not compatible with the ARCA analysis as the CA was too low to read accurately. It is clear from Figure 3-4 and Figure 3-5 that CA decreases significantly with increasing plasma contact time with the exception of 30 and 60 seconds - between which there is no statistically significant difference ($P<0.05$). A CA range of between 100 and 10˚ can be generated after relatively low exposure time, indicating that plasma treatment time is the most labile parameter influencing HDPE surface chemistry.

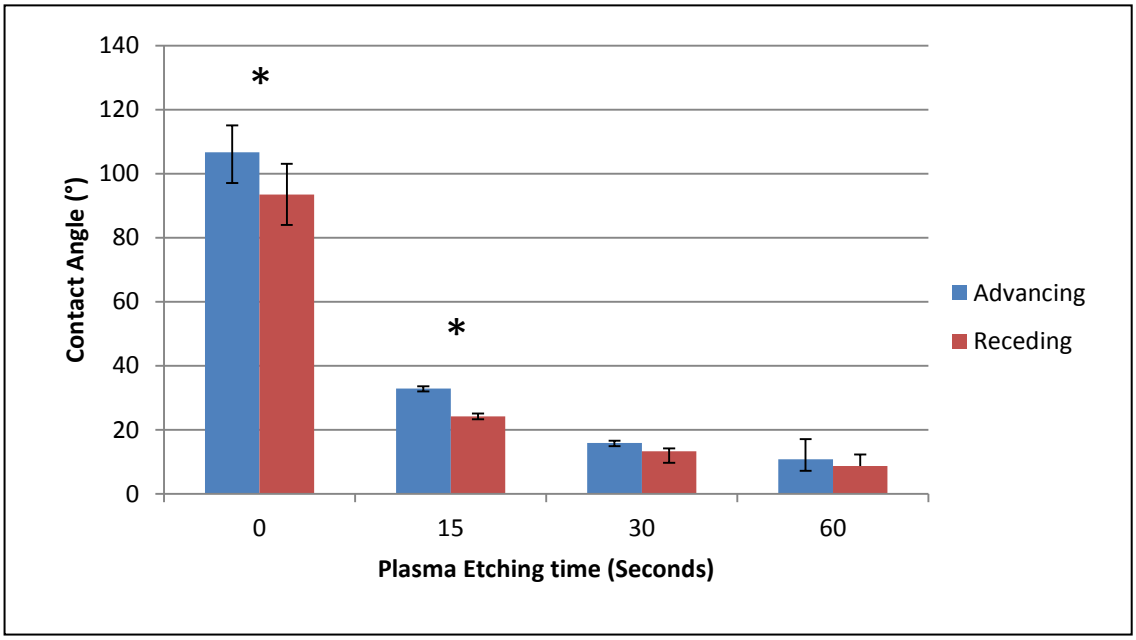

Figure 3-4: ARCA and increasing plasma contact time

High density polyethylene films were plasma etched for 60, 30, 15 and 0 seconds at 60 watts. Advancing and receding contact angle (°) of water was measured on 5 different samples; error bars represent standard deviation between average ARCA of ≥ 4 different samples. Graph shows a rapid decrease in contact angle with increasing plasma etching time, a significant difference was observed between all time points except 30 and 60 seconds for adancing and receding contact angle $P<0.001$). * indicates contact angles significantly different to other treatments.

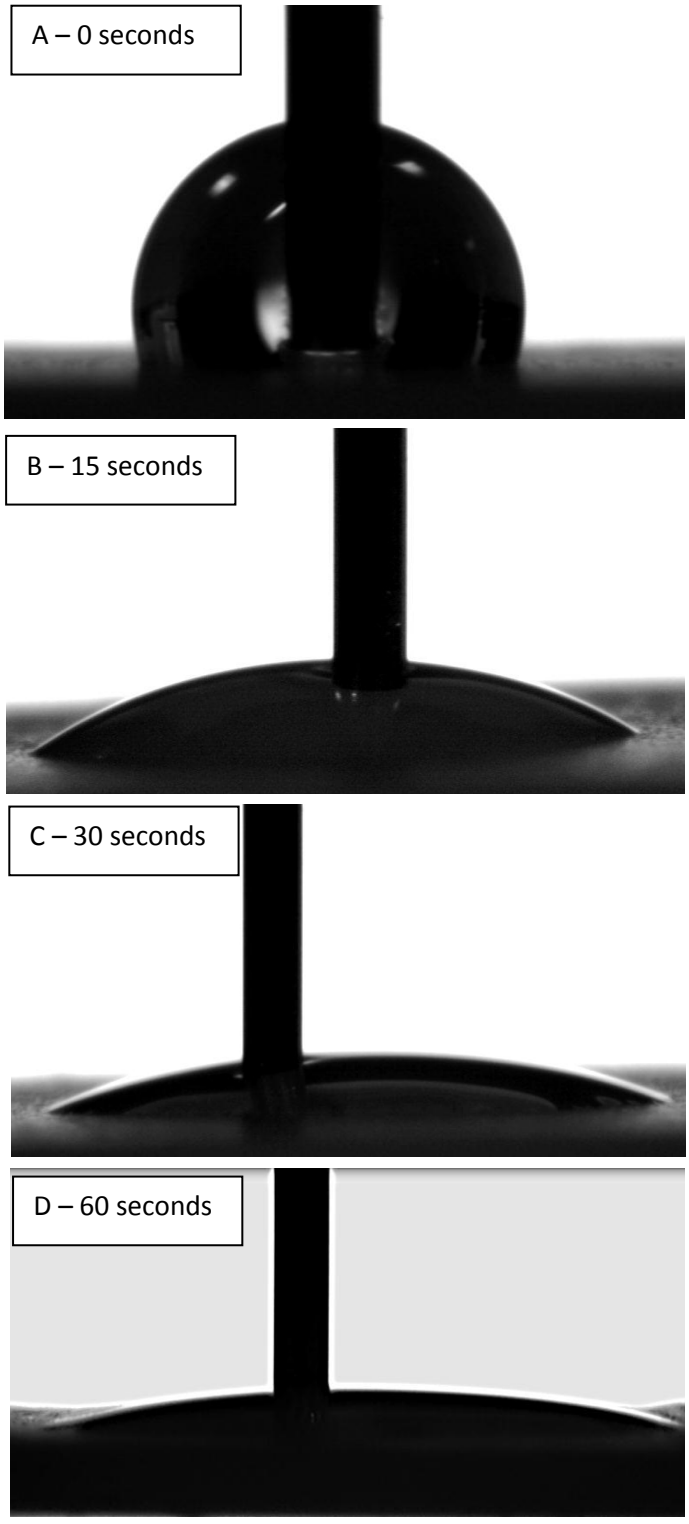

Figure 3-5: Images of ARCA and increasing plasma contact time

High density polyethylene films were plasma etched for 60, 30, 15 and 0 seconds at 60 watts. Images of advancing and receding contact angle (°) for each time point are shown from image A - D respectively. The angle at the edge of each droplet can be seen to decrease with increasing plasma contact time.

3.3.1.1 Plasma treatment chamber variation:

Plasma is chaotic, and despite the most consistent experimental procedure, variation in surface treatment will occur. This is due to the nature of the excited species that form plasma. In order to semi-quantitatively observe the variation throughout two different plasma systems; the Polaron barrel etcher (Figure 3-6) and a larger industrial grade plasma system (Figure 3-8). HDPE films were placed on the chamber platforms and exposed to plasma for 30 seconds at 60 watts and 109 seconds at 807 watts in the barrel etcher and industrial plasma system respectively. After treatment the films were analysed by sessile drop CA. Figure 3-7 shows a difference in CA of approximately 15° generated at the periphery of the chamber platform when compared to the centre. This variation indicates a range of plasma intensity occurs within the chamber. The centre of the platform between 4 and 6 cm width and 4-10cm length offers a more intense and consistent region, as indicated by the low CA which varies by no more than 5°.

The larger platform of the industrial grade system offered a more consistent CA of between 40 - 45° (Figure 3-9), with the exception of a region to the centre front of the chamber which peaks to about 60°. Overall the standard deviation of both plasma systems chamber variation is approximately 7°. By placing samples in the consistent regions during the etching process significant inconsistencies to the frit treatments were avoided.

Figure 3-6: Platform inside Polaron barrel etcher chamber

Image shows the inside of the Polaron pt7150 plasma barrel etcher, 24 well plate lid acted as etching stage on which samples were placed. Chamber measured at approximately 10 cm width by 14cm length.

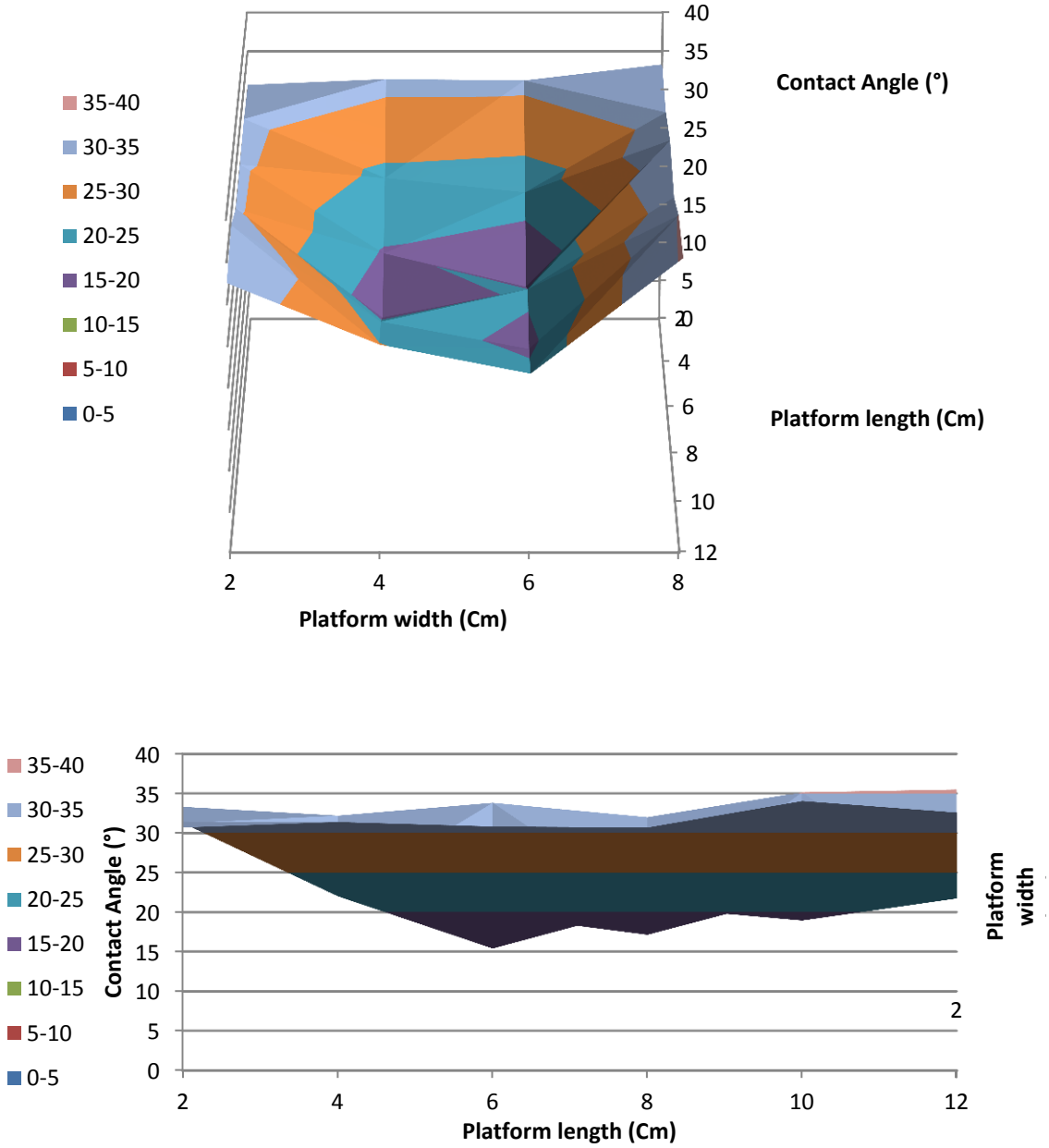

Figure 3-7: Variation within plasma chamber

3D surface chart shows variation in contact angle of HDPE films plasma etched for 30 seconds at 60 Watts. Top and bottom images represent the same graph at angles slightly above and almost horizontal to the 3D charts. Position of the top 3D chart is the equivalent to facing the plasma etching chamber length, bottom 3D chart is the equivalent to facing the width of the plasma etching chamber. 6-1 on the z-axis represents length of etching chamber, left to right represent width of chamber.

Figure 3-8: Multiple platforms of industrial grade plasma system

Image shows ten shelves of the industrial grade plasma system, each shelf is 45 x 45 cm and is capable of etching thousands of BioVyon™ frits.

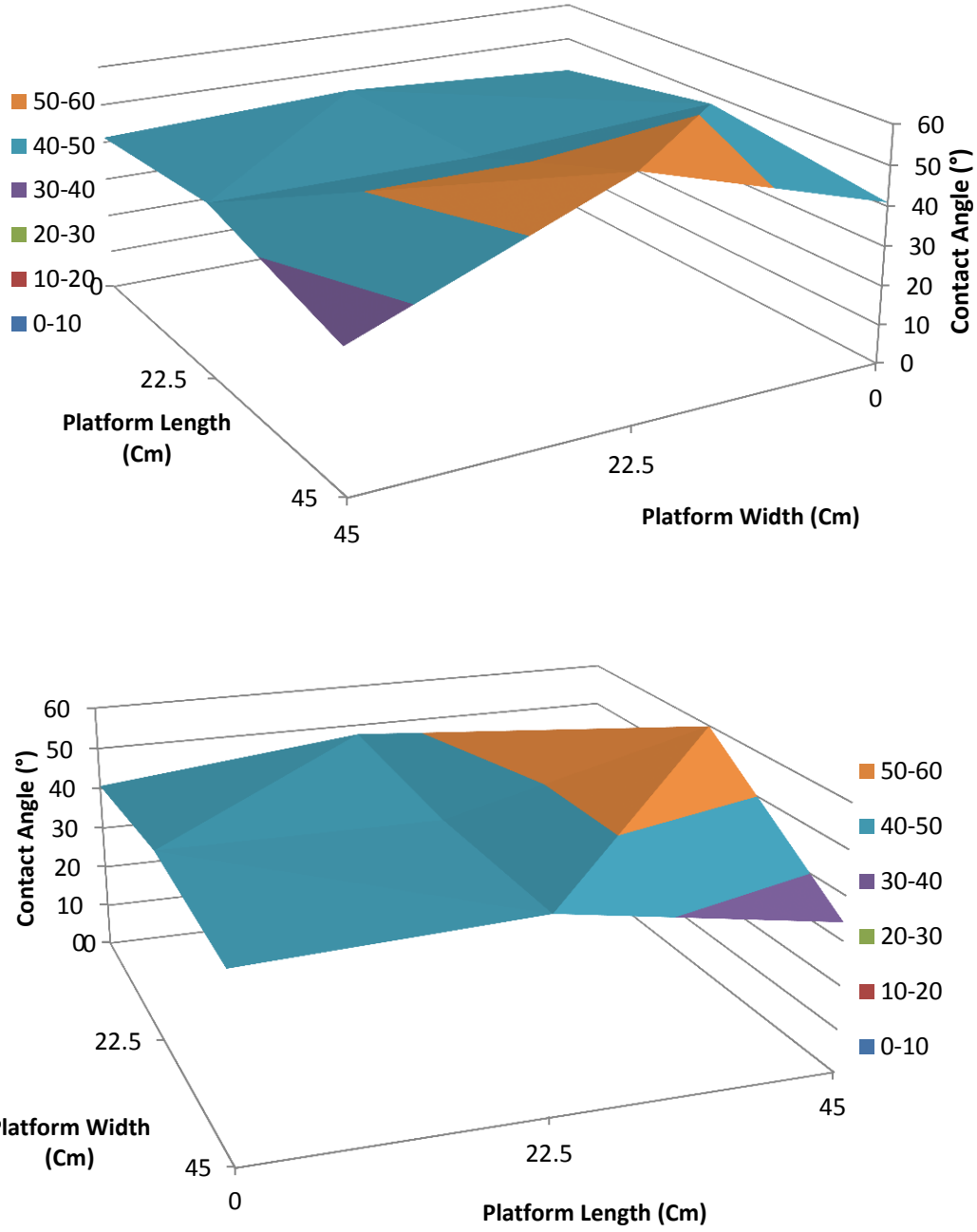

Figure 3-9: Variation within industrial grade plasma system

3D surface chart shows variation in contact angle of HDPE films plasma etched for 109 seconds at 800 Watts. Top and bottom images represent the same graph at angles diagonal to the front and rear of the chamber map. Position of the top 3D chart is the equivalent to facing the plasma etching chamber length, bottom 3D chart is the equivalent to facing the width of the plasma etching chamber.

3.3.2 Characterisation of surface chemistry generated by plasma system

It is well established that oxygen based plasma treatment generates oxygen moieties on polymer surfaces. So far, CA analysis has indicated an increase in hydrophilicity on LDPE and HDPE samples that have come into contact with plasma. Fourier transform infrared (FTIR) spectroscopy was used to identify the oxygen species generated.

The FTIR spectra in Figure 3-10 show absorbance peaks for untreated and plasma etched BioVyon ™ F frits, absorbance peaks are known to correspond to specific molecular bonds. Spectra a) represents the "footprint" for HDPE. Four significant peaks can be seen in this spectra; the first at 720-730 cm-1 which indicates the presence of CH_2 rocking. A second large absorbance peak is at approximately 1475 cm-1 and corresponds to CH_2 bending, the largest peak at approximately 3000 cm-1 corresponds to C-H bending (Section1.5).

The peaks highlighted on Spectra b) at 1716.7 cm^{-1} and 1369.5 cm^{-1} coincide to carbonyl and carboxyl groups respectively, although these peaks appear to be small, when compared directly to the untreated BioVyon™ absorbance spectra, it is clear that oxygen moieties are generated on the HDPE frit surface as a direct result of contact with plasma.

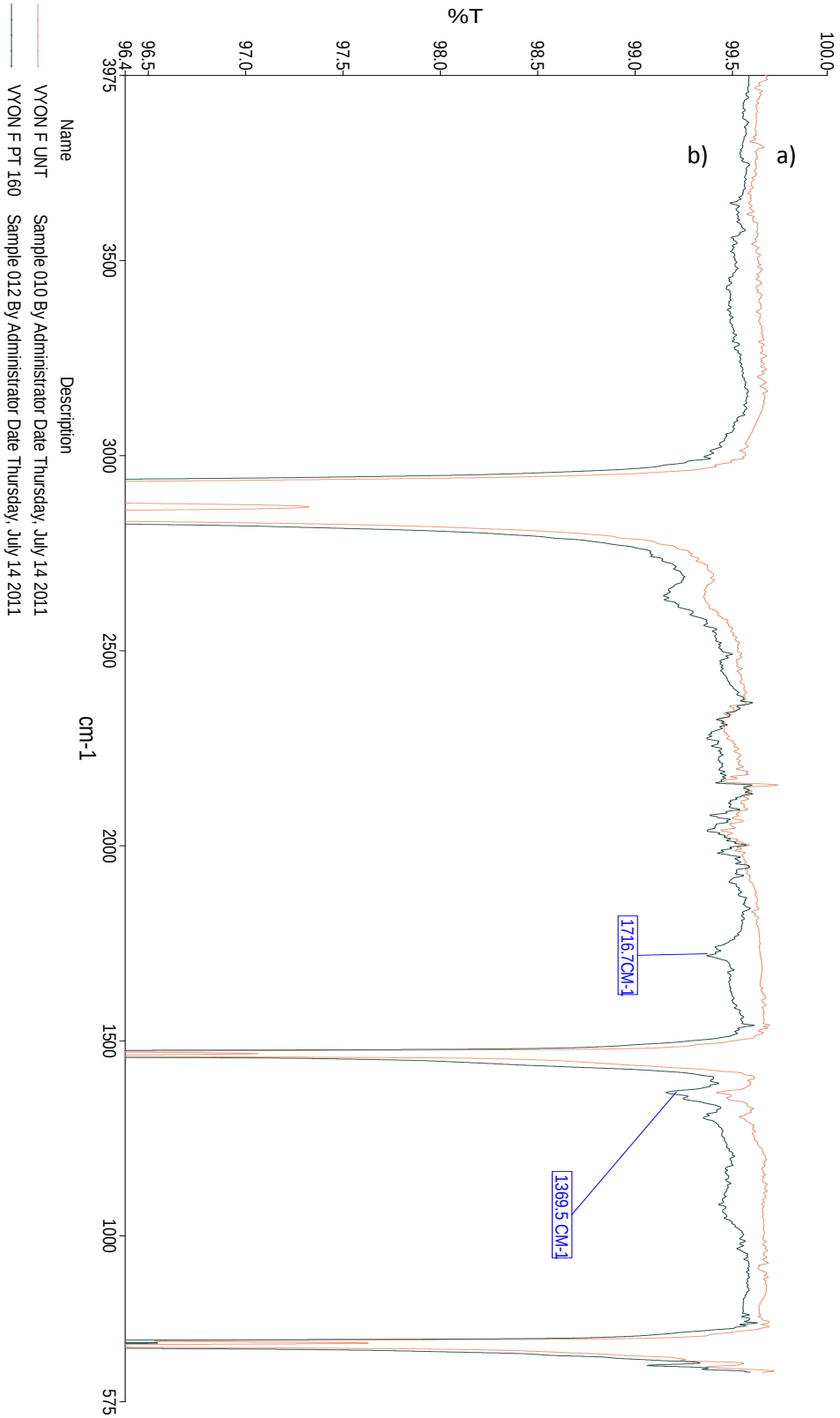

Figure 3-10: FTIR spectra of BioVyon™

Fourier transform infrared spectroscopy absorbance spectra of a) untreated BioVyon™ F frits and b) BioVyon™ F frits exposed to oxygen based plasma for 120 seconds at 60 Watts. Absorbance peaks can be observed in spectra b) at 1716.7cm^{-1} and 1369cm^{-1} which correspond to carbonyl and carboxyl groups respectively.

FTIR analysis indicated that COOH groups are a primary oxygen species generated during plasma etching, in order to use these groups in future chemical modification and surface conditioning it was necessary to quantify the number of COOH groups; this was achieved with the use of thionine acetate and toluidine blue fluorescent molecules.

Figure 3-11 indicates that after 120 seconds of exposure to oxygen plasma 1mm BioVyon F frits possess approximately 14-20 nmoles of COOH groups. The THA assay shows a near linear increase from 5nmoles after 15 seconds exposure. The TBO assay shows a more immediate increase and a smaller difference in COOH molarity from 30 seconds exposure onwards, relative to the THA assay. The variance in COOH groups quantified between THA and TBO could be due to structural differences between the fluorescent molecules effecting sensitivity or affinity for COOH groups present on the BioVyon™ surface.

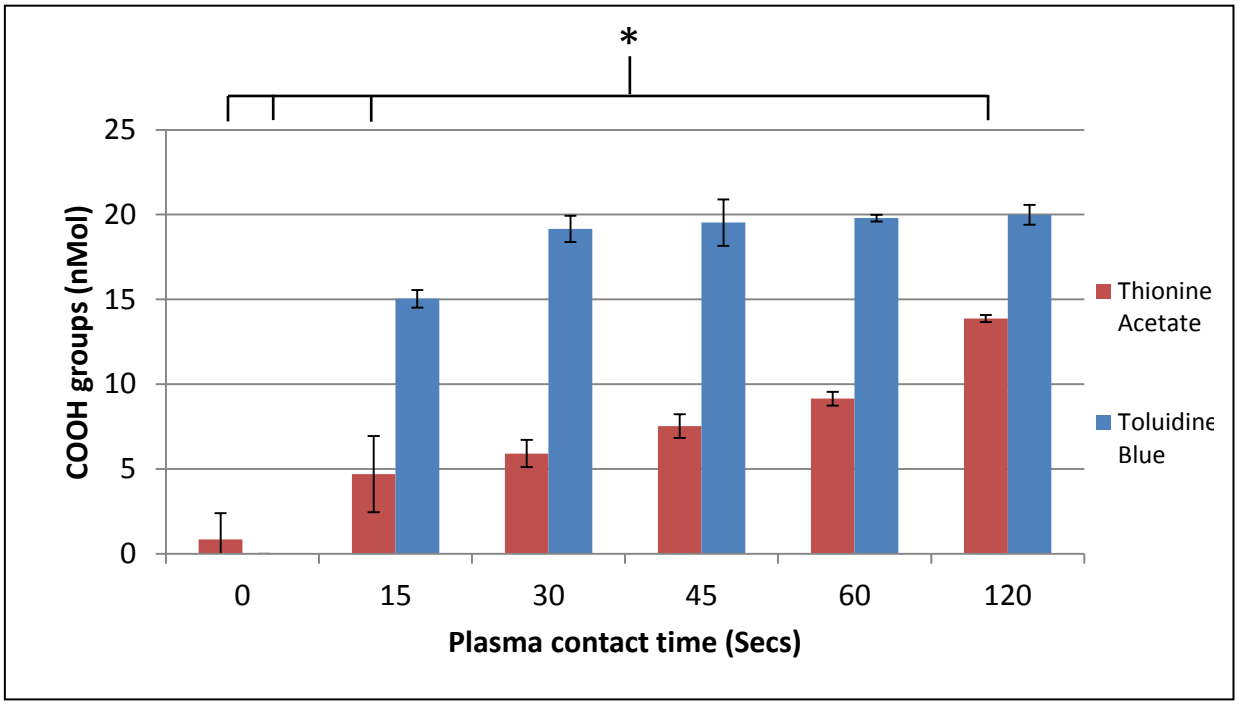

Figure 3-11: Effect of plasma contact time on COOH molarity

1mm Vyon F frits were plasma etched for 0, 15, 30, 45, 60 and 120 seconds at 60 watts in triplicate. Treated frits were submerged in solutions of 0.25mmol/L of Toluidine Blue (TBO) or 0.5mmol/L Thionine acetate (THA). The frits were washed x3 with distilled water, bound TBO and THA molecules removed with 500µl acetic acid and 100% ethanol respectively. 300µl samples were measured using a spectrometer at 595nm and the molar values extrapolated from a calibration curve. TBO and THA assays both indicate a significant increase in COOH groups with increasing plasma contact time ($P<0.001$). Significant difference between COOH groups at time points within the same assay data set denoted by *. A significant difference was observed at all time points between assay data sets ($P<0.05$).

3.3.2.1 BioVyon™ Surface chemistry compared to tissue culture plastic

Plasma is a common method employed to improve the surface of biomaterials for cell culture and is used commercially to modify tissue culture plastic. Using ARCA and TBO/THA assays plasma etched Biovyon™ and 2D BioVyon™ analogues were compared with tissue culture plastic. Figure 3-13 indicates that tissue culture plastic (TCP) has a very different absorbance spectra relative to plasma etched BioVyon™, it possesses the same three peaks at 720-730, 1475 and 3000 cm^{-1} corresponding to CH_2 rocking, CH_2 bending and C-H bending respectively. The benzene ring inherent within the structure of polystyrene (Figure 3-12) contribute to several other smaller peaks. A peak at 3025 cm^{-1} corresponds to alicyclic C-H bonds, moving down the wavelength a selection of small peaks can be seen between 2000 - 1700 cm^{-1}. These are overtone bands, which echo the fundamental frequencies at half the wavelength. The original peaks correspond to C-H in plane and out of plane bending and can be seen at 1068, 1027 and 906 cm^{-1}. The next large peak is at 1601cm^{-1} and corresponds to C-C double bonds in the benzene ring structure. Finally, a large peak can be observed at 1370 cm^{-1} which corresponds to carboxy groups present after contact with plasma generated via corona discharge. This peak is of a higher intensity than that of BioVyon ™ (Figure 3-10, Figure 3-13), suggesting a higher number of COOH are present on TCP than BioVyon™.

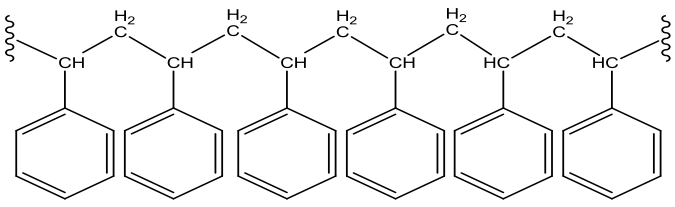

Figure 3-12: Structure of polystyrene

Image shows repeating carbon chain, with benzene ring structures of polystyrene.

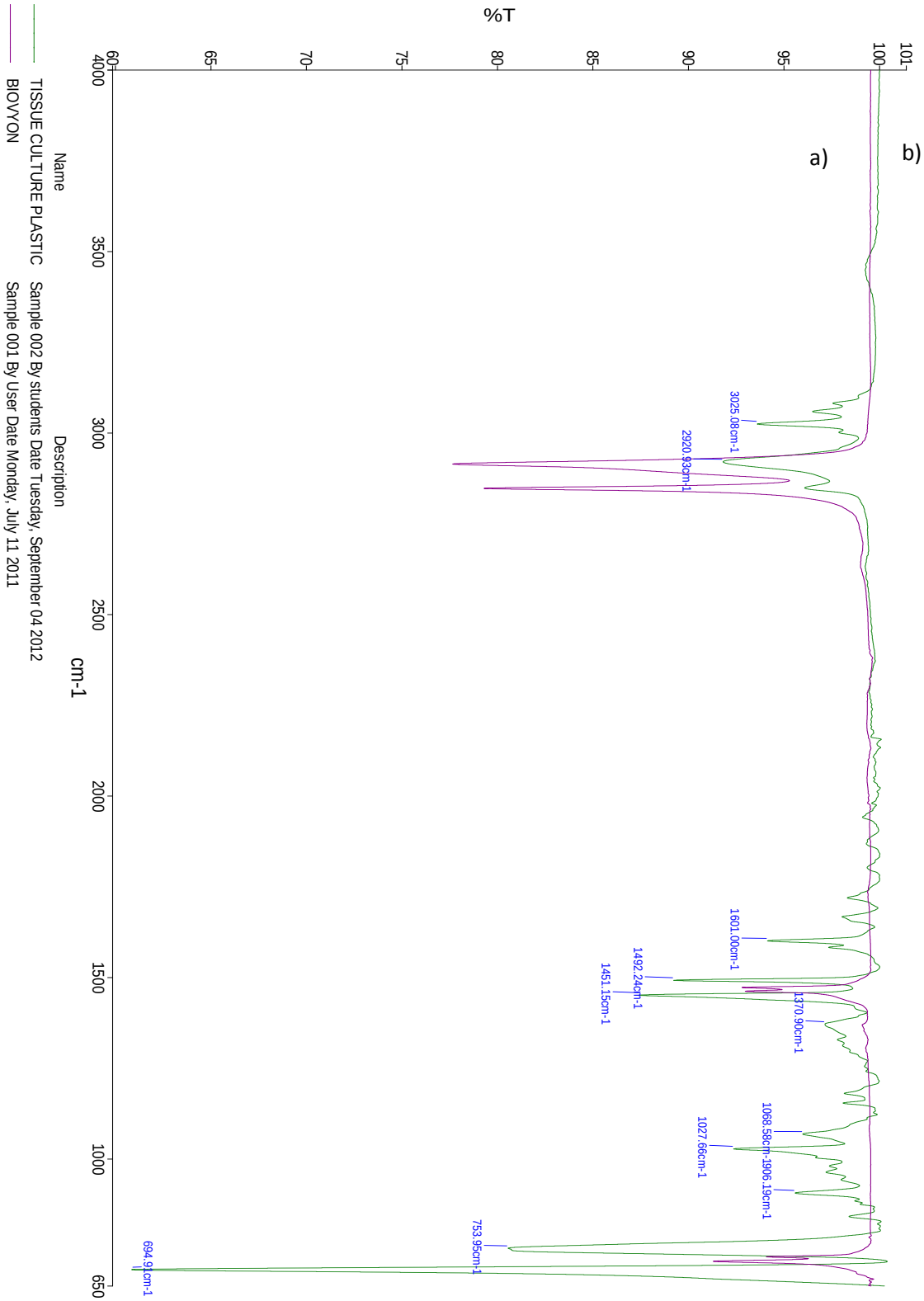

Fourier transform infrared spectroscopy absorbance spectra of a) BioVyon™ F frit exposed to oxygen based plasma for 60 seconds at 60 watts and b) tissue culture plastic. Absorbance peaks on spectra b) indicate alicyclic C-H bonds (3025 cm^{-1}) and C=C bonds (1601 cm^{-1}) present in the benzene ring structure. COOH groups and C-H bending correspond to peaks at 1370 cm^{-1} and between 1068 and 906 cm^{-1} respectively.

Figure 3-14 shows that TCP and Biovyon™ treated at 60 watts for 120 seconds possess between 35 – 43nmoles and 5 – 3 nMols of accessible COOH groups per cm^2 respectively. A significant difference of approximately 35 nmoles of COOH was observed between the materials (One way ANOVA, $P<0.05$). This data is supported by the higher transmittance of the peak at 1370 cm-1 in the absorbance spectra of TCP than BioVyon™ in Figure 3-13 indicating more COOH groups present on TCP than BioVyon™. Figure 3-15 and Figure 3-16 indicate thatTCP possesses a higher ARCA than BioVyon™ post plasma etching.

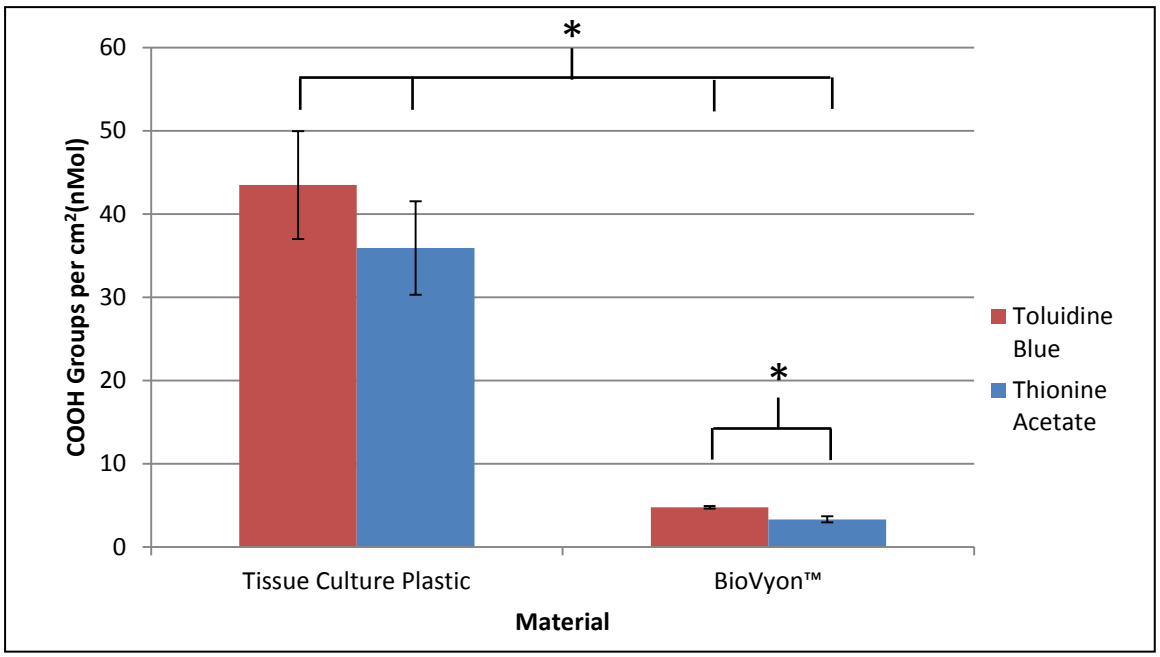

Figure 3-14: COOH molarity per cm^2 of BioVyon™ compared to tissue culture plastic

1mm Vyon F frits were plasma etched 60 seconds at 60 watts in triplicate. Treated frits and 6 well tissue culture plastic (TCP) plates were filled with and submerged in solutions of 0.25mmol/L of Toluidine Blue (TBO) or 0.5mmol/L Thionine acetate (THA) respectively. The frits and 6 well plates were washed x3 with distilled water, bound TBO and THA molecules removed with 500µl acetic acid and 100% ethanol respectively. 300µl samples were measured using a spectrometer at 595nm and the molar values extrapolated from a calibration curve. TBO and THA assays both indicate more COOH groups per cm² are generated on TCP relative to BioVyon™, the data sets for both assays are significantly different between materials ($P<0.05$). A significance difference was also observed in COOH groups on BioVyon™ between assay treatments ($P<0.05$). Significance difference denoted by *.

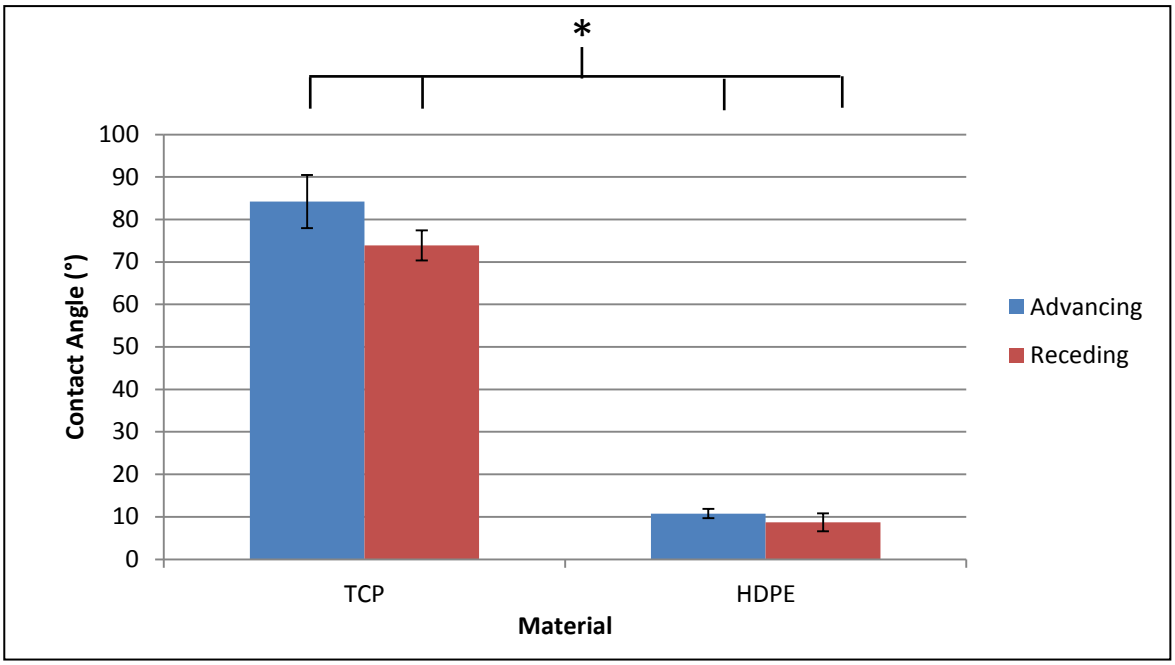

Figure 3-15: Contact angle of tissue culture plastic compared to BioVyon™ analogue

2D High density polyethylene (HDPE) BioVyon ™ analogues were plasma etched for 60 seconds at 60 watts and compared using advancing and receding contact angle (ARCA) to segments of tissue culture plastic (TCP) plates. ARCA (°) of water was measured on 5 different samples; error bars represent standard deviation between average ARCA of≥ 4 different samples. The data indicates that the contact angles on TCP was significantly higher than HDPE ($P<0.001$). Significance difference denoted by *.

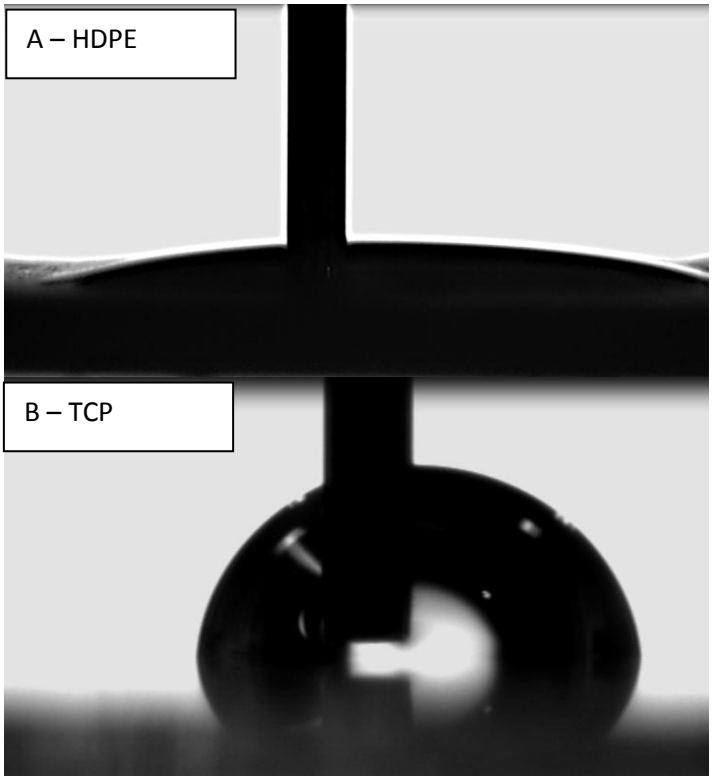

Figure 3-16: ARCA images of tissue culture plastic compared to BioVyon™ analogue

High density polyethylene (HDPE) BioVyon ™ analogues were plasma etched for 60 seconds at 60 watts and compared using advancing and receding contact angle (ARCA) to segments of tissue culture plastic (TCP) plates (Image A and B respectively). The angle at the edge of each droplet can be seen to be lower on HDPE than TCP.

3.3.3 Decay of oxygen groups generated by plasma systems

The ageing effect of plasma has been observed on a number of different materials, and is an important consideration for any biomaterial exposed to plasma. The surface chemistry generated by oxygen based plasma on polymers is known to change over time [274]. Oxygen groups such as carbonyl, hydroxyl and carboxyl groups are able to re-orientate from the surface to the internal environment of the polymer chains, via reptation motions [275]. This results in the reduction or "Decay" of these species on the surface. Interfacial forces and the surface environment effect the movement of polar oxygen groups, forcing regions highly populated with polar groups to orientate into the bulk polymer environment. The non-reversible nature of these group rotations can be attributed to clustering or hydrogen bonds between polar groups in the non-polar, internal environment [274].

In order to investigate the decay of oxygen moieties on BioVyon™, TBO assays and ARCA were applied BioVyon™ and 2D HDPE BioVyon™ analogues respectively. These methods assessed how the wettability and number of COOH groups changed on the materials surface over time, in different storage conditions. 2D HDPE BioVyon™ analogues were plasma etched for 60 seconds at 60 watts and immediately stored in either atmosphere (ATM) or phosphate buffered solution (PBS). ARCA was measured on ≥ 4 different samples at 0.5, 3 and 6 hours post etching to obtain data on short term decay. The data in Figure 3-17 indicates that hydrophilicity was reduced in both storage conditions within 6 hours after etching as shown by the increase in CA from 0.5 to 6 hours. No significant difference was observed between the ARCA of different storage

conditions at each time point, suggesting that the short term decay was not influenced by the storage environment.

In order to assess long term decay 2D HDPE BioVyon™ analogue ARCA was measured at 1,3,6,9 and 12 days post etching with oxygen plasma for 60 seconds at 60 watts. Figure 3-18 indicates that the samples stored in PBS had a lower advancing and receding CA than those stored in ATM over 12 days, a significant difference in CA was observed between storage conditions from 1 to 9 days, with the exception of the 9 day advancing CA and 12 day time points ($P<0.05$). The signficant increase in ARCA on HDPE stored in ATM compared to PBS up to 9 days suggests decay is reduced initially. However, there is no significant difference in HDPE ARCA at 12 days ($P<0.05$), suggesting that the decay of wettability may begin to slow or plateau over long term storage.

Approximately 2000 BioVyon™ Frits were plasma etched in the mass production chamber for 109 seconds at 800 Watts. The use of the TBO assay enabled quantification of carboxyl groups on the surface of the plasma etched HDPE throughout the frit surface. Long term decay of COOH groups can be seen in Figure 3-19. A significant decrease of approximately 4nMol in COOH groups can be seen after 6 months storage in PBS, (One way ANOVA, $P<0.05$).

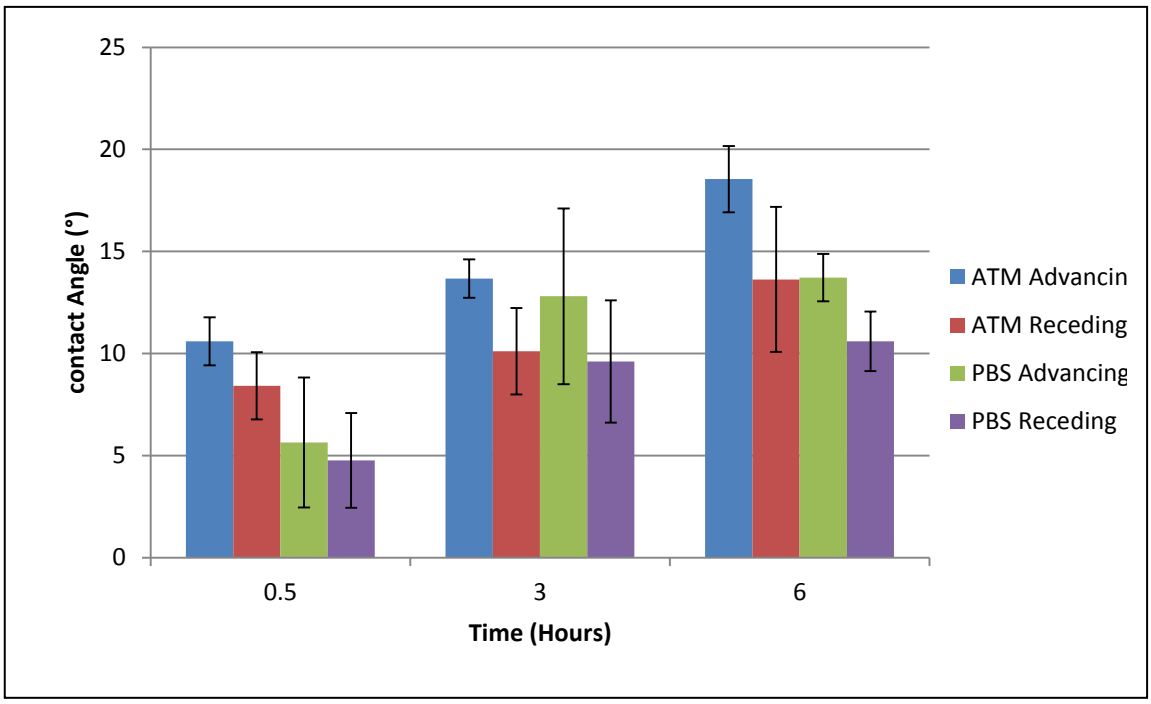

Figure 3-17: Short term decay

High density polyethylene (HDPE) films were plasma etched for 60 seconds at 60 watt and stored in either atmosphere (ATM) or a solution of phosphate buffered solution (PBS). Advancing and receding contact angle (ARCA) of samples was measured at 0.5, 3 and 6 hours after plasma etching; error bars represent standard deviation between average ARCA of ≥ 4 different samples. Results show no significant increase in CA from 0.5 to 6 hours for samples stored in PBS and ATM, no difference was seen between the storage conditions for each time point ($P>0.05$).

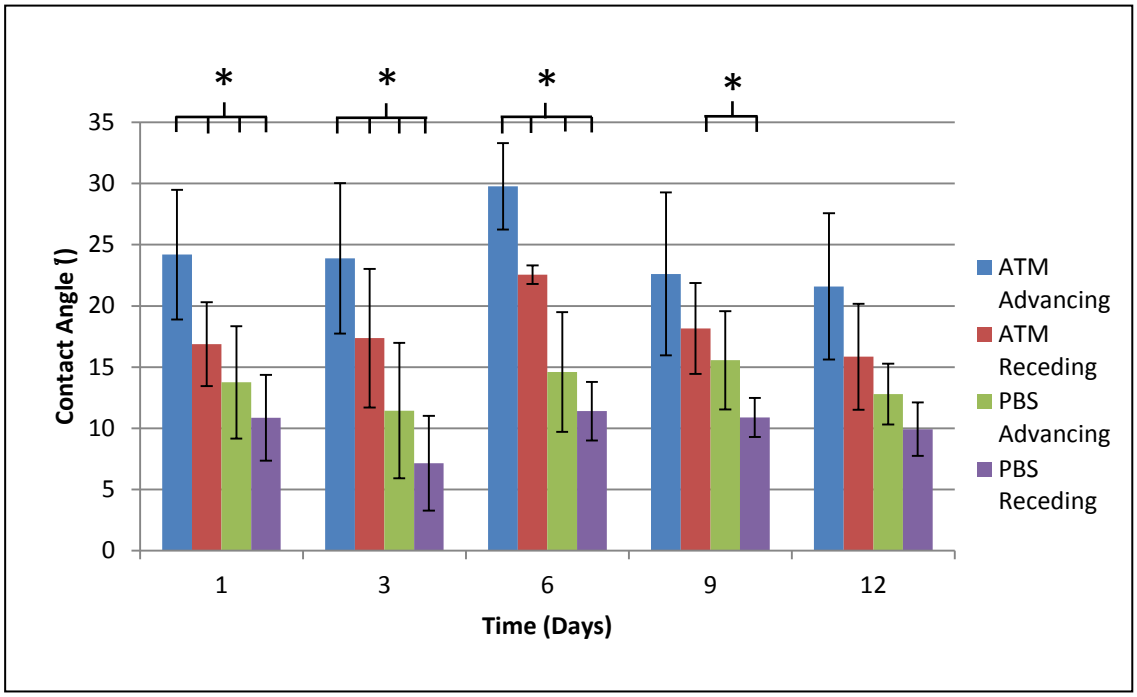

Figure 3-18: Long term decay

High density polyethylene (HDPE) films were plasma etched for 60 seconds at 60 watt and stored in either atmosphere (ATM) or a solution of phosphate buffered solution (PBS). Advancing and receding contact angle (ARCA) of samples was measured at 1,3,6,9 and 12 days after plasma etching; error bars represent standard deviation between average ARCA of ≥ 4 different samples. Results show no significant difference in ARCA of samples stored in PBS and ATM between different time points ($P>0.05$). A significant difference was seen between the storage conditions for each time point with the exception of the 9 days advancing contact angle and 12 days ($P<0.05$). Significant difference between contact angle of storage conditions denoted by *.

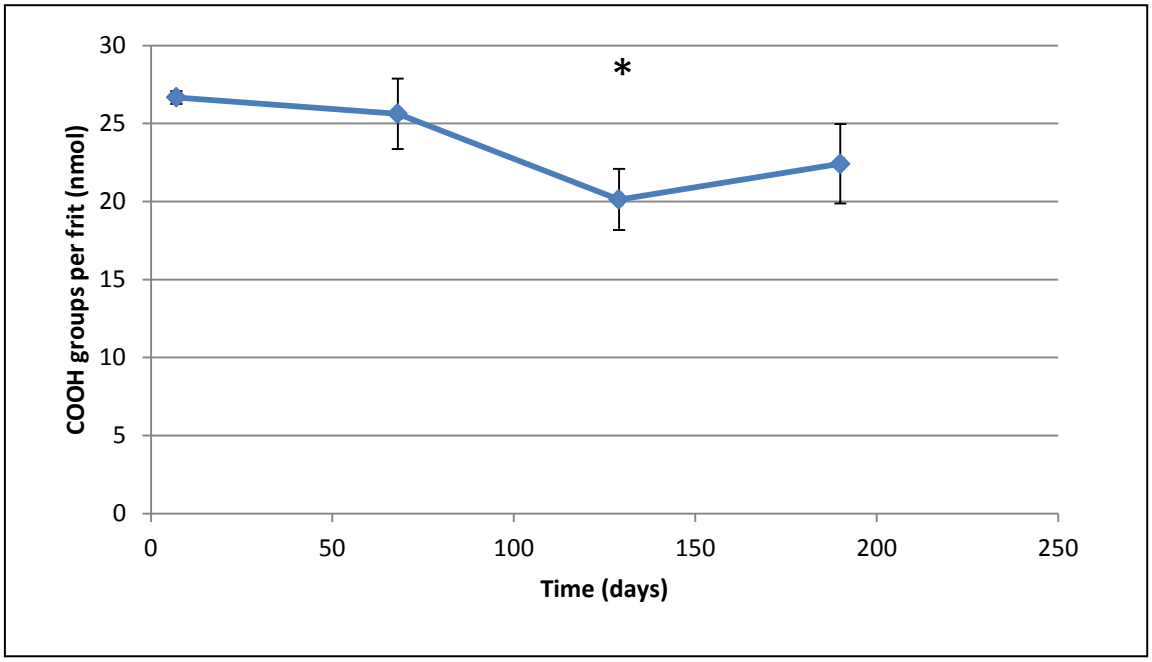

Figure 3-19: COOH decay

BioVyon Frits were plasma etched in the mass production etcher for 109 seconds at 800 watts. Treated frits submerged in solutions of 0.25mmol/L of Toluidine Blue (TBO). The frits were then washed with 10ml distilled water, bound TBO molecules removed with 500µl acetic acid. 300µl samples were measured using a spectrometer at 595nm and the molar values extrapolated from a calibration curve. TBO assay indicates gradual decrease in COOH groups per frit from approximately 27 to 2nmol over a period of 4 months before stabilising at 22nMol at 6 months. A significantly decreased number of COOH groups were observed at 129 days ($P<0.05$). Significant difference between COOH groups per frit (nmol) denoted by *.

3.3.4 Characterisation of surface roughness generated by plasma systems

Plasma is known to cause chain scission and ablation. This phenomenon is observed to take place more readily in amorphous regions of PE structures than the crystalline [230]. This is because methyl groups are more susceptible to oxidation than vinyl groups mid chain and more prevalent in amorphous regions of PE. This results in an uneven amount of ablation, and in turn, etching during contact with oxygen plasma. High density crystalline regions form surface topography as the low density amorphous regions are ablated and removed with gas flow. Due to the influence surface topography and roughness has on cellular responses it was necessary to characterise any changes to the PE surface generated during contact with plasma.

3.3.4.1 Atomic force microscopy (AFM)

In order to characterise the changes in surface topography due to the effects of oxygen plasma, five samples of untreated BioVyon™ were probed by AFM. Four different scan sizes were applied to these samples at 50, 10, 5 and 1µms (Figure 3-20). The same areas of the surfaces were then probed under identical parameters after being plasma etched for 60 seconds at 60 watts. This method provided a 3D image of the BioVyon™ surface as well as a quantitative measurement of the surface roughness before and after plasma etching.

Figure 3-20 and Figure 3-21 show the micro and nano scale topography respectively, at 50µm unique topography was used to navigate to the original scan areas post plasma etching as indicated by the red circles (Figure 3-20). The smaller scans reveal a clear

qualitative difference in nano topography, the presence of roughness can be seen when comparing the 1µm scans in Figure 3-21.

Quantitative measurement of five different samples using the AFM software indicated that the BioVyon™ had a higher average RMS roughness after plasma etching, however, no statistically significant difference was observed between the RMS values before and after plasma etching. Table 3-3 shows an increase at all scan sizes, with the largest difference at 50µm.

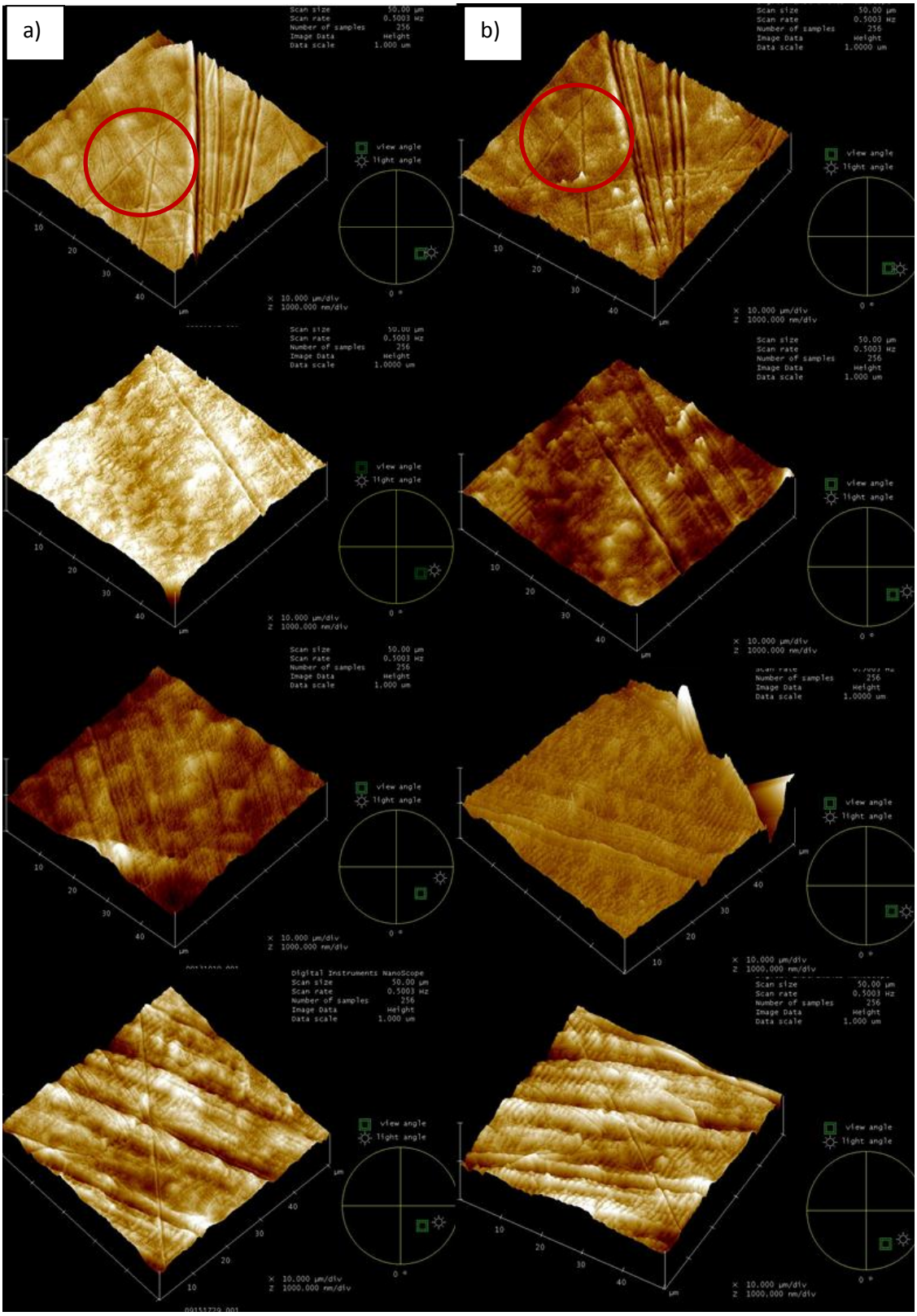

Figure 3-20: Range of AFM scans on BioVyon™

50µm AFM scans of 4 different BioVyon™ frits, a) untreated BioVyon™ and b) BioVyon™ plasma etched for 60 seconds at 60 watts. Images show similar micro topography before and after etching (Inicate by red circle); indicating area of investigation has been located successfully after treatment.

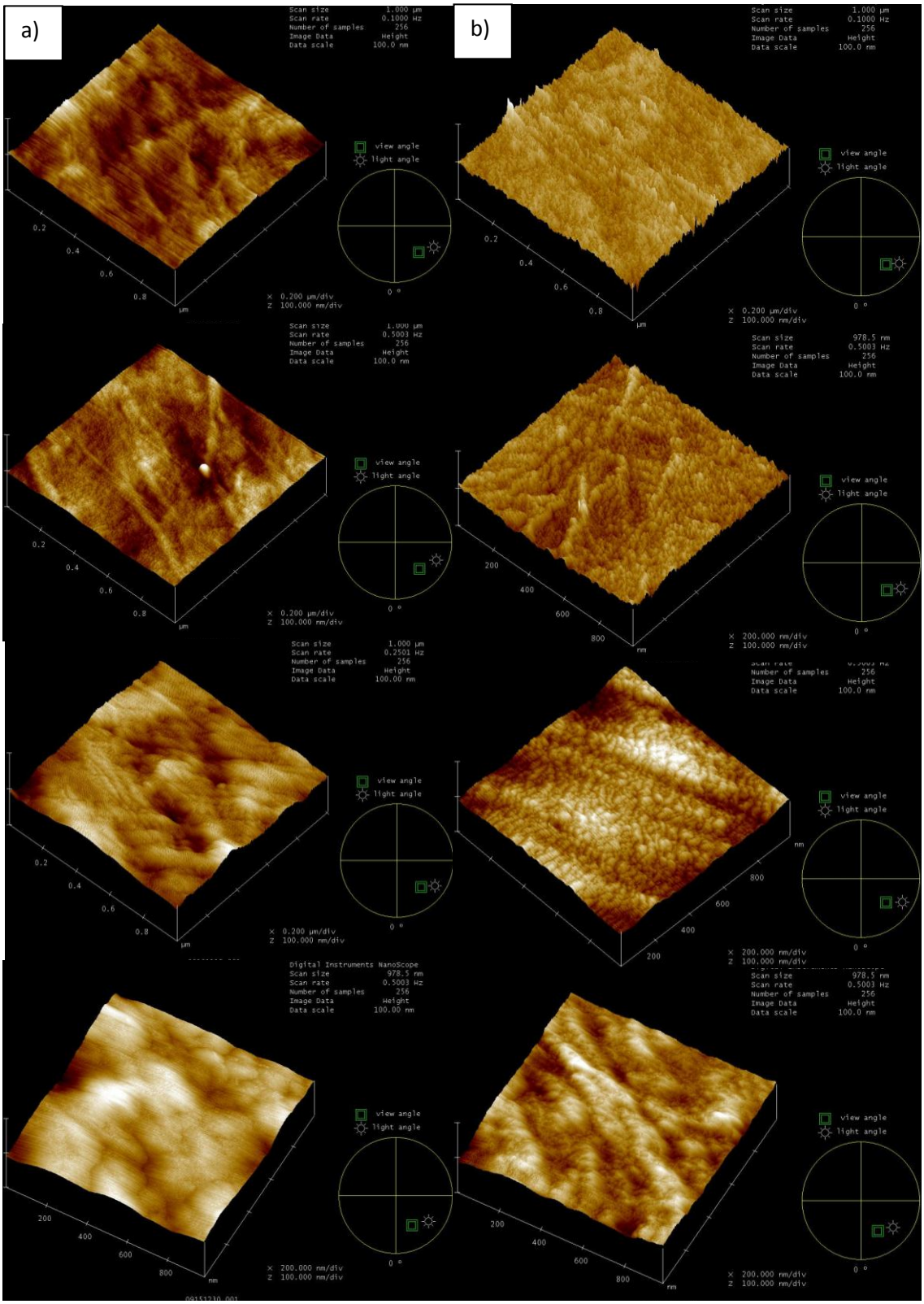

Figure 3-21: 1µm AFM scans of BioVyon™

1µm AFM scans of 4 different BioVyon™ frits, a) Untreated BioVyon™ and b) BioVyon™ plasma etched for 60 seconds at 60 watts. Images show an increase in the prevalence of nano topography after etching.

Scan size (µm)	Untreated BioVyon™ RMS (nm)	Plasma etched BioVyon™ RMS (nm)	Difference (nm)
50	46.79 ± 16.40	51.2486 ± 18.64	4.45
10	13.32 ± 4.72	15.253 ± 5.72	1.933
5	8.024 ± 2.24	10.5178 ± 3.12	2.49
1	4.7128 ± 1.92	5.2192 ± 1.47	0.506

Table 3-3: AFM roughness measurements

Table showing roughness measurements (RMS - Average root mean square) for untreated and plasma etched BioVyon™. An increase in roughness was seen between the untreated and plasma etched roughness measurements for each scan size.

3.3.4.2 Scanning electron microscopy (SEM)

The internal surface topography of the BioVyon™ was another key area of characterisation, as seeded cell populations will come into direct contact with it. In order to obtain qualitative data on the internal pore surfaces, untreated frits and frits plasma etched for 60 seconds at 60 watts were sputter coated for SEM analysis. Figure 3-22 shows a range of magnifications of the BioVyon™ surface, images a) and e) show the macrostructure for both untreated and plasma etched BioVyon™, although no difference between surface topography can be seen at this scale it is interesting to note the sintered particulates approximately 150-200µm in diameter which form the BioVyon™ structure.

Images c) and d) in Figure 3-23 show patches of micro scale topography on the surface of an individual sintered PE particulate at 1000x magnification. A clear difference can be seen between images e) and f) showing that the plasma etched BioVyon™ in f) has more prominent ridges relative to the untreated BioVyon™ in image e). Finally, magnification at 50,000x shows hollows generated by plasma in between ridges in image h), these hollows are not present in image g).

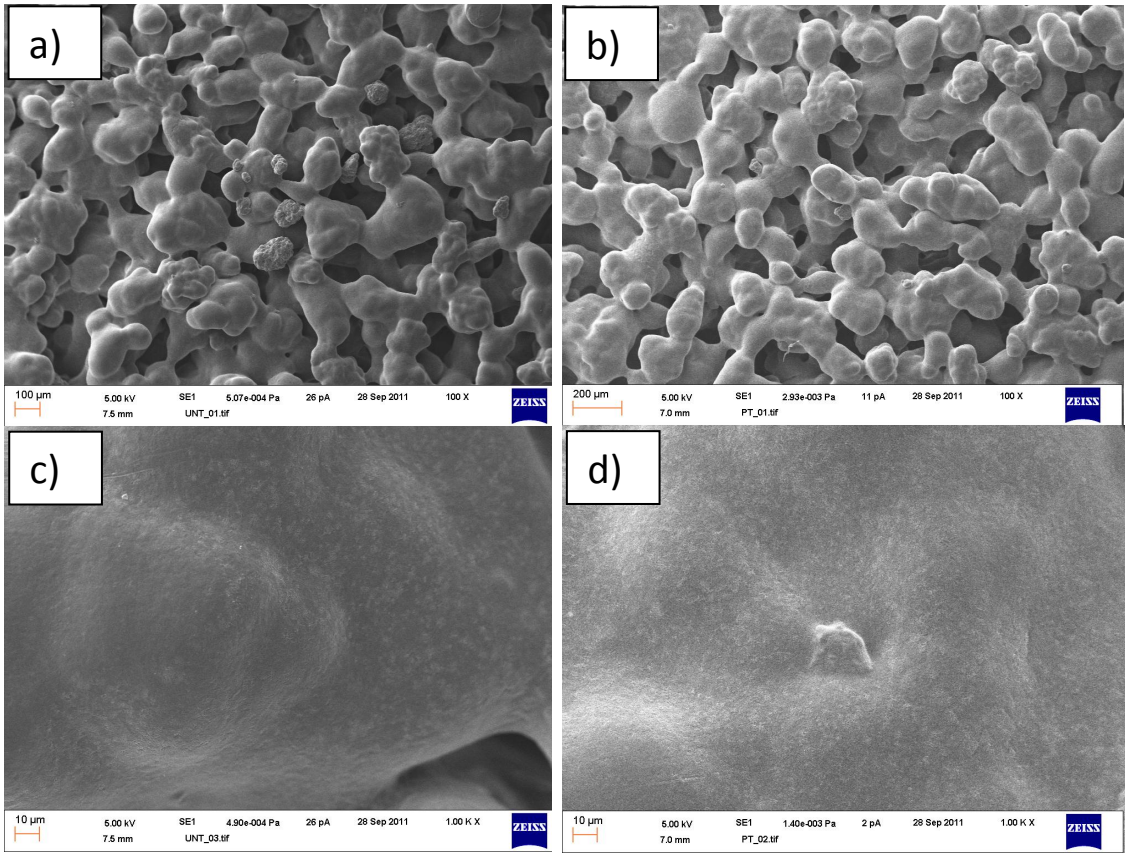

Figure 3-22: Microscale SEM images of BioVyon™

Images showing SEM images of untreated BioVyon™ a) and c), and BioVyon™ plasma etched for 60 seconds at 60 watts b) and d)). Images a) and b) taken at 100x magnification, images c) and d) taken at 1000x magnification. Overview of microscale topography show no obvious difference between Biovyon™ samples before and after treatment.

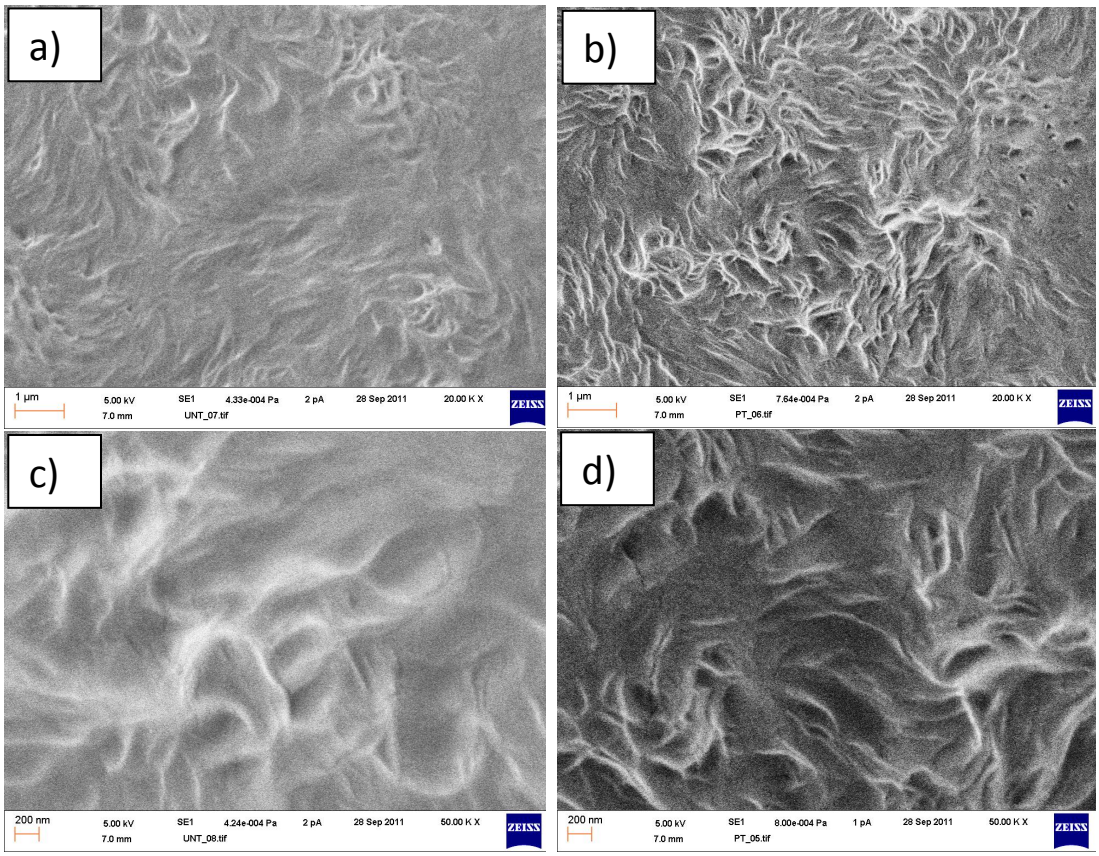

Figure 3-23: Nanoscale SEM images of BioVyon™

Images showing SEM images of untreated BioVyon™ a) and c), and BioVyon™ plasma etched for 60 seconds at 60 watts b) and d). Images c) and c) taken at 20,000x magnification, images c) and d) taken at 1000x magnification. Ridges and hollows are more prominent in the plasma etched BioVyon™ samples in images b) and d) relative to the untreated BioVyon™ samples in images a) and c).

3.3.5 Depth of plasma etching penetration in 3D BioVyon™

Due to the unpredictable, labile nature of plasma several factors are known to affect the deposition of oxygen moieties on the surface of polymers. Pressure, wattage, and time have all been investigated and suitably characterised in section 3.3.1. Plasma masking is another phenomenon affecting plasma etching; it is caused by the presence or structure of a substrate preventing optimal contact between plasma and polymer surfaces.

In order to investigate the effect of masking, SEM images were taken of the central structure of 2mm thick BioVyon™ frits. Untreated BioVyon™ frits and BioVyon™ plasma etched for 60 seconds at 60 watts were cut in half and positioned for imaging in an environmental SEM. Figure 3-24 image a) and b) show the warped regions of HDPE that have been cut by a scalpel, the surface directly behind these regions remained unchanged. Image d) clearly shows a more prominent surface roughness, with more hollows and ridges than the untreated surface in image c). This indicates that plasma is still etching the surfaces throughout the 2mm thick BioVyon™. In order to quantify the masking affect 2D HDPE BioVyon™ analogues were plasma etched for 20 seconds at 60 watts. 2mm thick BioVyon™ strips were placed over the samples to simulate the masking effect in the centre of a frit. ARCA was used to measure the change in surface wettability between samples with and without a BioVyon™ mask.

Figure 3-25 shows a significant difference between the ACA of 2D HDPE masked and the control 2D HDPE after plasma treatment ($P<0.01$). Advancing contact angle increased by approximately 17°, from this we can deduce that wettability decreases by approximately half through 2mm of BioVyon™ post plasma etching.

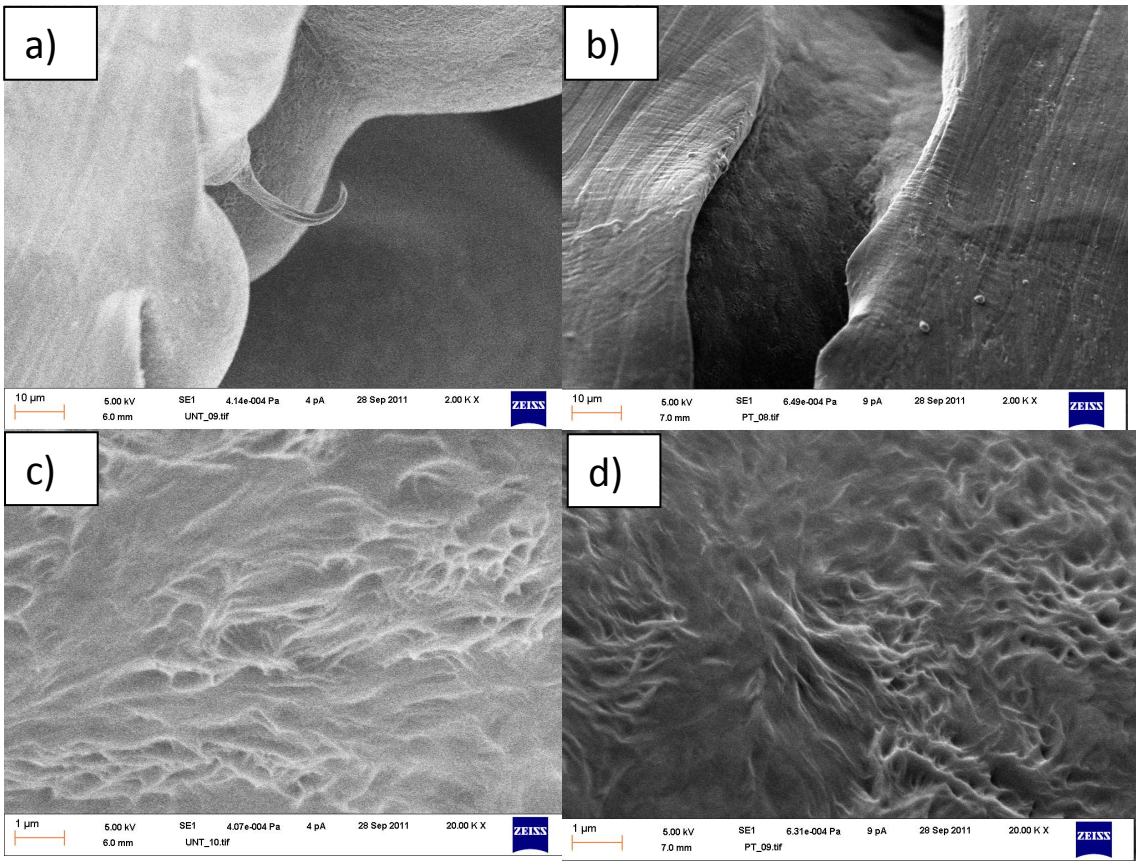

Figure 3-24: SEM images of BioVyon™ central structure

Images showing SEM images of untreated BioVyon™ a), c) and BioVyon™ plasma etched for 60 seconds at 60 watts b) and d). Images taken at 2000x a) and b) and 20,000x magnification c) and d) (unusual structure in a) is a PE fibril caused by cutting/warping of BioVyon™). Image d) indicates the etching has modified the topography in the centre of the frit.

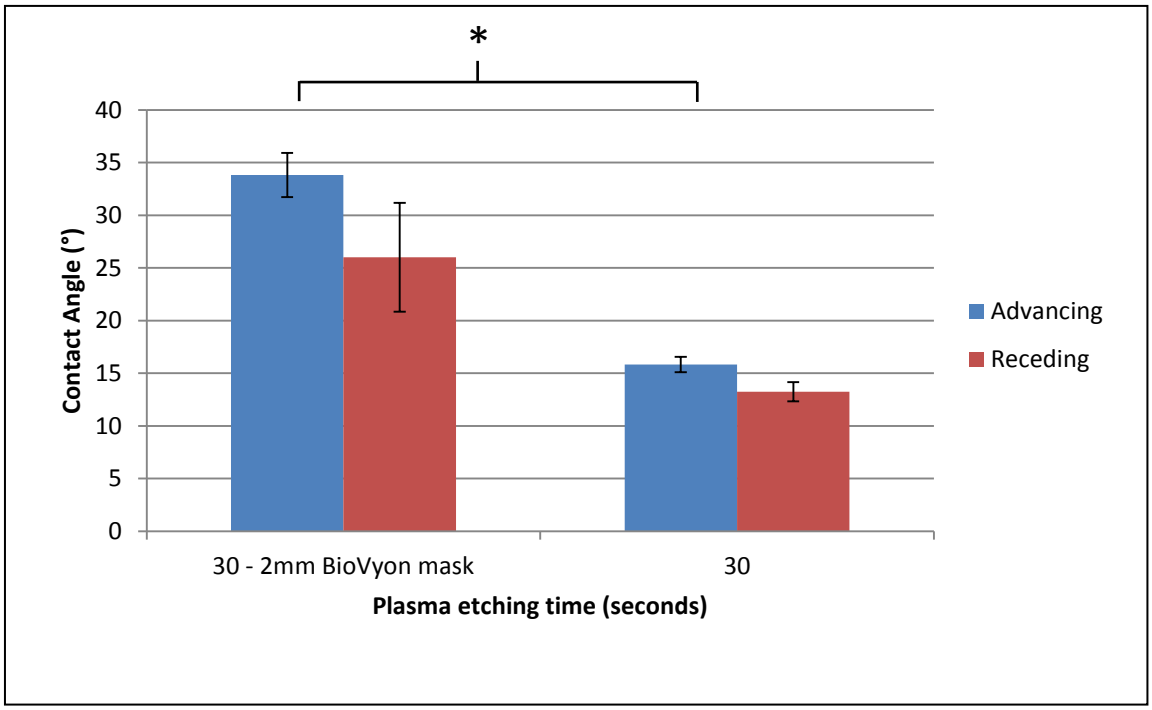

Figure 3-25: ARCA with BioVyon™ mask

Graph showing ARCA of 2D HDPE film covered with 2mm thick BioVyon™ compared to uncovered 2D HDPE. Both samples were plasma etched for 30 seconds at 60 Watts. ARCA of samples was measured at 30 minutes after plasma etching; error bars represent standard deviation between averages ARCA of ≥ 4 different samples. Results show a significant difference in ACA between samples. A significant difference can be seen between the HDPE film masked with 2mm BioVyon and the control sample. The increased contact angle on the mask sample indicates that wettability was decreased ($P<0.01$). Significant difference is denoted by *.

3.4 Discussion

This chapter has incorporated a range of techniques to characterise the structure, surface chemistry and surface topography of BioVyon™ before and after plasma etching. These findings have been discussed in relation to cell culture and how similar factors in current literature have been known to influence cells. Finally, the physical properties of BioVyon™ have been critically evaluated for potential as a mass cell culture system.

3.4.1 Structure

Initially the macrostructure of varying grades of BioVyon™ were characterised, pore size and surface area were investigated. Three grades of Vyon particulate provided a range of pore sizes (Table 3-1); once sintered Vyon F possessed a mean pore size of approximately 70µm in combination with a high porosity (Figure 3-1). This grade of particulate was selected for further investigation over Vyon M and HP which held a minimum pore size too small for cell infiltration and low porosity respectively.

The pore size of Vyon F was approximately three times larger than mammalian cells, allowing for easy infiltration and passage of cell populations into the internal structure. Other 3D culture materials such as Alvetex® possesses pores of between 10-20µm diameter [111], if at full capacity with cell populations these discs are limited to 200µm due to the diffusion limit of oxygen [108-110]. Despite the 1mm thickness of the BioVyon F frits, oxygen and nutrients are able to diffuse throughout the culture system due to the larger pore diameter indicated by mercury porosimetry (Figure 3-1).

The endocrine pancreas is one of the most specialised tissue types in the body. The islets of Langerhans are highly pervaded with capillaries and range in diameter from 50-500µm (Section 1.2.1.). Analysis of BioVyon™ suggests it will provide a suitable environment for β-cells, with pores large enough to hold small islets while promoting sufficient oxygen diffusion throughout its structure.

3.4.2 Surface chemistry

Oxygen plasma was applied to BioVyon™ to improve the chemical properties of the surface for cell culture. It was necessary to characterise the chemical species generated on the HDPE surface, and the factors affecting surface wettability.

Plasma contact time was the most significant factor influencing wettability of HDPE (Figure 3-4), large variation in wattage and pressure did not significantly influence ARCA of BioVyon™ analogues (Figure 3-2, Figure 3-3). Despite the control over pressure, wattage and plasma contact time, variation in ARCA and COOH groups on 2D HDPE and BioVyon™ frit samples respectively was shown across the treatment platforms of two separate etching systems (Figure 3-7, Figure 3-9). Although this effect can be reduced by plasma treating samples in the centre of the plasma etching platform where variation is minimal, this remains a limitation of the larger mass etching system. Variation in ARCA throughout BioVyon™ frits is an inevitable factor associated with plasma; however, it may prove beneficial when considering protein absorption. Previous studies applying oxygen plasma to PE have shown that a range of CA can still promote cellular adhesion and growth (Figure 1-7) [162]. A range of surface wettability and therefore charge could function to selectively absorb a variety of proteins by their side chains. It is clear from

the data in Figure 3-25 that a plasma etched BioVyon™ frit possesses a range of wettability due to the masking effect of the porous structure.

The application of oxygen plasma to polymers is known to generate a range of oxygen species. FTIR analysis of etched BioVyon™ frits indicated the primary groups generated include carbonyl, carboxyl and hydroxyl groups (Figure 3-10).These groups are known to promote protein absorption and in turn cell adhesion, a similar effect can be seen on tissue culture plastic. Comparing BioVyon™ and TCP surfaces at a molecular level is important as polystyrene plasma treated by corona discharge has been used in tissue culture for over 50 years, and is a well-established method of cell culture [144]. Comparison of the FTIR footprints of plasma etched BioVyon™ and TCP show that the only oxygen moiety these materials share is COOH as indicated by the peak at 1370 cm^{-1} in Figure 3-13. The difference in polymer structure and the type of plasma used can account for this variation. Polystyrene contains benzene ring structures which may be more susceptible to oxidation, favouring the generation of COOH groups. Furthermore, corona discharge is more intense plasma generated in atmosphere which in turn could account for the differences observed.

The differences in the oxygen species generated was supported by the comparative THA and TBO assay data in Figure 3-14, and the ARCA data in Figure 3-15. These findings suggested that the low ARCA, or high wettability of BioVyon™ was a result of the carbonyl and hydroxyl groups present after plasma etching (Figure 3-16). The same effect was not produced by COOH alone which are approximately eight times higher on TCP compared to BioVyon™ (Figure 3-16).

It appears that the benefit of benzene ring structures and a surface of COOH groups is long term stability; TCP can be stored for months without any reduction in its functional properties, this is not the case with plasma etched BioVyon™. Figure 3-17 and Figure 3-18 indicate that in atmospheric conditions ARCA increases rapidly by 8° over 6 hours and 4° over 6 days suggesting that oxygen groups generated by the plasma etching are susceptible to decay. By storing the plasma etched samples in PBS it was hoped that the decay would be reduced or prevented, as observed in previous studies on polydimethylsiloxane [266]. There was little evidence to support this in Figure 3-17 as the decrease in advancing contact angle of PBS stored samples after 30 minutes was comparable to the atmospheric samples. However Figure 3-18 indicates that the ARCA measurements of PBS stored samples plateaus over a period of 12 days, suggesting decay was not only reduced but completely halted over long periods of time, as indicated by long term study of COOH groups (Figure 3-19).

The characterisation of surface chemistry generated by oxygen plasma shows that BioVyon™ can be treated to generate a consistent, well defined surface chemistry with properties similar to TCP. This treatment can be preserved by storage in an appropriate media, and maintained at a standard suitable for the infiltration, adhesion and growth of cells.

3.4.3 Surface topography

Oxygen plasma has an etching effect on the surface of polymers. It was important to analyse this effect on BioVyon™ to compare and understand its significance relative to other materials. AFM scans and quantitative roughness measurements both indicated that roughness was increased after plasma etching; this is well established in literature [230, 251, 266].

Due to the manufacturing process, particulates in contact with a surface flatten during sintering generating plateaued regions on one side of BioVyon™ first. These regions provided an ideal platform for analysis with AFM; microscale topography was used to navigate to the original scanning areas. This meant that the same sample and section of BioVyon™ could be analysed before and after treatment with oxygen plasma for 60 seconds at 60 watts (Figure 3-20). Comparison between the scans at 50 and 1µm show that the nano scale topography was altered with larger microscale topography becoming more prominent in the 50µm scans and a more consistent increase in nanoscale roughness in the 1µm scans (Figure 3-20 and Figure 3-21). This etching effect was due to the nature of the HDPE surface and the ratio of amorphous to crystalline regions. The nano scale peaks observed to increase in the plasma etched 2D cross section are crystalline regions and appear prominent after etching due to the removal of amorphous regions surrounding them, which are more susceptible to chemical attack from the oxygen plasma. Quantitative measurement supported this, although no statistically significant difference was observed in roughness between untreated and etched samples as measured by RMS ($P>0.05$). A difference of a few nanometres could be seen to decrease from 50 - 1µm (Table 3-3). At a 1µm scan size a difference of only

0.5nm was observed. Relative to literature investigating cell response to surface roughness this is a very small difference, as supported by statistical analysis which was not found to be significant (P>0.05) [177].

The findings using AFM were supported by SEM analysis, at a nanoscale there was a clear difference in the topography of BioVyon™ before and after plasma treatment, more prominent ridges and hollows were present on the surface after 60 seconds contact with plasma at 60 watts compared to untreated surface (Figure 3-23). It is important to note that the surface in the SEM images appear different to the AFM scans as these are images of the sintered BioVyon™ surface, unlike the flattened regions of the frits, they possess a unique topography. The use of SEM to image the internal surface of plasma etched frits has also shown that despite the masking effect discussed earlier, etching is still visible in the centre of the frits (Figure 3-24). This indicates that the plasma is influencing both the physical and chemical properties throughout the frits, as ARCA was also decreased relative to untreated samples on 2D HDPE despite a 2mm BioVyon™ mask (Figure 3-25).

These methods have shown that post plasma etching, BioVyon™ possesses an average nanoscale topography depth of 5nm. Previous literature has investigated a range of materials and cell lines, and while these may not be directly comparable to BioVyon™ it is interesting to note that both microscale and nanoscale topography have been observed to influence cell response [171, 173, 177]. Studies exposing osteoblasts to trenches of varying widths indicated that they did not respond to topography of a width less than 10µm [171]. However, rat fibroblasts were found to orientate themselves in response to topography between 1-5µm in width [173]. While this work may be relevant

to the larger topographical structures, the surface of BioVyon™ is primarily composed of a consistent nanoscale roughness; a similar surface with topography depth as low as 44nm elicited a direct response from macrophages [177].

Work conjugating peptide sequences to polyurethane surfaces by varying lengths of PEG, found that a difference of 16nm in height between the pentapeptide GRGD improved the adhesion and growth of HUVEC endothelial cells over 36 hours [183]. It can be suggested that rather than the direct influence of roughness, this response may have been caused by the increased contact of integrin to peptides due to the variation in height. This in turn may have improved access to binding sites at a molecular level. This study is comparable to BioVyon™ which offers a similar roughness at the nanoscale.

Overall the methods used to characterise surface roughness generated by plasma etching have provided excellent proof of principle; etching has been quantitatively analysed by AFM and was found to increase roughness by approximately 0.5 nm. Direct imaging of the BioVyon™ surface support these measurements, the effects of plasma etching are clearly shown at both the micro and nano scale. BioVyon™ offers a unique and complex surface post plasma treatment which holds potential as a platform for further modification.

4 Conditioning BioVyon™ surface for cell adhesion and growth

4.1 Introduction

Conditioning a novel biomaterial for cell culture is a complex task due to the vast number of factors involved such as; surface chemistry, protein adsorption, surface area, nutrient and oxygen diffusion. All must be taken into account and are compounded by the complexity of the cell response and cellular requirements such as cell seeding, adhesion, spreading, cell to cell interaction, and growth factors. This chapter focuses on cellular adhesion and factors which have an immediate affect such as protein absorbance and seeding efficiency, with the primary aim of sustaining cellular survival and growth over a significant period of time.

4.2 Cell adhesion

Adhesion of a cell population to a 3D scaffold is the most important factor influencing cell culture, and affects the growth of the cell population. Various factors influenced cell seeding and had to be explored before optimisation of the BioVyon™ environment could begin.

4.2.1 Optimising cell adhesion

Initial experimentation was required to determine if plasma etching (PT) improved the adhesion and infiltration of cells. Populations of Min-6 were seeded (As described in section 2.2.16.2) onto BioVyon™ frits plasma etched for 60 seconds at 60 watts and untreated frits. The graph in Figure 4-1 shows a significant increase in cell adhesion to the plasma etched BioVyon™ frits ($P<0.05$), with approximately 450,000 and 40,000 cells adhered to plasma etched frits and untreated frits respectively. This is supported by the images below the graph which show that the cell suspension is unable to infiltrate the untreated frit due to the low wettability (Figure 4-1, c).

The effect of adhesion incubation time was compared between BioVyon™ frits plasma etched for 60 and 120 seconds at 60 watts. A similar pattern of adhesion can be seen from 0.5 to 5 hours incubation time between the two treatment times. A linear increase is observed from 0.5 hours to 2 hours, with a cell population of approximately 700,000 and 300,000 cells adhered on frits treated for 120 and 60 seconds respectively. Figure 4-2 shows the adhered populations plateau at 3 hours before fluctuating slightly from 4 to 5 hours. Overall, a significant difference is seen between plasma etching times after 1 hour ($P<0.05$), with frits treated for 120 seconds adhering a significantly higher number of Min-6 compared to the 60 second treated frits. Figure 4-2 indicates that after 2 hours incubation cell adhesion begins to plateau; further increases in cell number could have been due to cell proliferation. As a result the 2 hour incubation time was adopted for all future experiments involving cell adhesion.

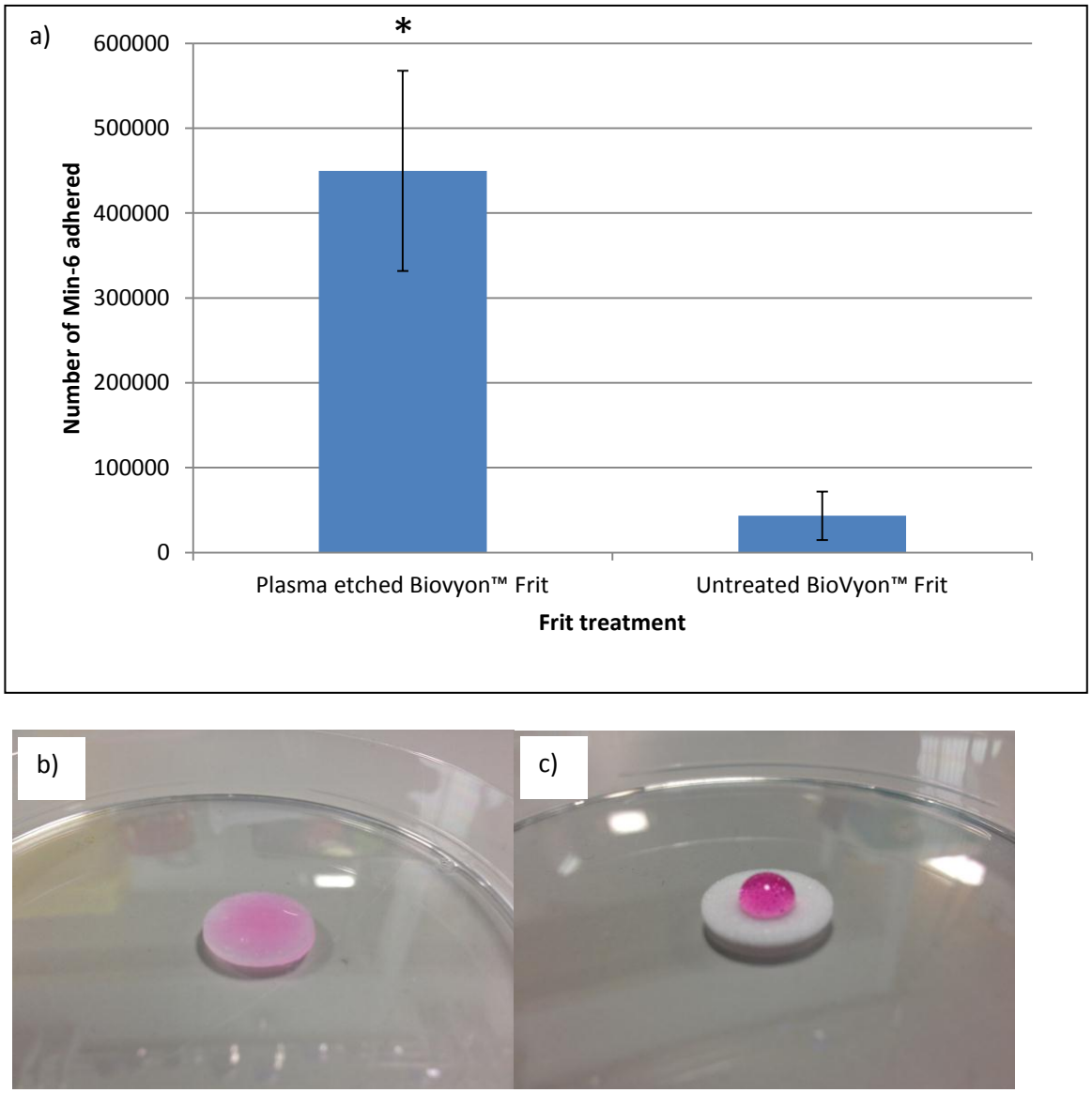

Figure 4-1: Cell adhesion before and after plasma treatment

BioVyon™ frits were plasma etched for 60 seconds at 60 watts, seeded with 200µl of cell suspension containing Min-6 (Described in Section 2.2.16.4). The cell number of each sample was calculated by comparison of absorbance value to a calibration curve; error bars represent variation between four frits seeded with the same cell population, n = 4. Graph a) shows Min-6 adhered to each frit type. Image b) shows cell media absorbed throughout the plasma etched frit structure, image c) shows cell media held as a droplet on the surface of an untreated frit. Graph a) indicates a significant increase in cell adhesion on plasma etched frits compared to the untreated frit, with approximately 450,000, and 40,000 Min-6 adhering respectively ($P<0.05$). This is due to the difference in wettability, as indicated by images b) and c). Significance difference between cell number adhered is denoted by *.

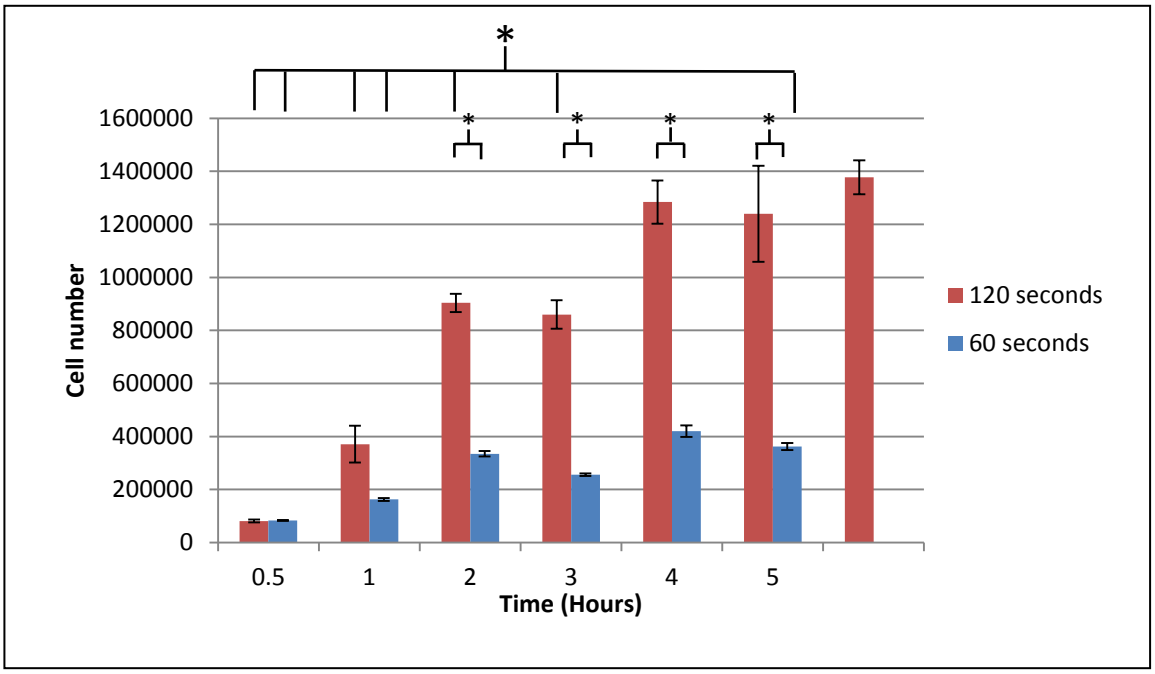

Figure 4-2: Cell adhesion and incubation time

BioVyon™ frits were plasma etched for 60 and 120 seconds at 60 watts, seeded with 200µl of cell suspension containing $1x10^6$ Min-6, and incubated for 2 hours (Described in section 2.2.16.4). The cell number of each sample was calculated by comparison of absorbance value to a calibration curve; error bars represent variation between three frits seeded with the same cell population, n = 3. A significant difference in cell number over incubation time was observed (Two-way ANOVA, $P<0.001$), a significant difference in cell number was observed at 0.5, 1 and 5 hours and 0.5, 1, 2 and 3 hours on frits plasma etched for 60 and 120 seconds respectively (Two-way ANOVA, $P<0.001$). Frits treated for 120 seconds adhered a significantly higher number of Min-6 compared to the 60 second treated frits between 2 and 5 hours (T-test, $P<0.05$). * indicates a significant difference in cell number between incubation times and plasma etching treatment times.

The volume of cell suspension seeded onto BioVyon™ was investigated as a factor influencing cell adhesion, contact between cells and the surface of the frits is affected by the solution surrounding the porous structure. BioVyon™ frits were plasma etched for 60 seconds at 60 watts, weighed and soaked in water, before being weighed again. The difference in weight was compared between three frits and used to calculate the volume of water filling the porous structure.

Weight before (g)	Weight after (g)	Difference (g)	Volume (µl)
0.0928	0.1704	0.0776	78

Table 4-1: BioVyon™ F internal volume

Three BioVyon™ F frits were weighed and submerged in water. Once removed they were re-weighed with water contained within the porous structure, the volume was calculated from the difference in the weight and found to be approximately 78µl.

To investigate the effect of varying volumes of cell suspension on adhesion, BioVyon™ frit were plasma etched for 60 seconds at 60 watts and seeded with $1x10^6$ Min-6 re-suspended in volumes increasing from 40µl to 200µl. Figure 4-3 shows that as seeding volume increases from 40µl to 80µl so does the number of cells adhered. After 80µl the cell number adhered appears to plateau with a gradual decrease to 200µl and an increase in error associated with the larger seeding volumes. It is interesting to note the sudden decrease in adhesion as the seeding volume increases past the frits internal capacity.

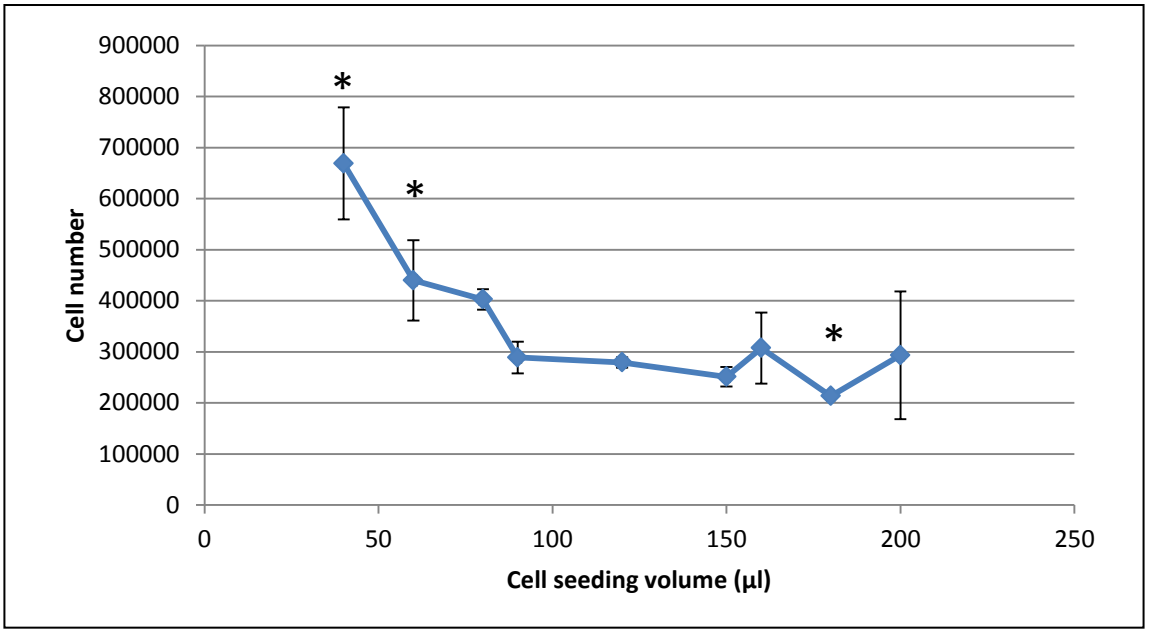

Figure 4-3: Cell adhesion and seeding volume

BioVyon™ frits were plasma etched for 60 at 60 watts, seeded with 40, 60, 80, 90, 120, 150, 160, 180 and 200µl of cell suspension containing $1x10^6$ Min-6, and incubated for 2 hours (Described in Section 2.2.16.4). The cell number of each sample was calculated by comparison of absorbance value to a calibration curve; error bars represent variation between three frits seeded with the same cell population, n = 3. As seeding volume increases from 40µl to 80µl the number of cells adhered decreases significantly (One-way ANOVA, $P<0.01$). 40, 60 and 180µl seeding volumes show a significantly different adhered cell number compared to the other volumes (One-way ANOVA, $P<0.01$). Significant difference in cell number adhered is denoted by *.

4.2.2 Cell adhesion and protein absorbance

It is well established that proteins promote cell adhesion by absorbing to materials and in turn adhering to cell integrins [144]. In order to observe the effect absorbed protein has on initial cell adhesion, cells suspensions in volumes of media with and without 10% FBS were seeded on BioVyon™ frits and tissue culture plastic (TCP) of comparable surface area. Figure 4-4 shows cell adhesion was signifcantly higher on both materials with FBS in the suspension volume as opposed to cells seeded without FBS ($P<0.05$).

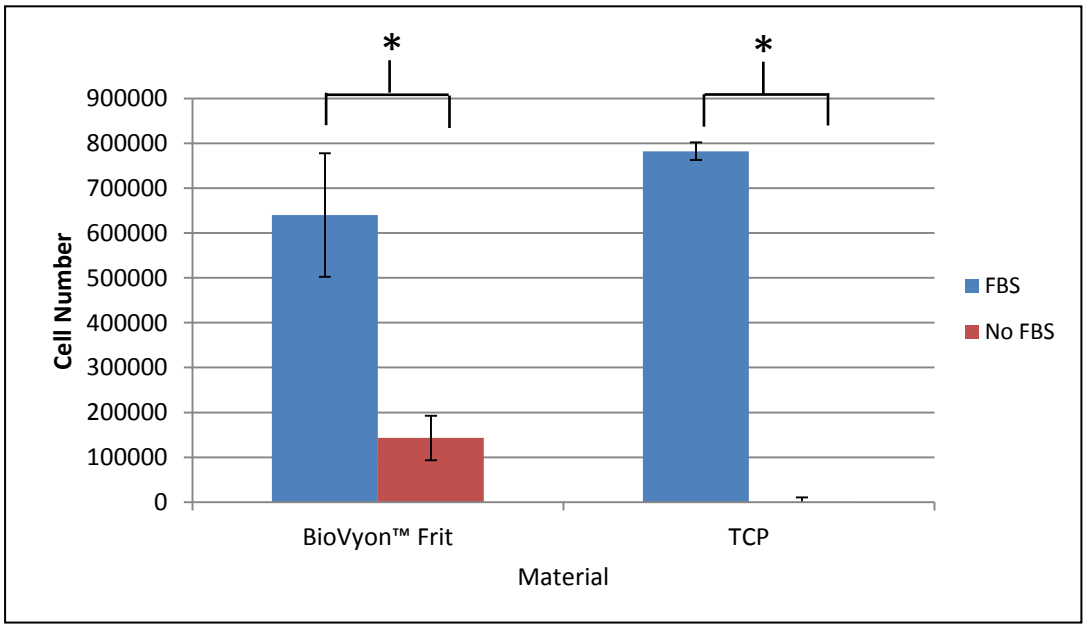

Figure 4-4: Cell adhesion with and without FBS

BioVyon™ frit plasma etched for 120 seconds at 60 watts and 12 well TCP plates of a comparative surface area were seeded with 40µl containing $1x10^6$ Min-6, and incubated for 2 hours (Described in Section 2.2.16.4). TCP plate cell suspension volume was increased to 1ml to ensure entire area was submerged to promote consistent cell adhesion. The cell number of each sample was calculated by comparison of absorbance value to a calibration curve; error bars represent variation between three frits seeded with the same cell population, n = 3. Cell adhesion was significantly higher on both materials with FBS in the suspension volume as opposed to cells seeded without FBS ($P<0.05$). Significant difference in cell number adhered is denoted by *.

4.2.2.1 Optimising protein adsorbance

Plasma etching affects wettability which in turn influences how proteins interact and adsorb to the surface of BioVyon™. The time of contact between BioVyon™ and oxygen plasma results in the generation of oxygen groups which contribute to surface wettability. Investigation of surface wettability on protein adsorption and cell adhesion would aid optimisation of the BioVyon™ internal environment for cell culture.

In order to assess how plasma contact time influences protein absorbance BioVyon™ frits were exposed to oxygen plasma for increasing lengths of time and then submerged in media containing FBS. After incubation the frits were washed and the protein desorbed using a 1% SDS solution, and quantified using a BCA assay. Figure 4-5 shows that as plasma contact time increased from 1 second to 50 seconds the quantity of FBS absorbed to the surface increases by approximately 0.38mg. The quantity of protein absorbed appeared to plateau from 50 to 120 seconds. Min-6 were then seeded on BioVyon™ frits treated in the same way as in Figure 4-5, to ascertain how the quantity of absorbed FBS influences cellular adhesion. Figure 4-6 shows that while contact with plasma has a positive affect on cell adhesion, increasing plasma contact time does not significantly increase cell adhesion beyond 20 seconds. A significant increase in adhered cell number can be seen in Figure 4-6, with cell number increasing from approximately 36,000 to 450,000 within 20 seconds of plasma contact time ($P<0.001$).

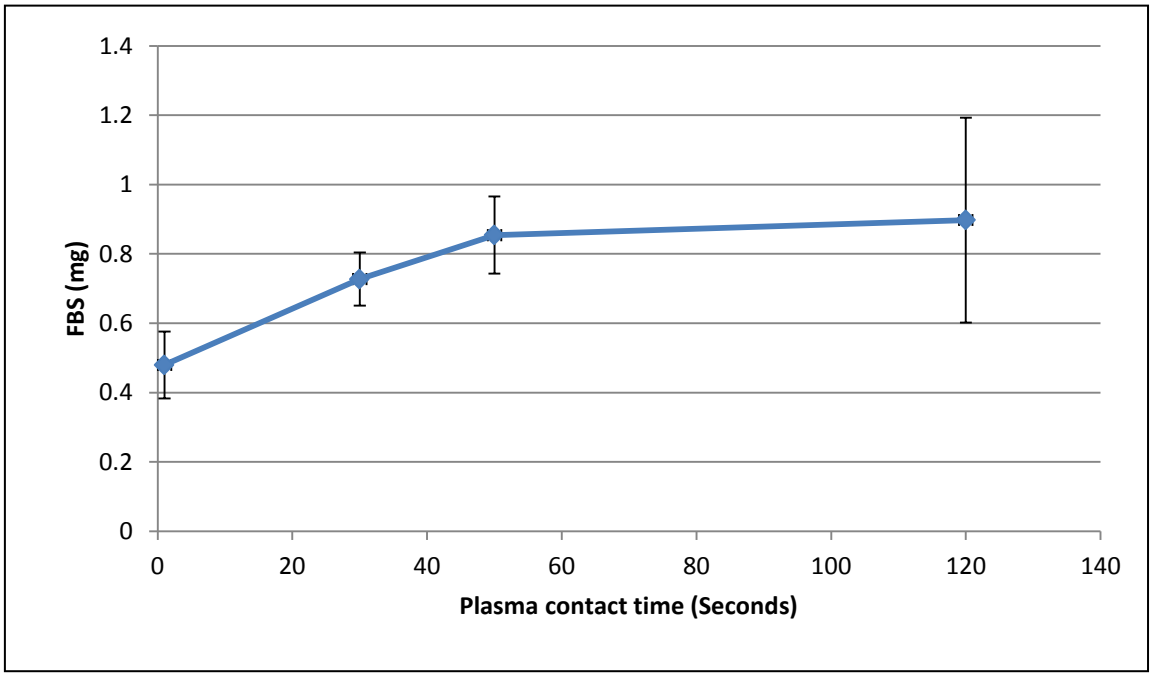

Figure 4-5: Protein adsorption with increasing plasma contact time

BioVyon™ frits were plasma etched for 1, 30, 50 and 120 seconds at 60 watts and soaked in 200µl media containing 10% FBS (20.3mg) foetal bovine serum (FBS) and incubated at 37°C for 1 hours before being washed with 800µl PBS. Frits were then transferred to 24 well suspension plates and submerged in 250µl of a 1% sodium dodecyl sulphate (SDS) solution, and incubated for 1 hour. SDS and unbound protein were then diluted with 750µl PBS, 25µl samples were transferred to a 96 well plate and incubated with 200µl BCA working reagent for 30 minutes before being measured using a spectrometer (Thermo, multiscan ascent)at 540nm. Bound protein was quantified by comparison of absorbance value to a calibration curve; error bars represent variation between three frits exposed to oxygen based plasma for different periods of time, n = 3. Protein adsorbance appeared to increase with increasing plasma contact time. While no statistically significant difference was observed, a clear increase in FBS absorbance can be seen from from 1 to 60 seconds ($P>0.05$).

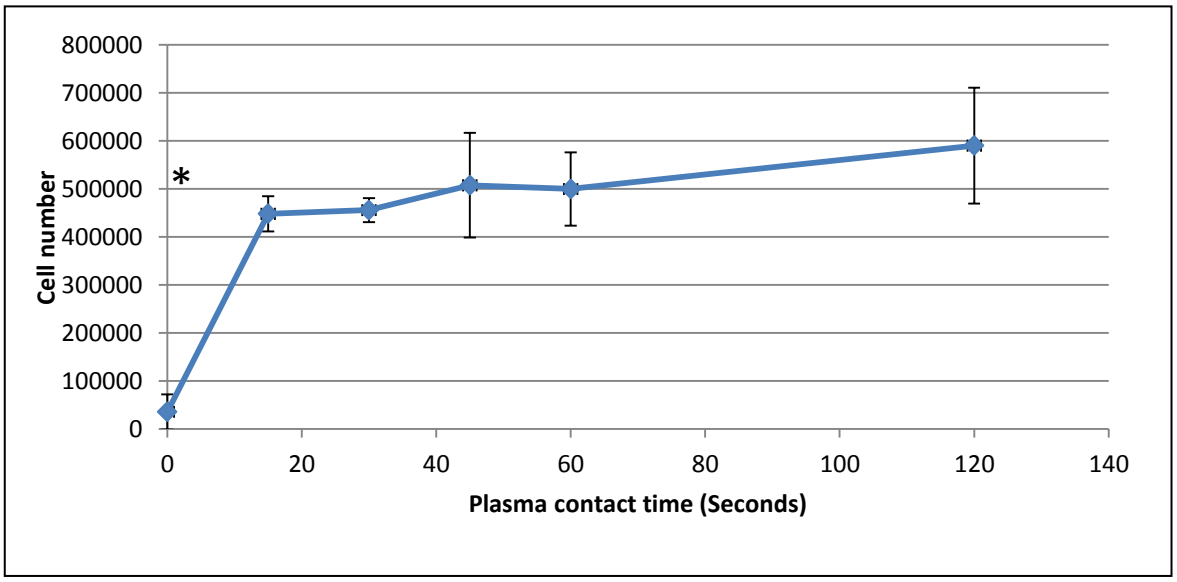

Figure 4-6: Cell adhesion and increasing plasma contact time

BioVyon™ frits were plasma etched for 0, 15, 30, 45, 60 and 120 seconds at 60 watts and seeded with 1×10^6 Min-6 in 200µl of cell suspension and incubated for 1 hour (Described in section 2.2.16.4). The cell number of each sample was calculated by comparison of absorbance value to a calibration curve; error bars represent variation between three frits seeded with the same cell population, n = 3. A gradual increase in cell population can be seen from 15 to 120 seconds. A significant difference in adhered cell number can be seen as plasma contact time increases from 0 to 15 seconds ($P<0.001$). Significant difference in adhered cell number is denoted by *.

4.2.3 Functionalising the BioVyon™ surface

The oxygen groups generated by contact with plasma offered anchorage sites for other chemical groups and potential for further functionalisation of BioVyon™. Amine groups have been used to bind short chain peptides, proteins and other molecules to the surface of biomaterials [276, 277]. Various surface treatments were tested, via protein absorbance and cell adhesion, in order to assess their suitability for cell culture.

4.2.3.1 Amine surface, cell growth/adhesion versus APTES

Aminopropyltriethoxysilane (APTES) is a molecule which can form covalent bonds with carboxyl groups and crosslink with other APTES molecules to effectively coat the surface of a material. This has been shown to functionalise the surface of materials with methyl and amine groups (Figure 4-8) [278, 279].

Plasma etched BioVyon™ frits were incubated with APTES at different concentrations for 24 hours at 90°C, in order to optimise the quantity bound to the surface of the frits. A methyl orange (MO) assay was utilised to quantify the amount of amine groups generated after treatment with APTES. Figure 4-8 shows a decrease in amine groups as the APTES in solution concentration decreases so does the quantity of amine groups available on the frit surface.The 0.1% solution of APTES was significantly lower than the other solutions depositing 0.68 nMol of amine groups ($P<0.01$). 1, 10 and 50% solutions deposited approximately 92 ,120 and 129 nMols of amine groups respectively. The image in Figure 4-8 shows frits incubated with decreasing solutions of APTES and stained with MO assay. The image supports the graph as it provides a qualitative assessment of the number and consistency of the amine groups throughout the frit structure. It is interesting

to note that the error associated with the 50 and 1% samples in the graph appear to have inconsistent spread throughout the frits in the images. A large dark spot of orange is present in the 50% solution frit, and darker specks of MO can be seen on the 1% solution frit. There appeared to be some orange colouration on the periphery of the frit incubated in the 0.1% APTES solution.

Biovyon™ F frits wth amine groups covalently bound to carboxyl groups were provided by Porvair filtration and compared using a MO assay to frits incubated with a 10% ATPES solution. Figure 4-9 shows that treatment with APTES generates a statistically higher quantity of amine groups, approximately 3.6 times more than than amine groups bound directly to the carboxy groups on the frit surface ($P<0.01$). To assess the suitability of amine functionalization for protein absorbance and cell adhesion, BioVyon™ frits treated with APTES, covalently bound amine frits, plasma etched frits and TCP of comparable surface area were submerged in 40µl media containg 10% FBS and incubated for 24 hours. The treated frits and TCP were then diluted with 200µl of PBS and the diffused FBS measured using a BCA assay, the quantity of FBS bound to the frits was calculated using the reverse method (Figure 4-10) (section 2.2.17). Figure 4-10 shows the quantity of FBS absorbed to each frit and the TCP. The amine frits absorbed a significantly higher quantity of FBS compared to the ATPES, PT and TCP ($P <0.001$). The PT frits seemed to absorb the lowest quantity of FBS, when compared to APTES treated frits and TCP, however the difference was not significant at approximately 0.11mg FBS.

BioVyon™ frits treated in the same way as frits in Figure 4-10, after incubation with 10% FBS in media they were seeded with $1x10^6$ Min-6 in a 40µl for 2 hours. Unadhered cells were removed by washing three times with PBS. Remaining Min-6 were quantified using

an LDH assay. Figure 4-11 indicated that APTES adhered a significantly lower number of cells than the other frits and TCP ($P<0.001$). Approximately 173,000 Min-6 were adhered on frits treated with 10% APTES compared to amine frits and plasma etched frits which adhered approximately 719,000 and 795,000 respectively. TCP adhered the highest cell population with approximately 845,000 Min-6. It is interesting to note that when comparing Figure 4-10 to Figure 4-11 the materials that absorbed the highest quantity of protein did not adhere the highest number of cells.

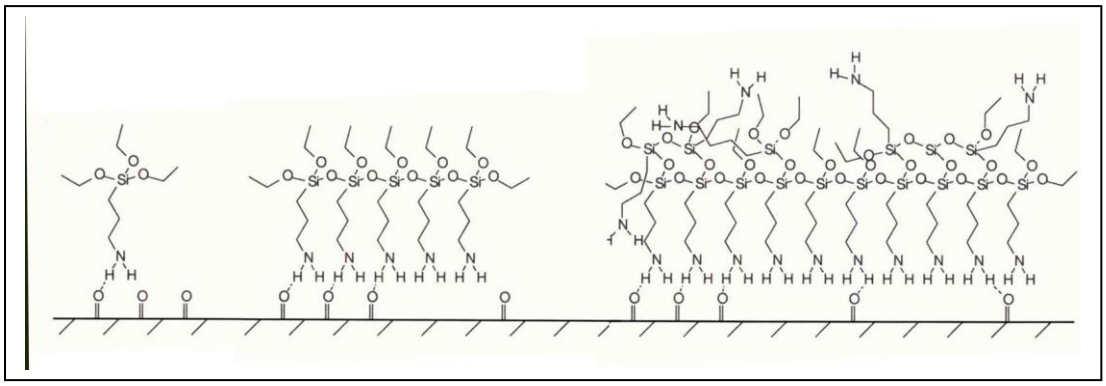

Figure 4-7: Aminopropyltriethoxysilane binding to carbonyl groups

Image shows theoretical orientation of Aminopropyltriethoxysilane (APTES) molecules on the suface of a material with carbonyl groups with increasing time and concentration.

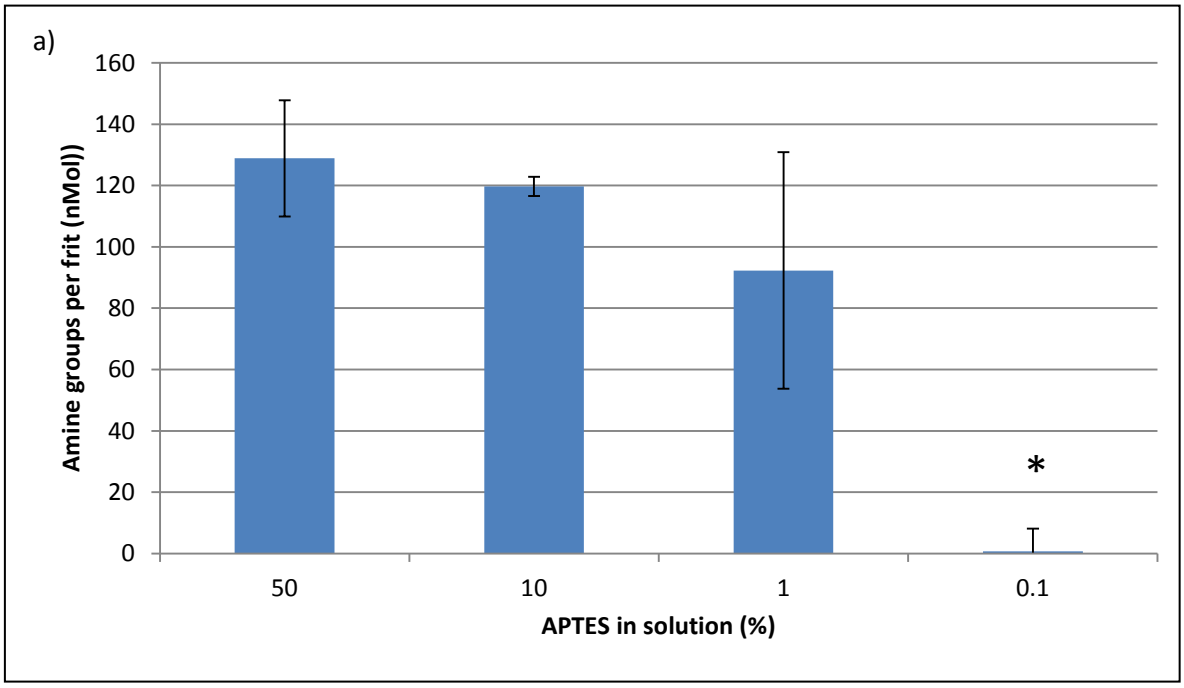

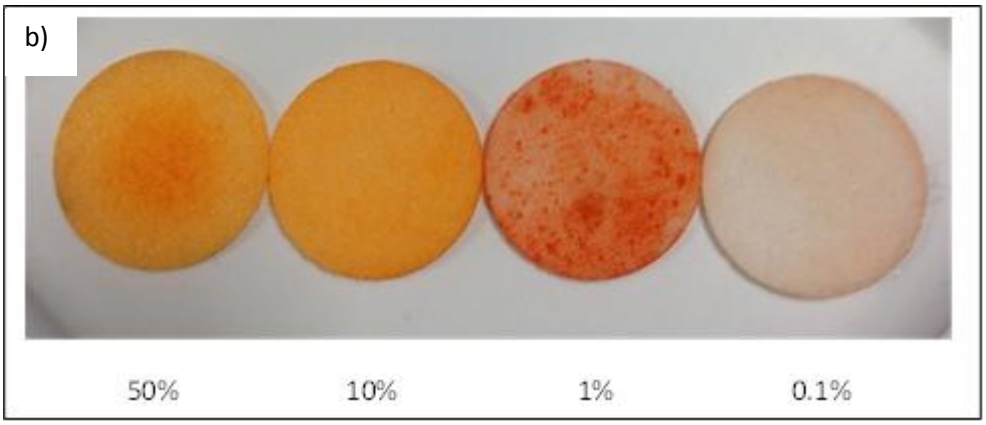

Figure 4-8: Range of amine groups generated with different % APTES in solution

BioVyon™ frits were plasma etched with an industrial plasma etcher for 116 seconds at 807 watts and treated with APTES (Described section 2.2.15). 50µl samples were measured using a spectrometer at 492nm and the molar values extrapolated from a calibration curve. MO assay indicates that there is a decrease in amine groups on the surface of frits treated with decreasing concentrations of APTES. Image below graph indicates the consistency of the orange MO molecules bound to amine groups within the frit structure, 10% APTES shows a consistent orange colour, 50 and 1% APTES solution show a dark spot central to the frit and bright patches on the surface respectively. 0.1% shows little if any orange colour and is the only solution generating amine groups significantly lower than the other solution concentrations ($P<0.01$). Significant difference of amine groups per frit (nMol) is denoted by *.

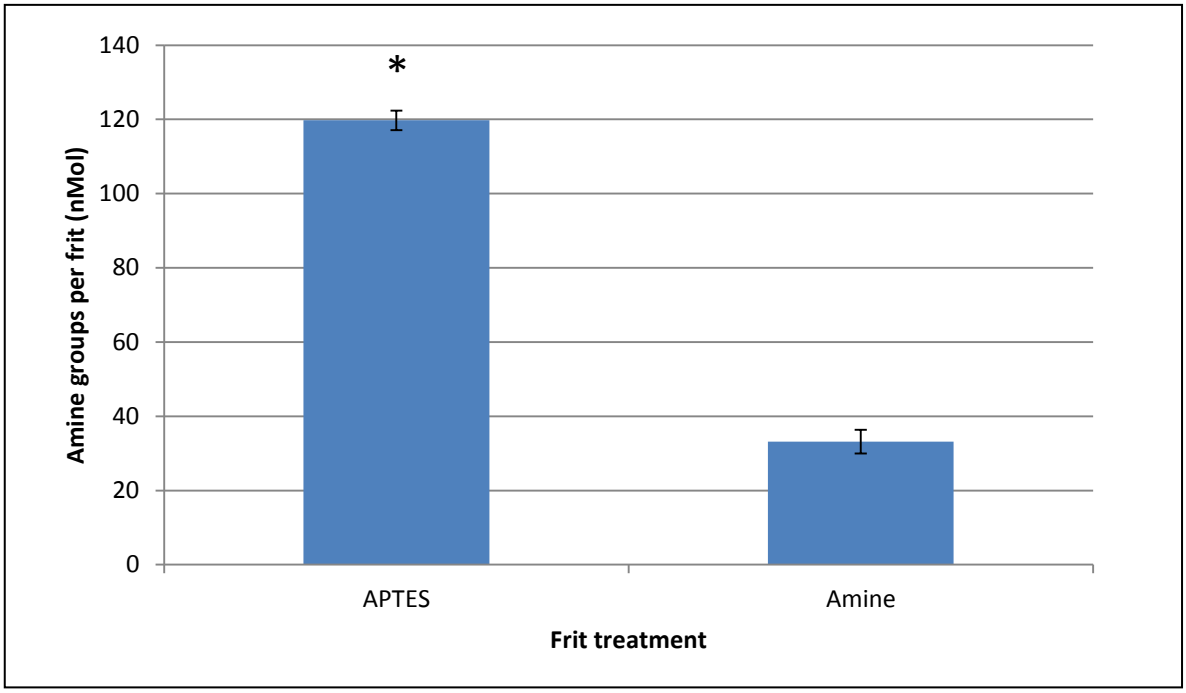

Figure 4-9: Amine group comparison on BioVyon™ frits

BioVyon™ frits were plasma etched with an industrial plasma etcher for 116 seconds at 807 watts and treated with aminopropyltriethoxysilane (APTES) before staining with methyl orange (MO) (Described section 2.2.15). Amine frits were provided by Porvair Filtration. 50µl samples were measured using a spectrometer at 492nm and the molar values extrapolated from a calibration curve. The graph indicates that the ATPES treated frits possessed approximately four times the amount of amine groups than the amine treated frits provided by Porvair filtration, a significant difference was observed ($P<0.01$). Significant difference in amine groups per frit (nMol) is denoted by *.

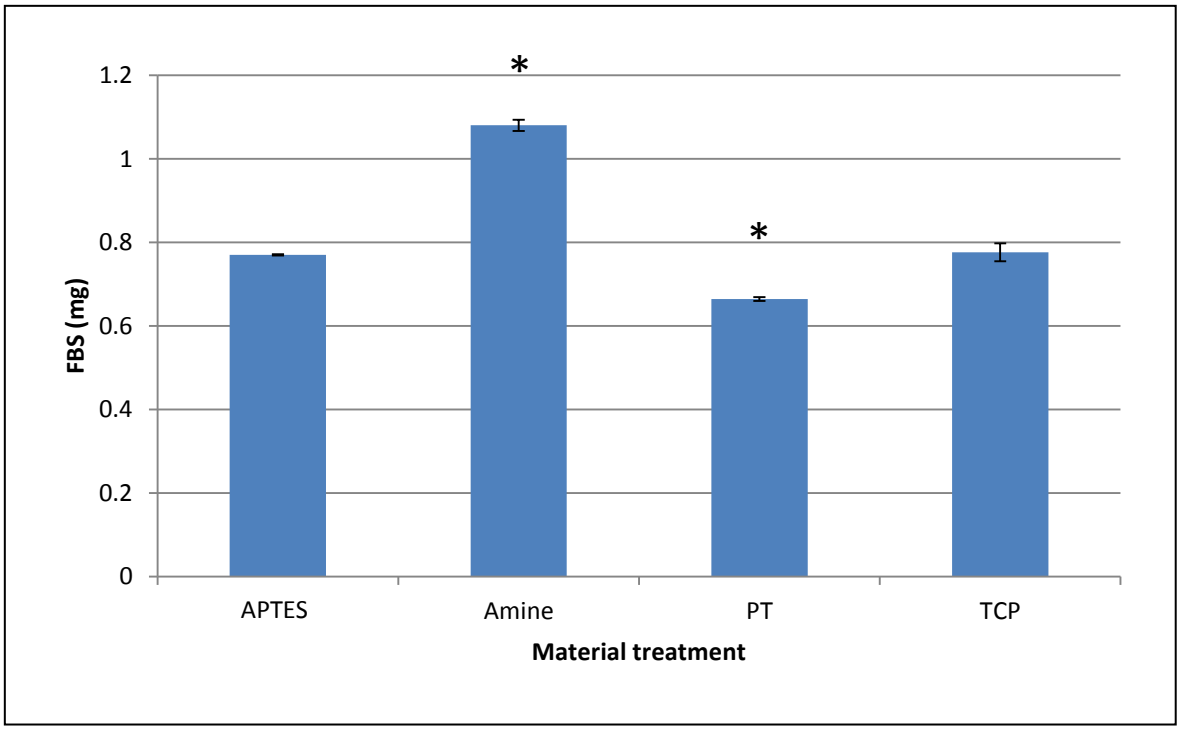

Figure 4-10: Protein absorbed to functionalised BioVyon™ frits and tissue cultue plastic

BioVyon™ frits were plasma etched (PT) with an industrial plasma etcher for 116 seconds at 807 watts and treated with 10%, aminopropyltriethoxysilane (APTES) (Described section 2.2.15). Amine frits were provided by Porvair Filtration. Treated frits and tissue culture plastic (TCP) 24 well plates were then soaked in 40µl (38µl for TCP to account for decreased surface area) media containing 10% (4.06mg) foetal bovine serum (FBS) and incubated at 37̊C for 2 hours. Frits were diluted with 200µl PBS and resuspended to aid diffusion of protein, 50µl samples were then added to 625µl of BCA working reagent and incubated at room temperature for 1 and 48 hours for the PT, TCP and ATPES, Amine samples respectively. Samples were then measured using a spectrometer (Thermo, multiscan ascent)at 540nm, and bound protein quantified using the reverse method. Absorbance values were compared to a calibration curve generated using the same incubation time with BCA working reagent as the samples; error bars represent variation between three BioVyon™ frits and TCP wells, n = 3. Graph indicates that the amine treated BioVyon™ frits and the plasma etched BioVyon™ frits adsorbed a significantly higher and lower quantity of FBS respectively, in comparison to the other materials ($P < 0.001$). Significant FBS quantity (mg) denoted by *.

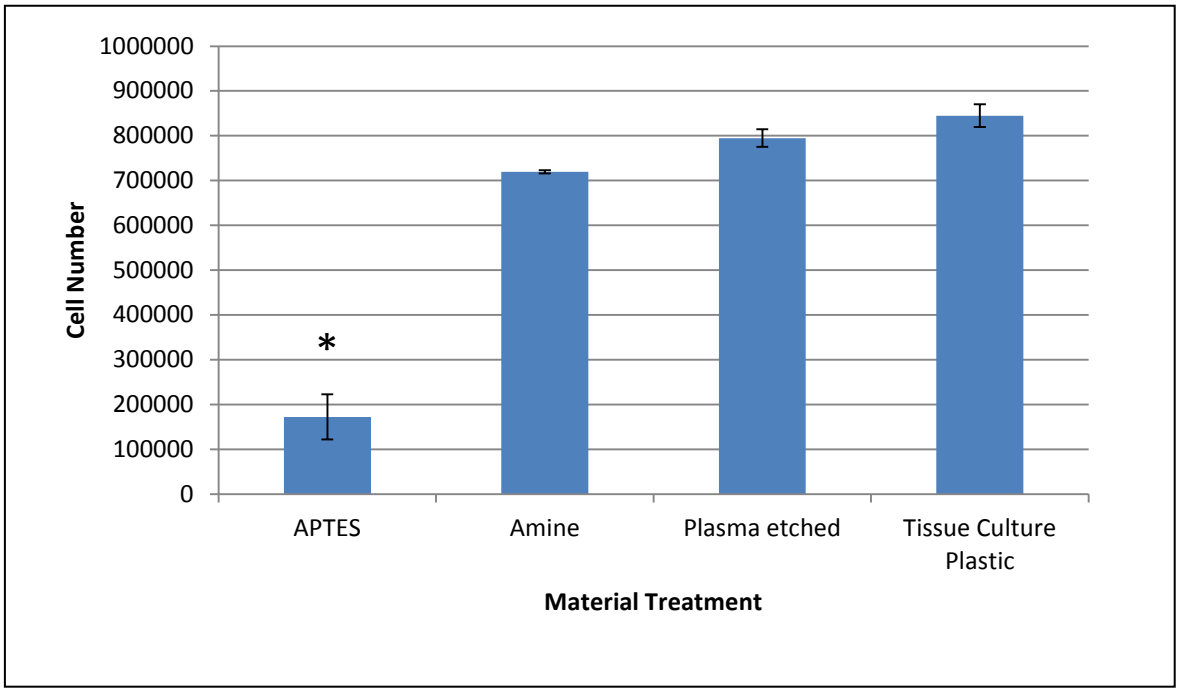

Figure 4-11: Cells adhered to functionalised BioVyon™ frits and tissue cultue plastic

BioVyon™ frits were plasma treated (PT) with an industrial plasma etcher for 116 seconds at 807 watts and treated with 10%, aminopropyltriethoxysilane (APTES) (Described section 2.2.15). Amine frits were provided by Porvair Filtration. Treated frits and tissue culture plastic (TCP) 24 well plates were then seeded with 40µl of cell suspension containing 1×10^6 Min-6 and incubated for 2 hours (Described in Section 2.2.16.4). The cell number of each sample was calculated by comparison of absorbance value to a calibration curve; error bars represent variation between three frits seeded with the same cell population, n = 3. Graph indicates that ATPES is the only treatment with a significantly decreased adhered cell number, with a cell population of approximately 170,000 adhered compared to the other materials, which adhered over 700,000 Min-6 ($P<0.001$). Significant difference in cell number adhered is denoted by *.

4.3 Discussion

This chapter has evaluated BioVyon™ as a cell culture system using methods to quantify cellular adhesion and protein absorbance and how factors such as plasma etching, volume of cell suspension and incubation time can influence adhesion. These factors have been explored and optimised to significantly improve the number of cells adhering to the internal BioVyon™ environment. The potential of further functionalising the surface of BioVyon™ using oxygen groups generated by plasma as anchorage sites was also investigated, the use of amine groups and there influence on protein will be considered in this section and compared to current literature.

4.3.1 Cell adhesion

Before contact with oxygen plasma BioVyon™ is almost completely unwettable and as a result it was impossible for cell suspensions to enter and adhere to the internal structure. The images in Figure 4-1 shows that the 200µl of cell suspension was contained on the surface of the hydrophobic, untreated frit. By comparison the frit exposed to oxygen plasma for 120 seconds possesses a wettability allowing for the saturation of media and cells into the porous structure. The presence of oxygen groups on the surface of hydrophobic polymer surfaces such as HDPE (Section 3.3) are vital for cell adhesion, as established in a variety of previous studies [144, 150, 156].

Once cell suspensions are seeded on and into plasma etched frits, three primary factors have been found to influence adhesion; the incubation time between cells and the

surface, the volume of the cell suspension, and the time of contact the frit has had with oxygen plasma. Two of these factors were investigated simultaneously, Figure 4-2 shows the adhered cell numbers of populations incubated from 1 to 6 hours on frits exposed to oxygen plasma for 60 and 120 seconds. The incubation time for both sets of data follow a similar pattern. There was an increase in cell adhesion from 0.5 to 2 hours before decreasing slightly to 3 hours, then plateauing after 4 hours.

It can be suggested that two hours is the optimal adhesion time for both plasma contact time sets. The slight decrease after two hours could be due to cells unadhering over time, once all avaliable adhesion sites on the BioVyon™ surface were taken. During the adhesion process (section 1.3.2), cell integrins may have removed partially bound protein causing cells to unadhere. Alternatively transient cell to cell adhesion could occur between adhered cells and cells in suspension, removing cells from the Biovyon™ [213].

The increase in cell populations after 3 hours (Figure 4-2), may not be due to further adhesion but proliferation. Min-6 population doubling time is approximaltey 1 generation per 24 hours Figure 2-9 can be used to calculate the theoretical increase in population after 6 hours. 0.228 generation doublings applied to a population of 900,000 cells (Approximate number adhered after 2 hours on frits in contact with plasma for 120 seconds) is approximately 200,000 cell divisions. This combined with the increase in variation observed for the 120 plasma contact data set after 4 hours is strongly suggestive of sporadic cell proliferation amongst the population.

The 60 second plasma contact data set showed a similar pattern of cell adhesion, however the number of cells adhered at each time point was significantly lower than the 120 second contact set. At the 2 hour adhesion time point a difference of approximately

565,000 cells was observed. That the decrease in plasma contact time has had a negative influence on cell adhesion may be due to a decrease in protein absorbance (Discussed in Section 4.3.2)

Different volumes of cell suspension were seeded onto BioVyon™ frits. A rapid decline in cell adhesion from 40µl to 90µl was observed in Figure 4-3. At low suspension volumes the cells are completely held within the frit structure and in a low volume there is a higher likelihood that the cells integrins will encounter an adhesion site on protein bound to the surface of the BioVyon™ or adhere to an adhered cell. As the suspension volume increases from 40µl, the volume increases and the likelihood of cell to adhesion site contact decreases, and so does cellular adhesion.

The BioVyon™ F frits have an internal volume of approxmiatley 80µl (Table 4-1), once the suspension volume increases to 90µl the frits are saturated and the volume is no longer held entirely within the porous structure. As a result the cells in suspension may not contact the BioVyon™ surface. This is supported by the data in Figure 4-3 as cell adhesion drops from approximately 400,000 to below 300,000 from 80µl to 90µl seeding volume.

As the volume increases from 150 to 200µl the cell adhesion appears to fluctuate and error increases, suggesting inconsistent adhesion resulting from cells in suspension failing to contact the BioVyon™ structure, or variation in protein adsorption. Overall these experiments have concluded that a frit exposed to the plasma for the longest, seeded with the lowest suspension volume for 2 hours is optimal for cellular adhesion.

4.3.2 Protein absorbance

Cell adhesion and protein absorbance are linked. This is a well established concept, and one that must be investigated throroughly before the BioVyon™ cultivation system can be optimised fully. Initially frits and TCP of comparable surface area were seeded with $1x10^6$ Min-6 in suspensions with or without FBS. Figure 4-4 indicated that in both materials protein is vital for cellular adhesion as Min-6 seeded without FBS adhered a significantly lower population of cells. The 3D structure of BioVyon™ alone may have been a factor contributing to an adhered population of approximately 143,000 as Min-6 without FBS in the media. Large clusters of cells may have formed via transient cell to cell adhesion, mediated through CAM molecules and integrins. This process may have caused cells to become trapped in the smaller BioVyon™ pores. These populations may then have endured washing prior to anaylsis with LDH assay (Section 2.2.16.4). Alternatively, the Min-6 may have synthesised and secreted their own proteinaceous microexuadate and adsorbed directly to the material surface independently of FBS in the media [151, 156].

BioVyon™ frits exposed to plasma for increasing periods of time indicate that adsorption of protein to the BioVyon™ surface was influenced by surface chemistry,. Figure 4-5 shows a trend, FBS absorption to BioVyon™ increases with increasing plasma contact time, from 1 to 50 seconds. The increase in protein absorbance is linked to the quantity of oxygen groups generated with increased plasma contact time, as more oxygen groups contribute to a hydrophilic or polar surface chemistry proteins are more readily adsorbed [162].

The plateau in protein adsroption after 50 seconds could be attributed to the beginning of an effect known as solvation, in which the surface becomes so positively charged, that a layer of water is bound with enough attraction to prevent or reduce interactions at a molecular level between proteins and the HDPE surface [165]. Alternatively, the surface of the frits may have been completely saturated with proteins constituting FBS.

Cellular adhesion with increasing plasma contact time followed the trend in protein adsorption in Figure 4-5; a low level of cell adhesion corresponded to the low protein adsorption. This is likely due to a limited amount of adhesion sites avaliable to cells. After 15 seconds plasma exposure the adhered cell population gradually increased by approximately 60,000 cells, after which a lot of variation was observed between frits. As the plasma contact time increases, the surface chemistry from 50 – 120 seconds (Figure 4-5) also shows a high amount of variation between protein adsorption on the frits, perhaps influencing the same variation on cell adhesion (Figure 4-6).

This variation could be associated with the random nature of protein adsorption. It can be speculated that within the FBS, albumin, a primary component of FBS, competes for the majority of the polar adsorption sites [162, 280]. Adsorption of albumin may improve with increasing contact angle, displacing other larger proteins suitable for cellular adhesion, such as fibronectin [162]. Due to the random nature of protein adsorption and the inability to control specific protein adsorption and orientation on the BioVyon™ surface, the optimisation of surface chemistry with oxygen plasma and addition of FBS alone may not be an effective method to condition the BioVyon™ for cell culture.

4.3.3 Functionalisation

The oxygen moieties generated by oxygen plasma held potential as anchoring groups for further chemical modification. APTES was investigated to discover if the functionality of the BioVyon™ surface could be improved. APTES in solution incubated with inorganic subtrates is known to deposit layers of amine and methyl groups [278, 281]. In order to optimise the generation of the functional layer of amine groups a range of APTES concentrations were incubated with plasma etched frits for 24 hours at 90 ˚C. Figure 4-8 indicated that the 10% APTES solution produced the most consistent treatment, and had the lowest variation in amine groups generated between frits.

The spots and darker regions observed in the frits treated with 10% and 1% solutions (Image b), Figure 4-8), are caused due to the MO dye binding to regions of the BioVyon™ surface with a high density of APTES molecules, crosslinked and layered during the incubation process. This variation appears to be influenced entirely by the concentration of APTES molecules present in solution. The temperature of the incubation environment is hostile to the oxygen treatment generated by exposure to plasma. As a result the 1% APTES concentration may have a sporadic and inconsistent APTES layer due to the decay (Section3.3.3) of carboxyl groups before a layer of APTES could be generated. A return to a hydrophobic surface chemistry in turn may have reduced the bonding of APTES molecules to the BioVyon™ surface. The 50% APTES solution shows a darker circle of amine groups central to the frit (Image, Figure 4-8) this may be due to the circular momentum of the incubator in combination with the increased quantity of APTES molecules in solution leading to increased crosslinking and in turn amine groups.

Porvair Filtration supplied frits with amine groups covalently bound to oxygen moieties on the surface. These were compared to the APTES treated frits. Figure 4-9 shows that the 10% APTES functionalised frits possessed approximately 3.6 times as many amine groups as the covalently bound amine frits suppied by Porvair Filtration. This shows that the APTES modification effectively increases surface funcationality of the BioVyon™ post plasma etching. The nature of APTES to crosslink results in an increase in functionality relative to the initial population of oxygen groups.

Due to the complexities of protein adsorption and cellular adhesion, it was vital to observe how these factors are influenced by the functionalisations. Due to the interactions between amine groups and the BCA assay the reverse method was applied to protein quantification protocols (Section 2.2.17). Figure 4-10 shows that the amine and APTES amine functionalised surfaces adsorbed a higher quantity of protein compared to frits exposed to plasma alone. This has been observed in other literature, and is due to the interaction between amine groups and corresponding carboxy groups on protein. The constituent proteins in FBS appear to favour the amine bound surface and adhere in turn more readily [274]. This however however does not correspond to the cell adhesion observed on first treated in the same way. It can be seen in Figure 4-11 that cellular adhesion on the amine functionalised frits was lower than both the plasma etched frits and TCP, despite a higher quantity of protein adsorption. There are several reasons why the amine surface may offer a suitable environment for protein adsorption but not cell adhesion. The adsorption process is heavily influced by the surface charge, and cell adhesion in turn is influenced by the structure of the proteins the cells come into contact with. A strong charge, or polar surface is known to the denature proteins adsorbed to the

surface, a certain folding is often necessary for the adhesion of cellular integrins [164, 282]. If the surface adsorbs proteins too strongly the proteins may become denatured or fold in an inaccessible way, reducing cellular adhesion, as observed with the amine frits in Figure 4-11 [164]. APTES frits showed a statistically lower number of adhered cells relative to the other treatments. The nature of the APTES molecule crosslinking may result in chains or sections of the APTES molecules being removed. This may be influenced by the attempted adhesion of cells and shear stress elicited during the seeding process.

These experiements have indicated that despite the advantage of increasing surface functionlisation with APTES, the treatment appears to be uncontrollable and is susceptible to the random process of protein adsorption. The amine bound frits appear to harbour comparative cell numbers, and hold potential as covalent anchoring groups for other molecules such as short chain peptides. This functionalisation holds potential to develop BioVyon™ as a cell culture system.

5 Mimicking the environment of the pancreas

5.1 Introduction

Biomaterials in tissue engineering function to mimic an environment in the body to grow, or cultivate a target tissue. The pancreatic islet is a relatively simplistic environment to mimic, the peri-insular basement membrane consists of two primary proteins, laminin 511 and collagen IV, these proteins adhere β-cell integrins in the periphery of the islets [70-72]. The β-cells central to the islet are adhered directly to other cells of the endocrine system, such as alpha and delta cells (Section 1.2.1). So far the biomaterial BioVyon™ has been developed and optimised for cell adhesion and assessed as a cultivation system. This chapter will investigate how effective BioVyon™ is at mimicking and harbouring Min-6 cell populations in three dimensions as well as protecting the β cell phenotype.

5.2 Peri-insular basement membrane protein adsorption

The ability of BioVyon™ to adsorb protein was exploited to coat the surface with proteins mimicking the peri insular basement membrane (BM). Plasma etched BioVyon™ frits were incubated in solutions of foetal bovine serum (FBS), laminin, collagen and a combination of both laminin and collagen. These proteins adsorbed to the surface during the 2 hour incubation and the quantities measured using a BCA assay (Described in section 2.2.16.1).

Figure 5-1 shows that a significantly higher quantity of collagen was adsorbed onto the surface of the frits and TCP, compared to laminin and laminin/collagen ($P<0.001$).

A higher quantity of laminin and collagen seems to adsorb to frits compared to TCP, with the exception of the combination of laminin/collagen. The only significant difference in protein adsorbance between materials was with laminin ($P<0.001$). The combination of proteins adsorbed less than both single protein solutions incubated with the frits. A higher quantity appeared to adsorb onto the TCP when compared to the frits. BioVyon™ frits incubated with BM proteins (Described in section 2.2.16.1) were analysed by scanning electron microscopy (SEM) to observe any topographical changes to the surface after protein adsorption had taken place. Figure 5-2 to Figure 5-6 show micro and nanoscale topography of BioVyon™ frits plasma etched for 116 seconds at 807 watts, and incubated with FBS, laminin, collagen and laminin/collagen. Overall the frits incubated with proteins share a underlying topography to the plasma etched control frits (Figure 5-2). However, cuboidal structures, microscale agglomerations, prominent ridges and nano scale, enveloping coatings can be seen on the surface of frits incubated with FBS (Figure 5-3), Laminin (Figure 5-4), Collagen (Figure 5-5) and laminin/Collagen (Figure 5-6) respectively. These topographies are noticeably different to the control frit surface and clearly influenced by the protein treatment.

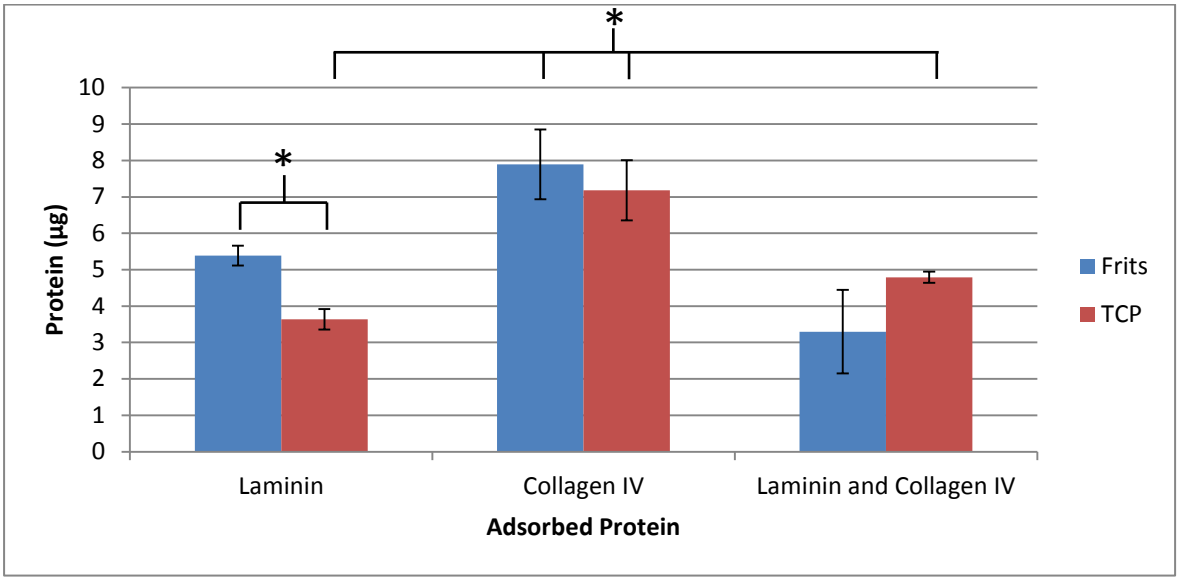

Figure 5-1: Peri insular basement membrane protein adsorption

BioVyon™ frits were plasma etched (PT) with an industrial plasma etcher for 116 seconds at 807 watts. Treated frits and tissue culture plastic (TCP) 24 well plates were incubated for 2hours in 40µl (38µl for TCP to account for decreased surface area) of a solution containing each protein (Described in section 2.2.16.1). After incubation frits were diluted with 200µl PBS and resuspended to aid diffusion of protein, 50µl samples were then added to 625µl of BCA working reagent and incubated at room temperature for 48 hours. 300µl samples were then measured using a spectrometer (Thermo, multiscan ascent)at 540nm, and bound protein quantified using the reverse method (Described in section 2.2.17). Absorbance values were compared to a calibration curve generated using the same incubation time with BCA working reagent as the samples; error bars represent variation between three BioVyon™ frits and TCP wells, n = 3. Graph shows that the highest quantity of protein adsorbed to both frits and TCP was Collagen IV, all protein quantities adsorbed to TCP were significantly different and laminin was the only protein to adhere significantly higher quantity to frits compared to TCP (Two-way ANOVA, $P<0.001$). * Indicates a significant difference in cell populations between treatments or materials.

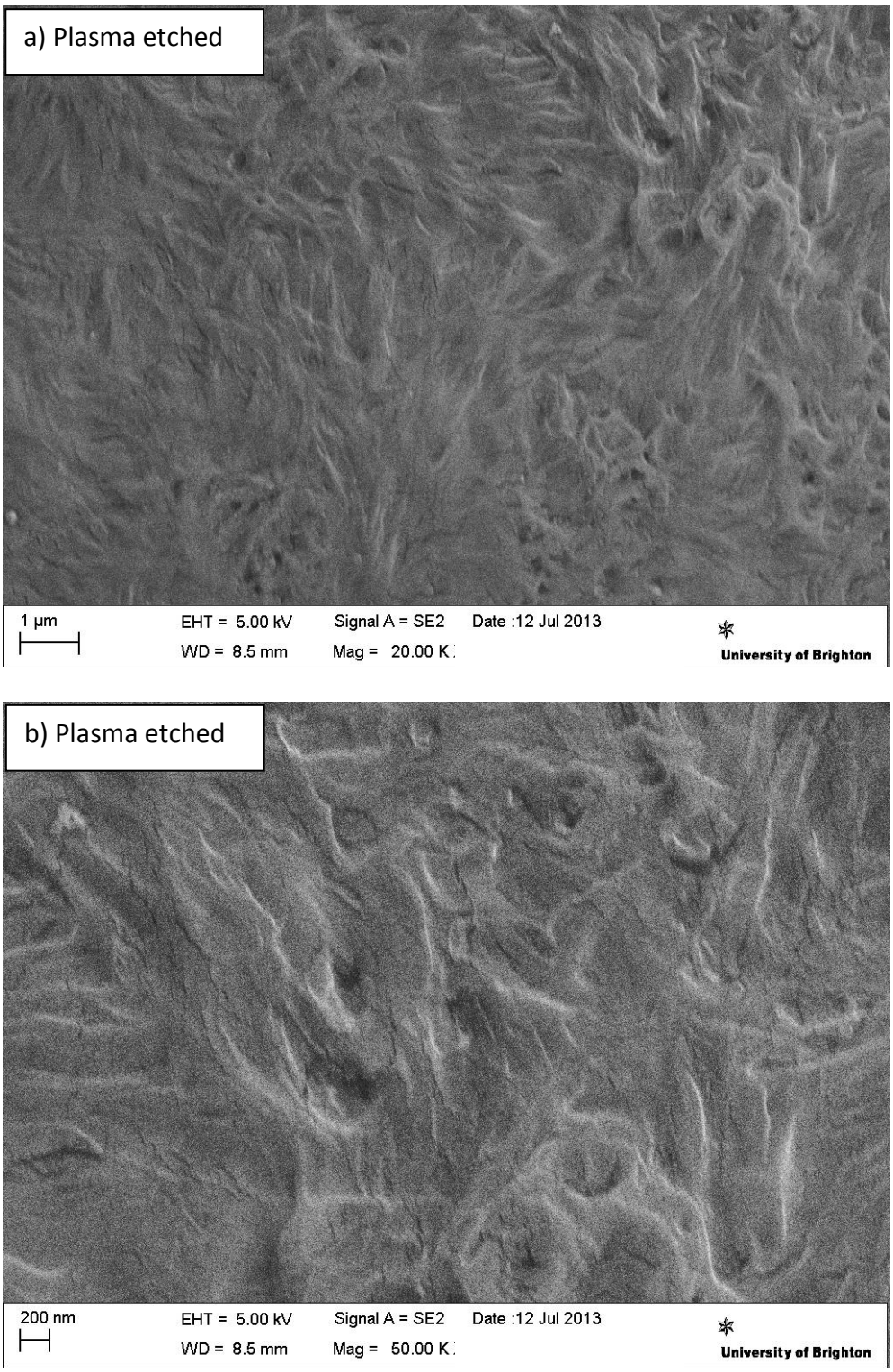

Figure 5-2: SEM images of plasma etched BioVyon™

SEM images of BioVyon™ frits plasma etched for 116 seconds at 807 watts. Image a) was taken at 20,000x magnification, b) 50,000x magnification. Surface appears typical of high density polyethylene (HDPE) post exposure to oxygen plasma, hollows and ridges are prominent in a), fissures and cracks can be seen clearly in b).

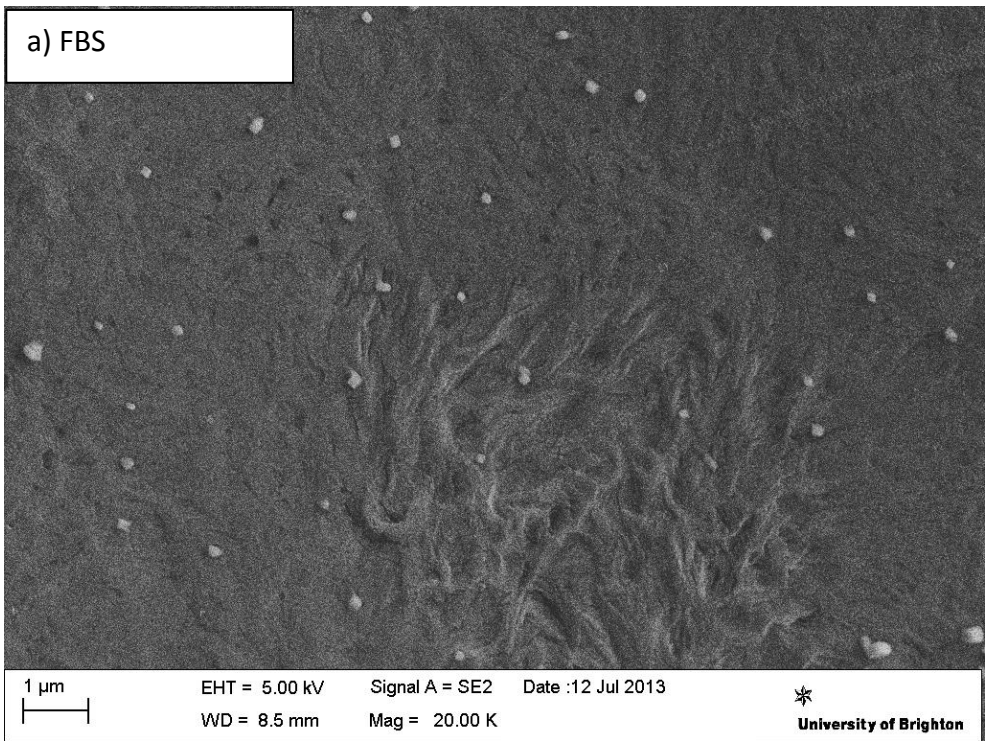

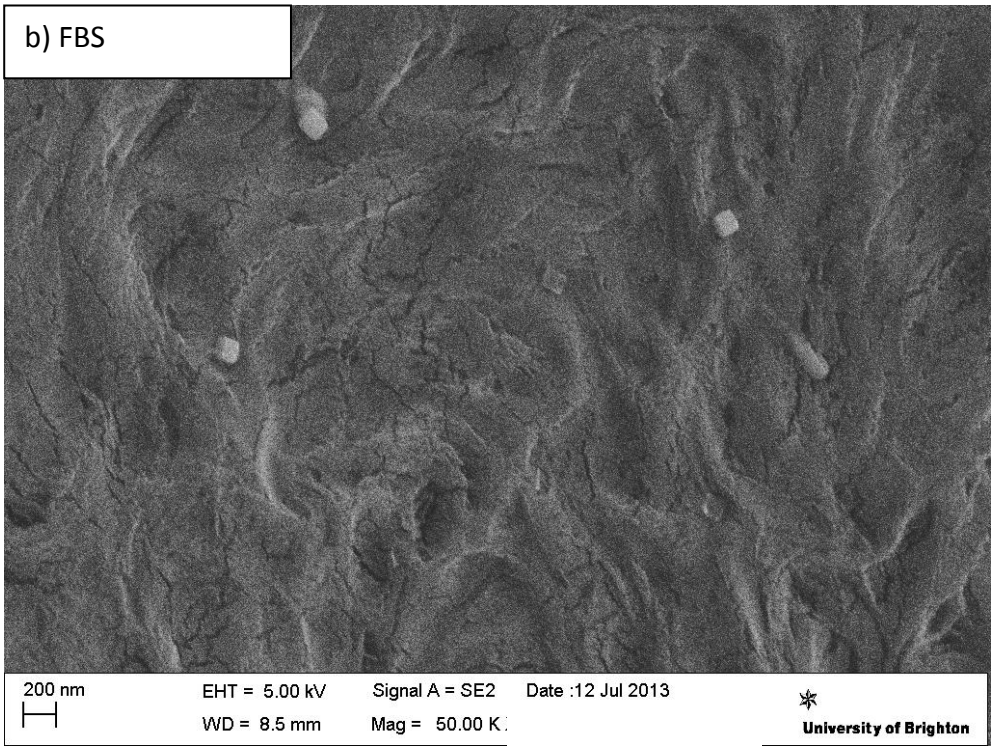

Figure 5-3: SEM images of plasma etched BioVyon™ and FBS

SEM images of BioVyon™ frits plasma etched for 116 seconds at 807 watts, and incubated with foetal bovine serum (FBS) (Described in 2.2.16.1). Image a) was taken at 20,000x magnification b) 50,000x magnification. Surface appears similar to plasma etched BioVyon™ with slightly less topography. Cuboidal structures approximately 100nm wide seen in a) and b) share a similar size and shape to salt crystals.

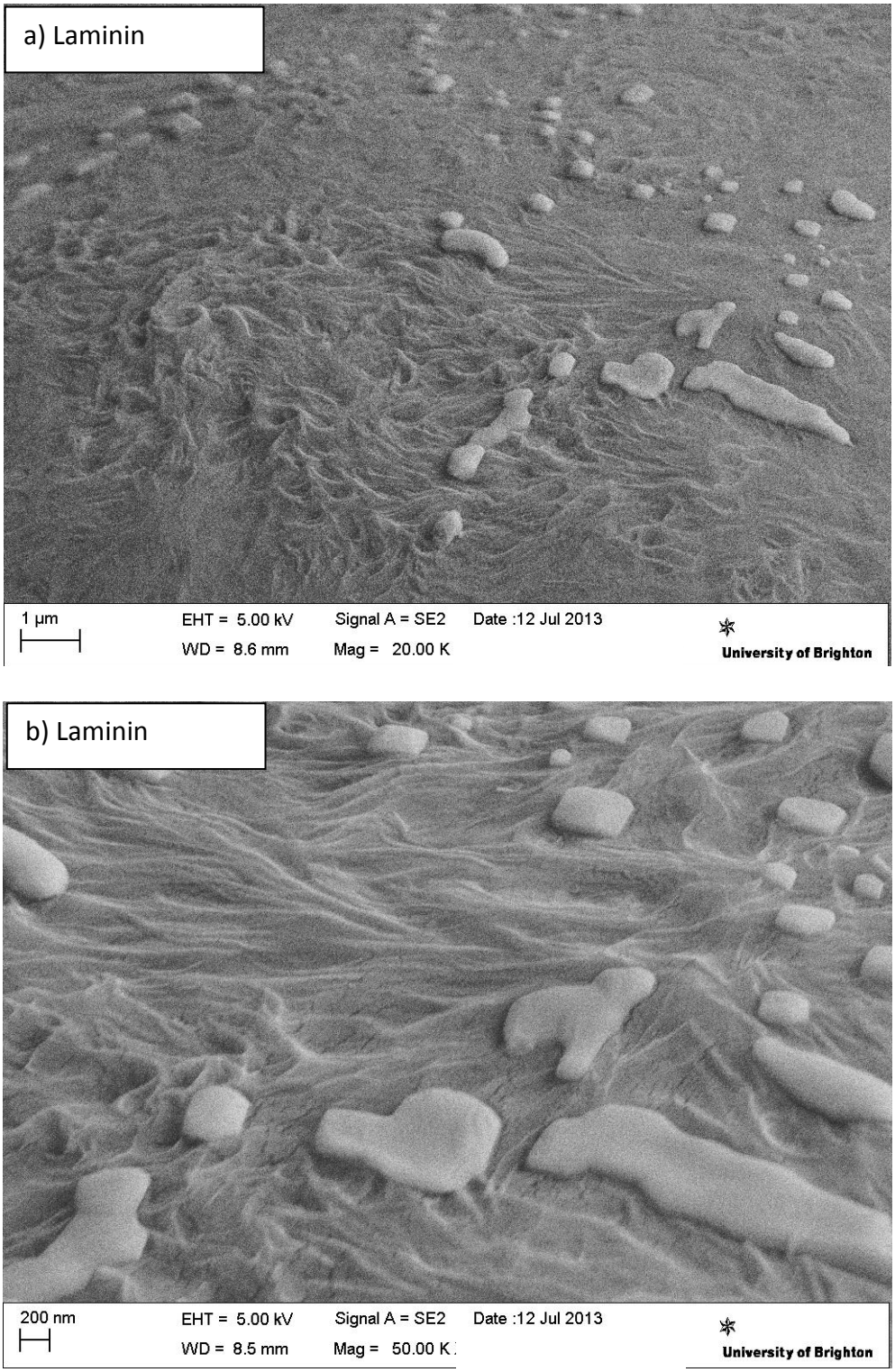

Figure 5-4: SEM images of plasma etched BioVyon™ and laminin

SEM images of BioVyon™ frits plasma etched for 116 seconds at 807 watts, and incubated with laminin (Described in 2.2.16.1). Image a) was taken at 20,000x magnification b) 50,000x magnification. Surface appears similar to plasma etched BioVyon™, several prominent agglomerations can be seen on the familiar surface topography.

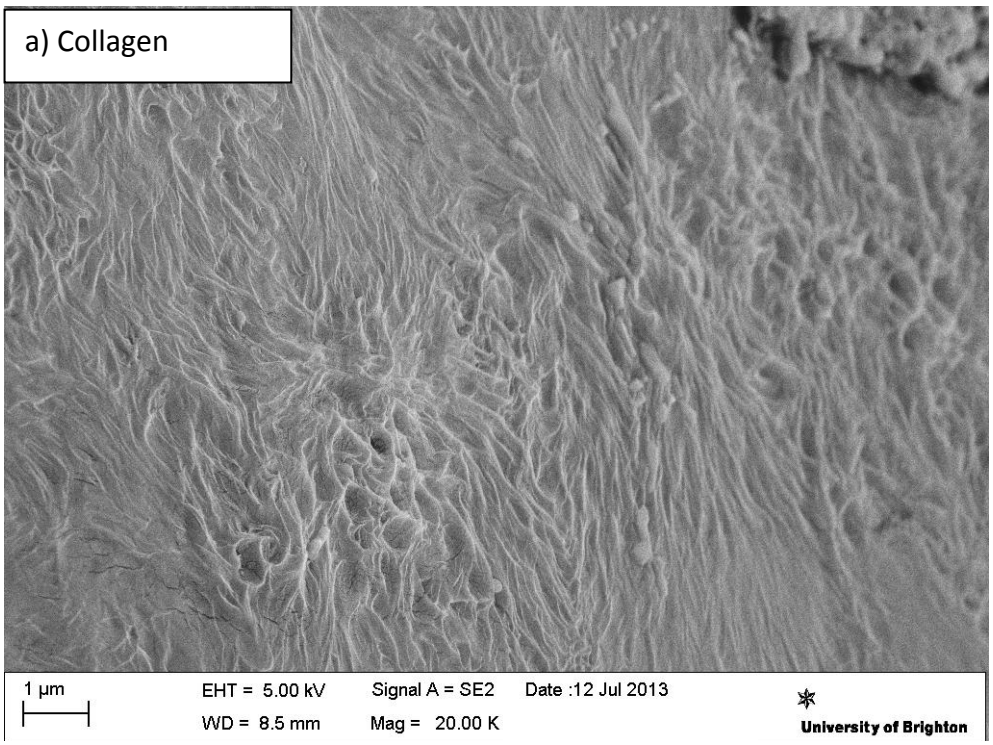

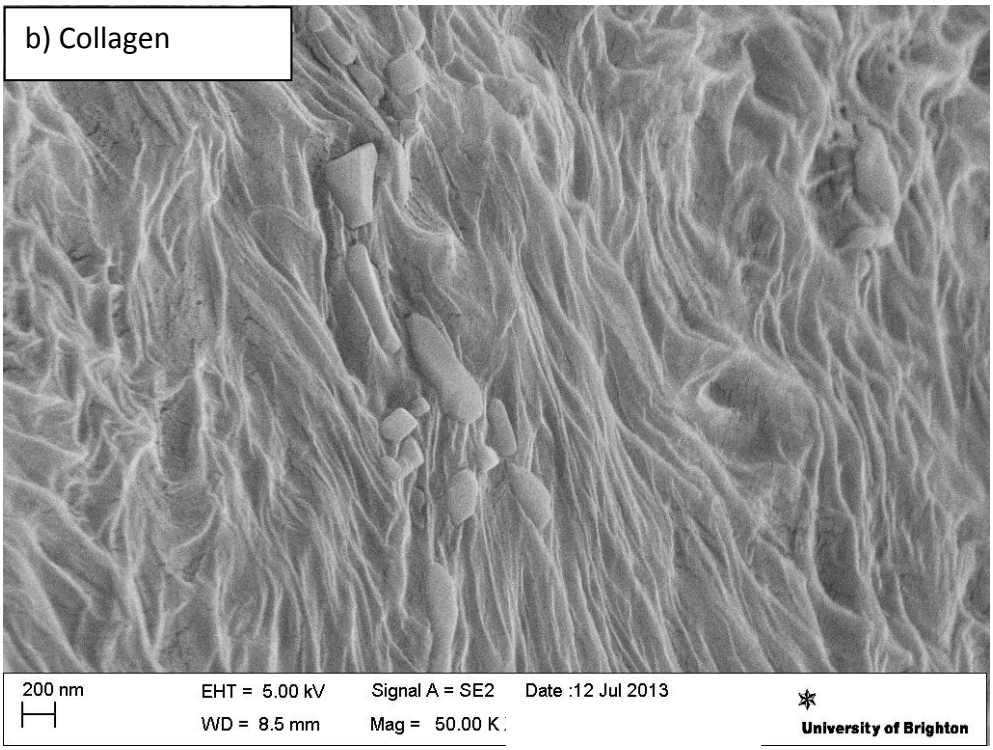

Figure 5-5: SEM images of plasma etched BioVyon™ and collagen

SEM images of BioVyon™ frits plasma etched for 116 seconds at 807 watts, and incubated with collagen (Described in 2.2.16.1). Image a) was taken at 20,000x magnification b) 50,000x magnification. Ridge topography appears to be more common and clearly defined in a)compared to plasma etched Biovyon™. Semi cuboidal structures present in b) are between 100nm and 400nm in size.

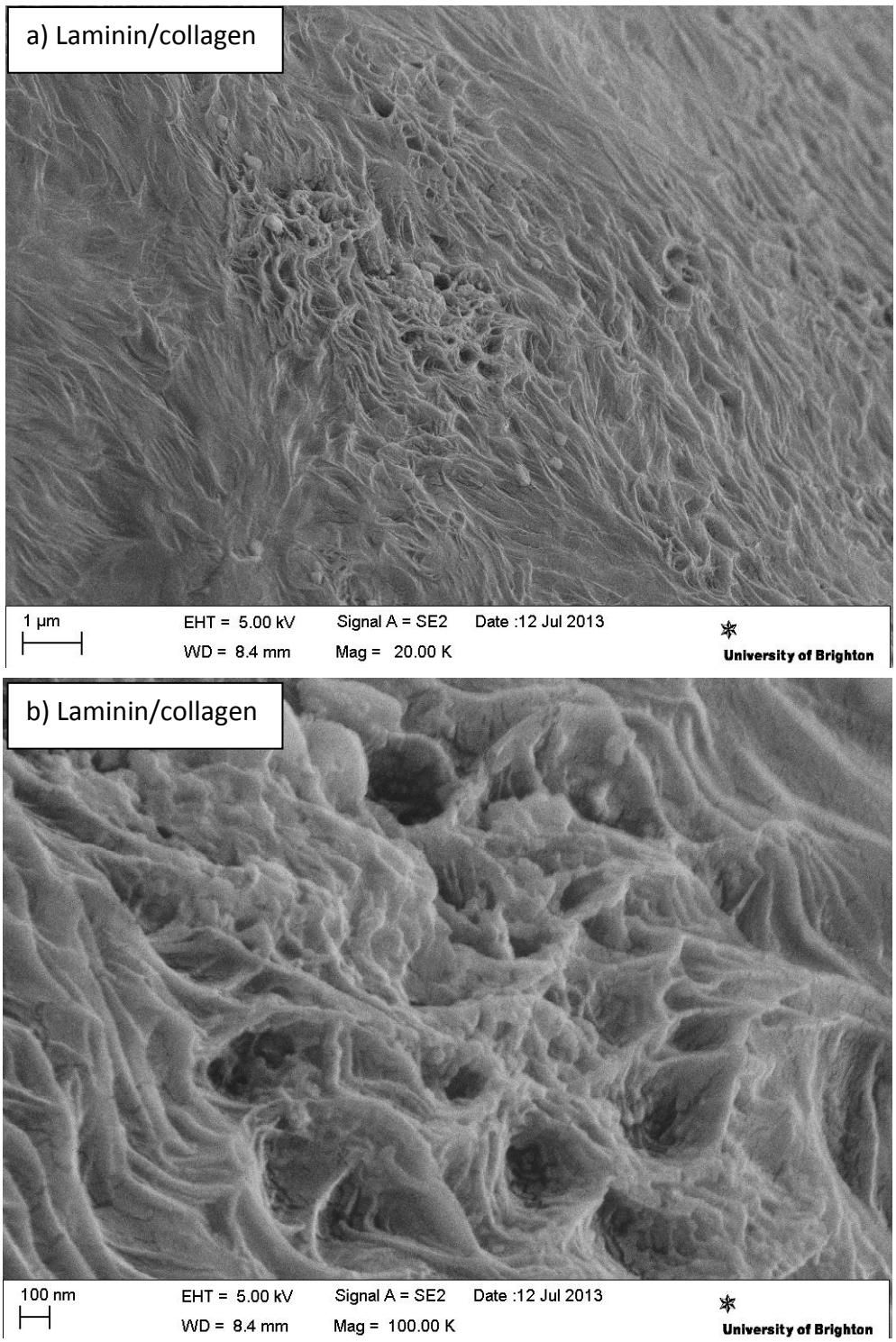

Figure 5-6: SEM images of plasma etched BioVyon™ and laminin/collagen

SEM images of BioVyon™ frits plasma etched for 116 seconds at 807 watts, and incubated with laminin and collagen (Described in 2.2.16.1). Image a) was taken at 50,000x magnification b) 100,000x magnification. Topography in image a) contains prominent ridges and hollows, with noticeable spheres positioned sporadically on the BioVyon™ surface. Increaseed magnification in b) shows a nanoscale coating, of rough spheres, enveloping the consistent ridge and hollow topography.

5.3 Cell adhesion

In order to assess the suitability of BioVyon™ for β-cell cultivation, three different populations of Min-6 were seeded onto frits and a two dimensional TCP control modified with BM proteins. The cell population initially adhered were quantified using an LDH assay (Described in 2.2.16.4). Figure 5-7 shows how cell adhesion is influenced on frits and TCP by four different protein treatments, and how this varies between three separate cell populations.

Figure 5-7, graphs a) and b) show a similar pattern of cell adhesion, TCP adhered more cells than frits in all treatments, a significant difference was apparent between laminin and laminin/collagen treated materials ($P<0.05$). The quantity of cells adhered between protein treatments is similar between graphs a) and b) with TCP adhering significantly more cells on laminin and laminin/collagen compared to the other protein treatments ($P<0.05$). Graph c) indicated that the third cell population did not follow a similar adhesion pattern to the first two populations. Cell adhesion appeared to be higher on frits treated with FBS and laminin compared to TCP, and a significant difference was observed between all protein treatments on TCP ($P<0.05$).

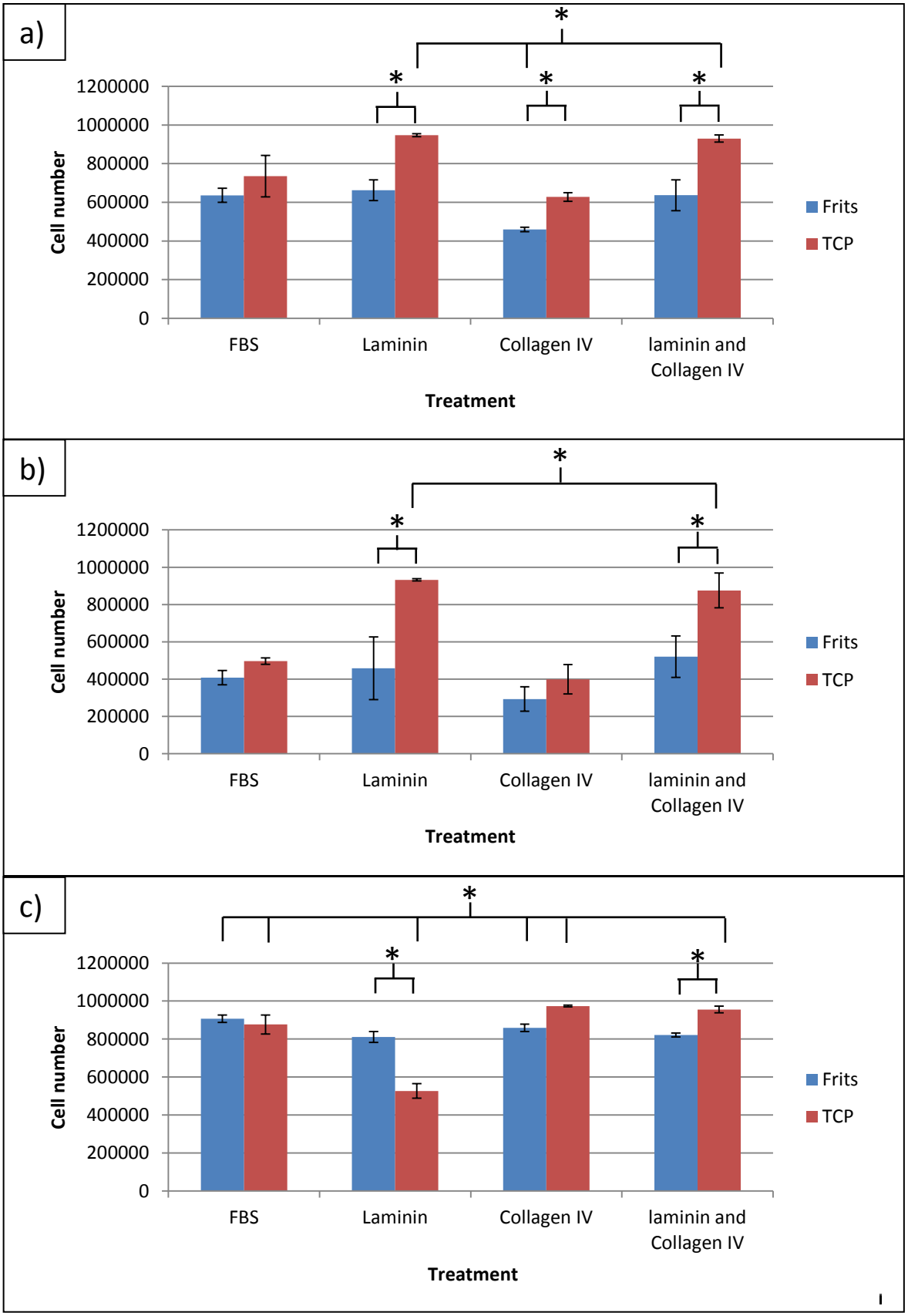

Figure 5-7: Cell adhesion to BioVyon™ frits and TCP incubated with BM proteins

BioVyon™ frits were plasma etched for 116 seconds at 807 watts. Treated frits and tissue culture plastic (TCP) 24 well plates were incubated for 2 hours in 40µl (38µl for TCP to account for decreased surface area) of a solution containing one of each peri insular basement membrane (BM) protein (Described in section 2.2.16.1). Prepared frits and TCP were then seeded with cell

suspension containing Min-6 (Described in Section 2.2.16.2) and the cell numbers initially adhered quantified on separate groups of frits, in triplicate using an LDH assay (Described in section 2.2.16.4). Graphs a) to c) show adhesion to frits and TCP for three different cell populations, the order of which corresponds to the figures later in this section. The cell number of each sample was calculated by comparison of absorbance value to a calibration curve; error bars represent variation between three frits seeded with the same cell population, n = 3. Graphs a) to c) show cell numbers on frits from three different cell populations. Graph a) shows a significant difference was observed in cell adhesion between TCP and frits with all treatments except FBS (Two-way ANOVA, $P<0.05$). Graph b) shows that a significant difference was observed in cell adhesion between TCP and frits treated with laminin and laminin/collagen (Two-way ANOVA, $P<0.05$). Graph c) shows that significant difference was observed in cell adhesion between TCP and frits treated with laminin and laminin/collagen (Two-way ANOVA, $P<0.05$).* Indicates a significant difference in cell populations between treatments or materials.

5.4 Cell growth

In order to investigate how the Min-6 cell populations responded over time within the modified BioVyon™ frits and TCP environments, three populations of adhered Min-6 were quantified after 3, 9 and 12 days culture using an LDH assay (Described in 2.2.16.4). The graphs in Figure 5-8 show cell number on frits treated with four different proteins over time, between three different cell populations.

Graphs a) to c) in Figure 5-8 provided a comparison between frit protein treatments over time, a two way ANOVA was used to show that there was a significant difference in cell number over time for each population ($P<0.001$). All three Min-6 populations show a different response over time. The Min-6 populations in graph a) appeared to fluctuate, decreasing at 9 days. Graph b) shows a rapid increase from approximately 500,000 cells to over 1,000,000 in 15 days. Graph c) shows a steady decline in cell number from a high number of Min-6 initially adhered.

The frit protein treatments appeared to follow the same basic pattern of cell number over time. Laminin and FBS treated frits often held a significantly higher number of cells compared to other treatments, with the exception of graph a) 15 days in which laminin treated frits held a lower number of cells ($P<0.001$).

The graphs in Figure 5-9 show cell number on TCP treated with four different proteins over time, between three different cell populations. Graphs a) to c) provided a comparison between TCP protein treatments over time, a two way ANOVA was used to

show that there was a significant difference in cell number over time for the populations in graph b) and c) ($P<0.001$).

Similarly to the frits all three Min-6 populations show a different response over time. The Min-6 populations in Figure 5-9 graph a) show varied cell number at three days, before remaining constant within 800,000 to 1,000,000 from 9 to 15 days. Graph b) also shows some variation in cell number at 3 days followed by a rapid increase from below 1,000,000 cells to approximately 1,750,000 cells at 15 days. Graph c) shows a rapid decline in cell number from a high number of Min-6 initially adhered, with the exception of TCP treated with FBS, on which cell number remained relatively constant and significantly different to the other treatments ($P<0.001$). The cell number between TCP protein treatments appeared much more varied compared to the frits, with FBS and laminin treated TCP deviating significantly from the other treatments in graphs a) and c) ($P<0.001$).

Cell populations were compared separately between frits and TCP treated with a single protein. Figure 5-10, Graphs a) to c) provided a comparison between frits and TCP treated with FBS over time. A two way ANOVA was used to show that there was a significant difference in cell number over time for all cell populations (graph a) to c)) ($P<0.001$). Cell number appeared to follow a similar pattern on both materials. Graph a) shows a higher cell number on frits after 3 days followed by TCP at 9 days ($P<0.05$). This is at variance with graph c) which shows consistently higher cell numbers on TCP from 3 to 15 days ($P<0.001$).

Figure 5-11, Graphs a) to c) provided a comparison between frits and TCP treated with laminin over time. A two way ANOVA was used to show that there was a significant

difference in cell number over time in graphs a) and b) ($P<0.001$). Cell number appeared to follow a similar pattern on both materials with the exception of graph c), which shows a difference in cell number of approximately 250,000 cells at 3 days. Graphs a) and b) show an increased cell number at 9 and 15 days, however, significant difference was only observed in graph a) at these time points ($P<0.01$).

Figure 5-12, Graphs a) to c) provided a comparison between frits and TCP treated with collagen over time. A two way ANOVA was used to show that there was a significant difference in cell number over time in all cell populations (graphs a) to c) ($P<0.01$). Variation in cell number can be seen at 3 days in graph a) with the higher cell number fluctuating between TCP and frits from 9 to 15 days respectively. Cell number was higher on TCP after 9 and 15 days in graph b), but a significant increase was observed at 3 and 9 days in graph c) ($P<0.05$).

Graphs a) to c) provided a comparison between frits and TCP treated with laminin/collagen over time. A two way ANOVA was used to show that there was a significant difference in cell number over time in all cell populations (graphs a) to c) ($P<0.01$). Similarly to collagen (Figure 5-12, graph a) variation in cell number can be seen at 3 days in graph a) with the higher cell number fluctuating between TCP and frits from 9 to 15 days respectively. Cell number was higher on TCP 3 to 15 days in graph b), but a statistical increase was observed after 3 and 9 days in graph c) ($P<0.001$).

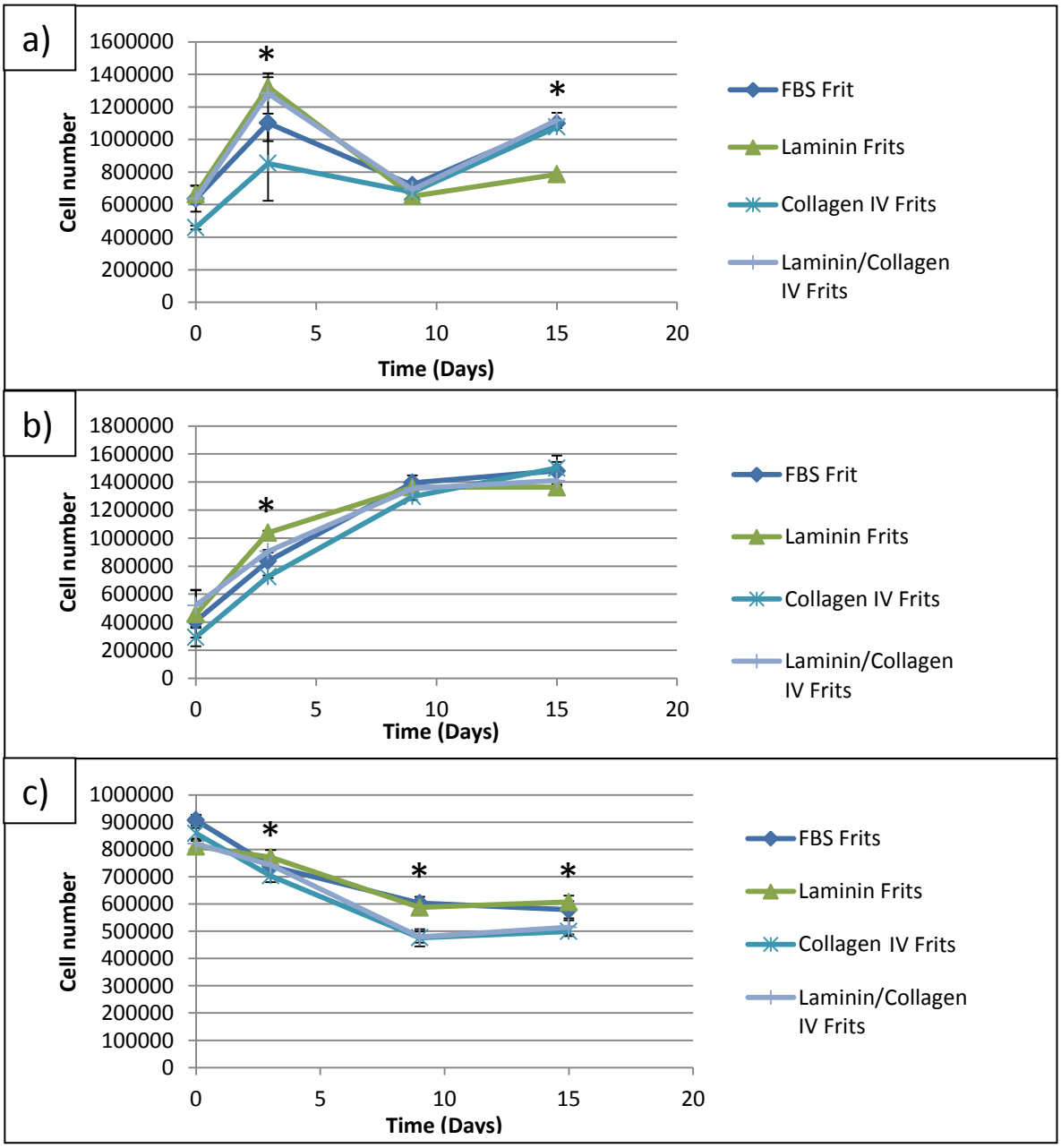

Figure 5-8: Cell populations over time on BioVyon™ frits incubated with BM proteins

BioVyon™ frits were plasma etched for 116 seconds at 807 watts. Treated frits were incubated for 2 hours in 40µl of a solution containing one of each peri insular basement membrane (BM) protein (Described in section 2.2.16.1). Prepared frits were then seeded with cell suspension containing Min-6 (Described in Section 2.2.16.2) and the cell numbers quantified on separate groups of frits, in triplicate at 0, 3, 9 and 15 days using an LDH assay (Described in section 2.2.16.4). Graph a) shows a significant fluctuation in cell number (Two-way ANOVA, $P<0.001$). Graph b) shows a significant increase in cell number from 3 to 15 days (Two-way ANOVA, $P<0.001$). Graph c) shows a significant decrease in cell number from 3 to 15 days (Two-way ANOVA, $P<0.001$).* indicates cell numbers that are significantly different to other treatments at time points.

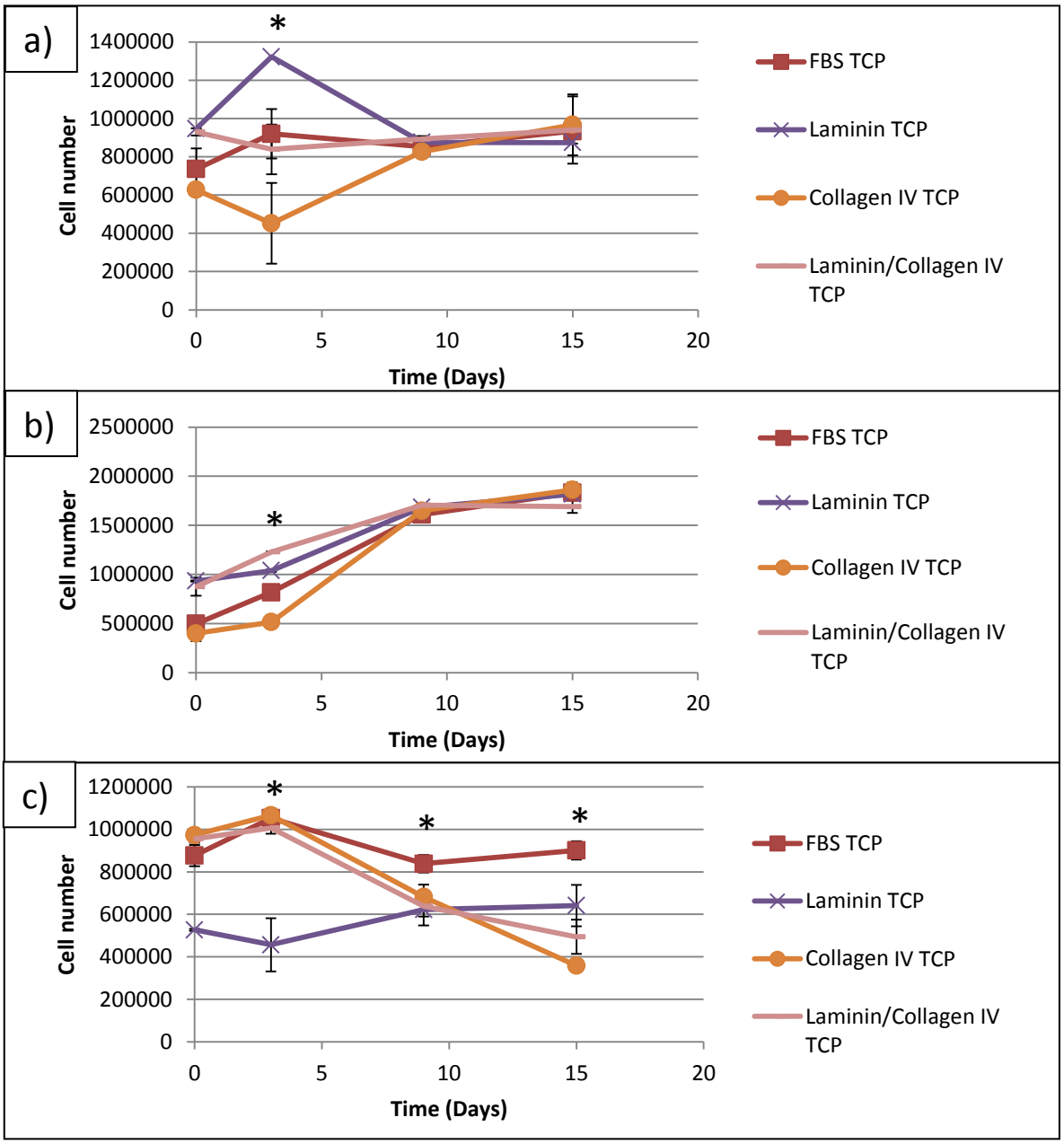

Figure 5-9: Cell populations over time on TCP incubated with BM proteins

24 well TCP plates were incubated for 2 hours in 38µl of a solution containing one of each peri insular basement membrane (BM) protein (Described in section 2.2.16.1). Prepared TCP plates were then seeded with cell suspension containing Min-6 (Described in Section 2.2.16.2) and the cell numbers quantified in separate wells, in triplicate at 0, 3, 9 and 15 days using an LDH assay (Described in section 2.2.16.4). Graph a) shows no significant difference was observed between treatments over time (Two-way ANOVA, $P>0.05$). Graph b) shows a significant increase in cell number with increasing time (Two-way ANOVA, $P<0.001$). Graph c) shows a significant difference in cell number with increasing time (Two-way ANOVA, $P<0.001$).* indicates cell numbers that are significantly different to other treatments at time points.

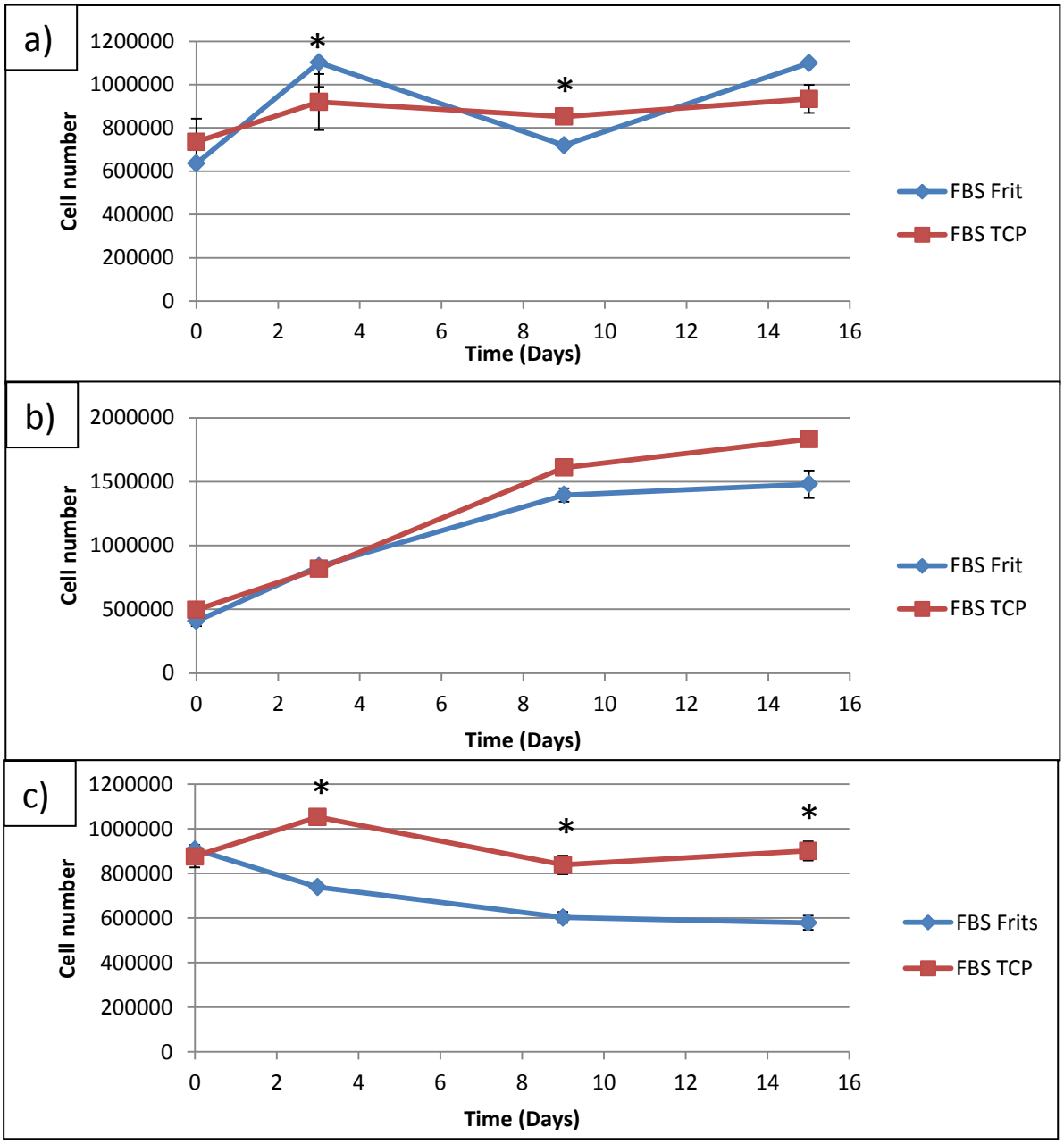

Figure 5-10: Cell populations over time on BioVyon™ frits and TCP incubated with FBS

Methods as in Figure 5-8 and Figure 5-9 for Frits and TCP respectively, materials treated with FBS. Graphs a) to c) show cell numbers on frits from three different cell populations. Graph a) shows there is a significant fluctuation in cell number over time (Two-way ANOVA, $P<0.001$), a significantly higher cell number on frits and TCP can be seen at 3 and 9 days respectively, with no difference at 15 days (Two-way ANOVA, $P<0.05$). Graph b) shows there is a significant increase in cell number over time (Two-way ANOVA, $P<0.001$), and no significant difference between cell number on the materials over time (One-way ANOVA $P>0.05$). Graph c) shows there is a significant decrease in cell number over time (One-way ANOVA, $P<0.001$). * indicates cell numbers that are significantly different to other treatments at time points.

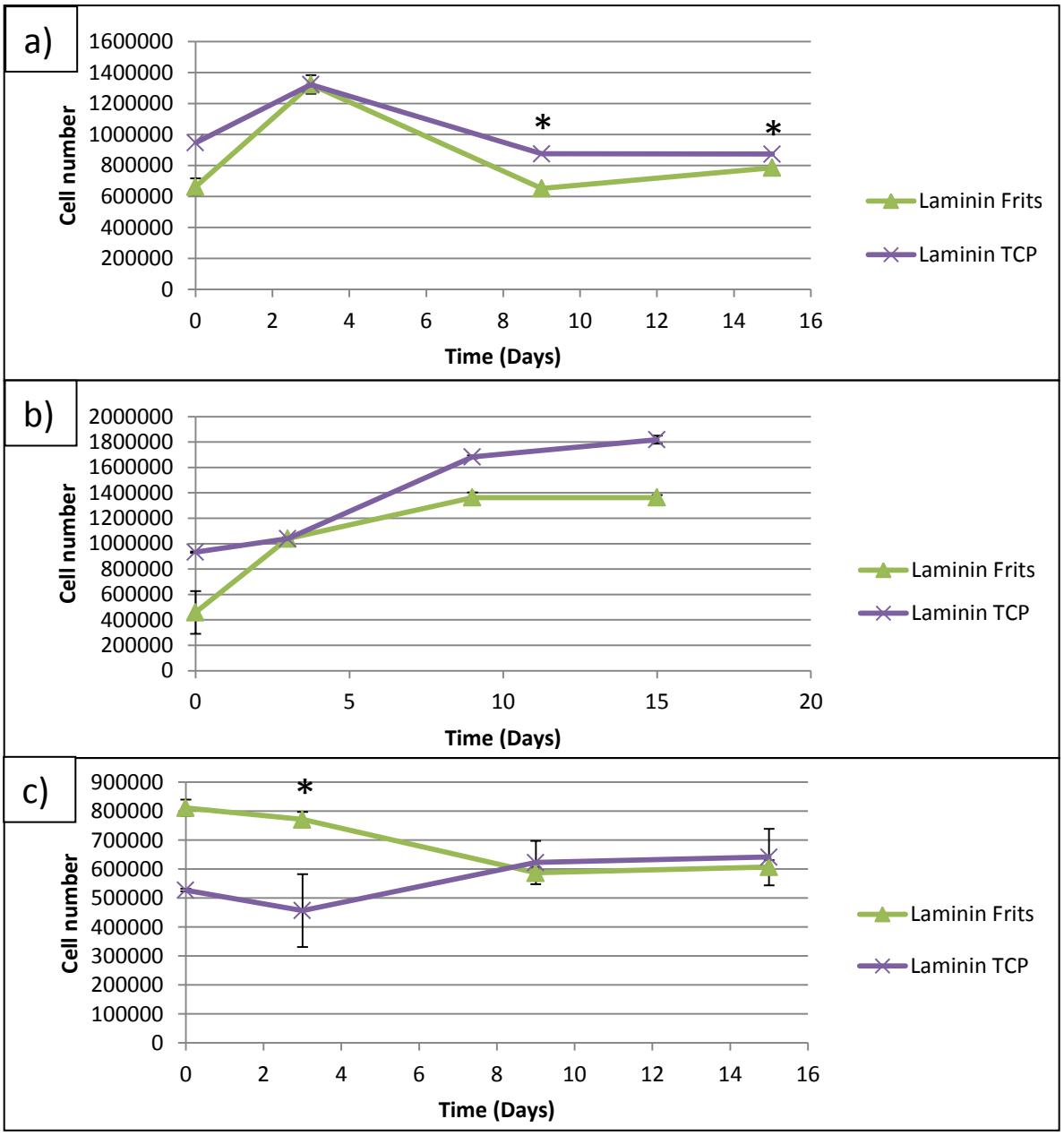

Figure 5-11: Cell populations over time on BioVyon™ frits and TCP incubated with Laminin

Methods as in Figure 5-8 and Figure 5-9 for Frits and TCP respectively, materials treated with Laminin. Graphs a) to c) show cell numbers on frits from three different cell populations. Graph a) shows there is a significant fluctuation in cell number over time (Two-way ANOVA, $P<0.001$), a significantly higher cell number was observed on laminin treated TCP at 9 and 15 days compared to frits (Two-way ANOVA $P<0.01$). Graph b) shows there is a significant increase in cell number over time (Two-way ANOVA, $P<0.001$), but no significant difference was observed between materials (Two-way ANOVA $P>0.05$).Graph c) shows there is no statistical difference in cell number over time (One-way ANOVA $P<0.001$), a significantly higher cell number was observed on laminin treated frits at 9 days compared to TCP (One-way ANOVA, $P<0.01$). * indicates cell numbers that are significantly different to other treatments at time points.

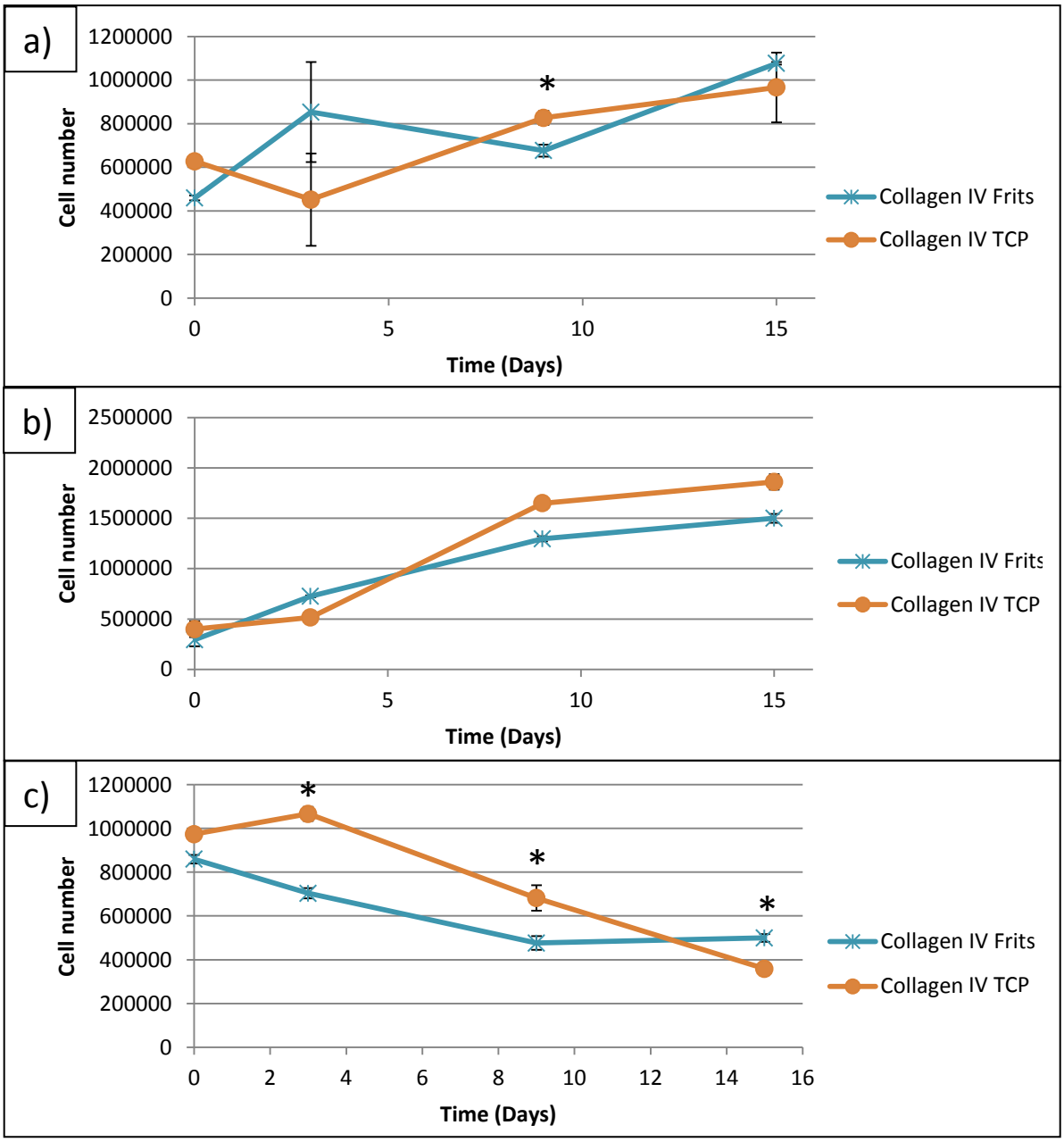

Figure 5-12: Cell populations over time on BioVyon™ frits and TCP incubated with Collagen IV

Methods as in Figure 5-8 and Figure 5-9 for Frits and TCP respectively, materials treated with Collagen IV. Graphs a) to c) show cell numbers on frits from three different cell populations. Graph a) shows there is a significant increase in cell number over time (One-way ANOVA $P<0.01$), a significantly higher cell number was observed on collagen treated TCP at 9 days compared to frits (Two-way ANOVA $P<0.01$). Graph b) shows there is a significant increase in cell number over time (One-way ANOVA $P<0.001$), but no significant difference was observed between materials (Two-way ANOVA, $P>0.05$). Graph c) shows there is significant decrease in cell number over time (One-way ANOVA $P<0.001$), a significantly higher cell number was observed on collagen treated TCP at 3 and 9 days compared to frits (Two-way ANOVA $P<0.05$), with the exception of 15 days when a higher number of cells are observed on frits ($P<0.05$).* indicates cell numbers that are significantly different to other treatments at time points.

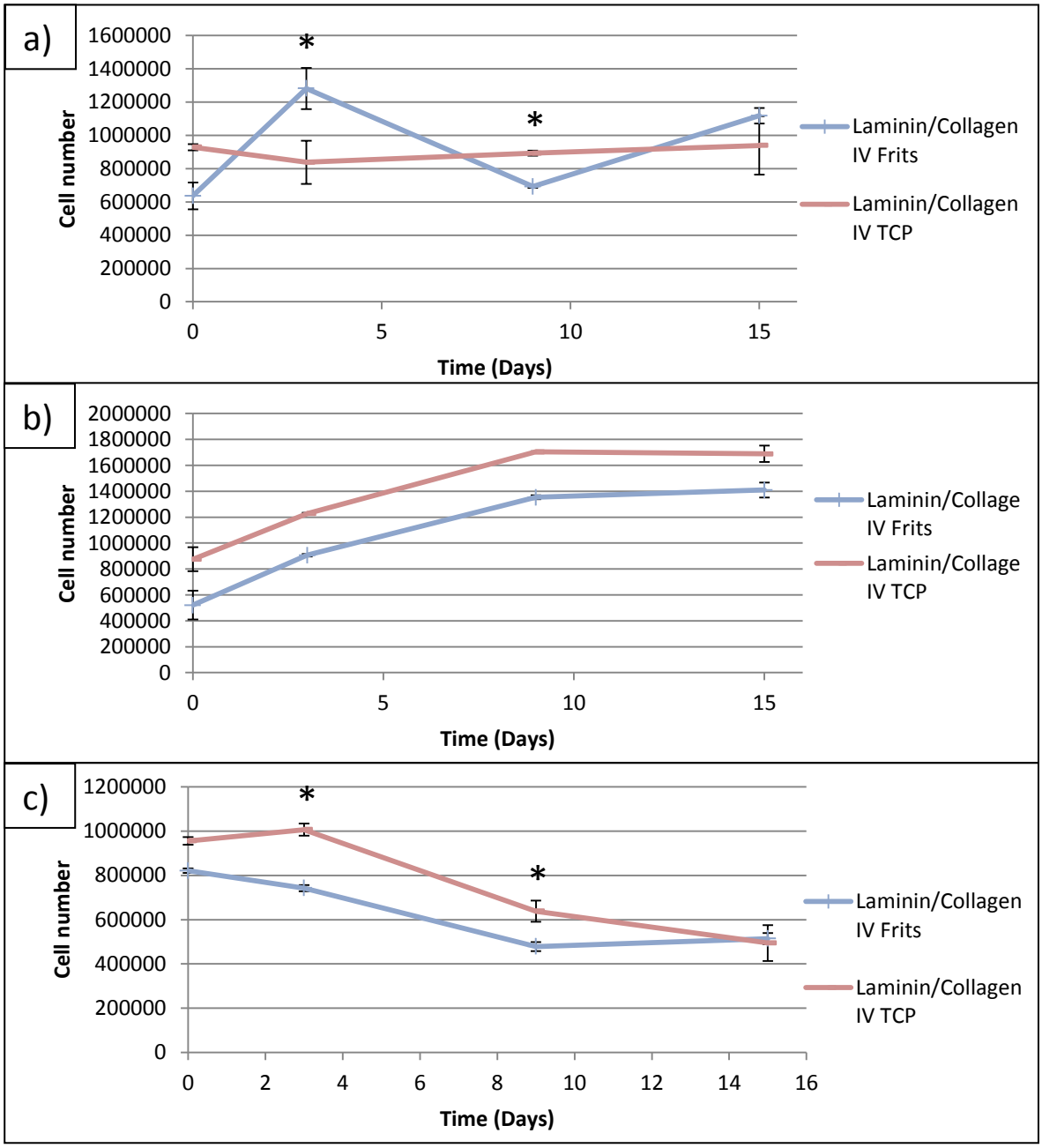

Figure 5-13: Cell populations over time on BioVyon™ frits and TCP incubated with Laminin/Collagen IV

Methods as in Figure 5-8 and Figure 5-9 for Frits and TCP respectively, materials treated with Laminin/Collagen IV. Graphs a) to c) show cell numbers on frits from three different cell populations. Graph a) shows there is a significant fluctuation in cell number over time (One-way ANOVA, $P<0.05$), a significantly higher cell number was observed on laminin/collagen treated frits at 3 compared to TCP (Two-way ANOVA $P<0.05$), at 9 days however a higher cell number was observed in laminin/collagen frits (One-way ANOVA $P<0.05$). Graph b) shows there is a significant increase in cell number over time (One-way ANOVA $P<0.001$), but no significant difference was observed between materials (Two-way ANOVA $P>0.05$). Graph c) shows there is significant decrease in cell number over time (One-way ANOVA $P<0.001$), a significantly higher cell number was observed on laminin/collagen treated TCP at 3 compared to frits at 3 and 9 days (Two-way ANOVA $P<0.001$).* indicates cell numbers that are significantly different to other treatments at time points.

5.5 Cell viability

Flourescent staining was used to investigate the viability of the adhered cell populations on protein treated frits and TCP. Two different frits and TCP wells were stained with hoescht and propidium iodide (HPI) (section 2.2.16.6) and calcein-AM (section 2.2.16.7), per protein treatment, at 15 days. This method also provided a qualitative comparison to the quantification of cell number using the LDH assay.

Images a) in Figure 5-14, Figure 5-16, Figure 5-18 and Figure 5-20 show Min-6 populations adhered to protein treated frits and stained with HPI. All protein treatments show Min-6 adhered around high density polyethylene (HDPE) particulates, and within the porous structure. Blue flouresence indicated cellular DNA. Frits treated with laminin (Figure 5-16) and laminin/collagen (Figure 5-20) appeared to be more densly populated compared to the other treatments. Images a) in Figure 5-15, Figure 5-17, Figure 5-19 and Figure 5-21 show the fluorescent green of Calcein AM staining which indicated viable cell populations within the porous frit structure.

Images b) in Figure 5-14, Figure 5-16, Figure 5-18 and Figure 5-20 show adhered Min-6 populations in protein treated TCP wells and stained with HPI. The HPI staining of TCP reveals a pattern of cell adhesion that varies between protein treatments. FBS shows densely packed cell clusters, with high fluorescence, interspersed with small sporadic regions of unpopulated TCP (Figure 5-14). This is at variance with laminin which shows a relatively consistent monolayer of adhered Min-6 (Figure 5-16), and a lower fluorescence compared to FBS. Small groups of cells in a monolayer populate TCP treated with collagen

(Figure 5-18), and have a high fluorescence, this is similar for the laminin/collagen treated TCP (Figure 5-20).

Images b) in Figure 5-15, Figure 5-17, Figure 5-19 and Figure 5-21 show calcein AM staining on TCP and reveals cell adhesion patterns at variance with the HPI staining. FBS appears to have an almost confluent population of cells with a weak fluorescence, and small regions of unpopulated TCP (Figure 5-15). Calcein AM staining of laminin is at variance with the HPI staining, small tightly packed groups of cells have a strong fluorescence, and are sporadically adhered (Figure 5-17). Cell populations seem less tightly packed on collagen treated TCP with larger regions of unpopulated TCP and a weak florescence compared to frits (Figure 5-19). Laminin/collagen treated TCP possesses a unique and consistent pattern of cell adhesion, with clearly defined borders to the cell monolayers (Figure 5-21).

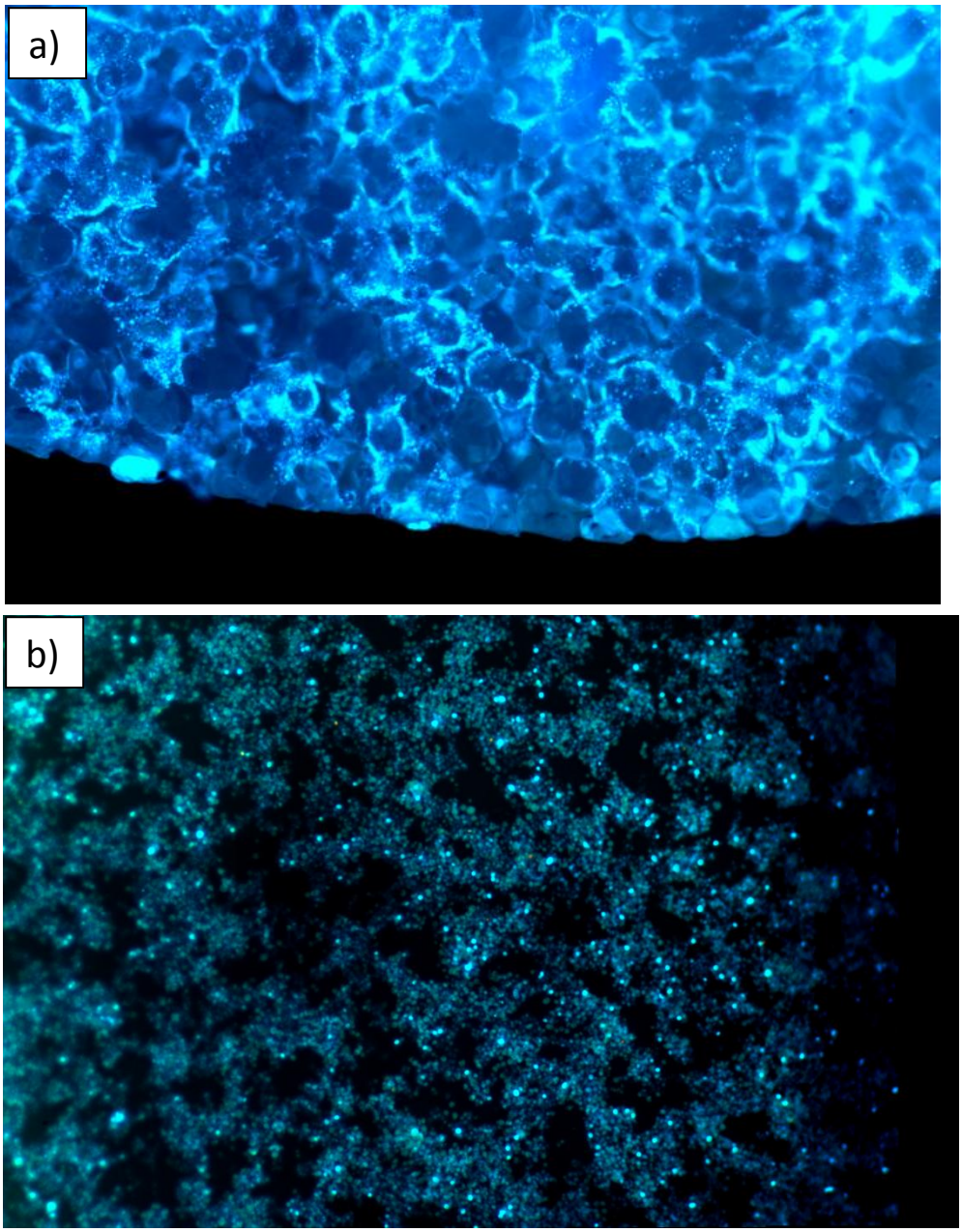

Figure 5-14: Cell populations on BioVyon™ frits and TCP incubated with FBS after 15 days

BioVyon™ frits were plasma etched for 116 seconds at 807 watts. Treated frits and tissue culture plastic (TCP) 24 well plates were incubated for 2 hours in 40µl (38µl for TCP to account for decreased surface area) of a solution containing FBS(Described in section 2.2.16.1). Prepared frits and TCP were then seeded with cell suspension containing Min-6 (Described in Section 2.2.16.2). After 15 days the frits and TCP were stained with Hoescht and propidium iodide (HPI) (Described in section 2.2.16.6) images were taken at x 5 magnification. Image a) shows cell populations within the BioVyon™ structure. Flourescent blue colour indicates clusters of cells in and around the darker, partially coalesced high density polyethylene (HDPE) particulates. Image b) shows cell populations in a 24 well TCP plate, cells appear confluent around sporadic, unpopulated regions.

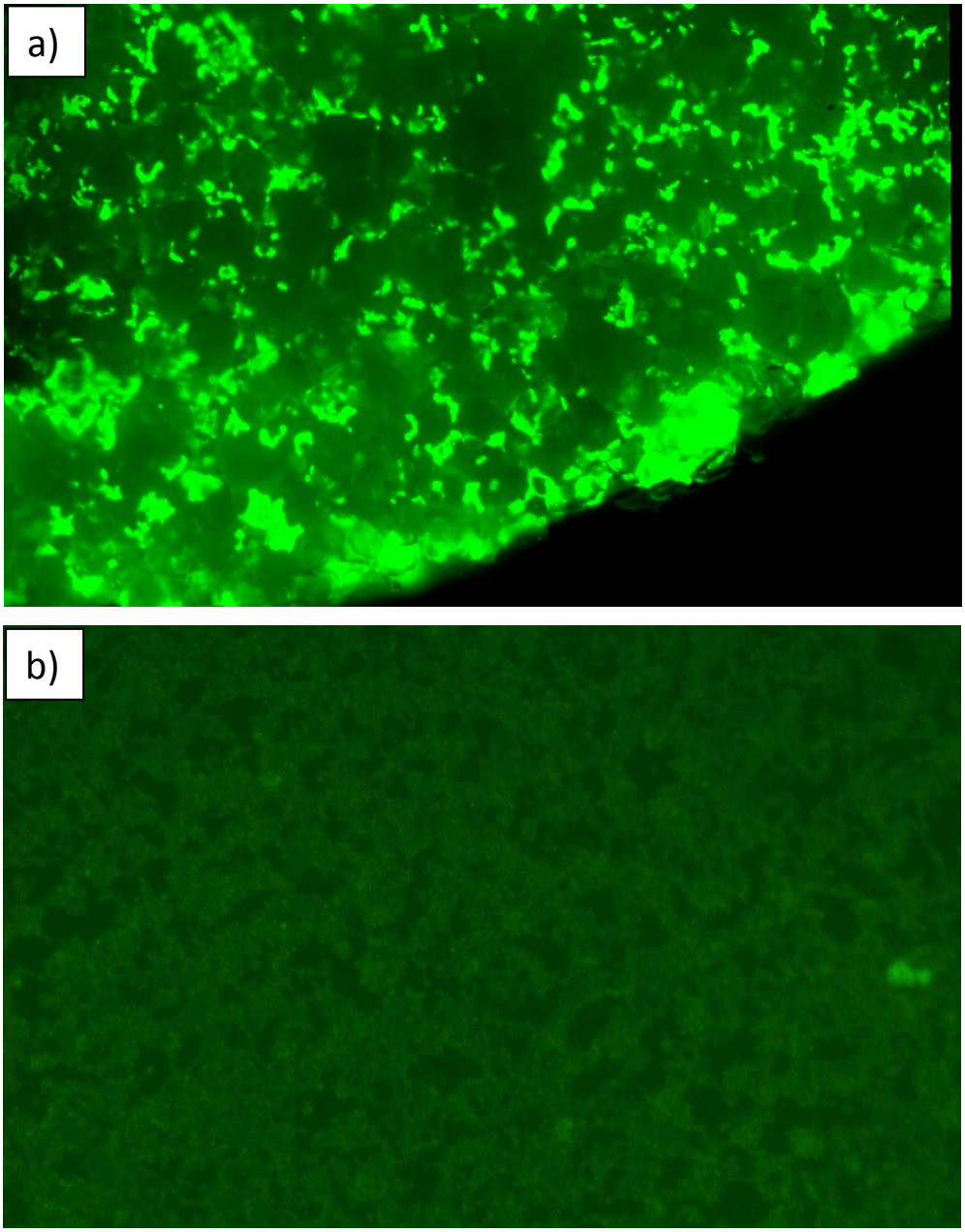

Figure 5-15: Cell populations on BioVyon™ frits and TCP incubated with FBS after 15 days

BioVyon™ frits were plasma etched for 116 seconds at 807 watts. Treated frits and tissue culture plastic (TCP) 24 well plates were incubated for 2 hours in 40µl (38µl for TCP to account for decreased surface area) of a solution containing FBS (Described in section 2.2.16.1). Prepared frits and TCP were then seeded with cell suspension containing Min-6 (Described in Section 2.2.16.2). After 15 days the frits and TCP were stained with Calcein AM (Described in section 2.2.16.7) images were taken at x 5 magnification. Image a) shows cell populations within the BioVyon™ structure. Flourescent green colour indicates clusters of cells in and around the darker, partially coalesced high density polyethylene (HDPE) particulates. Image b) shows cell populations in a 24 well TCP plate, cells appear confluent around sporadic, unpopulated regions.

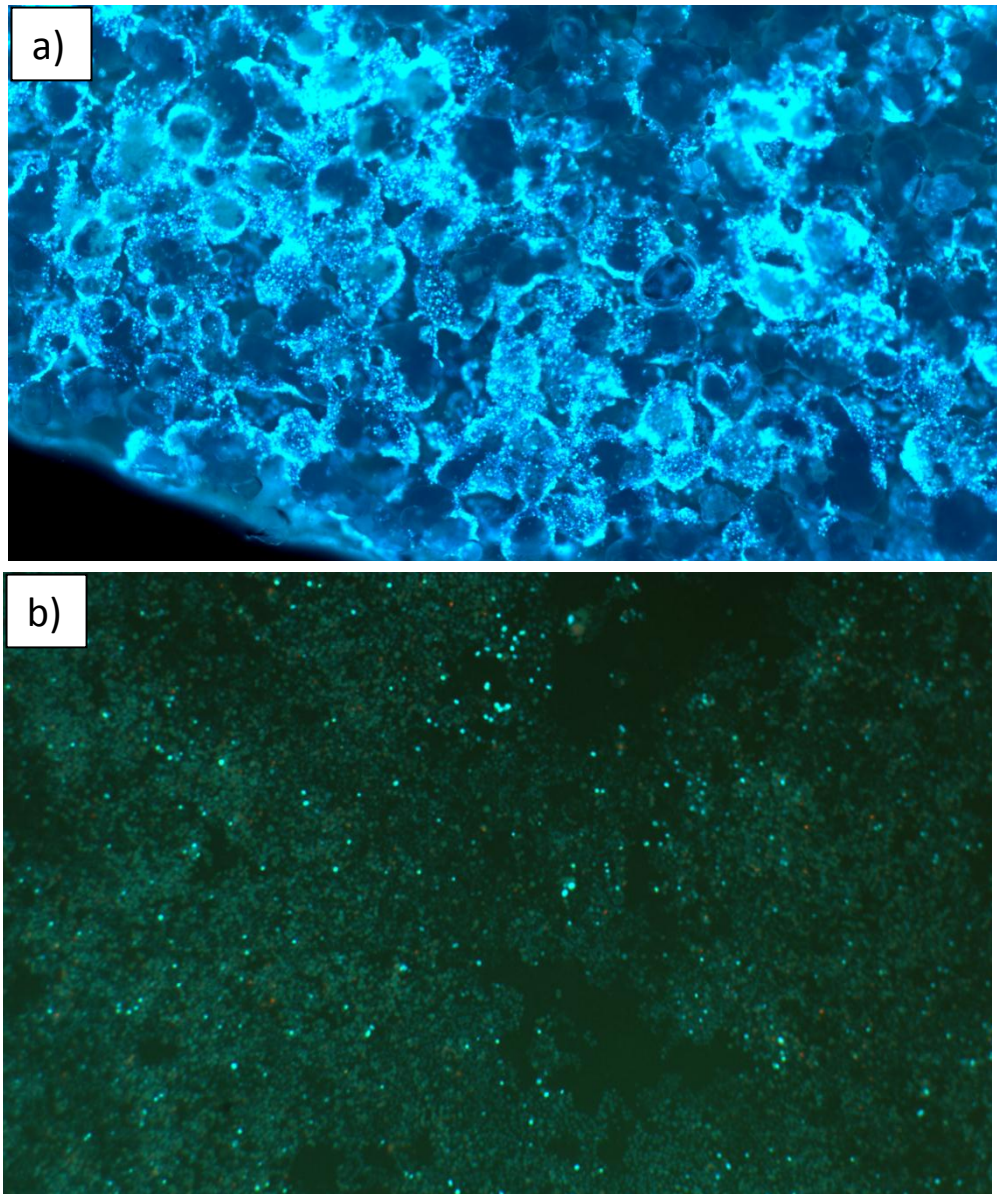

Figure 5-16: Cell populations on BioVyon™ frits and TCP incubated with laminin after 15 days

BioVyon™ frits were plasma etched for 116 seconds at 807 watts. Treated frits and tissue culture plastic (TCP) 24 well plates were incubated for 2 hours in 40µl (38µl for TCP to account for decreased surface area) of a solution containing laminin (Described in section 2.2.16.1). Prepared frits and TCP were then seeded with cell suspension containing Min-6 (Described in Section 2.2.16.2). After 15 days the frits and TCP were stained with Hoescht and propidium iodide (HPI) (Described in section 2.2.16.6) images were taken at x 5 magnification. Image a) shows cell populations within the BioVyon™ structure. Flourescent blue colour indicates clusters of cells in and around the darker, partially coalesced high density polyethylene (HDPE) particulates. Image b) shows cell populations in a 24 well TCP plate, cells appear confluent around sporadic, unpopulated regions.

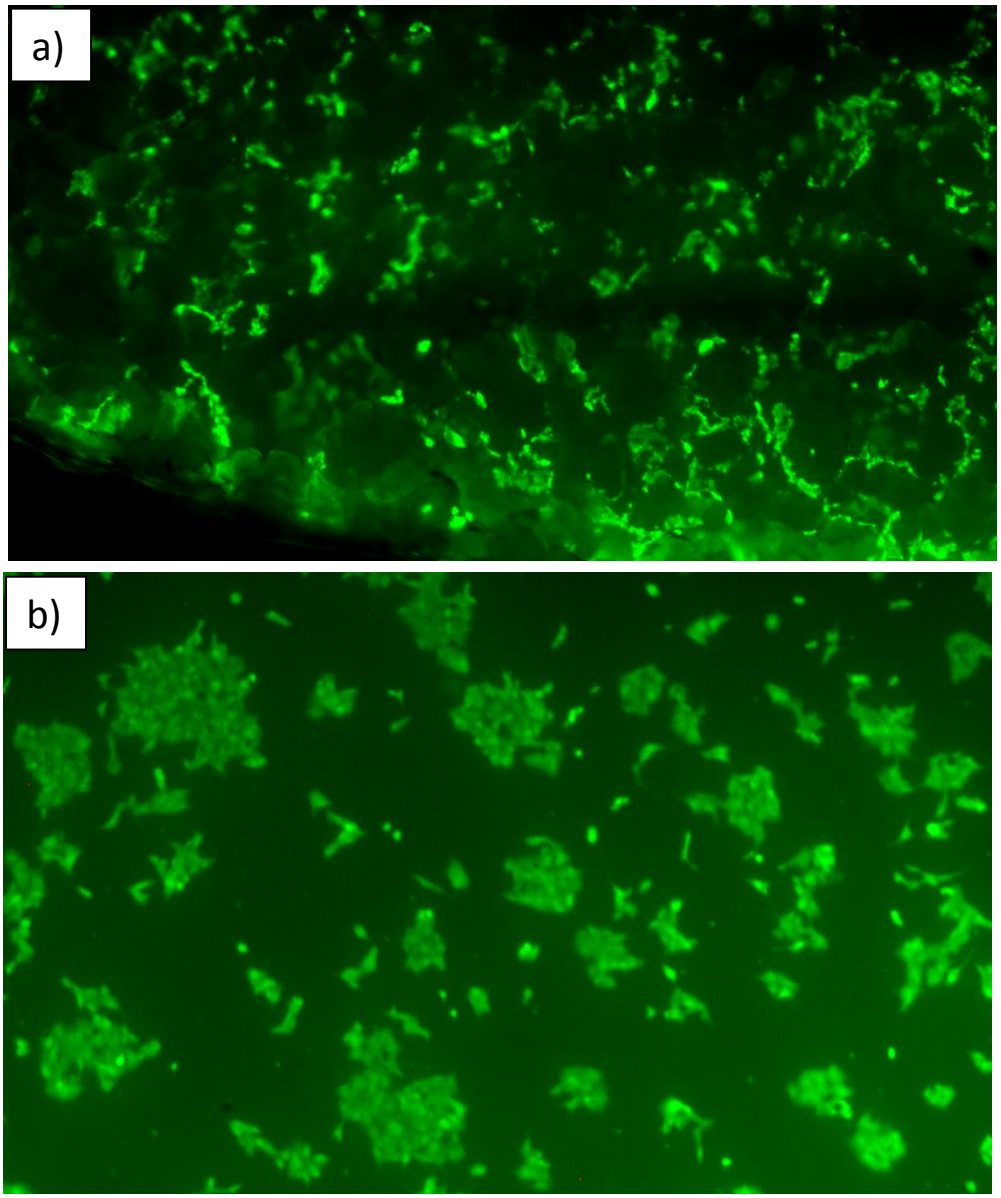

Figure 5-17: Cell populations on BioVyon™ frits and TCP incubated with laminin after 15 days

BioVyon™ frits were plasma etched for 116 seconds at 807 watts. Treated frits and tissue culture plastic (TCP) 24 well plates were incubated for 2 hours in 40µl (38µl for TCP to account for decreased surface area) of a solution containing laminin (Described in section 2.2.16.1). Prepared frits and TCP were then seeded with cell suspension containing Min-6 (Described in Section 2.2.16.2). After 15 days the frits and TCP were stained with Calcein AM (Described in section 2.2.16.7) images were taken at x 5 magnification. Image a) shows cell populations within the BioVyon™ structure. Flourescent green colour indicates clusters of cells in and around the darker, partially coalesced high density polyethylene (HDPE) particulates. Image b) shows cell populations in a 24 well TCP plate, cells appear confluent around sporadic, unpopulated regions.

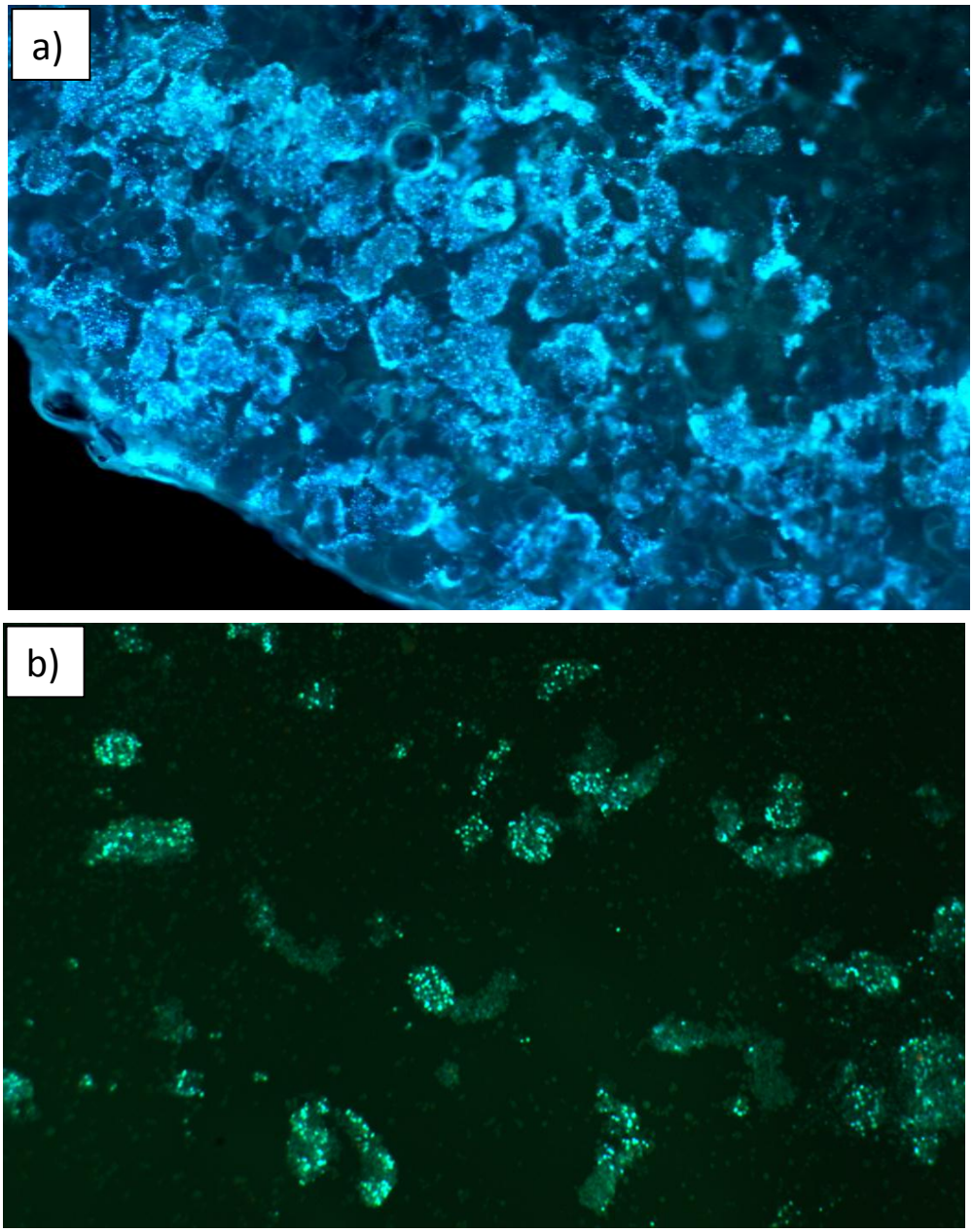

Figure 5-18: Cell populations on BioVyon™ frits and TCP incubated with collagen IV after 15 days

BioVyon™ frits were plasma etched for 116 seconds at 807 watts. Treated frits and tissue culture plastic (TCP) 24 well plates were incubated for 2 hours in 40µl (38µl for TCP to account for decreased surface area) of a solution containing collagen (Described in section 2.2.16.1). Prepared frits and TCP were then seeded with cell suspension containing Min-6 (Described in Section 2.2.16.2). After 15 days the frits and TCP were stained with Hoescht and propidium iodide (HPI) (Described in section 2.2.16.6) images were taken at x 5 magnification. Image a) shows cell populations within the BioVyon™ structure. Flourescent blue colour indicates clusters of cells in and around the darker, partially coalesced high density polyethylene (HDPE) particulates. Image b) shows cell populations in a 24 well TCP plate, cells appear to form small groups compared to the other treatments.

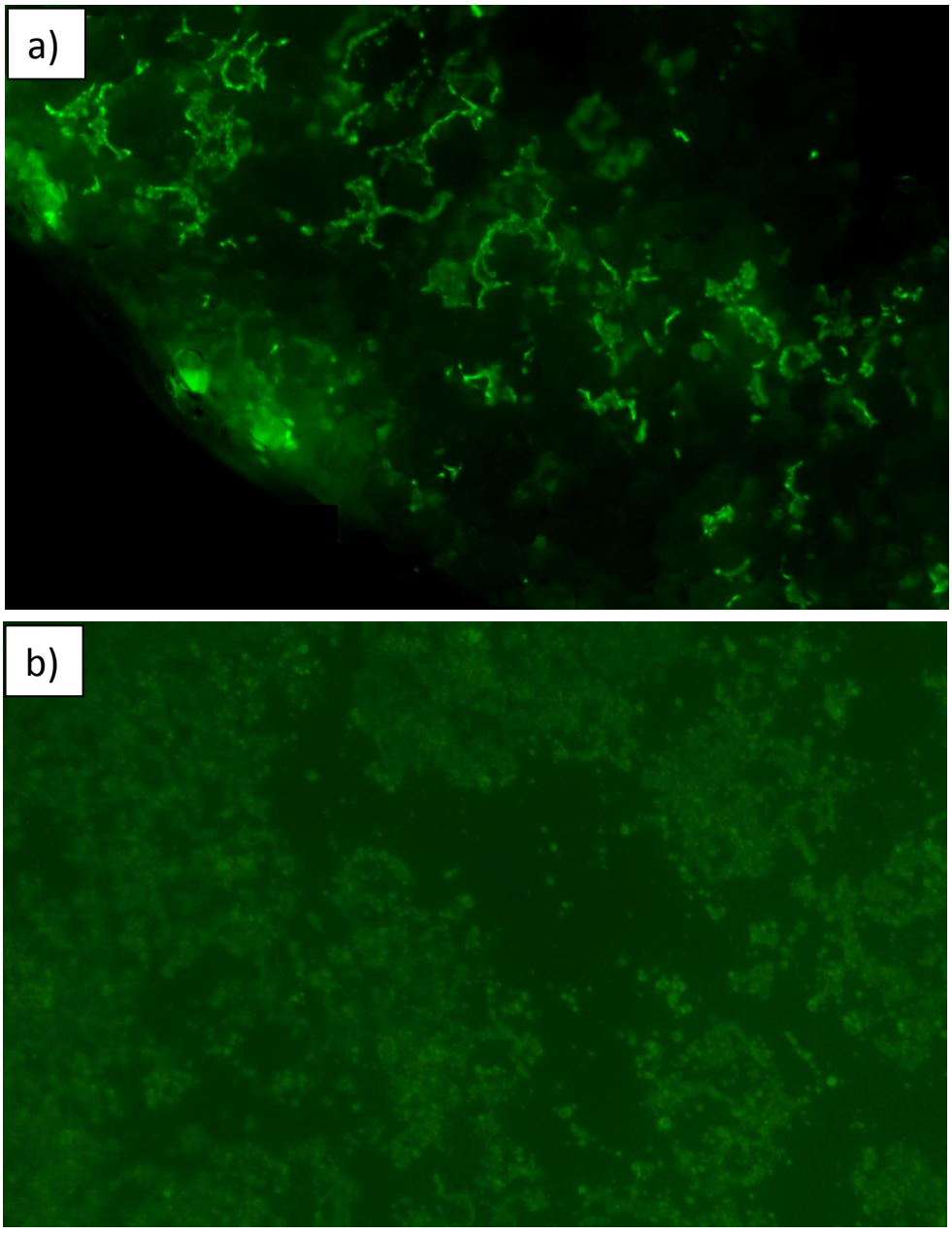

Figure 5-19: Cell populations on BioVyon™ frits and TCP incubated with collagen IV after 15 days

BioVyon™ frits were plasma etched for 116 seconds at 807 watts. Treated frits and tissue culture plastic (TCP) 24 well plates were incubated for 2 hours in 40µl (38µl for TCP to account for decreased surface area) of a solution containing collagen(Described in section 2.2.16.1). Prepared frits and TCP were then seeded with cell suspension containing Min-6 (Described in Section 2.2.16.2). After 15 days the frits and TCP were stained with Calcein AM (Described in section 2.2.16.7) images were taken at x 5 magnification. Image a) shows cell populations within the BioVyon™ structure. Flourescent green colour indicates clusters of cells in and around the darker, partially coalesced high density polyethylene (HDPE) particulates. Image b) shows cell populations in a 24 well TCP plate, cells appear confluent around large sporadic, unpopulated areas.

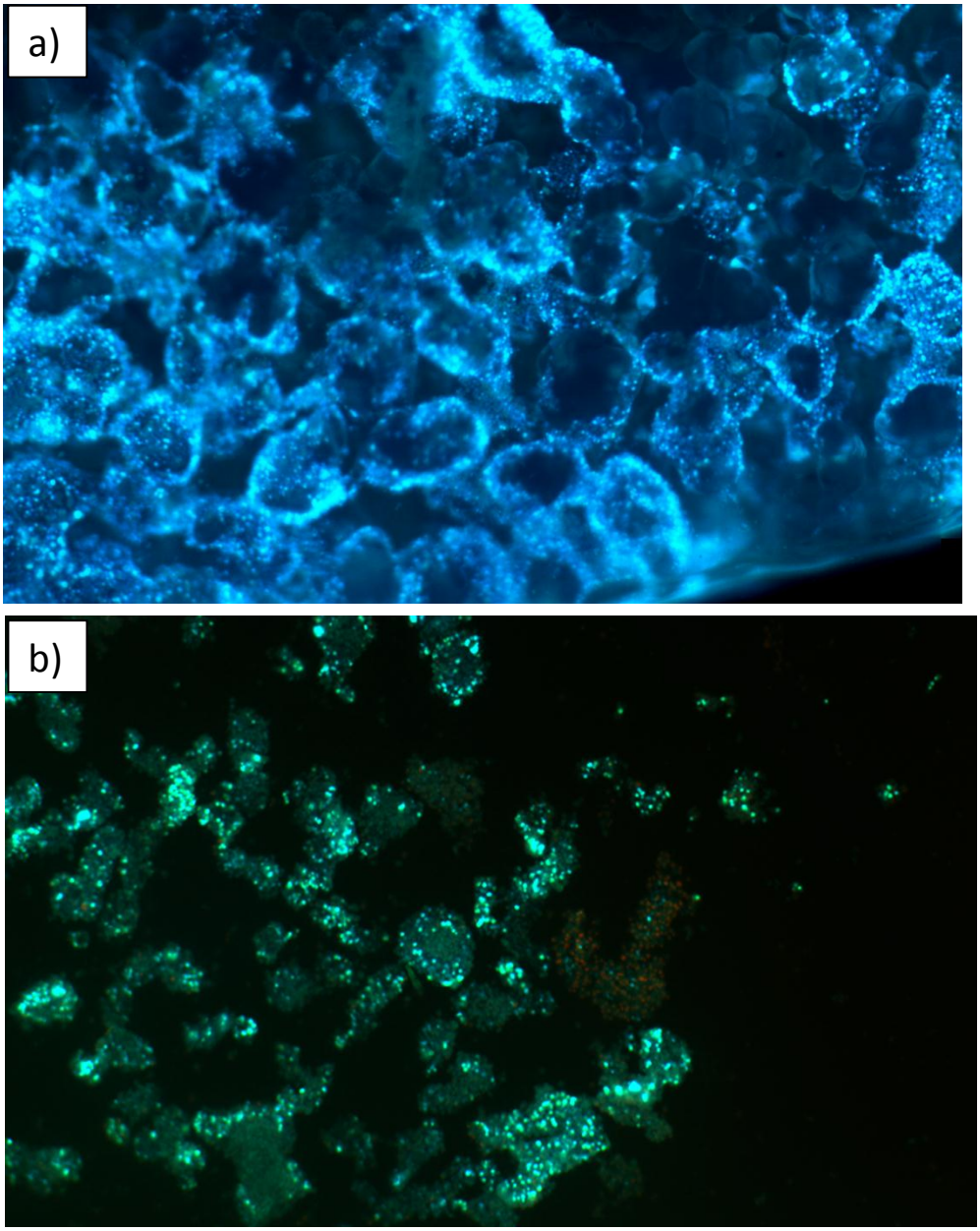

Figure 5-20: Cell populations on BioVyon™ frits and TCP incubated with laminin/collagen IV after 15 days

BioVyon™ frits were plasma etched for 116 seconds at 807 watts. Treated frits and tissue culture plastic (TCP) 24 well plates were incubated for 2 hours in 40µl (38µl for TCP to account for decreased surface area) of a solution containing laminin/collagen (Described in section 2.2.16.1). Prepared frits and TCP were then seeded with cell suspension containing Min-6 (Described in Section 2.2.16.2). After 15 days the frits and TCP were stained with Hoescht and propidium iodide (HPI) (Described in section 2.2.16.6) images were taken at x 5 magnification. Image a) shows cell populations within the BioVyon™ structure. Flourescent blue colour indicates clusters of cells in and around the darker, partially coalesced high density polyethylene (HDPE) particulates. Image b) shows cell populations in a 24 well TCP plate, cells appear to form small groups, some of which are populated by cells with a flouresecent red colour.

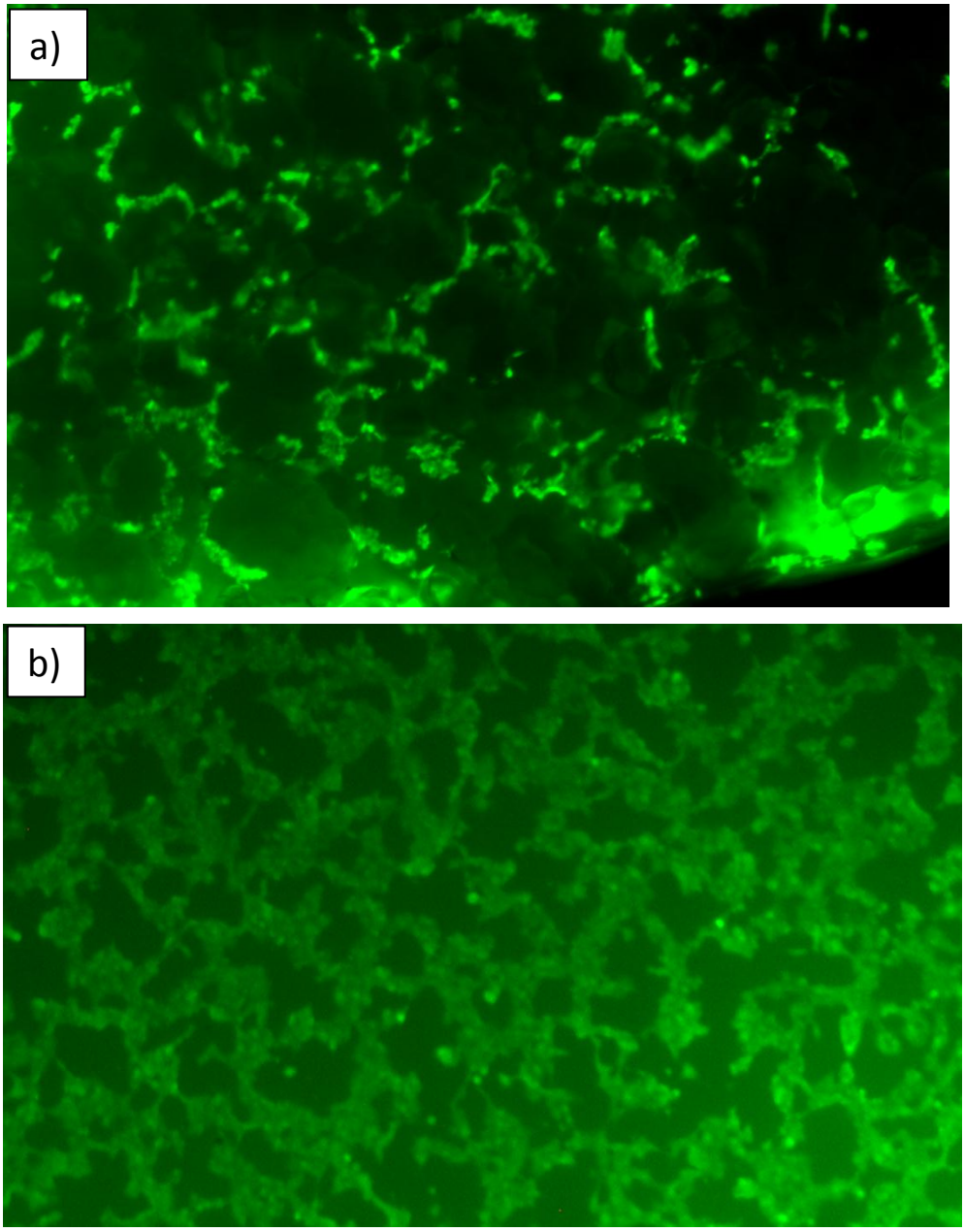

Figure 5-21: Cell populations on BioVyon™ frits and TCP incubated with laminin/collagen IV after 15 days

BioVyon™ frits were plasma etched for 116 seconds at 807 watts. Treated frits and tissue culture plastic (TCP) 24 well plates were incubated for 2 hours in 40µl (38µl for TCP to account for decreased surface area) of a solution containing collagen (Described in section 2.2.16.1). Prepared frits and TCP were then seeded with cell suspension containing Min-6 (Described in Section 2.2.16.2). After 15 days the frits and TCP were stained with Calcein AM (Described in section 2.2.16.7) images were taken at x 5 magnification. Image a) shows cell populations within the BioVyon™ structure. Flourescent green colour indicates clusters of cells in and around the darker, partially coalesced high density polyethylene (HDPE) particulates. Image b) shows cell populations in a 24 well TCP plate, cells appear confluent around sporadic, unpopulated areas.

5.6 β-cell phenotype

In order to assess how the phenotype of the Min-6 cell line was affected by long term culture on BioVyon™ frits and TCP treated with BM proteins, cell populations were exposed to a glucose challenge and the insulin secreted measured using an insulin ELISA (Section 2.2.16.3).

Initially it was necessary to observe how a decrease from 5mmol/L to 0mmol/L and increase to high glucose concentrations at 25mmol/L influenced the Min-6 cell lines insulin secretion on frits and TCP. The graphs in Figure 5-22 show insulin secretion on frits and TCP treated with four different proteins in media containing 5, 0 and 25 mmol/L glucose concentrations after 3 days culture. A two way ANOVA was used to show that there was no significant difference in insulin secretion at different glucose concentrations (Graphs a) and b) ($P>0.05$). A high amount of variation between frits and TCP replicates within the same protein treatment can be seen, resulting in no significant difference in insulin secretion between protein treatments at different glucose concentration for frits and TCP ($P>0.05$), with the exception of laminin treated TCP in 25mmol/L glucose. Overall the protein treated TCP generated a higher insulin secretion from adhered cell populations compared to the frits at 5mmol/L. At 0mmol/L cells secreted below 40 ng of insulin per 100,000 cells on both materials. At 25mmol/L the insulin secreted on the protein treated frits continued to decrease, in contrast to the TCP on which insulin increased on all protein treatments except laminin ($P<0.01$).

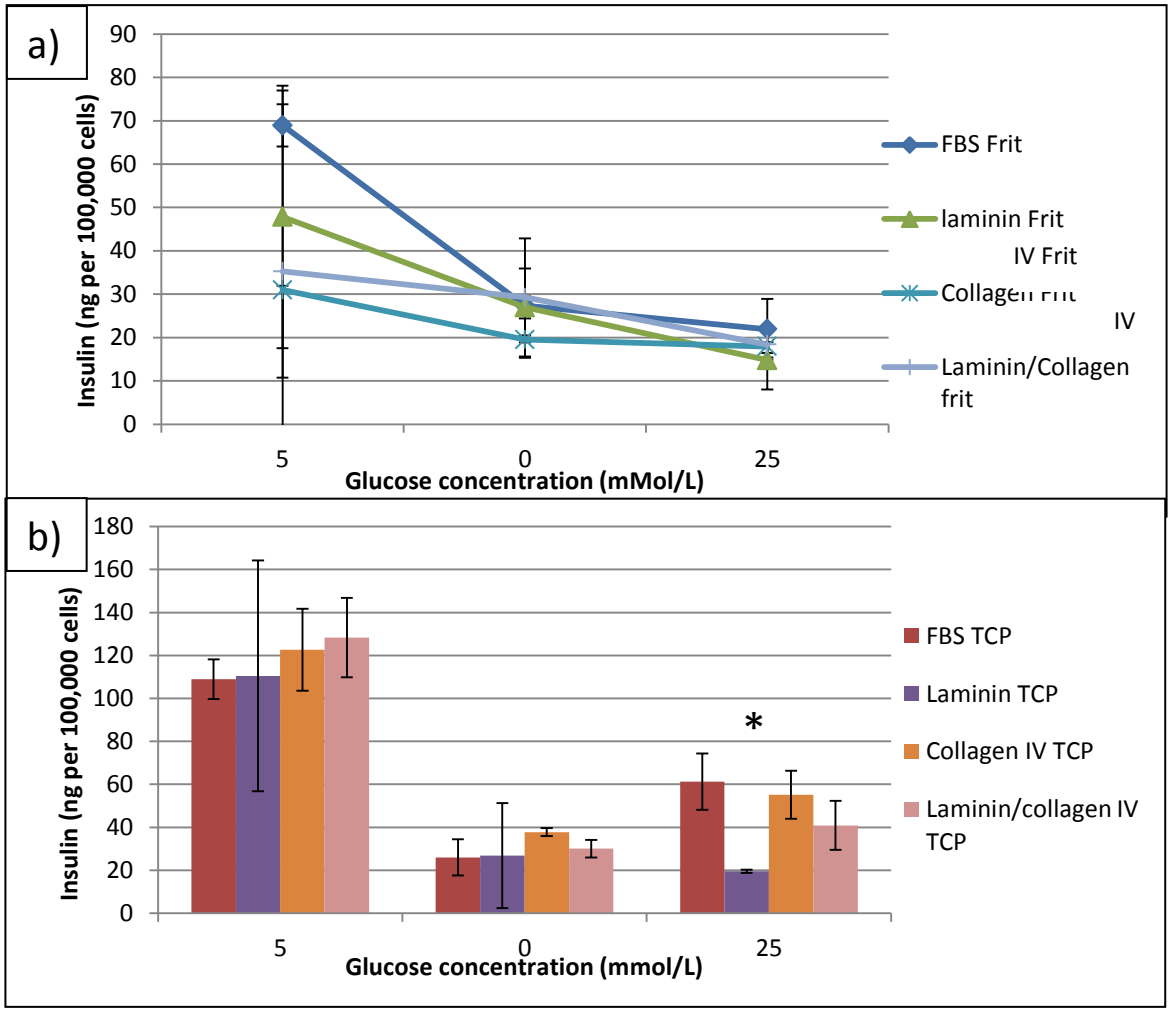

Figure 5-22: Insulin release to fluctuating glucose concentrations on BioVyon™ frits and TCP

BioVyon™ frits were plasma etched for 116 seconds at 807 watts. Treated frits and tissue culture plastic (TCP) 24 well plates were incubated for 2 hours in 40µl (38µl for TCP to account for decreased surface area) of a solution containing one of each peri insular basement membrane (BM) protein (Described in section 2.2.16.1). Prepared frits and TCP were then seeded with cell suspension containing Min-6 (Described in Section 2.2.16.2). After 3 days cell populations were exposed to a glucose challenge and the insulin released in media containing 5, 0 and 25mmol/L glucose quantified using an ELISA (Described in section 2.2.16.3). The quantity of insulin (ng) secreted was calculated per 100,000 cells using the cell numbers quantified after the glucose challenge with an LDH assay (Described in section 2.2.16.4). Graph a) and b) show insulin secretion from cell populations on frits and TCP treated with BM proteins respectively. Error bars represent variation between three frits seeded with the same cell population, n = 3. Graphs a) to c) show cell numbers on frits from three different cell populations. Graph a) shows there is no significant difference in insulin secreted over varying glucose concentrations on frits (Two-way ANOVA, $P>0.05$), and no significant difference in insulin secretion between frits treated with proteins (One-way ANOVA $P>0.05$). Graph b) shows there is no significant difference in insulin secreted over varying glucose concentrations on TCP (One-way ANOVA $P>0.05$), a significant decrease in insulin secretion was observed on TCP treated with Laminin at 25mmol/L glucose compared to the other treatments (One-way ANOVA $P<0.01$). * indicates insulin levels that are significantly different to other treatments at time points.

Graphs a) to c) in Figure 5-23 show insulin secretion on frits treated with four different proteins over time, between three different cell populations. Graphs a) to c) provided a comparison between frit protein treatments over time, a two way ANOVA was used to show that there was a significant difference in insulin secretion over time for each population ($P<0.001$). All three Min-6 populations show a similar pattern of insulin secretion, with variations between the quantities of insulin secreted per protein treatment . The Min-6 populations in graph a) secreted between 20 and 60 ng of insulin per 100,000 cells at 3 days which gradually increased to between 100 and 140 ng of insulin per 100,000 cells. Graph b) shows a similar pattern, a small increase was observed from 3 to 9 days before a rapid increase from 9 to 15 days of insulin secretion to between 120 and 180 ng of insulin per 100,000 cells. Graph c) shows more variation in insulin secretion between protein treatments than graphs a) and b), the initial insulin secretion is similar at 3 days. Insulin secretion appears to vary considerably between 50 and 150 ng of insulin per 100,000 cells at 9 days, before gradually increasing to below 150 ng of insulin per 100,000 cells. At 9 days Laminin/collagen treated frits secreted a significantly higher quantity of insulin compared to the other treatments at 15 days ($P<0.01$).

Graphs a) to c) in Figure 5-24 show insulin secretion on TCP treated with four different proteins over time, between three different cell populations. Graphs a) to c) provided a comparison between frit protein treatments over time, a two way ANOVA was used to show that there was a significant difference in insulin secretion over time for populations on graph b) and c) ($P<0.001$). The Min-6 populations in graph a) show a plateaued insulin secretion which starts high at 3 days within 80 to 150 ng of insulin per 100,000 cells. In all protein treatments but laminin the insulin secretion decreases, which is at variance with

the other cell populations. Graph b) shows a tight, consistent plateau of insulin secretion from 3 to 9 days between 40 and 80ng of insulin per 100,000 cells, before increasing rapidly to between 100 and 160 ng of insulin per 100,000 cells. Graph c) shows a steady increase in insulin secretion from 3 to 15 days on TCP treated with collagen and laminin/collagen, a significantly lower secretion of insulin was observed on laminin and FBS treated TCP at 15 days ($P<0.001$).

To aid statistical analysis, cell populations were compared separately between frits and TCP treated with a single protein. Figure 5-25, graphs a) to c) provided a comparison between frits and TCP treated with FBS over time. A two way ANOVA was used to show that there was a significant difference in insulin secretion over time for the cell population in graph b) ($P<0.001$). Graph a) shows a higher insulin secretion on TCP after 3 days compared to frits, insulin secretion then increase on frits from 3 to 15 days ($P<0.05$). Graph b) shows an increase in insulin secretion on both materials, with a significantly higher secretion on TCP at 3 and 9 days, which is surpassed by frits at 15 days ($P<0.05$). Graph c) shows a similar pattern of insulin secretion to graph a), insulin secretion on frits increases from 3 to 15 days, insulin secretion on TCP peaks at 9 days before decreasing at 15 days.

Figure 5-26 graphs a) to c) provided a comparison between frits and TCP treated with laminin over time. A two way ANOVA was used to show that there was a significant difference in insulin secretion over time for the cell populations in graphs b) and c) ($P<0.001$). Graph a) shows that TCP treated with laminin resulted in a consistently higher insulin secretion compared to frits, however a significant difference was only observed at 9 days ($P<0.05$). Graph b) shows a similar pattern of insulin secretion between materials,

with a reduced insulin secretion at 9 days followed by a rapid increase at 15 days. Graph c) shows a gradual increase in insulin secretion from 3 to 15 days, with laminin treated TCP appearing to secrete higher quantities of insulin at all time points.

Figure 5-27, graphs a) to c) provided a comparison between frits and TCP treated with collagen over time. A two way ANOVA was used to show that there was a significant difference in insulin secretion over time for the cell populations in graphs b) and c) ($P<0.001$). Graph a), a large variation can be seen in insulin secretion at 3 days, collagen treated TCP secreted a high quantity of insulin initially before decreasing. The opposite can be seen on collagen treated frits. Graph b) shows a similar pattern of insulin secretion between materials, with a reduced insulin secretion at 9 days followed by a rapid increase at 15 days, similar to laminin (Figure 5-26, graph b)). Graph c) shows a gradual increase in insulin secretion from 3 to 15 days on collagen treated TCP, insulin secretion on frits however appears to plateau from 9 to 15 days.

Figure 5-28 graphs a) to c) provided a comparison between frits and TCP treated with laminin/collagen over time. A two way ANOVA was used to show that there was significant difference in insulin secretion over time for all cell populations (graphs a) to c) ($P<0.001$). Graph a), shows a similar pattern to collagen, a significant difference can be seen in insulin secretion at 3 days initially on TCP, before decreasing. The opposite can be seen on laminin/collagen treated frits ($P<0.05$). Graph b) shows a reduced insulin secretion at 9 days followed by a rapid increase at 15 days, similar to laminin and collagen (Figure 5-26, graph b and Figure 5-27 graph b). Graph c) shows a gradual increase in insulin secretion on both materials from 3 to 15 days with laminin/collagen treated TCP secreting a higher quantity compared to frits.

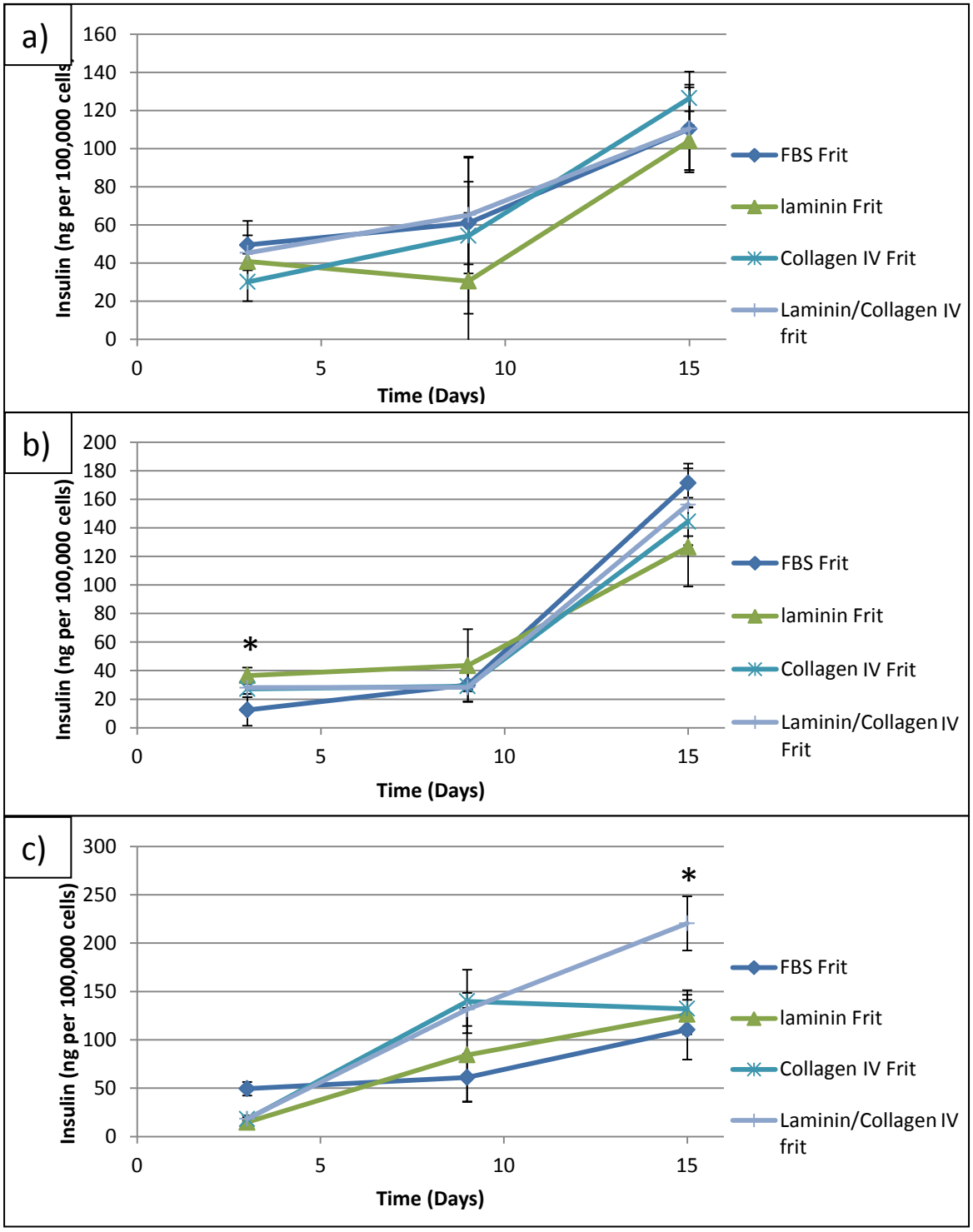

Figure 5-23: Insulin release to glucose challenge on BioVyon™ frits

Methods as in Figure 5-22 for frits and TCP respectively. At 3, 9 and 15 days different cell populations were exposed to a glucose challenge. The insulin released in media containing 25mmol/L glucose quantified using an ELISA (Described in section 2.2.16.3). The quantity of insulin (ng) secreted was calculated per 100,000 cells, using the cell numbers quantified after the glucose challenge with an LDH assay (Described in section 2.2.16.4). Graph a), b) and c) shows there is a statistical increase in insulin secretion over time (Two-way ANOVA, $P<0.001$). * indicates insulin levels that are significantly different to other treatments at time points.

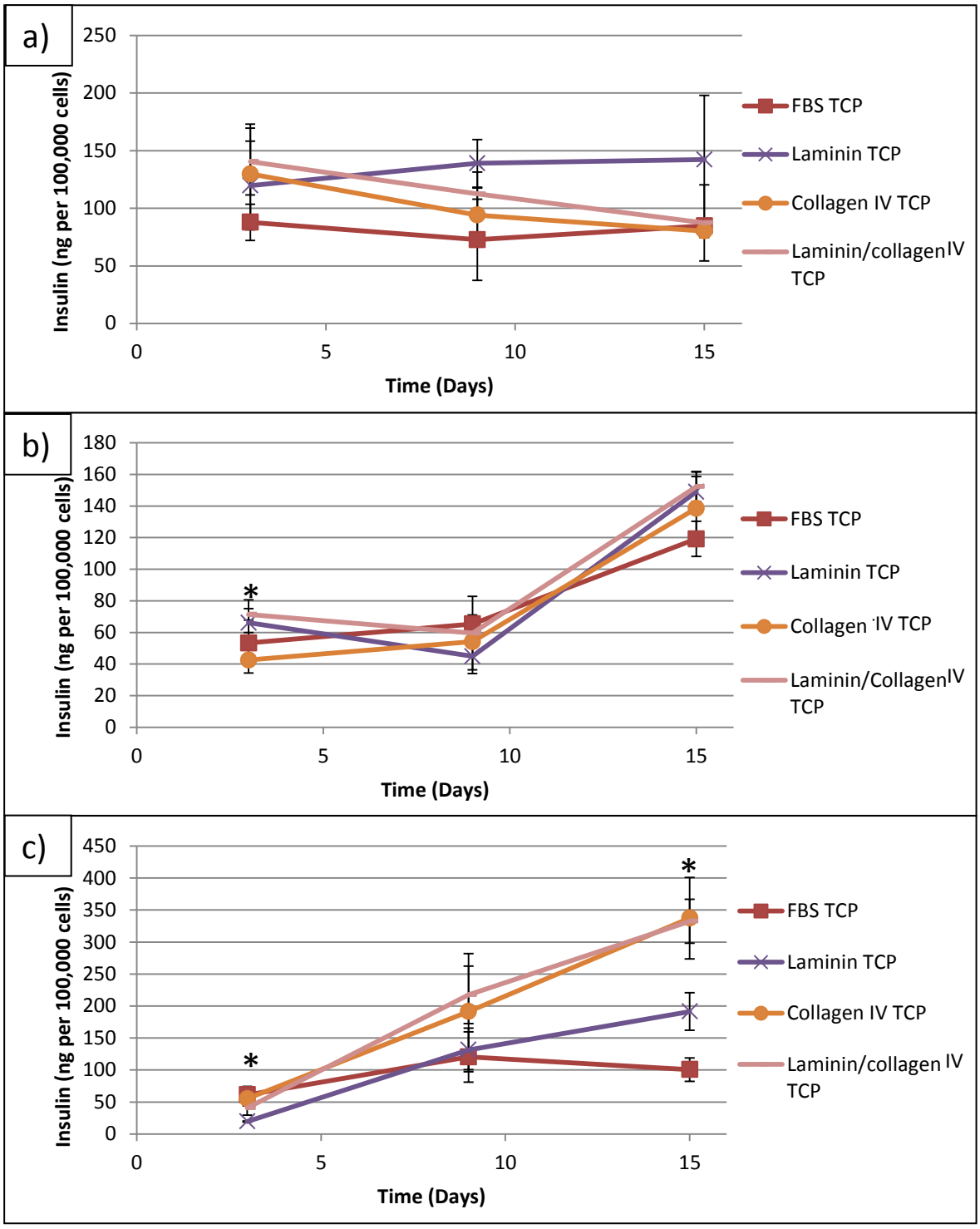

Figure 5-24: Insulin release to glucose challenge on TCP over time

Methods as in Figure 5-23 for frits and TCP respectively. Graph a) shows there is no significant difference in insulin secretion over time (Two-way ANOVA, $P>0.05$). Graph b) and c) shows there is a significant increase in insulin secretion over time (Two-way ANOVA, $P<0.001$), Collagen and Laminin/collagen treated TCP secreted a higher quantity of insulin compared to the other treatments at 15 days (Two-way ANOVA, $P<0.001$). * indicates insulin levels that are significantly different to other treatments at time points.

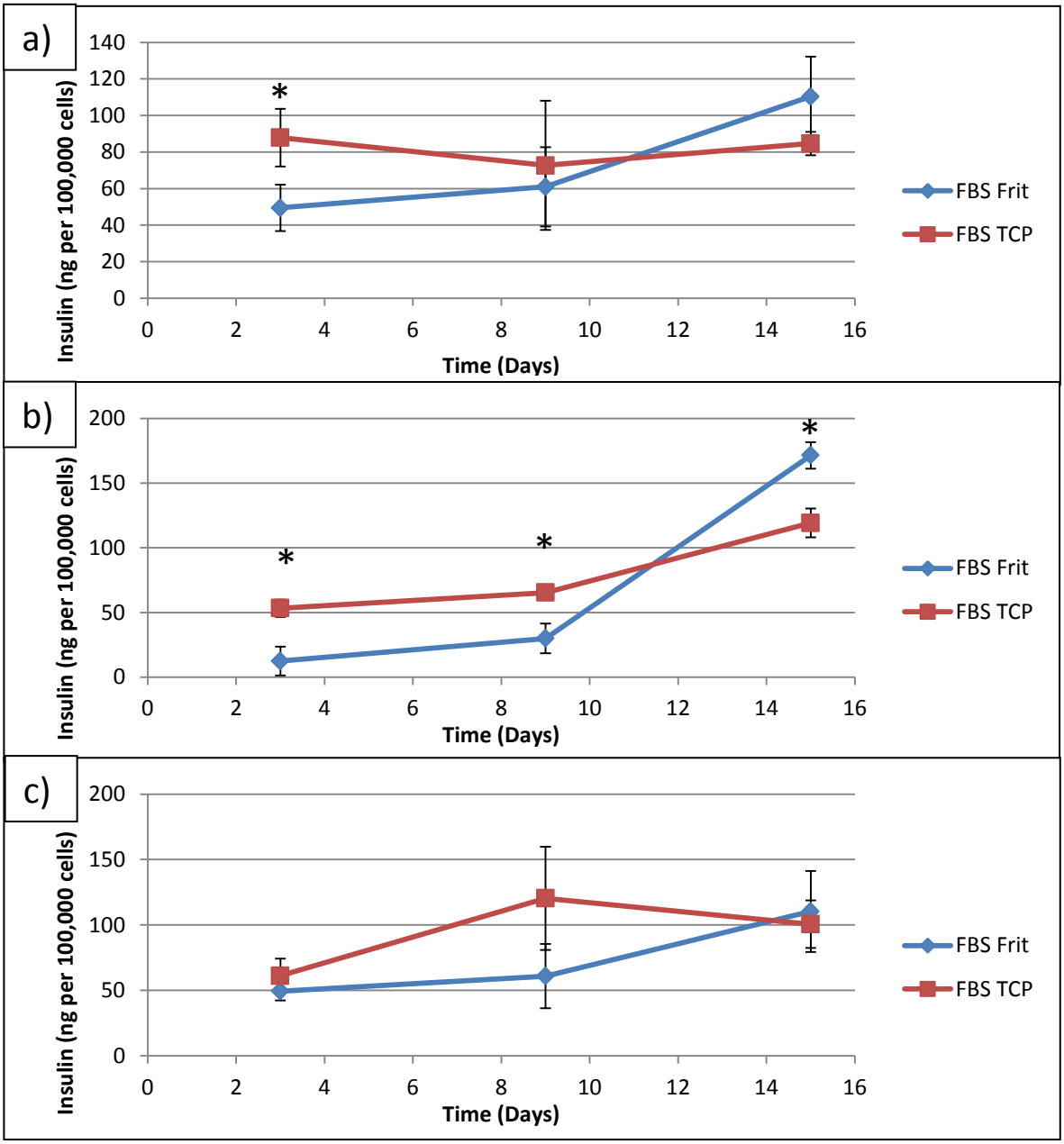

Figure 5-25: Insulin release to glucose challenge on BioVyon™ and TCP incubated with FBS

Methods as in Figure 5-23 for frits and TCP respectively. Graph a) shows there is no significant difference in insulin secretion over time (Two-way ANOVA, $P>0.05$), Graph b) shows there is a significant increase in insulin secretion over time (Two-way ANOVA, $P<0.001$). Graph c) shows there is no significant difference in insulin secretion over time (Two-way ANOVA, $P>0.05$). * indicates insulin levels that are significantly different to other treatments at time points.

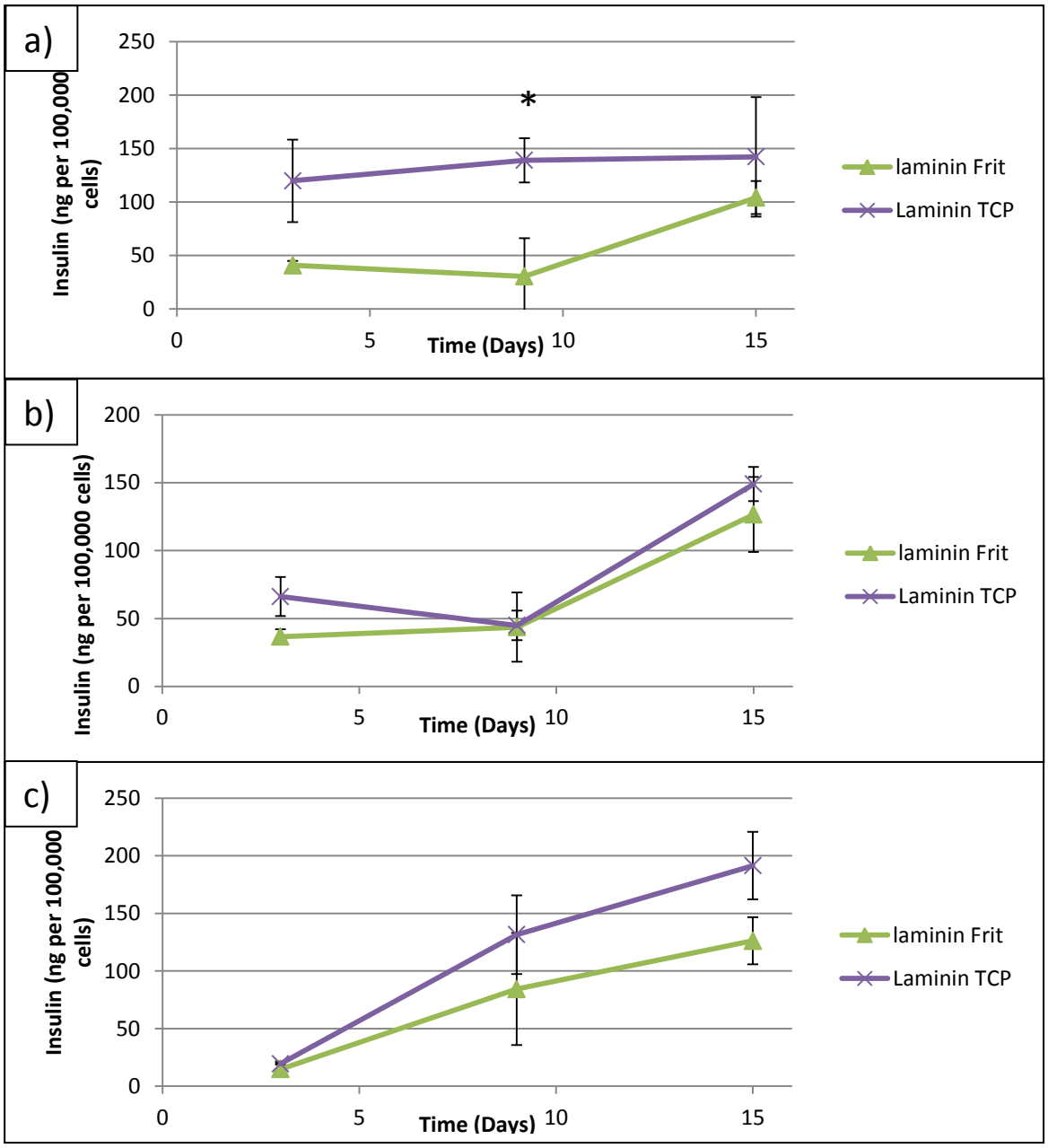

Figure 5-26: Insulin release to glucose challenge on BioVyon™ and TCP incubated with Laminin

Methods as in Figure 5-23 for frits and TCP respectively. Graph a) shows there is no significant difference in insulin secretion over time (Two-way ANOVA, $P>0.05$), Graph b) and c) shows there is a significant increase in insulin secretion over time (Two-way ANOVA, $P<0.001$), * indicates insulin levels that are significantly different to other treatments at time points.

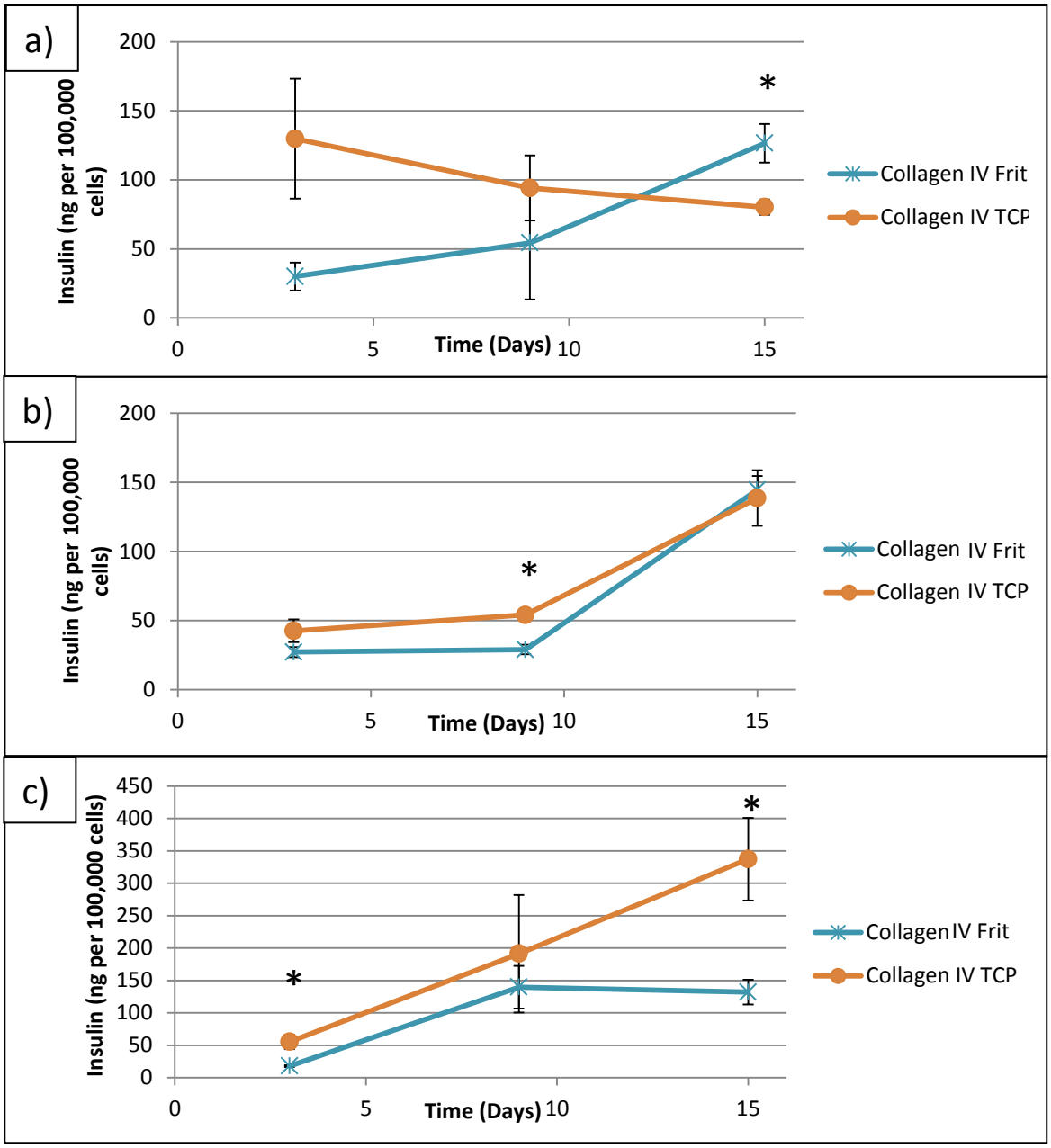

Figure 5-27: Insulin release to glucose challenge on BioVyon™ and TCP incubated with Collagen IV

Methods as in Figure 5-23 for frits and TCP respectively. Graph a) and c) shows there is no significant difference in insulin secretion over time (Two-way ANOVA, $P>0.05$), Graph b) shows there is a significant increase in insulin secretion over time (Two-way ANOVA, $P<0.001$).* indicates insulin levels that are significantly different to other treatments at time points.

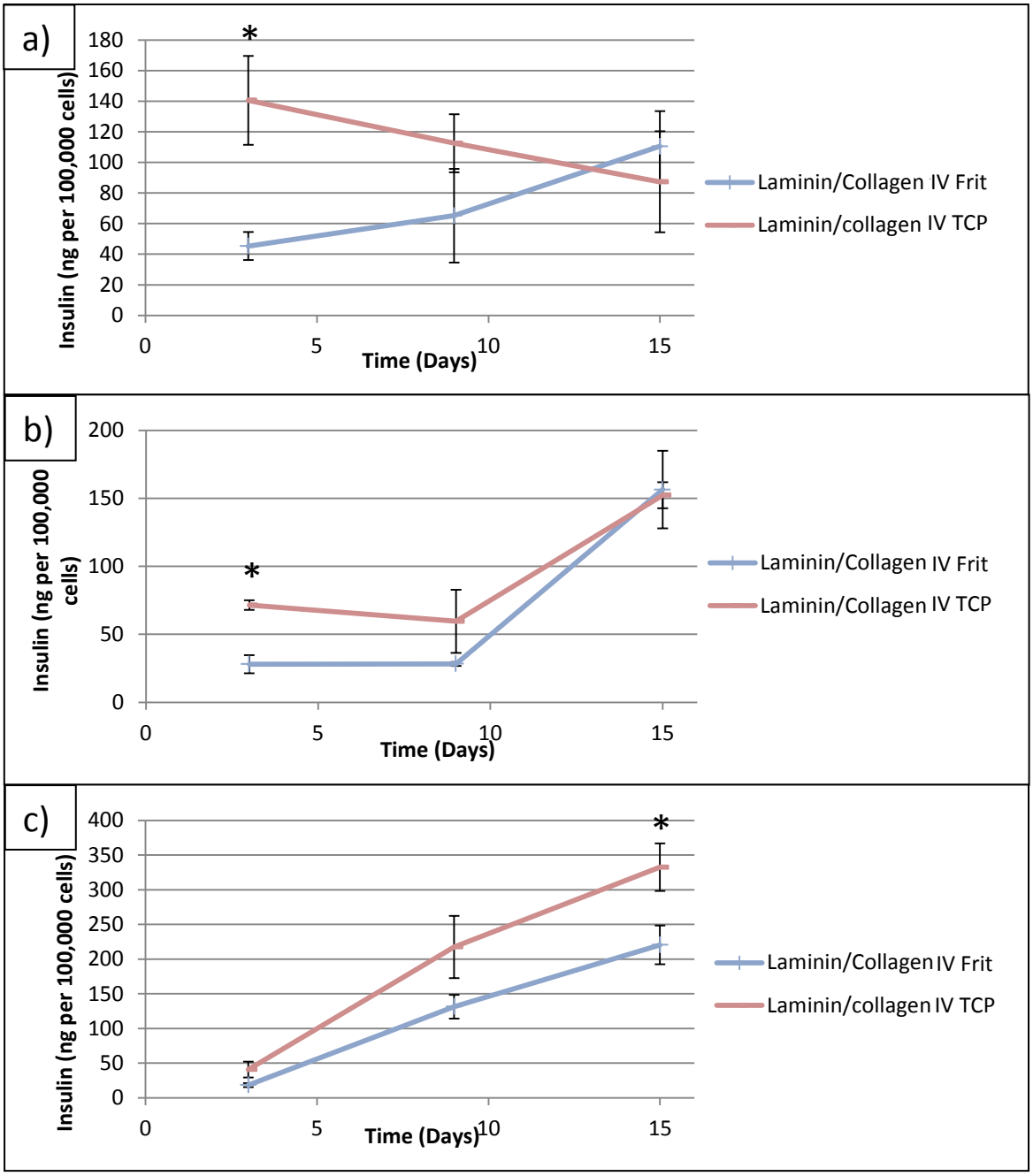

Figure 5-28: Insulin release to glucose challenge on BioVyon™ and TCP incubated with Laminin/collagen IV

Methods as in Figure 5-23 for frits and TCP respectively. Graph a), b) and c) shows there is significant difference in insulin secretion over time (Two-way ANOVA, $P<0.05$), * indicates cell numbers that are significantly different to other treatments at time points.

5.7 Discussion

This chapter has investigated how a three dimensional culture environment mimicking the proteinaceous structure of the endocrine pancreas has influenced the phenotype of the Min-6 cell line. Initial protein adsorbance to the surface of plasma etched BioVyon™ frits was analysed quantitatively and qualitatively using a BCA assay and SEM respectively. Cell populations were then seeded on the modified frits and growth and viability observed using LDH assay and a multitude of fluorescent stains. Finally, insulin secretion, the β-cell phenotype was assessed over time on frits coated with a range of peri-insular basement membrane proteins using an insulin ELISA. For each experiment the frits were compared to a TCP control to observe any difference between the two dimensional and three dimensional environments and the effect they have on the cell popualtions. The results observed on BioVyon™ will be evaluated and compared to recent literature.

5.7.1 Protein adsorption

The proteins selected to modify the surface of the Biovyon™ frits are known to form the lamina lucida interna, a layer of the periinsular basement membrane which adheres and supports β-cell populations (Section 1.2.2). Collagen IV, Laminin 511 and a combination of the two proteins were incubated with plasma modified frits and TCP, proteins adsorb to positively charged polymer surfaces and a BCA assay was used to quantify the quantities bound [162, 166]. Collagen was adsorbed at the highest quantity to frits and TCP, several factors have been identified which contribute to protein adsorption such as size, charge

and stability [277]. The results shown in Figure 5-1 indicates collagen adsorbs more readily, it can be speculated that the structure of collagen promotes its adsorption to the surface of the materials more readily than laminin.

Laminin and collagen appeared to adsorb more readily to frits than TCP wells of a comparable surface area. A significant difference was observed in the adsorption of laminin between frits and TCP ($P<0.001$). The increased adsorption of laminin and collagen in frits could have been due the plethora of oxygen moieties generated on BioVyon™ compared to TCP. Contributing to the higher wettability observed on plasma etched frits and HDPE exposed to oxygen plasma in comparison to TCP (Figure 3-15). Hydroxyl groups may have promoted hydrogen bonding to the positively charged regions of collagen and laminin, increasing adsorption [274].

The increased adsorption of both proteins to TCP from the laminin/collagen treatment may be due to TCP adsorbing the proteins in such a way as to promote protein-protein adhesion between collagen and laminin. Collagen is known to contain several binding motifs for proteins such as perlectins, heparin sulphate proteoglycans and enactins, this enables crosslinking in the peri-insular basement membrane [63, 69, 73, 84].

SEM analysis of the protein treated frits show cuboidal crystal structures and agglomerations (Figure 5-3 to Figure 5-6) which are absent on the plasma etched control frits (Figure 5-2). The primary limitation of SEM is that the samples must be exposed to a vacuum before analysis. This may have impacted the surface of the BioVyon™ exposed to protein treatment. During SEM analysis the decrease in pressure may have resulted in the evaporation of a water layer vital in sustaining the structural relevance of protein for cellular adhesion [283]. The agglomerations observed in Figure 5-4 graphs a) and b), may

have been formed druing the evaporation of the water layer. This may have resulted in the proteins unfolding and hydrophobic regions, normally protected internally in a polar solution, shifting to the outside of the protein structure. This in turn may have resulted in protein-protein interactions between the hydrophobic regions and a resulting agglomeration forming the structures observed in Figure 5-3 to Figure 5-6 [284, 285]. SEM analysis provided a complementary, qualitative analysis which supported the presence of proteins adsorbed to the BioVyon™ surface prior to cell seeding.

5.7.2 Cell adhesion

It was important to analyse the cell populations over time within the frit and TCP environments treated with BM proteins. Initially cells were seeded onto each material after 2 hours incubation in serum free media and the number adhered quantified using a reverse method. The materials were washed to remove any unadhered cells. These were then quantified and the number adhered calculated from the number originally seeded. This enabled quantification of cell number without sacrificing the adhered cell population.

Figure 5-7 graph a) to c) show cell adhesion to four different protein treatments on frits and TCP. In order to understand the pattern of cell adhesion between protein treatments and the variation between cell populations it is useful to consider the status of the cell once seeded. Prior to the seeding process a monolayer of Min-6 were trypsinised using a solution of enzymes that hydrolyse protein. This process indiscriminately cleaved the

extracellular proteins adhering (such as integrins, dystroglycans and lutherans (Figure 1-3) the Min-6 cell monolayer to the TCP surface they were cultured on.

Once seeded onto the treated materials, the cell adhesion molecules may have been removed, decreased or active. The random nature of trypsinisation may have contributed to the variation between cell populations and this may have influenced the pattern of adhesion and the number adhered to the materials.

Laminin treated materials were observed to adhere the highest number of cells (Figure 5-7, graphs a) and b)). This mirrors the abundance of adhesion sites located on the globular domain of the laminin structure, that are known to adhere a plethora of β-cell adhesion molecules (Section 1.2.2.2 and 1.4.3.). Collagen and FBS were also observed to adhere cell populations and possess integrin adhesion sites and proteins that promote cellular adhesion respectively.

Overall, the laminin and laminin/collagen treated TCP was the only material found to have significantly increased the cell adhesion compared to the other treatments in in graphs a) and b) (Figure 5-7) ($P<0.05$). However, a large number of cells were adhered in all cell populations on all treatments. Considering they were seeded in serum free media it can be suggested that any adhesion observed was mediated by the protein adsorbed to the material. Thus the desired environment had been achieved and cells were adhered to BM proteins in a two dimensional or three dimensional environment.

5.7.3 Cell growth

Once seeded onto the treated materials, the cell populations were cultured in protein treated frits and TCP for 3, 9 and 15 days. At each time point the number of cells were

quantified. This provided information as to how the populations were growing within the environment they were exposed to. Cell number was compared between protein treatments on the same material and between materials with the same protein treatment over time.

Figure 5-8, graphs a) to c) and Figure 5-9 graphs a) to c) show a similar pattern of growth from the same cell populations on TCP and frits. In Figure 5-8 and Figure 5-9 graphs a) shows plateau in cell number from 9 to 15 days (Or at least the smallest difference in cell number at 15 days from the number initially adhered). Graphs b) Figure 5-8 show an increase in growth, and graphs c) show a decrease in growth.

The differences observed could be explained by the number of cells adhered initially, the populations in graphs b) Figure 5-8 have a relatively low adhesion at 2 hours (between 200,000 and 500,000 cells) and resulted in a cell population that increases from 3 to 15 days. The opposite pattern of cell growth can be seen on some treatments in graphs c) Figure 5-8, frits and TCP with a high number of cells adhered initially (between 750,000 and 925,000 cells) appear to decrease over time. Graphs a) Figure 5-8 show that an initial cell number of approximately 600,000 seem to plateau after 15 days. This may have been an effect of confluency, a phenomenon commonly encountered on TCP. Proliferating cell monolayers reach a state of complete confluency when there is no more space in which to grow. The Min-6 cell line are susceptible to this state and become apoptotic as a result. This may be the reason why a high number of cells adhered initially on TCP and frits reduced in number over 15 days, due to active mechanisms causing apoptosis or an absence of signals inducing proliferation .The opposite is apparent of populations with a

low number adhered initially, the absence of cell to cell contact, or abundance of space available to grow may have promoted proliferation on both materials.

Variation between treatments was observed on both materials (Figure 5-8 and Figure 5-9), however, the cell numbers followed the same basic pattern on the frits. This suggests that the initial quantity of proteins adsorbed may have lost relevance, and failed to influence the proliferation of the cell population beyond initial cell adhesion.

Variation between cell number on TCP protein treatments provided an interesting insight into the influence protein treatment has in a two dimensional environment. Not only did the proteins adsorbed have a significant impact on the cell numbers initially adhered, but an effect was seen over time, specifically after 3 days of culture on TCP. Figure 5-9, graphs a) to c) show significant differences between cell number on the different protein treatments at 3 days ($P<0.001$), suggesting that protein adsorbed on a two dimensional TCP environment are able to influence adhered cell numbers more significantly than proteins adsorbed to the frits. This may be due to a multitiude of factors contributing to cell death and proliferation on the different environments over time. The seeding process is a chaotic environment, reliant on protein adsorption, correct alignment and abundance of adhesion sites, cell contact and integrity of adhesion molecules. This may have resulted in cells adhering initially and then unadhering from the frits and TCP surface.

The influence adhesion has on the growth of the population is compounded by the environment post seeding, the type and number of integrin adhesion may have influenced metabolism, proliferation and in turn cell to cell adhesion. Without the correct extracellular signalling cell populations may have become apoptotic or quiescent within the frit or cultured on the TCP controls.

Comparison of protein treatment between the two materials indicated that TCP cell number was significantly higher in the populations in graphs b) and c) for all treatments except laminin ($P<0.05$) (Figure 5-10 to Figure 5-13). This observation supports the idea that protein treatment was more influential on the TCP than the frits.

The environment within the frits may have been more susceptible to changes in surface treatment, due to increased shear forces or flow of media. After initial adhesion, media containing FBS was used to nourish the cells on the materials. Proteins in FBS may have crosslinked, covered or replaced laminin, collagen or laminin/collagen treatments on the frits more readily than proteins bound to the TCP surfaces. This in turn may have have reduced the influence of the adsorbed proteins of the BM. Furthermore, it is known that many cell lines including the Min-6 can secrete their own extracellular matrix proteins, after the initial adhesion to the frits cells may have secreted and generated their own proteins influencing the surrounding environment [198, 286]. This may have been promoted by the environment in the frits and functioned to produce the consistently observed between cell number on the different frit protein treatments.

5.7.4 Cell viability

Cell populations cultured for 15 days were stained with Hoescht and propidium iodide (HPI) and Calcein AM to assess cell viability after long term culture on the TCP and frit environments. HPI and Calcein AM move passively through the cell membrane to interact with DNA and cytosolic esterases respectively [287]. Viability is indicated by the combination of stains in HPI, propidium iodide is unable to pass into viable cells with a sustained membrane integrity. The presence of blue fluorescence and not red indicates

that the cells stained are viable. Calcein AM fluoresces green in the presence of cytosolic esterases, if the green fluorescence is sustained within the cell, this indicates membrane integrity. In combination these stains provide a powerful test of viability.

Graphs a) in Figure 5-14 to Figure 5-21 shows HPI and Calcein AM staining of Min-6 cells adhered to frits treated with different proteins. The HPI shows a strong blue fluorescence from the cell populations, which appear to be adhered within the porous structure of the frits. The high flouresence on all protein treatments may have been due to the three dimensional structure of the frits, and cells in the depth of the pores adding to the flourescence. The HPI also appears to stain the surface of the frits, providing a clear image of the surrounding material. The Calcein AM staining shows a strong green fluorescence within the cells adhered to frits treated with all four proteins. This may again be compounded by cells in the depths below the surface. Overall the staining observed on the frits indicates that at 15 days the cells adhered are viable.

Graphs b) in Figure 5-14 to Figure 5-21 shows HPI and Calcein AM staining of Min-6 cells adhered to TCP treated with different proteins. The staining of the Min-6 on TCP is remarkably different to the frits. The pattern of cell adhesion is unique to the protein treatment, the most significant of which were observed on laminin and laminin/collagen treated TCP (Graphs b) Figure 5-17 and Figure 5-21). The second most striking observation was that the fluorescence of both stains appeared to be much less intense than the cell populations on the frits. This may be due to the fact that a monolayer is being stained and compared to cells on a 3D material. However, if the cells stained with Calcein AM on FBS treated TCP (graph b) in Figure 5-15) are compared to the cells on TCP treated with laminin (graph b) Figure 5-17) a difference in fluorescence intensity can be seen. This

suggests either a reduction in the cytosolic esterases, or a lack of membrane integrity, resulting in the flouresence effectively leaking out of the cells. This is supported by the presence of red flouresence in the HPI stained, protein treated TCP.

Overall it appears that the cells are more viable on the frits than the TCP environment between all protein treatments. It is interesting to note that cell monolayers would normally become over confluent and apoptotic on a TCP environment once cultured beyond approximately seven days. The success of the cell populations on the TCP may be due to protein pre-treatment in combination with an increased frequency of media change. This may have functioned to remove apoptotic cells and sustain the population.

5.7.5 Cell phenotype

In addition to analysing the growth and viability of the cell populations cultured on BioVyon™ and TCP treated with BM proteins, it was necessary to assess the phenotype of the Min-6 cell line. As a β-cell line the Min-6 are known to produce and secrete insulin in response to fluctuations in glucose concentrations [199].

This response was assessed in Min-6 cultured on frits and TCP treated with BM proteins at 3 days, Figure 5-22 graphs a) and b) indicated that the insulin secretion in ng per 100,000 cells continued to decrease from 5, to 0 to 25mmol/L glucose on the frit environment compared to the TCP on which a slight increase from 0 to 25mmol/L glucose concentration was observed. In a physiological environment, native β-cells would be expected to secrete a higher quantity of insulin in response to an increase in glucose concentration at 25mmol/L than the lower glucose at 5mmol/L. The observed response in

Figure 5-22 on both materials does not mirror the natural response of native β-cells. This can be attributed to the fact that the Min-6 are a cell line in a synthetic environment, after trypsinisation and resuspension, resulting in a reduction in cell to cell adhesion and the formation of gap junctions vital for efficient insulin secretion [11]. This could explain a slightly reduced efficiency in insulin production and secretion.

If the two materials are compared (Figure 5-22), it is clear that there is less variation between protein treatments and a higher quantity of insulin secreted on the TCP than the frits. This suggests that the phenotype is sustained more effectively on TCP after 3 days culture than on the frits. This experiment showed that the Min-6 cell line responded to fluctuations in glucose concentrations, and is a suitable model to investigate the effect of protein treatments over time.

The insulin secretion of the Min-6 cell lines were then assessed over time on frits and TCP treated with different proteins. Figure 5-23 shows that all three cell popualtions secreted a significantly higher quantity of insulin over time on all treatments ($P<0.001$). A similar pattern was observed in TCP, however, on one of the three populations insulin secretion appeared to decrease in all protein treatments except laminin (graph a), Figure 5-24). This suggests that the environment in the frits is as effective as TCP at sustaining the insulin phenotype. The three dimensional environment in combination with large populations of proliferating Min-6 may have resulted in an increased number of cell to cell adhesion and the formation of gap junctions necessary for rapid secretion, of large quantities of insulin.

The quantity of insulin secreted on the frits appears to show less variation between treatments than the TCP, supporting the idea that adsorbed proteins are more influential on the TCP than the frit environment. If insulin secretion on the individual protein

treatments are considered and compared between the materials, it is clear that overall, a slightly higher quantity of insulin was secreted on the TCP compared to the frits (Figure 5-25 to Figure 5-28)

However, in FBS treated materials the quantity of insulin secreted appears to increase beyond that secreted by cell population on TCP at 15 days (Figure 5-25). The same pattern was observed on frits treated with collagen ($P<0.05$) (Graph a, Figure 2-27) and laminin/collagen (Graph a, Figure 5-28). This suggests that the β-cell phenotype is not only protected after long term culture on the frit environmet but may be improved over time as the cell populations grow. The proliferation of the Min-6 cells in combination with the potential secretion of extracellular proteins may be generating an environment that begins to mimic the natural proteinaceous structure within the endocrine pancreas.

6 Conclusion

This study was the first to investigate the potential of BioVyon™ as a novel biomaterial to mass culture a β-cell line. The modification of BioVyons™ surface chemistry and unique three dimensional (3D) structure in combination with the adsorption of proteins to mimic the pancreatic islet, resulted in a novel culture environment. The observation of Min-6 growth and sustained phenotype cultured on this material provided an original contribution to knowledge.

This chapter will conclude with the following:

- A summary of the key findings from each chapter
- A comparison of key findings to current literature
- A consideration of the methodological limitations
- Implications of this research and futher work

6.1 Key findings

So far a number of exciting milestones have been reached in the investigation of BioVyon™ as a novel biomaterial to culture the Min-6 cell line. The BioVyon™ structure has been well characterised and detailed analysis has provided a clear understanding of its capabilities. Oxygen plasma has been used to alter and improve the surface; post plasma etching BioVyon™ was found to be susceptible to cellular infiltration and surface

conditioning. These treatments were optimised and the BioVyon™ surface rendered suitable for protein adsorption, which aided and promoted cellular adhesion.

Proteins specific to the functional peri-insular basement membrane were employed to modify the BioVyon™ surface. Reliable quantification of cell number was also achieved using a LDH assay. This, in turn, was used to analyse growth of cell populations seeded onto BioVyon™. Finally, the phenotype of the Min-6 populations cultured on the modified BioVyon™ was analysed and compared to tissue culture plastic (TCP) controls over 15 days.

6.1.1 BioVyon™ characterisation and development

Several primary elements of the BioVyon™ structure were investigated; the macro structure, the micro and nano scale topography and the surface chemistry. These were characterised before and after treatment with oxygen plasma, the influence of which was analysed with several techniques and compared to TCP.

The 1mm BioVyon™ F frits were shown to possess a porosity suitable for effective passage and diffusion of seeded cell populations and oxygen respectively (Section 3.2). Two separate plasma etching systems were employed to modify the BioVyon™ frits, and the effects of oxygen plasma characterised, directly with FTIR and THA/TBO assays, and indirectly using ARCA respectively (Section 3.3). The primary factor influencing surface chemistry on the BioVyon™ was found to be contact time with oxygen plasma (Figure 3-4 and Figure 3-11). With optimisation it was found that a wettability comparable to TCP

could be generated within the frit structure (Figure 3-15). Furthermore , the nature of the plasma generated a range of wettability throughout the frit thickness (Section 3.3.5). The chemistry of the HDPE particulates forming the BioVyon™ frits resulted in the generation of several oxygen species, as opposed to a pure population of COOH groups generated on the polystyrene used for TCP (Section 3.3.2.1). The range of oxygen groups generated were found to be susceptible to decay in the atmosphere. This was also found to be reduced and the oxygen groups sustained if the treated frits were stored in an appropriate media (Section 3.3.3).

Finally, the micro and nano scale topography was visualised and assessed using SEM and AFM. These topographies were not found to be significantly influenced by contact with plasma. A difference of approximately 0.5nm was observed at the lowest scan size, this scale of topography was not directly comparable with previous literature due to the huge number of cell lines and materials investigated (Section 3.3.4 and 3.4.3). The most relevant study assessed macrophage response to topography size as low as 44nm [177], despite the similarity, BioVyon™ possesses its own, unique surface and may have influenced cells differently. In conclusion it was found that the influence of oxygen plasma on Biovyon™ was complex, but with understanding and optimisation an appropriate treatment was applied that was suitable for cell culture.

6.1.2 Conditioning and surface modification of the BioVyon™ frits

The most important factors influencing cell adhesion were investigated in chapter three. This not only involved exploring the logistics of seeding cells into the porous structure, but also investigating protein adsorbance to the chemically optimised surface.

Using basic capillary action to seed cell suspensions into the BioVyon frits structure, it was found that the incubation time of cells within the frits influenced adhesion, and that 2 hours was optimal before cell proliferation interfered with quantification of the adhered cell numbers (Figure 4-2). The volume of the cell suspension seeded was another factor investigated.

The BioVyon™ frits were found to hold an internal volume of approximately 80µl (Table 4-1). By reducing the volume in which cells were seeded and the incubation time, it was speculated that the contact between cell integrins and adhesion sites on adsorbed proteins were increased. It is well established that cell adhesion is mediated by proteins. This was systematically investigated on the surface of frits. Initially it was found that cell adhesion was significantly reduced when seeded without serum proteins to mediate adhesion (Figure 4-4). The final factor contributing to cell adhesion was plasma contact time with the BioVyon™ surface, an increase in wettability was shown to increase protein adsorbance and in turn cell adhesion (Figure 4-5 and Figure 4-6).

The oxygen species generated on the surface of BioVyon™ were exploited for further modification and functionalization (Section 4.2.3). The application of the silane linker APTES were found to generate four times the number of accessible amine groups compared to direct binding of amine groups to existing COOH groups at a ratio of 1:1 (Figure 4-9).

Chapter 4 indicated that Biovyon™ holds the ability to adhere a number of cells similar to that of TCP of a comparable surface area. The process of cell adhesion was optimised and the factors influencing it explored. The influence of protein adsorption on cell adhesion was applied and understood with relevance to the BioVyon™ surface. Finally, BioVyon™

shows potential for further functionalization, providing a surface susceptible to several chemical modifcations, such as covalent bonding with amine groups, silane linker crosslinking and potentially peptide conjugation.

6.1.3 Mass cultivation and mimicking the pancreas

In order to fufill the aims of the project, the BioVyon™ environment was modified using appropriate proteins to mimic the pancreatic basement membrane. Min-6 cells were then cultured on this environment and analysed over time. Cell growth and insulin secretion were assessed at 3, 9 and 15 days to obtain an idea of how the cell populations behaved in the BioVyon™ environment and how this compared to existing TCP culture methods.

The quantities of protein adsorbed to the surface of the frits and TCP were investigated initially, and it was found that the plasma etched BioVyon™ surface chemistry adsorbed a higher quantity of laminin and collagen than TCP of a comparable surface area (Figure 5-1). This was confirmed qualitatively by SEM imaging which indicated proteinaceous aglomerations on the frits surface after protein treatment (Figure 5-2 to Figure 5-6).

Overall, this showed that BioVyon™ is capable of being modified via protein adsorption to mimic psysiological environments.

Although variation was observed between three different cell populations seeded and adhered onto the frits treated with a range of BM proteins, the number adhered were comparable to TCP (Figure 5-7). The initial number of cells adhered may have had an influence on the cell populations growth as three different patterns of growth were

observed on the frits and TCP. Two of the three populations showed an increase in cell number over 15 days and cell viability of cells cultured in the frits after 15 days were found to be better than that of TCP (section 5.5). This suggests that the 3D environment prevents or reduces the affect of confluency.

Analysis of insulin secretion in the Min-6 cell line using an insulin ELISA indicated that the cells responded appropriately to a glucose challenge compared to previous literature [78]. The response observed to high glucose concentrations was protected and improved in the BioVyon™ environment over 15 days (Figure 5-23). The absence of any consistent significant difference in cell number and insulin secretion between protein treatments on the frits, suggests that the protein treatment lost relevance over time. In contrast to TCP, on which cell growth and insulin secretion showed more variation between treatments (Figure 5-8, Figure 5-9, Figure 5-23, Figure 5-24).

Overall the environment created within the BioVyon™ frits was found to harbour large quantities of Min-6, these populations have been observed to proliferate and the insulin phenotype preserved and improved over long periods of cell culture.

6.2 Evaluation of results and comparison to current literature

The primary aim of this research was to investigate the potential of BioVyon™ to mass culture β-cell populations. In order to do so it was necessary to mimic the 3D and structural aspects of the pancreatic islet. The theory behind this study and the key findings will be critically evaluated and compared to current literature.

6.2.1 The three dimensional structure of BioVyon™

Various methods of 3D culture exist; highly porous, solid scaffolds similar to BioVyon™ such as Alevtex ® have been successful in culturing large populations of different cells, including hepatocytes, adipocytes and neurones [288-290]. Gels such as Matrigel ® have been employed to entrap and sustain β-cell analogues [78, 291].

Microgravity culture methods have also been used to generate pseudoislets that better mimic the *in-vivo* adhesion between cells of the pancreatic islet [292]. It was hypothesised that the 3D structure of BioVyon™ in combination with a surface chemistry comparable to current TCP would support 3D growth and promote appropriate cell to cell contact in the Min-6 cell line.

Cell to cell contact between β-cells is key to efficient insulin secretion in the pancreatic islet. This has been well established through observations of native β-cells and β-cell lines exposed to increased concentrations of glucose [62, 293-295]. Cell adhesion molecules (CAMS) play an important role in the formation of gap junctions between β-cells, these junctions are known to promote the influx of Ca^{2+} ions between cells [218, 220, 221]. The influence of these junctions was elucidated by an experiment in which the yellow dye luciferase was added to one side of a pseudoislet formed from Min-6. The dye was observed to flow rapidly thorugh the islet via the network of gap junctions, eventually fluorescing throughout the islet [219]. Ca^{2+} ions in turn initiate insulin exocytosis, and mediate a collective, pulsatile secretion of insulin throughout a population of β-cells [62].

Culturing β-cells in 3D as pseudoislets has been found to improve insulin secretion due to improved cell to cell adhesion [293, 296], an observation which supports the current

paradigm shift from two dimensional cell culture to three dimensional methods (Section 1.1.6). It can be speculated that mimicking the three dimensional structure of the pancreatic islet provides cell to cell adhesion at all angles around an individual cell as opposed to the limited adhesion between cells in a monolayer.

The results of long term growth and visualisation of cell populations within the frit structure indicated that structures similar to pseudoislets cultured in microgravity were not achieved. However, cell viability was improved on the frit environment, and in some cases insulin secretion in the cell populations appeared to be improved on the Biovyon™ compared to TCP. This suggests that the porous structure did offer some benefit, the effects of which may have been heavily influenced by initial viability and numbers of cell populations adhered.

6.2.2 Mimicking the peri-insular basement membrane

As well as the 3D aspect of mimicking the pancreas another key area of consideration is the proteinacious structures surrounding native β-cells. The peri-insular basement membrane is vital for the development and maintenance of the β-cell phenotype (Section 1.4.1). These were passively adsorbed to the surface of BioVyon™ in an effort to combine the 3D environment with the proteins β-cells would be directly adhered to in the endocrine pancreas. Anaylsis of protein adsorption indicated that the cells would have come into direct contact and adhered to these proteins (Figure 5-1).

The literature most relevant to this work is that of Weber *et al* (2008) who, using matrigel and a process of light photoinitiation incorporated various isoforms of the proteins that form the peri-insular BM into a 3D culture environment [78]. Approximately 50,000 Min-6

were encapsulated in the proteinaceous gel, these populations were exposed to a glucose challenge at 1, 5 and 10 days [78]. The glucose challenge was conducted at lower concentration than this study, with encapsulated Min-6 being exposed to 1.1mMol for 45 min followed by 16.7mMol for 1 hour [78]. A significant increase in insulin secretion was observed after 5 days on gels containing laminin and collagen IV, before plateauing from 5 to 10 days [78].

This study can be partially compared to this work as the Min-6 cells were in contact with the same proteins used (Collagen IV and laminin 511) at a comparable quantity in a 3D environment. However, the most significant difference would be the structure of the proteins in the gel. This may have been significantly different to the proteins adsorbed to the surface of the BioVyon™, as the structure and folding are strongly influenced by a positively charge polymer surface [164, 274, 277].

The number of cells grown over time is not shown in Weber *et al's* (2008) work, however it can be speculated that the plateau in insulin secretion observed after 5 days could be due to the Min-6 cell populations reaching a state of confluency in the gel which was at a volume of 30µl. This in turn could have influenced the quantity of insulin secreted per cell. The insulin secretion oberserved on the frits showed an increasing insulin secretion over a longer period of time, for all cell populations (Figure 5-23) ($P<0.001$). Although the quantities of insulin cannot be directly compared between Min-6 populations on the BioVyon™ and the hydrogel, it does indicate that the cells may have continued to grow and the insulin phenotype may have improved on the frits beyond 15 days.

The peri-insular basement membrane is formed of a collection of proteins, of which laminin and collagen IV are known to directly adhere to β-cells (Section 1.2.2). The ratio of

these proteins found in the BM is another important factor influencing the type and number of integrins adhered. This in turn may affect intracellular pathways. Weber *et al* (2008) incorporated a combination of BM proteins into Matrigel ® at specific ratios [78]. Laminin and collagen IV were entrapped by photoinitiation which polymerised the proteins in the gel structure at ratios of 25:75, 50:50, 75:25. Min-6 populations cultured in these environments were assessed for viability and insulin release in response to glucose at different time points [78]. The most significant finding was that a ratio of 25:75 collagen IV to laminin resulted in the highest level of insulin release compared to other protein ratios after 5 days, and remained consistent over 10 days. The authors speculate the success of this protein combination was due to its similarity to the ratio found naturally in the BM.

In the present study a combination of laminin and Collagen IV was seeded onto plasma etched BioVyon™ frits in an attempt to generate a ratio similar to the peri-insular BM (Figure 5-1). One of three cell populations indicated a significant increase in insulin secretion at 15 days on the laminin/collagen treatment compared to the other proteins ($P<0.01$) (Figure 5-23). Further work is required to identify the ratio at which laminin and collagen IV were adsorbed to the surface of the BioVyon™. The adsorption of proteins to polymer surfaces is known to be chaotic and uncontrollable, and so it is unclear whether applying the proteins at different concentrations will provde precise control over the ratio at which they are adsorbed.

Overall, the large porous structure of BioVyon™ offered a more advantageous environment for mass cell culture compared to the gel investigated in the work of Weber *et al* (2008) [78]. The results of the Min-6 culture in Matrigel® suggested the cell

populations became quiescent, as insulin secretion began to plateau after 5 days [78]. This may have been due to reduced space preventing cell proliferation or the omnipresent nature of the gel impeding the development of a physiological standard of β-cell phenotype. The results observed in this study suggest that the vacuous nature of BioVyon™ not only promoted proliferation but also insulin secretion up to 15 days.

6.3 Methodological limitations

The primary limitation encountered during this project was due to the 3D nature of the BioVyon™. All methods of cell anaylsis normally applied to 2D methods of cell culture had to be adapted for the porous structure of the frits. This prevented simple quantification of cell number via counting using a haemocytometer, and it was necessary to employ assays on samples of the cell population supernatants.

Further, complications arose when staining cell populations adhered to the frits. Only the first 0.2mm of the cell populations growing within BioVyon™ could be visualised using fluorescent staining, providing a qualitative glimpse of the pheriphery of the frits.

Cell populations had to be sacrificed at each time point during the long term cell culture trials to assess number and in turn growth. As a result different populations on separate frits were used to plot cell number over time. It was not possible using the techniques described to quantify the cell number at 3, 9 and 15 days for one population, and so the experiments were dependant on the cell population seeded between frits behaving in the same way on the frit and TCP environments.

Despite these limitations, three cell populations were seeded onto three frits per time point, adhesion did not vary between frits seeded with the same cell population. By repeating the trial with three separate populations the influence of adhesion on cell growth and insulin secretion was made apparent, the n number of these trials supports the integrity of the findings.

6.4 Further work:

A clear challenge of BioVyon™ modification is the adsorption of proteins. The process itself is uncontrollable and it is difficult to control the ratio at which they adsorb and the folding post adsorption. A potential solution to this is to apply short chain peptide sequences.

Laminin is a key protein in the peri-insular matrix and possesses an abundance of binding sites for primary adhesion molecules in β-cells such as integrins, lutherans and dystroglycans (Section 1.2.2). Two primary cell binding domains have been identified within laminin, the long arm of the α chain, and sections of the β and γ chain, which in previous studies have been identified as the E8 and P1 fragments, respectively [65, 297].

Throughout the laminin structure, a few specific amino acid sequences have been implicated in integrin adhesion. The tail end of the α-chain consists of five globular domains in which the majority of peptide sequences with an affinity to specific integrins have been identified. Muscle cells, neurones, hepatocytes, and a range of tumour cell lines have been observed to adhere to this region [297-299]. IKLLI and IKVAV are sequences derived from the α1 chain globular domain and hold an affinity for integrin

α3β1 which is known to be expressed by β-cells and an undefined adhesion molecule weighing 110kDa respectively [291, 300].

The β1 and γ1 chains of laminin also contain significant adhesion sequences. LRE and PDSGR are located on the γ1 and β1 chains, respectively. Their adhesion molecules are unknown, however, they have been implicated in β-cell adhesion. YIGSR is a also found on the β1 chain and is known to bind to an undefined 67kda receptor protein [88, 96, 291, 301]. There is an abundance of different peptide sequences within laminin that warrant continued investigation on a 3D environment.

Collagen is another key structural component of the peri-insular BM and has been shown to influence β-cells. GFOGER is the only sequence that is known to block integrin α2β1 and so may be another sequence that could potentially influence β-cells through adhesion molecules [81]. Further work by Weber *et al* (2007) investigated the function of short chain peptides derived from both laminin and collagen I, similar to the previous investigation these peptides were covalently bound to PEG molecules prior to incorporation into the gels via photo polymerisation [291]. A range of peptides were investigated, derived from laminin and collagen. The peptides promoting the highest level of viability in Min-6 populations were IKLLI and IKVAV, which are peptide sequences derived from laminin α1 chain [291]. Both peptides sustained Min-6 populations at approximately 85% viability over 10 days, showing a better response than PDSGR and YIGSR which are derived from the laminin β1 chains. These peptides were unable to sustain as many viable Min-6 with the viability dropping to approximately 70 and 68% after 10 days respectively [291].

Weber *et al* (2007) employed a similar tactic to this study, developing PEG gels with a combination of peptides. It was found that Min-6 cultured in IKVAV and YIGSR hydrogels secreted the highest levels of insulin, consistently over 10 days. It is interesting to note that a combination of peptides from different regions of laminin produced the best response from the encapsulated Min-6. Furthermore, the combination of IKVAV and YIGSR generated a significantly better response from the Min-6 than they did individually [291]. This study shows that short chain peptides can preserve the β-cell phenotype as effectively as whole proteins if displayed to cell populations in an appropriate concentration and combination. The presence of YIGSR and IKVAV promoted insulin secretion in response to glucose at a level comparable to collagen IV and laminin at a ratio of 25:75 [78, 291]. At this level of investigation, specificity between proteins isoforms cannot be applied directly to peptide sequences. The peptides used are the minimal number of amino acids required to block cell adhesion molecules, and so lack the specificity of the whole protein.

It would be expected that the Min-6 population exposed to peptide sequences innate in laminin isoforms, would up-regulate appropriate adhesion molecules via outside – in signalling. Thus, triggering specific intracellular pathways and promoting expression of the β-cell phenotype. This work supports the use of short chain peptides in conditioning and generating an environment on which β-cells can be mass cultured and potentially differentiated from stem cells [291].

The generation of COOH groups on BioVyon™ from contact with oxygen plasma would provide an ideal anchor for the conjugation of short chain peptides, and enable control over the number and type of peptide conjugated. This in turn could influence the types of

integrin adhesion from β-cells seeded into the environment. Modification of a polymer surface may offer a more appropriate surface than Matrigel®, providing adhesive sequences similar to the peri-insular basement membrane in combination with an increased likelihood of cell to cell contact in comparision with the enivironment of a gel.

Cell seeding is another area that could be developed, basic capillary action and the factors influenced it were investigated initially, and then used as a foundation to continue work on the more advanced aims of the study. The results observed in this study suggest that the cell popualtions are influenced by the number of cells initially adhered to the BioVyon™ environment. Basic capillary action was applied to seed cell populations to the frits, more advanced seeding techniques could be employed to seed more consistently throughout the porous structure, aiding cell to cell adhesion and nutrient transfer.

Hydrodynamic cell seeding involves the use of pressurised flow of cell suspension through a scaffold in order to maximise cell attachment and distribution, as well as providing a more suitable environment for cell growth via a constant flow of media, mimicking the physiological levels of oxygen and nutrients supplied *in vivo* [302-305].

Studies using variations of hydrodynamic flowing cell suspension techniques, such as the manual “multi-pass” seeding technique, and the use of unidirectional fluid flow and directional fluid flow perfusion bioreactors all proved more successful than simple dynamic and static techniques [306-308]. These methods distributed cells within the scaffolds uniformly resulting in a higher cellular density after culture. However, interestingly, the level of cell seeding efficiency was shown to decrease with increasing

cell density, which contrasts with other studies and may have been due to saturation of the ethylene terephthalate scaffold [306]. Furthermore, use of this seeding technique showed that even cardio myocytes, which are sensitive to low levels of oxygen, were maintained in a collagen based scaffold, while being distributed evenly and maintaining the cellular phenotype [309].

A more recent study incorporating an oscillating perfusion flow of an initial cell suspension followed by media throughout a polyactive scaffold showed a high level of cell seeding efficiency, distribution and cellular viability. The action of a constant flow of media was thought to have removed any dead cells unbound to the surface of the polymer; resulting in more viable cells growing within the scaffold [303]. Furthermore the oscillating flow and sheer stress exerted on the cell suspension clusters aided distribution within the complex pore structure and all its orientations. The cells were also separated into smaller aggregates. These factors may have aided distribution within the scaffold [303]. This contrasts with the static technique where the cells attach to the bottom of the pores in large aggregates due to the effects of gravity [310, 311].

Alterations in the geometry of the stirring flask led to the investigation and use of the wavy walled bioreactor (WWB) [312]. Studies have shown that the altered geometry and operating conditions can affect several important hydrodynamic parameters. These include the oxygen concentration, agitation rate and mixing time of cell suspensions [313]. Overall, the hydrodynamic environment of the WWB promoted cellular viability due to effective oxygen and nutrient mixing within the bioreactor, also lower shear stresses and turbulence were found in the WWB compared to the stirring flask [313].

Initially studies focused on the formation of cellular aggregates within the bioreactor independently of scaffolds; however the use of WWB for seeding chondrocytes on PGA scaffolds showed excellent results. The scaffolds in the sinusoidal waved wall lobes of the WWB showed high cell seeding efficiency with 100% cell attachment over 3 days as well as >80% cell viability after 24 hours [302].

The use of WWBs aimed to decrease the shear velocity and increase circulation of a normal stirring flask, increasing the movement of the cell suspension through the scaffolds. This, therefore, increased the number of collisions between the scaffold surface and the cells [314]. It is thought that the flow of the culture media around the scaffolds created an optimal hydrodynamic environment, supporting the externally seeded cells which aided the growth of cells internally via cellular communication or mechanotransduction [315]. It would be of interest to apply a flow system to the BioVyon™ frits, which, due to the large porous structure would seem compatible with a constant flow of both media and cell suspensions.

Overall the modification of BioVyon™ has proved to be successful in harbouring and promoting proliferation in a large population of Min-6. Long term growth showed protection of the β-cell phenotype, and an improved viability relative to TCP controls of a comparable surface area.

These observations show that BioVyon™ holds unquestionable potential as a mass culture system and offers a unique and dynamic platform for further development. Modification to promote relevance of the surface to the peri-insular basement membrane would generate a 3D culture environment that truly mimics the endocrine pancreas.

7 References

[1] Stefan Y, Orci L, Malaisse-Lagae F, Perrelet A, Patel Y, Unger RH. Quantitation of endocrine cell content in the pancreas of nondiabetic and diabetic humans. Diabetes. 1982;31:694-700.

[2] Suckale J, Solimena M. Pancreas islets in metabolic signalling - focus on the beta cell. Frontiers in bioscience. 2008;13:7156-71.

[3] Cabrera O, Berman DM, Kenyon NS, Ricordi C, Berggren P-O, Caicedo A. The unique cytoarchitecture of human pancreatic islets has implications for islet cell function. Proceedings of the National Academy of Sciences of the United States of America. 2006;103:2334-9.

[4] Edwards JL, Vincent AM, Cheng HT, Feldman EL. Diabetic neuropathy: Mechanisms to management. Pharmacology & Therapeutics. 2008;120:1-34.

[5] Tu E, Twigg SM, Semsarian C. Sudden death in type 1 diabetes: The mystery of the [`]dead in bed' syndrome. International Journal of Cardiology. 2010;138:91-3.

[6] Daneman D. Type 1 diabetes. The Lancet. 2006;367:847-58.

[7] Johnson RP, Craig SW. An intramolecular association between the head and tail domains of vinculin modulates talin binding. J Biol Chem. 1994;269:12611-9.

[8] Alberti KG, Zimmet PZ. Definition, diagnosis and classification of diabetes mellitus and its complications. Part 1: diagnosis and classification of diabetes mellitus provisional report of a WHO consultation. Diabet Med. 1998;15:539-53.

[9] Zipris D. Epidemiology of type 1 diabetes and what animal models teach us about the role of viruses in disease mechanisms. Clinical Immunology. 2009;131:11-23.

[10] Gorsuch AN, Spencer KM, Lister J, McNally JM, Dean BM, Bottazzo GF, et al. Evidence for a long prediabetic period in type I (insulin-dependent) diabetes mellitus. Lancet. 1981;2:1363-5.

[11] Harold Rifkin M, Daniel Porte J, MD. ellenberg and Rifkins: Diabetes Mellitus, Theory and Practice: Elsevier; 1990.

[12] Long AE, Bingley PJ. The epidemiology of childhood diabetes. Paediatrics and Child Health. 2009;19:304-8.

[13] Knip M, Siljander H. Autoimmune mechanisms in type 1 diabetes. Autoimmunity Reviews. 2008;7:550-7.

[14] Patterson CC, Dahlquist GG, Gyürüs E, Green A, Soltész G. Incidence trends for childhood type 1 diabetes in Europe during 1989-2003 and predicted new cases 2005-20: a multicentre prospective registration study. The Lancet. 2009;373:2027-33.

[15] IDF DIabetes Atlas 5th edition. International Diabetes Federation; 2011.

[16] Diabetes UK. Key Statisitcs on diabetes. 2010.

[17] Street CN, Rajotte RV, Korbutt GS. Stem cells: a promising source of pancreatic islets for transplantation in type 1 diabetes. Curr Top Dev Biol. 2003;58:111-36.

[18] Thomas J. Insulin: Discovery and Development: The Open University; 1993.

[19] Shapiro AMJ, Lakey JRT, Ryan EA, Korbutt GS. Islet transplantation in seven patients with type 1 diabetes mellitus using a glucocorticoid-free immunosuppressive regimen. The New England Journal of Medicine. 2000;343:230-8.

[20] International Islet Transplant Registry (ITR). ITR Newsletter 2001;8:1-20.

[21] Ryan EA, Paty BW, Senior PA, Bigam D, Alfadhli E, Kneteman NM, et al. Five-Year Follow-Up After Clinical Islet Transplantation. Diabetes: A Journal of the American Diabetes Association. 2005;54:2060-9.

[22] Gaglia JL, Shapiro AMJ, Weir GC. Islet Transplantation: Progress and Challenge. Archives of Medical Research. 2005;36:273-80.

[23] Miszta-Lane H, Mirbolooki M, James Shapiro AM, Lakey JRT. Stem cell sources for clinical islet transplantation in type 1 diabetes: Embryonic and adult stem cells. Medical Hypotheses. 2006;67:909-13.

[24] Thomson JA, Itskovitz-Eldor J, Shapiro SS, Waknitz MA, Swiergiel JJ, Marshall VS, et al. Embryonic Stem Cell Lines Derived from Human Blastocysts. Science. 1998;282:1145-7.

[25] Wiles MV, Keller G. Multiple hematopoietic lineages develop from embryonic stem (ES) cells in culture. Development. 1991;111:259-67.

[26] Svendsen CN, Smith AG. New prospects for human stem-cell therapy in the nervous system. Trends in Neurosciences. 1999;22:357-64.

[27] Klug MG, Soonpaa MH, Koh GY, Field LJ. Genetically selected cardiomyocytes from differentiating embronic stem cells form stable intracardiac grafts. The Journal of Clinical Investigation. 1996;98:216-24.

[28] Zhang C-p, Fu X-b. Therapeutic potential of stem cells in skin repair and regeneration. Chinese Journal of Traumatology (English Edition). 2008;11:209-21.

[29] Sato T, Liu X, Basma H, Togo S, Sugiura H, Nelson A, et al. IL-4 induces differentiation of human embryonic stem cells into fibrogenic fibroblast-like cells. Journal of Allergy and Clinical Immunology. 2011;In Press, Corrected Proof.

[30] Dai W, Field LJ, Rubart M, Reuter S, Hale SL, Zweigerdt R, et al. Survival and maturation of human embryonic stem cell-derived cardiomyocytes in rat hearts. Journal of Molecular and Cellular Cardiology. 2007;43:504-16.

[31] Mitjavila-Garcia MT, Simonin C, Peschanski M. Embryonic stem cells: Meeting the needs for cell therapy. Advanced Drug Delivery Reviews. 2005;57:1935-43.

[32] Soria B, Roche E, BernÃ¡ G, LeÃ³n-Quinto T, Reig JA, MartÃ-n F. Insulin-secreting cells derived from embryonic stem cells normalize glycemia in streptozotocin-induced diabetic mice. Diabetes. 2000;49:157-62.

[33] Lumelsky N, Blondel O, Laeng P, Velasco I, Ravin R, McKay R. Differentiation of Embryonic Stem Cells to Insulin-Secreting Structures Similar to Pancreatic Islets. Science. 2001;292:1389-94.

[34] Okabe S, Forsberg-Nilsson K, Spiro AC, Segal M, McKay RDG. Development of neuronal precursor cells and functional postmitotic neurons from embryonic stem cells in vitro. Mechanisms of Development. 1996;59:89-102.

[35] Van Hoof D, D'Amour KA, German MS. Derivation of insulin-producing cells from human embryonic stem cells. Stem Cell Res. 2009;3:73-87.

[36] D'Amour KA, Bang AG, Eliazer S, Kelly OG, Agulnick AD, Smart NG, et al. Production of pancreatic hormone-expressing endocrine cells from human embryonic stem cells. Nat Biotech. 2006;24:1392-401.

[37] Kroon E, Martinson LA, Kadoya K, Bang AG, Kelly OG, Eliazer S, et al. Pancreatic endoderm derived from human embryonic stem cells generates glucose-responsive insulin-secreting cells in vivo. Nat Biotech. 2008;26:443-52.

[38] Zhang S. Beyond the petri dish. Nature Publishing group. 2004;22.

[39] Zhang D, Jiang W, Liu M, Sui X, Yin X, Chen S, et al. Highly efficient differentiation of human ES cells and iPS cells into mature pancreatic insulin-producing cells. Cell Res.19:429-38.

[40] Griffith LG, Swartz MA. Capturing complex 3D tissue physiology in vitro. Nat Rev Mol Cell Biol. 2006;7:211-24.

[41] Roskelley CD, Desprez PY, Bissell MJ. Extracellular matrix-dependent tissue-specific gene expression in mammary epithelial cells requires both physical and biochemical signal transduction. Proc Natl Acad Sci USA. 1994;91:12378-82

[42] Sarvetnick N. Pancreatic growth and regeneration: Karger Landes Systems; 1997.

[43] Beattie GM, Rubin JS, Mally MI, Otonkoski T, Hayek A. Regulation of proliferation and differentiation of human fetal pancreatic islet cells by extracellular matrix, hepatocyte growth factor, and cell-cell contact. . Diabetes: A Journal of the American Diabetes Association. 1996;45:1223-8.

[44] Phillips BW, Hentze H, Rust WL, Chen QP, Chipperfield H, Tan EK, et al. Directed differentiation of human embryonic stem cells into the pancreatic endocrine lineage. Stem Cells Dev. 2007;16:561-78.

[45] Datta N, Pham Q, Sharma U, Sikavitsas V, Jansen J, Mikos A. In vitro generated extracellular matrix and fluid shear stress synergistically enhance 3D osteoblastic differentiation. Proc Natl Acad Sci U S A. 2006;103:2488-93.

[46] Kang JY, Chung CW, Sung J-H, Park B-S, Choi J-Y, Lee SJ, et al. Novel porous matrix of hyaluronic acid for the three-dimensional culture of chondrocytes. International Journal of Pharmaceutics. 2009;369:114-20.

[47] Hu J, Feng K, Liu X, Ma PX. Chondrogenic and osteogenic differentiations of human bone marrow-derived mesenchymal stem cells on a nanofibrous scaffold with designed pore network. Biomaterials. 2009;30:5061-7.

[48] Graves CE, McAllister RG, Rosoff WJ, Urbach JS. Optical neuronal guidance in three-dimensional matrices. Journal of Neuroscience Methods. 2009;179:278-83.

[49] Debnath J, Brugge JS. Modelling glandular epithelial cancers in three-dimensional cultures. Nat Rev Cancer. 2005;5:675-88.

[50] Minami K, Okano H, Okumachi A, Seino S. Role of Cadherin-mediated Cell-Cell Adhesion in Pancreatic Exocrine-to-Endocrine Transdifferentiation. Journal of Biological Chemistry. 2008;283:13753-61.

[51] Gray HL. Grays' Anatomy. 38th ed: Chruchill Livingstone; 1995.

[52] Palade GE, Siekevitz P, Caro LG. Structure, Chemistry and Function of the Pancreatic Exocrine Cell. Ciba Foundation Symposium - The Exocrine Pancreas: Normal and Abnormal Functions: John Wiley & Sons, Ltd.; 2008. p. 23-55.

[53] Becker V. Histochemistry of the Exocrine Pancreas. Ciba Foundation Symposium - The Exocrine Pancreas: Normal and Abnormal Functions: John Wiley & Sons, Ltd.; 2008. p. 56-66.

[54] Bosco D, Armanet M, Morel P, Niclauss N, Sgroi A, Muller YD, et al. Unique arrangement of alpha- and beta-cells in human islets of Langerhans. Diabetes. 2010.

[55] Andralojc KM, Mercalli A, Nowak KW, Albarello L, Calcagno R, Luzi L, et al. Ghrelin-producing epsilon cells in the developing and adult human pancreas. Diabetologia. 2009;52:486-93.

[56] Konstantinova I, Lammert E. Microvascular development: learning from pancreatic islets. BioEssays. 2004;26:1069-75.

[57] Bonnerweir S, Orci L. NEW PERSPECTIVES ON THE MICROVASCULATURE OF THE ISLETS OF LANGERHANS IN THE RAT. Diabetes. 1982;31:883-9.

[58] Henderson JR, Moss MC. A MORPHOMETRIC STUDY OF THE ENDOCRINE AND EXOCRINE CAPILLARIES OF THE PANCREAS. Quarterly Journal of Experimental Physiology and Cognate Medical Sciences. 1985;70:347-56.

[59] Jansson LJ, Carlsson POC. Graft vascular function after transplantation of pancreatic islets. Diabetologia. 2002;45:749-63.

[60] Nikolova G, Lammert E. Interdependent development of blood vessels and organs. Cell and Tissue Research. 2003;314:33-42.

[61] Ashcroft FM. Adenosine 5'-Triphosphate-Sensitive Potassium Channels. Annual Review of Neuroscience. 1988;11:97-118.

[62] Jain R, Lammert E. Cell-cell interactions in the endocrine pancreas. Diabetes Obes Metab. 2009;11 Suppl 4:159-67.

[63] Timpl R. Structure and biological activity of basement membrane proteins. European Journal of Biochemistry. 1989;180:487-502.

[64] Paulsson M, Mats. Basement Membrane Proteins: Structure, Assembly, and Cellular Interactions. Critical Reviews in Biochemistry and Molecular Biology. 1992;27:93-127.

[65] Yurchenco P, Schittny J. Molecular architecture of basement membranes. The FASEB Journal. 1990;4:1577-90.

[66] Martinez-Hernandez A, Amenta PS. The basement membrane in pathology. Lab Invest. 1983;48:656-77.

[67] Hay ED. Cell Biology of Extracellualr Matrix. 2nd ed: Plenum Press; 1991.

[68] Chan FL, Inoue S. Lamina lucida of basement membrane: An artefact. Microscopy Research and Technique. 1994;28:48-59.

[69] Kragl M, Lammert E. Basement membrane in pancreatic islet function. Adv Exp Med Biol. 2010;654:217-34.

[70] Otonkoski T, Banerjee M, Korsgren O, Thornell LE, Virtanen I. Unique basement membrane structure of human pancreatic islets: implications for β-cell growth and differentiation. Diabetes, Obesity and Metabolism. 2008;10:119-27.

[71] Virtanen I, Banerjee M, Palgi J, Korsgren O, Lukinius A, Thornell LE, et al. Blood vessels of human islets of Langerhans are surrounded by a double basement membrane. Diabetologia. 2008;51:1181-91.

[72] Stendahl JC, Kaufman DB, Stupp SI. Extracellular Matrix in Pancreatic Islets: Relevance to Scaffold Design and Transplantation. Cell Transplantation. 2009;18:1-12.

[73] Jiang F-X, Naselli G, Harrison LC. Distinct Distribution of Laminin and Its Integrin Receptors in the Pancreas. Journal of Histochemistry & Cytochemistry. 2002;50:1625-32.

[74] Meyer T, BÃ¼hler C, Czub S, Beutner U, Otto C, Thiede A, et al. Selection of donor pigs for pancreatic islet transplantation may depend on the expression level of connective tissue proteins in the islet capsule. Transplant Proc. 1998;30:2471-3.

[75] Deijnen JHM, Suylichem PTR, Wolters GHJ, Schilfgaarde R. Distribution of collagens type I, type III and type V in the pancreas of rat, dog, pig and man. Cell and Tissue Research. 1994;277:115-21.

[76] Cirulli V, Beattie GM, Klier G, Ellisman M, Ricordi C, Quaranta V, et al. Expression and Function of αvβ3 and αvβ5 Integrins in the Developing Pancreas. The Journal of Cell Biology. 2000;150:1445-60.

[77] Hughes SJ, Clark A, McShane P, Contractor HH, Gray DWR, Johnson PRV. Characterisation of Collagen VI within the Islet-Exocrine Interface of the Human Pancreas: Implications for Clinical Islet Isolation? Transplantation. 2006;81:423-6 10.1097/01.tp.0000197482.91227.df.

[78] Weber LM, Hayda KN, Anseth KS. Cell-matrix interactions improve beta-cell survival and insulin secretion in three-dimensional culture. Tissue Eng Part A. 2008;14:1959-68.

[79] Boutaud A, Borza D-B, Bondar O, Gunwar S, Netzer K-O, Singh N, et al. Type IV Collagen of the Glomerular Basement Membrane. Journal of Biological Chemistry. 2000;275:30716-24.

[80] Kaido T, Yebra M, Cirulli V, Montgomery AM. Regulation of human beta-cell adhesion, motility, and insulin secretion by collagen IV and its receptor alpha1beta1. J Biol Chem. 2004;279:53762-9.

[81] Knight CG, Morton LF, Peachey AR, Tuckwell DS, Farndale RW, Barnes MJ. The collagen-binding A-domains of integrins alpha(1)beta(1) and alpha(2)beta(1) recognize the same specific amino acid sequence, GFOGER, in native (triple-helical) collagens. J Biol Chem. 2000;275:35-40.

[82] Kaido T, Yebra M, Cirulli V, Rhodes C, Diaferia G, Montgomery AM. Impact of defined matrix interactions on insulin production by cultured human beta-cells: effect on insulin content, secretion, and gene transcription. Diabetes. 2006;55:2723-9.

[83] Malinda KM, Kleinman HK. The laminins. The International Journal of Biochemistry & Cell Biology. 1996;28:957-9.

[84] Timpl R. Macromolecular organization of basement membranes. Current Opinion in Cell Biology. 1996;8:618-24.

[85] Colognato H, Yurchenco PD. Form and function: The laminin family of heterotrimers. Developmental Dynamics. 2000;218:213-34.

[86] Garbe JH, Gohring W, Mann K, Timpl R, Sasaki T. Complete sequence, recombinant analysis and binding to laminins and sulphated ligands of the N-terminal domains of laminin alpha3B and alpha5 chains. The Biochemical journal. 2002;362:213-21.

[87] Yurchenco PD, Cheng YS. Self-assembly and calcium-binding sites in laminin. A three-arm interaction model. Journal of Biological Chemistry. 1993;268:17286-99.

[88] Yamada H, Shimizu T, Tanaka T, Campbell KP, Matsumura K. Dystroglycan is a binding protein of laminin and merosin in peripheral nerve. FEBS Lett. 1994;352:49-53.

[89] Kikkawa Y, Moulson CL, Virtanen I, Miner JH. Identification of the binding site for the Lutheran blood group glycoprotein on laminin alpha 5 through expression of chimeric laminin chains in vivo. J Biol Chem. 2002;277:44864-9.

[90] Kikkawa Y, Miner JH. Review: Lutheran/B-CAM: a laminin receptor on red blood cells and in various tissues. Connect Tissue Res. 2005;46:193-9.

[91] Beck K, Hunter I, Engel J. Structure and function of laminin: anatomy of a multidomain glycoprotein. The FASEB Journal. 1990;4:148-60.

[92] Nikolova G, Jabs N, Konstantinova I, Domogatskaya A, Tryggvason K, Sorokin L, et al. The vascular basement membrane: a niche for insulin gene expression and Beta cell proliferation. Dev Cell. 2006;10:397-405.

[93] Banerjee M, Virtanen I, Palgi J, Korsgren O, Otonkoski T. Proliferation and plasticity of human beta cells on physiologically occurring laminin isoforms. Molecular and Cellular Endocrinology. 2012;355:78-86.

[94] Bosco D, Meda P, Halban PA, Rouiller DG. Importance of cell-matrix interactions in rat islet beta-cell secretion in vitro: role of alpha6beta1 integrin. Diabetes. 2000;49:233-43.

[95] Mankelow TJ, Burton N, Stefansdottir FO, Spring FA, Parsons SF, Pedersen JS, et al. The Laminin 511/521–binding site on the Lutheran blood group glycoprotein is located at the flexible junction of Ig domains 2 and 3. Blood. 2007;110:3398-406.

[96] Tashiro K, Monji A, Yoshida I, Hayashi Y, Matsuda K, Tashiro N, et al. An IKLLI-containing peptide derived from the laminin alpha1 chain mediating heparin-binding, cell adhesion, neurite

outgrowth and proliferation, represents a binding site for integrin alpha3beta1 and heparan sulphate proteoglycan. Biochem J. 1999;340 (Pt 1):119-26.

[97] Kreis T, Vale R. Guidebook to the extracellular metrix anchor and adhesion proteins. Oxford university press; 1999.

[98] Meda P, Bosco D. Communication of Islet Cells: Molecules and Functions

Molecular Basis of Pancreas Development and Function. In: Habener JF, Hussain MA, editors.: Springer US; 2001. p. 143-63.

[99] Ris F, Hammar E, Bosco D, Pilloud C, Maedler K, Donath MY, et al. Impact of integrin-matrix matching and inhibition of apoptosis on the survival of purified human beta-cells in vitro. Diabetologia. 2002;45:841-50.

[100] Kaido T, Perez B, Yebra M, Hill J, Cirulli V, Hayek A, et al. Alphav-integrin utilization in human beta-cell adhesion, spreading, and motility. J Biol Chem. 2004;279:17731-7.

[101] Thurmond DC, Gonelle-Gispert C, Furukawa M, Halban PA, Pessin JE. Glucose-Stimulated Insulin Secretion Is Coupled to the Interaction of Actin with the t-SNARE (Target Membrane Soluble N-Ethylmaleimide-Sensitive Factor Attachment Protein Receptor Protein) Complex. Molecular Endocrinology. 2003;17:732-42.

[102] Ringer S. A further Contribution regarding the influence of the different Constituents of the Blood on the Contraction of the Heart. J Physiol. 1883;4:29-42 3.

[103] Miller DJ. Sydney Ringer; physiological saline, calcium and the contraction of the heart. The Journal of Physiology. 2004;555:585-7.

[104] Eagle H. Nutrition Needs of Mammalian Cells in Tissue Culture. Science. 1955;122:501-4.

[105] Cooper GM, Hausman RE. The Cell: A molecular approach. 4th edition ed: ASM Press; 2007.

[106] Davis JM. Basic Cell culture: Oxford university press; 2001.

[107] Guppy M, Leedman P, Zu X, Russell V. Contribution by different fuels and metabolic pathways to the total ATP turnover of proliferating MCF-7 breast cancer cells. Biochem J. 2002;364:309-15.

[108] Torres Filho IP, Leunig M, Yuan F, Intaglietta M, Jain RK. Noninvasive measurement of microvascular and interstitial oxygen profiles in a human tumor in SCID mice. Proceedings of the National Academy of Sciences. 1994;91:2081-5.

[109] Rouwkema J, Rivron NC, van Blitterswijk CA. Vascularization in tissue engineering. Trends in Biotechnology. 2008;26:434-41.

[110] Carmeliet P, Jain RK. Angiogenesis in cancer and other diseases. Nature. 2000;407:249-57.

[111] Carnachan RJ, Bokhari M, Przyborski SA, Cameron NR. Tailoring the morphology of emulsion-templated porous polymers. Soft matter. 2006;2:608-16.

[112] Hayman MW, Smith KH, Cameron NR, Przyborski SA. Growth of human stem cell-derived neurons on solid three-dimensional polymers. Journal of Biochemical and Biophysical Methods. 2005;62:231-40.

[113] Asthana A, Kisaalita WS. Microtissue size and hypoxia in HTS with 3D cultures. Drug Discovery Today.

[114] Hutmacher DW, Sittinger M, Risbud MV. Scaffold-based tissue engineering: rationale for computer-aided design and solid free-form fabrication systems. Trends in Biotechnology. 2004;22:354-62.

[115] Gafni Y, Zilberman Y, Ophir Z, Abramovitch R, Jaffe M, Gazit Z, et al. Design of a filamentous polymeric scaffold for in vivo guided angiogenesis. Tissue Eng. 2006;12:3021-34.

[116] Brandley BK, Schnaar RL. Covalent attachment of an Arg-Gly-Asp sequece peptide to derivatizable polyacrylamide surfaces: Support of fibroblast adhesion and long-term growth. Analytical Biochemistry. 1988;172:270-8.

[117] Hynes RO. Integrins: a family of cell surface receptors. Cell. 1987;48:549-54.

[118] Beauvais-Jouneau A, Thiery J-P. Multiple roles for integrins during development. Biology of the Cell. 1997;89:5-11.

[119] Atala A, Lanza R, Thomson JA, Nerem r. Principles of regenerative medicine: Elsevier; 2011.

[120] Hynes RO. Integrins: versatility, modulation, and signaling in cell adhesion. Cell. 1992;69:11-25.

[121] LeBaron RG, Athanasiou KA. Extracellular matrix cell adhesion peptides: functional applications in orthopedic materials. Tissue Eng. 2000;6:85-103.

[122] Hersel U, Dahmen C, Kessler H. RGD modified polymers: biomaterials for stimulated cell adhesion and beyond. Biomaterials. 2003;24:4385-415.

[123] Petit V, Thiery JP. Focal adhesions: structure and dynamics. Biol Cell. 2000;92:477-94.

[124] Giancotti FG. Complexity and specificity of integrin signalling. Nat Cell Biol. 2000;2:E13-E4.

[125] Chen H-C, Appeddu PA, Parsons JT, Hildebrand JD, Schaller MD, Guan J-L. Interaction of Focal Adhesion Kinase with Cytoskeletal Protein Talin. Journal of Biological Chemistry. 1995;270:16995-9.

[126] Kwiatkowski DJ. Functions of gelsolin: motility, signaling, apoptosis, cancer. Curr Opin Cell Biol. 1999;11:103-8.

[127] Coll JL, Ben-Ze'ev A, Ezzell RM, RodrÃ-guez FernÃ¡ndez JL, Baribault H, Oshima RG, et al. Targeted disruption of vinculin genes in F9 and embryonic stem cells changes cell morphology, adhesion, and locomotion. Proceedings of the National Academy of Sciences of the United States of America. 1995;92:9161-5.

[128] Chiarugi P, Giannoni E. Anoikis: A necessary death program for anchorage-dependent cells. Biochemical Pharmacology. 2008;76:1352-64.

[129] Hildebrand JD, Schaller MD, Parsons JT. Paxillin, a tyrosine phosphorylated focal adhesion-associated protein binds to the carboxyl terminal domain of focal adhesion kinase. Mol Biol Cell. 1995;6:637-47.

[130] Chen H-C, Appeddu PA, Isoda H, Guan J-L. Phosphorylation of Tyrosine 397 in Focal Adhesion Kinase Is Required for Binding Phosphatidylinositol 3-Kinase. Journal of Biological Chemistry. 1996;271:26329-34.

[131] Schaller MD, Hildebrand JD, Shannon JD, Fox JW, Vines RR, Parsons JT. Autophosphorylation of the focal adhesion kinase, pp125FAK, directs SH2-dependent binding of pp60src. Mol Cell Biol. 1994;14:1680-8.

[132] Coutts AS, Adams CJ, La Thangue NB. p53 ubiquitination by Mdm2: A never ending tail? DNA Repair. 2009;8:483-90.

[133] Lim S-T, Chen XL, Lim Y, Hanson DA, Vo T-T, Howerton K, et al. Nuclear FAK Promotes Cell Proliferation and Survival through FERM-Enhanced p53 Degradation. Molecular Cell. 2008;29:9-22.

[134] IliÄ‡ Dk, Almeida EAC, Schlaepfer DD, Dazin P, Aizawa S, Damsky CH. Extracellular Matrix Survival Signals Transduced by Focal Adhesion Kinase Suppress p53-mediated Apoptosis. The Journal of Cell Biology. 1998;143:547-60.

[135] Cardone MH, Roy N, Stennicke HR, Salvesen GS, Franke TF, Stanbridge E, et al. Regulation of Cell Death Protease Caspase-9 by Phosphorylation. Science. 1998;282:1318-21.

[136] Romashkova JA, Makarov SS. NF-[kappa]B is a target of AKT in anti-apoptotic PDGF signalling. Nature. 1999;401:86-90.

[137] Datta SR, Katsov A, Hu L, Petros A, Fesik SW, Yaffe MB, et al. 14-3-3 Proteins and Survival Kinases Cooperate to Inactivate BAD by BH3 Domain Phosphorylation. Molecular Cell. 2000;6:41-51.

[138] Alahari SK, Reddig PJ, Juliano RL, Kwang WJ. Biological aspects of signal transduction by cell adhesion receptors. International Review of Cytology: Academic Press; 2002. p. 145-84.

[139] Cohen GM. Caspases: the executioners of apoptosis. Biochem J. 1997;326:1-16.

[140] Thornberry NA. Caspases: key mediators of apoptosis. Chemistry & Biology. 1998;5:R97-R103.

[141] Kuwana T, Bouchier-Hayes L, Chipuk JE, Bonzon C, Sullivan BA, Green DR, et al. BH3 Domains of BH3-Only Proteins Differentially Regulate Bax-Mediated Mitochondrial Membrane Permeabilization Both Directly and Indirectly. Molecular Cell. 2005;17:525-35.

[142] Cheng EHYA, Wei MC, Weiler S, Flavell RA, Mak TW, Lindsten T, et al. BCL-2, BCL-XL Sequester BH3 Domain-Only Molecules Preventing BAX- and BAK-Mediated Mitochondrial Apoptosis. Molecular Cell. 2001;8:705-11.

[143] Carrel A. A METHOD FOR THE PHYSIOLOGICAL STUDY OF TISSUES IN VITRO. The Journal of Experimental Medicine. 1923;38:407-18.

[144] Grinnell F, Danielli GHBaJF. Cellular Adhesiveness and Extracellular Substrata. International Review of Cytology: Academic Press; 1978. p. 65-144.

[145] Martin GR, Rubin H. Effects of cell adhesion to the substratum on the growth of chick embryo fibroblasts. Experimental Cell Research. 1974;85:319-33.

[146] Amstein CF, Hartman PA. Adaptation of plastic surfaces for tissue culture by glow discharge. J Clin Microbiol. 1975;2:46-54.

[147] Chu PK, Chen JY, Wang LP, Huang N. Plasma-surface modification of biomaterials. Materials Science and Engineering: R: Reports. 2002;36:143-206.

[148] Taylor AC. Attachment and spreading of cells in culture. Experimental Cell Research. 1961;8:154-73.

[149] Wolpert L, Macpherson I, Todd I. Cell Spreading and Cell Movement: an Active or a Passive Process? Nature. 1969;223:512-3.

[150] Curtis AS, Forrester JV, McInnes C, Lawrie F. Adhesion of cells to polystyrene surfaces. The Journal of Cell Biology. 1983;97:1500-6.

[151] Curtis A. Cell activation and adhesion. J Cell Sci. 1987;87:609-11.

[152] Pierschbacher MD, Ruoslahti E. Cell attachment activity of fibronectin can be duplicated by small synthetic fragments of the molecule. Nature. 1984;309:30-3.

[153] Akiyama SK, Yamada SS, Yamada KM. Characterization of a 140-kD avian cell surface antigen as a fibronectin-binding molecule. The Journal of Cell Biology. 1986;102:442-8.

[154] Pytela R, Pierschbacher MD, Ruoslahti E. A 125/115-kDa cell surface receptor specific for vitronectin interacts with the arginine-glycine-aspartic acid adhesion sequence derived from fibronectin. Proceedings of the National Academy of Sciences of the United States of America. 1985;82:5766-70.

[155] Parsegian VA, Gingell D. Red blood cell adhesion. III. Analysis of forces. J Cell Sci. 1980;41:151-7.

[156] Curtis ASG. Cell adhesion. Progress in Biophysics and Molecular Biology. 1973;27:315-70, IN7-IN8, 71-72, IN9-IN10, 73-74, IN11-IN12, 75-84.

[157] Elbert DL, Hubbell JA. Surface Treatments of Polymers for Biocompatibility. Annual Review of Materials Science. 1996;26:365-294.

[158] Vogler EA. Structure and reactivity of water at biomaterial surfaces. Advances in Colloid and Interface Science. 1998;74:69-117.

[159] Schneider R, Chadwick BR, Jankowski J, Acworth I. Determination of physicochemical parameters of solids covered with conditioning films from groundwaters using contact angles. Comparative analysis of different thermodynamic approaches utilizing a range of diagnostic liquids. Colloids and Surfaces A: Physicochemical and Engineering Aspects. 1997;126:1-23.

[160] Shafrin EG, Zisman WA. CONSTITUTIVE RELATIONS IN THE WETTING OF LOW ENERGY SURFACES AND THE THEORY OF THE RETRACTION METHOD OF PREPARING MONOLAYERS1. The Journal of Physical Chemistry. 1960;64:519-24.

[161] Lee JH, Park JW, Lee HB. characterization of hydroxyl group gradient surfaces prepared by water vapor plasma treatment. Polymer (Korea). 1990;14:646.

[162] Lee JH, Lee HB. A wettability gradient as a tool to study protein adsorption and cell adhesion on polymer surfaces. J Biomater Sci Polym Ed. 1993;4:467-81.

[163] Horbett TA, Lew KR. Residence time effects on monoclonal antibody binding to adsorbed fibrinogen. J Biomater Sci Polym Ed. 1994;6:15-33.

[164] Chinn JA, Posso SE, Horbett TA, Ratner BD. Postadsorptive transition in fibrinogen adsorbed to polyurethanes: Changes in antibody binding and sodium dodecy1 sulfate elutability. Journal of Biomedical Materials Research. 1992;26:757-78.

[165] Pierschbacher MD, Ruoslahti E. Influence of stereochemistry of the sequence Arg-Gly-Asp-Xaa on binding specificity in cell adhesion. J Biol Chem. 1987;262:17294-8.

[166] Lee JH, Kim HG, Khang GS, Lee HB, Jhon MS. Characterization of wettability gradient surfaces prepared by corona discharge treatment. Journal of Colloid and Interface Science. 1992;151:563-70.

[167] Lee JH, Jung HW, Kang I-K, Lee HB. Cell behaviour on polymer surfaces with different functional groups. Biomaterials. 1994;15:705-11.

[168] Lee JH, Lee JW, Khang G, Lee HB. Interaction of cells on chargeable functional group gradient surfaces. Biomaterials. 1997;18:351-8.

[169] Lee JH, Khang G, Lee JW, Lee HB. Interaction of Different Types of Cells on Polymer Surfaces with Wettability Gradient. Journal of Colloid and Interface Science. 1998;205:323-30.

[170] Curtis A, Wilkinson C. New depths in cell behaviour: reactions of cells to nanotopography. London: Portland Press Ltd; 1999.

[171] Zinger O, Anselme K, Denzer A, Habersetzer P, Wieland M, Jeanfils J, et al. Time-dependent morphology and adhesion of osteoblastic cells on titanium model surfaces featuring scale-resolved topography. Biomaterials. 2004;25:2695-711.

[172] Chauvy PF, Madore C, Landolt D. Variable length scale analysis of surface topography: characterization of titanium surfaces for biomedical applications. Surface and Coatings Technology. 1998;110:48-56.

[173] den Braber ET, Jansen HV, de Boer MJ, Croes HJE, Elwenspoek M, Ginsel LA, et al. Scanning electron microscopic, transmission electron microscopic, and confocal laser scanning microscopic observation of fibroblasts cultured on microgrooved surfaces of bulk titanium substrata. Journal of Biomedical Materials Research. 1998;40:425-33.

[174] Perizzolo D, Lacefield WR, Brunette DM. Interaction between topography and coating in the formation of bone nodules in culture for hydroxyapatite- and titanium-coated micromachined surfaces. Journal of Biomedical Materials Research. 2001;56:494-503.

[175] Den Braber ET, de Ruijter JE, Smits HTJ, Ginsel LA, von Recum AF, Jansen JA. Effect of parallel surface microgrooves and surface energy on cell growth. Journal of Biomedical Materials Research. 1995;29:511-8.

[176] Pritchard DJ, Morgan H, Cooper JM. Micron-Scale Patterning of Biological Molecules. Angewandte Chemie International Edition in English. 1995;34:91-3.

[177] Wójciak-Stothard B, Curtis A, Monaghan W, Macdonald K, Wilkinson C. Guidance and Activation of Murine Macrophages by Nanometric Scale Topography. Experimental Cell Research. 1996;223:426-35.

[178] Martin JY, Schwartz Z, Hummert TW, Schraub DM, Simpson J, Lankford J, et al. Effect of titanium surface roughness on proliferation, differentiation, and protein synthesis of human osteoblast-like cells (MG63). Journal of Biomedical Materials Research. 1995;29:389-401.

[179] Kieswetter K, Schwartz Z, Hummert TW, Cochran DL, Simpson J, Dean DD, et al. Surface roughness modulates the local production of growth factors and cytokines by osteoblast-like MG-63 cells. Journal of Biomedical Materials Research. 1996;32:55-63.

[180] Lohmann CH, Sagun R, Sylvia VL, Cochran DL, Dean DD, Boyan BD, et al. Surface roughness modulates the response of MG63 osteoblast-like cells to 1,25-(OH)2D3 through regulation of phospholipase A2 activity and activation of protein kinase A. Journal of Biomedical Materials Research. 1999;47:139-51.

[181] Boyan BD, Batzer R, Kieswetter K, Liu Y, Cochran DL, Szmuckler-Moncler S, et al. Titanium surface roughness alters responsiveness of MG63 osteoblast-like cells to 1α,25-(OH)2D3. Journal of Biomedical Materials Research. 1998;39:77-85.

[182] Wirth C, Comte V, Lagneau C, Exbrayat P, Lissac M, Jaffrezic-Renault N, et al. Nitinol surface roughness modulates in vitro cell response: a comparison between fibroblasts and osteoblasts. Materials Science and Engineering: C. 2005;25:51-60.

[183] Chung T-W, Liu D-Z, Wang S-Y, Wang S-S. Enhancement of the growth of human endothelial cells by surface roughness at nanometer scale. Biomaterials. 2003;24:4655-61.

[184] Ranella A, Barberoglou M, Bakogianni S, Fotakis C, Stratakis E. Tuning cell adhesion by controlling the roughness and wettability of 3D micro/nano silicon structures. Acta Biomaterialia. 2010;6:2711-20.

[185] Beattie GM, Montgomery AMP, Lopez AD, Hao E, Perez B, Just ML, et al. A Novel Approach to Increase Human Islet Cell Mass While Preserving β-Cell Function. Diabetes. 2002;51:3435-9.

[186] Lucas-Clerc C, Massart C, Campion JP, Launois B, Nicol M. Long-term culture of human pancreatic islets in an extracellular matrix: morphological and metabolic effects. Molecular and Cellular Endocrinology. 1993;94:9-20.

[187] Navarro-Alvarez N, Rivas-Carrillo JD, Soto-Gutierrez A, Yuasa T, Okitsu T, Noguchi H, et al. Reestablishment of microenvironment is necessary to maintain in vitro and in vivo human islet function. Cell Transplantation. 2008;17:111-9.

[188] Wang RN, Rosenberg L. Maintenance of beta-cell function and survival following islet isolation requires re-establishment of the islet-matrix relationship. The Journal of endocrinology. 1999;163:181-90.

[189] Beattie GM, Cirulli V, Lopez AD, Hayek A. Ex Vivo Expansion of Human Pancreatic Endocrine Cells. Journal of Clinical Endocrinology & Metabolism. 1997;82:1852-6.

[190] Cirulli V, Beattie GM, Klier G, Ellisman M, Ricordi C, Quaranta V, et al. Expression and function of alpha(v)beta(3) and alpha(v)beta(5) integrins in the developing pancreas: roles in the adhesion and migration of putative endocrine progenitor cells. J Cell Biol. 2000;150:1445-60.

[191] Crisera CA, Kadison AS, Breslow GD, Maldonado TS, Longaker MT, Gittes GK. Expression and role of laminin-1 in mouse pancreatic organogenesis. Diabetes. 2000;49:936-44.

[192] Jiang FX, Cram DS, DeAizpurua HJ, Harrison LC. Laminin-1 promotes differentiation of fetal mouse pancreatic beta-cells. Diabetes. 1999;48:722-30.

[193] Beattie GM, Rubin JS, Mally MI, Otonkoski T, Hayek A. Regulation of Proliferation and Differentiation of Human Fetal Pancreatic Islet Cells by Extracellular Matrix, Hepatocyte Growth Factor, and Cell-Cell Contact. Diabetes. 1996;45:1223-8.

[194] Like AA, Appel MC, Williams RM, Rossini AA. Streptozotocin-induced pancreatic insulitis in mice. Morphologic and physiologic studies. Lab Invest. 1978;38:470-86.

[195] Offield MF, Jetton TL, Labosky PA, Ray M, Stein RW, Magnuson MA, et al. PDX-1 is required for pancreatic outgrowth and differentiation of the rostral duodenum. Development. 1996;122:983-95.

[196] Lammert E, Gu G, McLaughlin M, Brown D, Brekken R, Murtaugh LC, et al. Role of VEGF-A in vascularization of pancreatic islets. Curr Biol. 2003;13:1070-4.

[197] Gu G, Wells JM, Dombkowski D, Preffer F, Aronow B, Melton DA. Global expression analysis of gene regulatory pathways during endocrine pancreatic development. Development. 2004;131:165-79.

[198] Lien S-M, Ko L-Y, Huang T-J. Effect of pore size on ECM secretion and cell growth in gelatin scaffold for articular cartilage tissue engineering. Acta Biomaterialia. 2009;5:670-9.

[199] Miyazaki J, Araki K, Yamato E, Ikegami H, Asano T, Shibasaki Y, et al. Establishment of a pancreatic beta cell line that retains glucose-inducible insulin secretion: special reference to expression of glucose transporter isoforms. Endocrinology. 1990;127:126-32.

[200] Gazdar AF, Chick WL, Oie HK, Sims HL, King DL, Weir GC, et al. Continuous, clonal, insulin- and somatostatin-secreting cell lines established from a transplantable rat islet cell tumor. Proc Natl Acad Sci U S A. 1980;77:3519-23.

[201] Santerre RF, Cook RA, Crisel RM, Sharp JD, Schmidt RJ, Williams DC, et al. Insulin synthesis in a clonal cell line of simian virus 40-transformed hamster pancreatic beta cells. Proceedings of the National Academy of Sciences of the United States of America. 1981;78:4339-43.

[202] Hynes RO. Integrins: Bidirectional, Allosteric Signaling Machines. Cell. 2002;110:673-87.

[203] Wang RN, Paraskevas S, Rosenberg L. Characterization of integrin expression in islets isolated from hamster, canine, porcine, and human pancreas. J Histochem Cytochem. 1999;47:499-506.

[204] Hato T, Pampori N, Shattil SJ. Complementary roles for receptor clustering and conformational change in the adhesive and signaling functions of integrin alphaIIb beta3. J Cell Biol. 1998;141:1685-95.

[205] Durbeej M, Henry MD, Ferletta M, Campbell KP, Ekblom P. Distribution of Dystroglycan in Normal Adult Mouse Tissues. Journal of Histochemistry & Cytochemistry. 1998;46:449-57.

[206] Ervasti J, Campbell K. A role for the dystrophin-glycoprotein complex as a transmembrane linker between laminin and actin. The Journal of Cell Biology. 1993;122:809-23.

[207] Williamson RA, Henry MD, Daniels KJ, Hrstka RF, Lee JC, Sunada Y, et al. Dystroglycan is essential for early embryonic development: disruption of Reichert's membrane in Dag1-null mice. Hum Mol Genet. 1997;6:831-41.

[208] Spence HJ, Dhillon AS, James M, Winder SJ. Dystroglycan, a scaffold for the ERK-MAP kinase cascade. EMBO Rep. 2004;5:484-9.

[209] Belkin AM, Smalheiser NR. Localization of cranin (dystroglycan) at sites of cell-matrix and cell-cell contact: recruitment to focal adhesions is dependent upon extracellular ligands. Cell Adhes Commun. 1996;4:281-96.

[210] Jiang FX, Georges-Labouesse E, Harrison LC. Regulation of laminin 1-induced pancreatic beta-cell differentiation by alpha6 integrin and alpha-dystroglycan. Mol Med. 2001;7:107-14.

[211] Udani M, Zen Q, Cottman M, Leonard N, Jefferson S, Daymont C, et al. Basal cell adhesion molecule/lutheran protein. The receptor critical for sickle cell adhesion to laminin. J Clin Invest. 1998;101:2550-8.

[212] Cirulli V, Baetens D, Rutishauser U, Halban PA, Orci L, Rouiller DG. Expression of neural cell adhesion molecule (N-CAM) in rat islets and its role in islet cell type segregation. J Cell Sci. 1994;107 (Pt 6):1429-36.

[213] Pincet F, Le Bouar T, Zhang Y, Esnault J, Mallet JM, Perez E, et al. Ultraweak sugar-sugar interactions for transient cell adhesion. Biophys J. 2001;80:1354-8.

[214] Hauge-Evans AC, Squires PE, Persaud SJ, Jones PM. Pancreatic beta-cell-to-beta-cell interactions are required for integrated responses to nutrient stimuli: enhanced Ca2+ and insulin secretory responses of MIN6 pseudoislets. Diabetes. 1999;48:1402-8.

[215] Yap AS, Brieher WM, Gumbiner BM. Molecular and functional analysis of cadherin-based adherens junctions. Annu Rev Cell Dev Biol. 1997;13:119-46.

[216] Luther MJ, Davies E, Muller D, Harrison M, Bone AJ, Persaud SJ, et al. Cell-to-cell contact influences proliferative marker expression and apoptosis in MIN6 cells grown in islet-like structures. Am J Physiol Endocrinol Metab. 2005;288:E502-9.

[217] Carvell MJ, Marsh PJ, Persaud SJ, Jones PM. E-cadherin interactions regulate beta-cell proliferation in islet-like structures. Cell Physiol Biochem. 2007;20:617-26.

[218] Ravier MA, Guldenagel M, Charollais A, Gjinovci A, Caille D, Sohl G, et al. Loss of connexin36 channels alters beta-cell coupling, islet synchronization of glucose-induced Ca2+ and insulin oscillations, and basal insulin release. Diabetes. 2005;54:1798-807.

[219] Rogers GJ, Hodgkin MN, Squires PE. E-cadherin and cell adhesion: a role in architecture and function in the pancreatic islet. Cell Physiol Biochem. 2007;20:987-94.

[220] Gilon P, Henquin JC. Influence of membrane potential changes on cytoplasmic Ca2+ concentration in an electrically excitable cell, the insulin-secreting pancreatic B-cell. J Biol Chem. 1992;267:20713-20.

[221] Gilon P, Ravier MA, Jonas JC, Henquin JC. Control mechanisms of the oscillations of insulin secretion in vitro and in vivo. Diabetes. 2002;51 Suppl 1:S144-51.

[222] Charollais A, Gjinovci A, Huarte J, Bauquis J, Nadal A, Martin F, et al. Junctional communication of pancreatic beta cells contributes to the control of insulin secretion and glucose tolerance. J Clin Invest. 2000;106:235-43.

[223] COWIE JMG. Polymers: Chemistry & Physics of Modern Materials. 2nd edition ed: Chapman & Hall; 1991.

[224] Fawcett EWea. British patent. Imperial chemical; 1937.

[225] Houwink R, Meyer KH, Pringsheim H, Waterman HI, Bergmann E, Mark H, et al. General discussion. Transactions of the Faraday Society. 1936;32:115-21.

[226] Brydson J. Plastics materials. 7th ed: Butterworth Heinemann; 1999.

[227] Ziegler K, Holzkamp E, Breil H, Martin H. Polymerisation von Äthylen und anderen Olefinen. Angewandte Chemie. 1955;67:426-.

[228] Francis C U. Use of the polyethylene catheter for jejunostomy feeding. The American Journal of Surgery. 1951;82:408-10.

[229] Burke B S. Precision-formed polyethylene implants for correction of mandibular contour. The American Journal of Surgery. 1956;92:538-44.

[230] Wu S. Polymer interface and adhesion: John Wiley and sons; 1982.

[231] Blais P, Carlsson DJ, Csullog GW, Wiles DM. The chromic acid etching of polyolefin surfaces, and adhesive bonding. Journal of Colloid and Interface Science. 1974;47:636-49.

[232] Kato K. Investigation of high-density polyethylene film surface treated with chromic acid mixture by use of 2,4-dinitrophenylhydrazine. II. Film surfaces treated at 70°C. Journal of Applied Polymer Science. 1977;21:2735-43.

[233] Mares F, Rocek J. Oxidation with chromium(VI)oxide. XI. dependence of oxidation rates of parraffins on structure. Coll Czech Chem Commun. 1961;26:2370-88.

[234] Briggs D, Brewis DM, Konieczko MB. X-ray photoelectron spectroscopy studies of polymer surfaces. Journal of Materials Science. 1979;14:1344-8.

[235] Greene RE. Tappi. 1965;48.

[236] Kreidl WH, Hartmann F. Plast Technol. 1955;1.

[237] Bradley A, Fales JD. Prospects for industrial applications of electrical discharge. Chem Tech. 1971;1:232.

[238] Marquis MA. Plasma Chemistry in Electrical Discharges. F. K. McTaggart. Elsevier, New York, 1967. xii + 246 pp., illus. $17.50. Topics in Inorganic and General Chemistry, vol. 9. Science. 1968;161:458.

[239] R.H.Hansen, H.Schonhorn. Journal of polymer science. 1966.

[240] Barbara HS. Infrared Spectroscopy: John Wiley and Sons; 2004.

[241] Guruvenket S, Rao GM, Komath M, Raichur AM. Plasma surface modification of polystyrene and polyethylene. Applied Surface Science. 2004;236:278-84.

[242] Lehocký M, Drnovská H, Lapčíková B, Barros-Timmons AM, Trindade T, Zembala M, et al. Plasma surface modification of polyethylene. Colloids and Surfaces A: Physicochemical and Engineering Aspects. 2003;222:125-31.

[243] Windawi H, Ho FFL. Applied electron spectroscopy for chemical analysis: John wiley; 1982.

[244] Ivanov VB, Behnisch J, Holländer A, Mehdorn F, Zimmermann H. Determination of Functional Groups on Polymer Surfaces Using FluorescenceLabelling. Surface and Interface Analysis. 1996;24:257-62.

[245] Behnisch J, Mehdorn F, Holländer A, Zimmermann H. Mechanistic approach to the plasma polymerization of acrylic acid by a pulsed MW(ECR) plasma. Surface and Coatings Technology. 1998;98:875-8.

[246] Nedelmann H, Weigel T, Hicke HG, Müller J, Paul D. Microwave plasma polymerization of acrylic acid on poly(ethylene terephthalate) track-etched membranes. Surface and Coatings Technology. 1999;116-119:973-80.

[247] Médard N, Soutif JC, Poncin-Epaillard F. Characterization of CO2 plasma-treated polyethylene surface bearing carboxylic groups. Surface and Coatings Technology. 2002;160:197-205.

[248] Médard N, Aouinti M, Poncin-Epaillard F, Bertrand P. ToF-SIMS ability to quantify surface chemical groups: correlation with XPS analysis and spectrochemical titration. Surface and Interface Analysis. 2001;31:1042-7.

[249] Morris VJ, Kirby AR, Gunning AP. Atomic force microscopy for biologists Imperial College Press; 1999.

[250] Minko S, Roiter Y. AFM single molecule studies of adsorbed polyelectrolytes. Current Opinion in Colloid & Interface Science. 2005;10:9-15.

[251] Rhodes NP, Wilson DJ, Williams RL. The effect of gas plasma modification on platelet and contact phase activation processes. Biomaterials. 2007;28:4561-70.

[252] Chiesa R, Tanzi MC, Alfonsi S, Paracchini L, Moscatelli M, Cigada A. Enhanced wear performance of highly crosslinked UHMWPE for artificial joints. Journal of Biomedical Materials Research. 2000;50:381-7.

[253] Minns RJ, Blamey JM, Blunn GW, Heath DV. The polyethylene wear of meniscal bearings in the early Minns meniscal knee replacement. The Knee. 1994;1:57-64.

[254] Ingham E, Fisher J. Biological reactions to wear debris in total joint replacement. Proceedings of the Institution of Mechanical Engineers, Part H: Journal of Engineering in Medicine. 2000;214:21-37.

[255] Canales V, Panisello JJ, Herrera A, Sola A, Mateo JJ, Caballero MJ. Extensive Osteolysis Caused By Polyethylene Particle Migration in an Anatomical Hydroxyapatite-Coated Hip Prosthesis: 10 Years' Follow-Up. The Journal of Arthroplasty. 2010;25:1115-24.e1.

[256] Streicher RM. IONIZING IRRADIATION FOR STERILIZATION AND MODIFICATION OF HIGH MOLECULAR-WEIGHT POLYETHYLENES. Plastics and Rubber Processing and Applications. 1988;10:221-9.

[257] Bragdon CR, Jasty M, Muratoglu OK, O'Connor DO, Harris WH. Third-body wear of highly cross-linked polyethylene in a hip simulator. The Journal of Arthroplasty. 2003;18:553-61.

[258] Muratoglu OK, O'Connor DO, Bragdon CR, Delaney J, Jasty M, Harris WH, et al. Gradient crosslinking of UHMWPE using irradiation in molten state for total joint arthroplasty. Biomaterials. 2002;23:717-24.

[259] Thomé IPS, Dagostin VS, Piletti R, Pich CT, Riella HG, Angioletto, et al. Bactericidal Low Density Polyethylene (LDPE) Urinary Catheters: Microbiological characterization and effectiveness. Materials Science and Engineering: C.

[260] Wellisz T. Clinical experience with the medpor porous polyethylene implant. Aesthetic Plastic Surgery. 1993;17:339-44.

[261] Romo Iii T, Sclafani AP, Sabini P. Use of Porous High-Density Polyethylene in Revision Rhinoplasty and in the Platyrrhine Nose. Aesthetic Plastic Surgery. 1998;22:211-21.

[262] Cenzi R, Farina A, Zuccarino L, Carinci F. Clinical Outcome of 285 Medpor Grafts used for Craniofacial Reconstruction. Journal of Craniofacial Surgery. 2005;16:526-30 10.1097/01.scs.0000168761.46700.dc.

[263] Arevalo-Silva CA, Eavey RD, Cao Y, Vacanti M, Weng Y, Vacanti CA. Internal Support of Tissue-Engineered Cartilage. Arch Otolaryngol Head Neck Surg. 2000;126:1448-52.

[264] Wu Y, Zhu L, Jiang H, Liu W, Liu Y, Cao Y, et al. Engineering cartilage substitute with a specific size and shape using porous high-density polyethylene (HDPE) as internal support. Journal of Plastic, Reconstructive & Aesthetic Surgery. 2010;63:e370-e5.

[265] coperation S. OPTIONS: MEDPOR® Biomaterial and Surgical Implants. 2011.

[266] Williams RL, Wilson DJ, Rhodes NP. Stability of plasma-treated silicone rubber and its influence on the interfacial aspects of blood compatibility. Biomaterials. 2004;25:4659-73.

[267] Good RJ, Koo MN. The effect of drop size on contact angle. Journal of Colloid and Interface Science. 1979;71:283-92.

[268] 10993-1 I. Biological evaluation of medical devices - part 1: Evaluation and testing. 2003.

[269] Cima LG, Vacanti JP, Vacanti C, Ingber D, Mooney D, Langer R. Tissue engineering by cell transplantation using degradable polymer substrates. J Biomech Eng. 1991;113:143-51.

[270] Vasita R, Katti DS. Growth factor-delivery systems for tissue engineering: a materials perspective. Expert Rev Med Devices. 2006;3:29-47.

[271] Massia SP, Hubbell JA. An RGD spacing of 440 nm is sufficient for integrin alpha V beta 3-mediated fibroblast spreading and 140 nm for focal contact and stress fiber formation. The Journal of Cell Biology. 1991;114:1089-100.

[272] Xu L-C, Siedlecki CA. Effects of surface wettability and contact time on protein adhesion to biomaterial surfaces. Biomaterials. 2007;28:3273-83.

[273] Spijker HT, Bos R, van Oeveren W, de Vries J, Busscher HJ. Protein adsorption on gradient surfaces on polyethylene prepared in a shielded gas plasma. Colloids and Surfaces B: Biointerfaces. 1999;15:89-97.

[274] Siow KS, Britcher L, Kumar S, Griesser HJ. Plasma Methods for the Generation of Chemically Reactive Surfaces for Biomolecule Immobilization and Cell Colonization - A Review. Plasma Processes and Polymers. 2006;3:392-418.

[275] Unger RH, Orci L. Glucagon and the a Cell. New England Journal of Medicine. 1981;304:1518-24.

[276] Ma Z, Mao Z, Gao C. Surface modification and property analysis of biomedical polymers used for tissue engineering. Colloids and Surfaces B: Biointerfaces. 2007;60:137-57.

[277] Dee KC, Puleo DA, Bizios R. Biocompatibility. An Introduction To Tissue-Biomaterial Interactions: John Wiley & Sons, Inc.; 2003. p. 173-84.

[278] Koga H, Kitaoka T, Isogai A. In situ modification of cellulose paper with amino groups for catalytic applications. Journal of Materials Chemistry. 2011;21:9356-61.

[279] Miller AG. Determination of particle size distribution of salt crystals in aqueous slurries. Powder Technology. 1978;21:275-84.

[280] Linke T, Doraiswamy S, Harrison EH. Rat plasma proteomics: Effects of abundant protein depletion on proteomic analysis. Journal of Chromatography B. 2007;849:273-81.

[281] Howarter JA, Youngblood JP. Surface Modification of Polymers with 3-Aminopropyltriethoxysilane as a General Pretreatment for Controlled Wettability. Macromolecules. 2007;40:1128-32.

[282] Ertel SI, Ratner BD, Horbett TA. Radiofrequency plasma deposition of oxygen-containing films on polystyrene and poly(ethylene terephthalate) substrates improves endothelial cell growth. Journal of Biomedical Materials Research. 1990;24:1637-59.

[283] Raschke TM. Water structure and interactions with protein surfaces. Current Opinion in Structural Biology. 2006;16:152-9.

[284] Ruotolo BT, Robinson CV. Aspects of native proteins are retained in vacuum. Current Opinion in Chemical Biology. 2006;10:402-8.

[285] Wolynes PG. Biomolecular folding in vacuo!!!(?). Proceedings of the National Academy of Sciences. 1995;92:2426-7.

[286] Uroic DS, Baudouin G, Ferguson LA, Docherty HM, Vallier L, Docherty K. A factor(s) secreted from MIN-6 beta-cells stimulates differentiation of definitive endoderm enriched embryonic stem cells towards a pancreatic lineage. Mol Cell Endocrinol. 2010;328:80-6.

[287] Bratosin D, Mitrofan L, Palii C, Estaquier J, Montreuil J. Novel fluorescence assay using calcein-AM for the determination of human erythrocyte viability and aging. Cytometry Part A. 2005;66A:78-84.

[288] Schutte M, Fox B, Baradez MO, Devonshire A, Minguez J, Bokhari M, et al. Rat primary hepatocytes show enhanced performance and sensitivity to acetaminophen during three-dimensional culture on a polystyrene scaffold designed for routine use. Assay Drug Dev Technol. 2011;9:475-86.

[289] Neofytou EA, Chang E, Patlola B, Joubert LM, Rajadas J, Gambhir SS, et al. Adipose tissue-derived stem cells display a proangiogenic phenotype on 3D scaffolds. J Biomed Mater Res A. 2011;98:383-93.

[290] Hayman MW, Smith KH, Cameron NR, Przyborski SA. Enhanced neurite outgrowth by human neurons grown on solid three-dimensional scaffolds. Biochem Biophys Res Commun. 2004;314:483-8.

[291] Weber LM, Hayda KN, Haskins K, Anseth KS. The effects of cell–matrix interactions on encapsulated β-cell function within hydrogels functionalized with matrix-derived adhesive peptides. Biomaterials. 2007;28:3004-11.

[292] Tanaka H, Tanaka S, Sekine K, Kita S, Okamura A, Takebe T, et al. The generation of pancreatic beta-cell spheroids in a simulated microgravity culture system. Biomaterials. 2013;34:5785-91.

[293] Hauge-Evans AC, Squires PE, Persaud SJ, Jones PM. Pancreatic beta-cell-to-beta-cell interactions are required for integrated responses to nutrient stimuli: enhanced Ca2+ and insulin secretory responses of MIN6 pseudoislets. Diabetes. 1999;48:1402-8.

[294] HALBAN PA, WOLLHEIM CB, BLONDEL B, MEDA P, NIESOR EN, MINTZ DH. The Possible Importance of Contact between Pancreatic Islet Cells for the Control of Insulin Release. Endocrinology. 1982;111:86-94.

[295] Jaques F, Jousset H, Tomas A, Prost A-L, Wollheim CB, Irminger J-C, et al. Dual Effect of Cell-Cell Contact Disruption on Cytosolic Calcium and Insulin Secretion. Endocrinology. 2008;149:2494-505.

[296] Bavamian S, Klee P, Britan A, Populaire C, Caille D, Cancela J, et al. Islet-cell-to-cell communication as basis for normal insulin secretion. Diabetes, Obesity and Metabolism. 2007;9:118-32.

[297] Edgar D, Timpl R, Thoenen H. The heparin-binding domain of laminin is responsible for its effects on neurite outgrowth and neuronal survival. EMBO J. 1984;3:1463-8.

[298] Timpl R, Johansson S, Vandelden V, Oberbaumer I, Hook M. CHARACTERIZATION OF PROTEASE-RESISTANT FRAGMENTS OF LAMININ MEDIATING ATTACHMENT AND SPREADING OF RAT HEPATOCYTES. Journal of Biological Chemistry. 1983;258:8922-7.

[299] Terranova VP, Rao CN, Kalebic T, Margulies IM, Liotta LA. Laminin receptor on human breast carcinoma cells. Proc Natl Acad Sci U S A. 1983;80:444-8.

[300] Gribova V, Crouzier T, Picart C. A material's point of view on recent developments of polymeric biomaterials: control of mechanical and biochemical properties. Journal of Materials Chemistry. 2011;21:14354-66.

[301] Masters KS, Anseth KS. CELL–MATERIAL INTERACTIONS. In: Peppas A, Sefton MV, editors. Advances in Chemical Engineering: Academic Press; 2004. p. 7-46.

[302] Bueno EM, Laevsky G, Barabino GA. Enhancing cell seeding of scaffolds in tissue engineering through manipulation of hydrodynamic parameters. Journal of Biotechnology. 2007;129:516-31.

[303] Wendt D, Marsano A, Jakob M, Heberer M, Martin I. Oscillating perfusion of cell suspensions through three-dimensional scaffolds enhances cell seeding efficiency and uniformity. Biotechnology and Bioengineering. 2003;84:205-14.

[304] Feng Z, Teng M. Perfusion bioreactor system for human mesenchymal stem cell tissue engineering: Dynamic cell seeding and construct development. Biotechnology and Bioengineering. 2005;91:482-93.

[305] Tatsuya K, Tetsuji Y, Reiko I, Akira M. Three-dimensional cell seeding and growth in radial-flow perfusion bioreactor for in vitro tissue reconstruction. Biotechnology and Bioengineering. 2006;93:947-54.

[306] Yan L, Teng M, Douglas AK, Larry CL, Shang-Tian Y. Effects of Filtration Seeding on Cell Density, Spatial Distribution, and Proliferation in Nonwoven Fibrous Matrices. Biotechnology Progress. 2001;17:935-44.

[307] Kim SS, Sundback CA, Kaihara S, Benvenuto MS, Kim BS, Mooney DJ, et al. Dynamic seeding and in vitro culture of hepatocytes in a flow perfusion system. Tissue Eng. 2000;6:39-44.

[308] Davisson T, Sah RL, Ratcliffe A. Perfusion increases cell content and matrix synthesis in chondrocyte three-dimensional cultures. Tissue Eng. 2002;8:807-16.

[309] Milica R, Michelle E, Liming Y, Robert L, Lisa EF, Gordana V-N. High-density seeding of myocyte cells for cardiac tissue engineering. Biotechnology and Bioengineering. 2003;82:403-14.

[310] Burg KJL, W. D. Holder J, Culberson CR, Beiler RJ, Greene KG, Loebsack AB, et al. Comparative study of seeding methods for three-dimensional polymeric scaffolds. Journal of Biomedical Materials Research. 2000;51:642-9.

[311] Vunjak-Novakovic G, Radisic M. Cell seeding of polymer scaffolds. Methods Mol Biol. 2004;238:131-46.

[312] Natarajan B, Metghalchi M, Tangborn A, Barabino G. Hydrodynamic evaluation of a novel bioreactor design. Bioprocess Eng Symp. 1992;23:1-6.

[313] Bahar B, Chang-Mateu IM, Gilda AB. Characterization of mixing in a novel wavy-walled bioreactor for tissue engineering. Biotechnology and Bioengineering. 2005;92:907-19.

[314] Bilgen B, Sucosky P, Neitzel GP. Flow characterization of a wavy-walled bioreactor for cartilage tissue engineering. Biotechnology and Bioengineering. 2006;95:1009-22.

[315] Grodzinsky AJ, Levenston ME, Jin M, Frank EH. CARTILAGE TISSUE REMODELING IN RESPONSE TO MECHANICAL FORCES. Annual Review of Biomedical Engineering. 2000;2:691-713.